VOL. 20 NO. 3 MARCH 1969
COMPLETING VOLUME 20
PUBLISHED MONTHLY

JOURNAL OF ELECTROANALYTICAL CHEMISTRY AND INTERFACIAL ELECTROCHEMISTRY

International Journal devoted to all Aspects of Electroanalytical Chemistry, Double Layer Studies, Electrokinetics, Colloid Stability, and Electrode Kinetics.

ELSEVIER

GENERAL INFORMATION

Types of contributions

(a) Original research work not previously published in other periodicals.
(b) Reviews on recent developments in various fields.
(c) Short communications.
(d) Bibliographical notes and book reviews.

Languages

Papers will be published in English, French or German.

Submission of papers

Papers should be sent to one of the following Editors:
Professor J. O'M. Bockris, John Harrison Laboratory of Chemistry, University of Pennsylvania, Philadelphia 4, Pa. 19104, U.S.A.
Dr. R. H. Ottewill, Department of Chemistry, The University, Bristol 8, England.
Dr. R. Parsons, Department of Chemistry, The University, Bristol 8, England.
Professor C. N. Reilley, Department of Chemistry, University of North Carolina, Chapel Hill, N.C. 27515, U.S.A.

Authors should preferably submit two copies in double-spaced typing on pages of uniform size. Legends for figures should be typed on a separate page. The figures should be in a form suitable for reproduction, drawn in Indian ink on drawing paper or tracing paper, with lettering etc. in thin pencil. The sheets of drawing or tracing paper should preferably be of the same dimensions as those on which the article is typed. Photographs should be submitted as clear black and white prints on glossy paper. Standard symbols should be used in line drawings, the following are available to the printers:

▼ ▽ ■ □ ● ◎ ▪ ◘ ◈ ▣ ▪ + ×

All references should be given at the end of the paper. They should be numbered and the numbers should appear in the text at the appropriate places.
A summary of 50 to 200 words should be included.

Reprints

Fifty reprints will be supplied free of charge. Additional reprints (minimum 100) can be ordered at quoted prices. They must be ordered on order forms which are sent together with the proofs.

Publication

The *Journal of Electroanalytical Chemistry and Interfacial Electrochemistry* appears monthly. For 1969, each volume has 3 issues and 4 volumes will appear.
Subscription price: Sfr. 316.— (U.S. $ 74.60) per year incl. postage. Additional cost for copies by air mail available on request. For subscribers in the U.S.A. and Canada, 2nd class postage paid at Jamaica, N.Y. For advertising rates apply to the publishers.

Subscriptions

Subscriptions should be sent to:

ELSEVIER SEQUOIA S.A., P.O. Box 851, 1001 Lausanne 1, Switzerland

ELECTROANALYTICAL CHEMISTRY AND INTERFACIAL ELECTROCHEMISTRY
Elsevier Sequoia S.A., Lausanne – Printed in The Netherlands

THEORY OF CHRONOPOTENTIOMETRY AT CYLINDRICAL ELECTRODES FOR ALL VALUES OF DIFFUSION COEFFICIENT, TRANSITION TIME AND ELECTRODE RADIUS

DAVID I. DORNFELD* AND DENNIS H. EVANS
Department of Chemistry, University of Wisconsin, Madison, Wis. 53706 (U.S.A.)
(Received September 30th, 1968)

The first derivation of a transition time equation for chronopotentiometry with cylindrical electrodes was that of PETERS AND LINGANE[1]. These authors utilized asymptotic expansions of the Bessel functions whose quotient appears in the Laplace transform of the concentration in the solution of the cylindrical form of the Fick's law equation with chronopotentiometric boundary conditions. Inverse transforms were obtained term by term giving a transition time equation whose validity was supported by satisfactory agreement with experimental data[1].

Nevertheless, it soon became apparent that the Peters and Lingane equation fails when the dimensionless parameter, θ, becomes large[2] ($\theta = D^{\frac{1}{2}}\tau^{\frac{1}{2}}/r_0$ where D is the diffusion coefficient of the electroactive species (cm^2/sec), τ is the transition time (sec) and r_0 is the radius of the cylindrical electrode (cm)). In the reduction of hydrogen ion, which has an exceptionally large D ($8.6 \cdot 10^{-5}$ cm^2/sec at 25° in 1 M KCl), at an electrode of 0.0252 cm radius, the Peters and Lingane equation failed for τ greater than about 4 sec ($\theta = 0.7$) even with two additional terms added to the series[2,3]. The improvement afforded by each new derived term is so slight that further extensions of the series in the Peters and Lingane equation seem unwarranted.

An equation valid for large values of θ may be derived by the methods of CARSLAW AND JAEGER[4]. The inversion theorem is applied directly to the Laplace transform of the concentration. The Bessel functions are written in the form of their series definitions, and term by term integration is performed. Using this procedure we have added another term to the equation given by CARSLAW AND JAEGER[4]. The result is:

$$i\tau^{\frac{1}{2}}/AC^\circ = [\pi^{\frac{1}{2}} nFD^{\frac{1}{2}}/2]R \tag{1}$$

$$R = \left[\pi^{\frac{1}{2}}\left(\frac{\ln \Psi}{4\theta} + \frac{(1+\ln \Psi)}{8\theta^3} + \frac{((3+\pi^2)/2 - \ln \Psi - 3(\ln \Psi)^2)}{64\theta^5}\right)\right]^{-1} \tag{2}$$

where i is the current (A), A the electrode area (cm^2), C° the concentration of the electroactive species (moles/cm^3), n the number of Faradays/mole of electrode reaction, F the Faraday and $\Psi = 4\theta^2/e^\gamma$ where γ is Euler's constant and θ was defined above.

R is the previously defined[2,3] cylindrical correction factor. It is the factor by which the value of $i\tau^{\frac{1}{2}}/AC^\circ$ pertaining to a plane electrode must be multiplied to

* Present address: Minnetonka High School, Excelsior, Minn.

obtain the theoretical value of $i\tau^{\frac{1}{2}}/AC^{\circ}$ for the cylindrical electrode. R is a function only of θ.

Numerous values of R were computed for θ between 0.8 and 20. Some of these are plotted in Fig. 1 along with the analogous values of R from the extended Peters and Lingane equation[3] and the experimental results for hydrogen ion reduction[2]. Equation (2) gives correct values of R for large θ but it begins to fail seriously for θ less than about 1.6 just as the earlier equation gives correct values of R for small θ but fails for θ above about 0.7. There remains a considerable region in which neither equation is adequate.

Values of R for θ between 0.2 and 2.2 were computed in an alternative way. The solution to the boundary value problem may be obtained in the form of an integral[4,5] which may be evaluated numerically. After making a substitution of variable ($U=ur_0$) and considering only the concentration at the electrode surface ($r=r_0$) the solution[4,5] takes the form:

$$\frac{i\tau^{\frac{1}{2}}}{AC^{0}} = \left[\frac{\pi^{\frac{1}{2}}nFD^{\frac{1}{2}}}{2}\right]\left[\int_0^{\infty} \frac{1-\exp(-\theta^2u^2)}{U^2} \frac{J_0(U)Y_1(U)-Y_0(U)J_1(U)}{J_1^2(U)+Y_1^2(U)}\,\mathrm{d}U\right]^{-\pi^{\frac{1}{2}}\theta} \tag{3}$$

where J_n and Y_n are Bessel functions of the first and second kind respectively of order n. The second factor of the right-hand side of eqn. (3) is again the cylindrical correction factor, R.

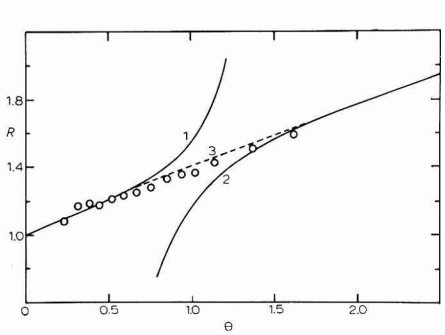

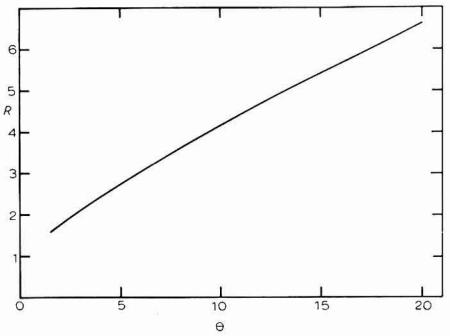

Figs. 1–2. Correction factor (R) for chronopotentiometry with cylindrical electrodes as a function of θ. $\theta = D^{\frac{1}{2}}\tau^{\frac{1}{2}}/r_0$.

Fig. 1: (1), extended Peters and Lingane equation[3]; (2), eqn. 2; (3) numerical results from eqn. (3), (- - -); (○), exptl. data for hydrogen ion reduction[2].

Fig. 2: Eqn. (2) for $1.6 \leqslant \theta \leqslant 20$.

The integral was evaluated numerically using the CDC 1604 computer and the Romberg trapezoidal extrapolation numerical integration technique. It was found that the function to be integrated was a well-behaved, smooth function of U in the region $0 \leq U \leq 25$. Therefore, the function was integrated over this region for $\theta = 0.20$, 0.25, 0.30 ... 2.20. Typically consecutive integrations agreed to within 0.1% when the number of intervals reached 256. The Romberg integral was always within 0.1% of the integral obtained using Simpson's rule.

In the region $U>25$, the function to be integrated is given quite accurately by $-U^{-2}$. This may be shown by noting that for $U>25$ and $\theta>0.2$, $e^{-\theta^2U^2}$ is always less than e^{-25}. In addition, for $U>25$, the portion of the function containing the Bessel functions reduces to -1.000. This may be shown by replacing the Bessel functions by their asymptotic forms[6]. Manipulation of the resulting expression yields minus unity for the asymptotic value. Computed values of the Bessel function expression are within one part per thousand of minus unity for $U>20$, so in this region the function to be integrated is given by $-U^{-2}$. The function has lost its dependence on θ, so a single value of the integral for $U\geq25$ will pertain to all values of θ to be considered. This integral is obtained directly and is given by $[1/U]_{25}^{\infty}=-1/25$. This value, along with the numerical results for $0\leq U\leq25$, permits us to obtain the total integrals in eqn. (3) and to calculate R for $\theta=0.20, 0.25, 0.30 \ldots 2.20$. These are presented in Table 1.

TABLE 1

CORRECTION FACTOR (R) FOR CHRONOPOTENTIOMETRY WITH CYLINDRICAL ELECTRODES AS A FUNCTION OF θ

$\theta = D^{\frac{1}{2}}\tau^{\frac{1}{2}}/r_0$

θ	R	θ	R	θ	R
0.20	1.086	0.90	1.368	1.60	1.628
0.25	1.108	0.95	1.388	1.65	1.646
0.30	1.128	1.00	1.407	1.70	1.664
0.35	1.149	1.05	1.426	1.75	1.682
0.40	1.170	1.10	1.444	1.80	1.700
0.45	1.190	1.15	1.463	1.85	1.718
0.50	1.210	1.20	1.482	1.90	1.735
0.55	1.230	1.25	1.501	1.95	1.753
0.60	1.250	1.30	1.519	2.00	1.770
0.65	1.270	1.35	1.538	2.05	1.788
0.70	1.291	1.40	1.556	2.10	1.805
0.75	1.310	1.45	1.574	2.15	1.822
0.80	1.330	1.50	1.592	2.20	1.840
0.85	1.349	1.55	1.610		

The validity of the $U\geq25$ integral is supported by the excellent agreement between the numerical method and each series solution in the regions where they overlap. The first five entries in Table 1 are within 0.1% of the values calculated from the extended Peters and Lingane equation[3]. The last two entries are within 0.1% of the values calculated from eqn. (2). Furthermore, when the integral for $0\leq U\leq25$ was computed for $\theta=20$ at the 0.001% error level and $-1/25$ was used for the $U\geq25$ integral, R was calculated to be 6.6273 compared to 6.6275 from eqn. (2).

The values of R from Table 1 are also plotted in Fig. 1. Since R is very nearly a linear function of θ, theoretical values of R for comparison with the experimental hydrogen reduction values were obtained by interpolation between the values in Table 1. The agreement between experiment and theory is satisfactory with an average error of 2.0%. There is a preponderance of low values suggesting a small systematic error in the measurement of i, τ, D or r_0.

The behavior of R for larger values of θ is shown in Fig. 2 where the values

were calculated from eqn. (2). The function increases smoothly with R reaching a value of about 6.6 at $\theta = 20$. For θ greater than about 5, R may be calculated with an uncertainty of less than 0.1% using only the terms through θ^3 in eqn. (2).

The relatively large values of R predicted for large θ represent a small but real increase in sensitivity. This increase arises from the fact that the charging of the electrical double layer limits the sensitivity of the chronopotentiometric method. For example, with planar electrodes it may be shown[7] that the quantity of electricity required to charge the double layer is 1.2 times the quantity arising from the Faradaic reaction at $C^\circ = 10^{-5}$ M and a theoretical τ of 10 sec (assuming $D = 10^{-5}$ cm^2/sec, average double layer capacitance = 20 μF/cm^2, potential change = 0.5 V, $n = 1$). Thus the larger part of the (average) current is expended in charging the double layer and a severely distorted chronopotentiogram with an enhanced transition time is observed. The resulting difficulties in interpretation have been amply demonstrated and several theoretical treatments which correct chronopotentiometric results for double layer charging have been reported[8–12].

However, owing to the enhanced mass transport by diffusion observed at non-planar electrodes, the effects of double layer charging may be minimized. For example with $\theta = 100$ ($D = 10^{-5}$ cm^2/sec, $\tau = 10$ sec, $r_0 = 10^{-4}$ cm) which is about the largest θ which might be practical, R (from eqn. (2)) is calculated to be 22.5. The result is that the relative quantity of electricity required to charge the double layer is only $1/R$ times that required for a planar electrode or only 0.05 times the quantity corresponding to the Faradaic reaction under the same conditions as stated above. A much less severely distorted chronopotentiogram would result.

The effect is even more pronounced for a spherical electrode. With $\theta = 100$ the spherical correction factor[13] is 114 and double layer charging would account for only about 1% of the total current.

The only practical way of obtaining very large θ is to construct electrodes of very small radius ($r_0 \approx 10^{-4}$ cm). The construction of such sub-miniature electrodes presents several difficulties, but this stratagem represents a relatively direct way of decreasing the adverse effects of double layer charging in chronopotentiometry.

Equation (2), the numerical results in Table 1, and the previous small θ-equation[1–3] provide the necessary theoretical basis for chronopotentiometry at cylindrical electrodes for any values of D, τ and r_0. An extensive table of computed values of R for $0 \leq \theta \leq 20$ will be provided on request.

ACKNOWLEDGEMENT

This work was supported by the National Science Foundation Research Participation for High School Teachers Program, 1968–69, GW-2887 (D.I.D.) and by National Science Foundation grant number GP-8350 (D.H.E.).

SUMMARY

The theory of chronopotentiometry at cylindrical electrodes has been extended to include large values of the parameter θ ($\theta = D^{\frac{1}{2}}\tau^{\frac{1}{2}}/r_0$). Satisfactory agreement was found between the theory and previously published data for the reduction of hydrogen ion.

REFERENCES

1 D. G. PETERS AND J. J. LINGANE, *J. Electroanal. Chem.*, 2 (1961) 1.
2 J. J. LINGANE, *J. Electroanal. Chem.*, 2 (1961) 46.
3 D. H. EVANS AND J. E. PRICE, *J. Electroanal. Chem.*, 5 (1963) 77.
4 H. S. CARSLAW AND J. C. JAEGER, *Conduction of Heat in Solids*, Oxford, London, 2nd ed., 1959, pp. 338–341.
5 D. G. PETERS, Ph.D. thesis, Harvard University, 1962, p. 22.
6 *Handbook of Mathematical Functions*, edited by M. ABRAMOWITZ AND I. A. STEGEN, Dover, New York, 1965, p. 364.
7 P. DELAHAY, *New Instrumental Methods in Electrochemistry*, Interscience, New York, 1954, p. 207–8.
8 J. J. LINGANE, *J. Electroanal. Chem.*, 1 (1960) 379.
9 A. J. BARD, *Anal. Chem.*, 35 (1963) 340.
10 D. H. EVANS, *Anal. Chem.*, 36 (1964) 2027.
11 M. L. OLMSTEAD AND R. S. NICHOLSON, *J. Phys. Chem.*, 72 (1968) 1950.
12 R. S. RODGERS AND L. MEITES, *J. Electroanal. Chem.*, 16 (1968) 1.
13 G. MAMANTOV AND P. DELAHAY, *J. Am. Chem. Soc.*, 76 (1954) 5319.

ELECTROANALYTICAL CHEMISTRY AND INTERFACIAL ELECTROCHEMISTRY
Elsevier Sequoia S.A., Lausanne – Printed in The Netherlands

EFFECTS OF NEGLECTING PRE-EXPONENTIAL TERMS IN ELECTROCHEMICAL KINETIC EQUATIONS

T. BIEGLER AND R. WOODS
Division of Mineral Chemistry, CSIRO, P.O. Box 124, Port Melbourne, Victoria 3207 (Australia)
(Received October 5th, 1968)

Electrochemical kinetic equations for reactions involving adsorbed intermediates are generally approached in modern treatments (*e.g.*, refs. 1 and 2) by the following kinds of arguments. The rate of an electrochemical reaction from absolute rate theory is

$$i = nF(\tau kT/h) \exp(-\Delta\bar{G}^{\circ\neq}/RT)\, \Pi a_R$$

where the rate is expressed in terms of the current i, $\Delta\bar{G}^{\circ\neq}$ is the standard electrochemical free energy of activation, Πa_R is the product of reactant activities, and the other terms have their usual significance. $\Delta\bar{G}^{\circ\neq}$ depends on the electrode potential according to

$$\Delta\bar{G}^{\circ\neq} = (\Delta\bar{G}^{\circ\neq})_{\phi=0} - \beta nF\phi$$

where ϕ is the electrode potential on an arbitrary reference scale and $(\Delta\bar{G}^{\circ\neq})_{\phi=0}$ is the standard electrochemical free energy of activation when $\phi = 0$ and β is the transfer coefficient.

The problem of introducing activities of chemisorbed species is conventionally overcome by expressing them as fractional surface coverages. A further complication arises because the free energy of adsorption is likely to decrease (and therefore $\Delta\bar{G}^{\circ\neq}$ to increase) with coverage when chemisorption is involved[3,4]. Two models have been proposed to account for this coverage-dependence of adsorption energy:

(i) The surface is assumed to be uniform and the standard free energy of adsorption a function of coverage,

$$\Delta G_\theta^\circ = \Delta G_0^\circ - RTg(\theta)$$

resulting in a proportionate increase in the standard free energy of activation of $\alpha RTg(\theta)$ where α is a symmetry factor. This is an induced heterogeneity model in which the adsorption energy is changed as a consequence of the presence of those particles already adsorbed[3,5].

(ii) The surface is supposed to possess intrinsic heterogeneity and to consist of a number of patches having different adsorption energies. The properties of the whole surface are obtained by summation of the properties of the individual patches[4,6,7].

Electrochemists usually formulate the forward rate of the adsorption charge transfer reaction

$$A + M \rightleftharpoons B\text{–}M + e \qquad \text{I}$$

as

$$i_1 = k_1 a_A (1-\theta) \exp(\beta F\phi/RT) \exp -\alpha g(\theta) \qquad (1)$$

where all terms independent of coverage, potential or reactant activities are incorporated in the rate constant, k_1; θ is the fractional coverage of surface species B. Note that the activity of reactant M, the electrode surface, is introduced as the term $(1-\theta)$ which is the fraction of the available electrode surface not covered by adsorbed species. This equation refers to the induced heterogeneity model, a point which is not always made explicit. In fact, general rate equations for the intrinsic heterogeneity model cannot be obtained without introducing restrictive assumptions[4,6,7] and the following derivations refer to the induced heterogeneity model.

The rate of the reverse reaction is written as:

$$i_{-1} = k_{-1}\,\theta \exp\{-(1-\beta)F\,\phi/RT\} \exp[(1-\alpha)g(\theta)] \qquad (2)$$

When the forward and reverse rates are considerably greater than any subsequent steps involving B, the equilibrium condition is given by $i_1 = i_{-1}$ from which

$$\{\theta/(1-\theta)\} \exp g(\theta) = (k_1/k_{-1})a_A \exp(F\phi/RT) \qquad (3)$$

Although the form of $g(\theta)$ is not always specified, two models are commonly assumed in electrochemical kinetic derivations based on the adsorption isotherm, (3):

(i) free energy of adsorption is independent of coverage, *i.e.*, $g(\theta) = 0$ (Langmuir model);

(ii) free energy of adsorption is linearly dependent on coverage, *i.e.*, $g(\theta) = f\theta$ (Temkin model).

In those cases where $g(\theta) \neq 0$, it has repeatedly been claimed (*e.g.*, refs. 1, 2 and 8) that the effects of the terms θ, $(1-\theta)$ and $\theta/(1-\theta)$ are negligible compared with the exponential terms involving θ, as long as θ is in the range 0.2–0.8. These pre-exponential terms are then ignored and the isotherm is written as:

$$\exp g(\theta) = (k_1/k_{-1})a_A \exp(F\phi/RT) \qquad (4)$$

In view of the fact that $\theta/(1-\theta)$ changes by a factor of 16 over this range of values of θ, it is by no means self-evident that this simplification is justified except at $\theta = 0.5$ in eqn. (3). It is the purpose of this communication to explore the consequences of excluding these pre-exponential terms.

THE ADSORPTION ISOTHERM

We consider the isotherm, (3), derived for reaction I. Rearrangement and differentiation give

$$\frac{d\phi}{d\theta} = \frac{RT}{F}\left[\frac{1}{\theta(1-\theta)} + g'(\theta)\right] \qquad (5)$$

where $g'(\theta)$ is the first derivative of $g(\theta)$. From this

$$\frac{d\theta}{d\phi} = \frac{F}{RT}\left[\frac{\theta(1-\theta)}{1+g'(\theta)\theta(1-\theta)}\right] \qquad (6)$$

Equations of similar form have been derived by HALE AND GREEF[9] with the

difference that these authors reversed the signs of the $g(\theta)$-terms in our eqns. (1) and (2). In other words, positive values of their $g(\theta)$ correspond to an increase in free energy of adsorption with increasing coverage. The significance of this sign reversal on the interpretation of the polynomial expressions proposed for $g(\theta)$ was not discussed by these authors.

For the Temkin model, $g'(\theta) = f$, we have

$$\{\theta/(1-\theta)\} \exp f\theta = (k_1/k_{-1})a_A \exp (F\phi/RT) \tag{7}$$

and

$$\frac{d\theta}{d\phi} = \frac{F}{RT}\left[\frac{\theta(1-\theta)}{1+f\theta(1-\theta)}\right] \tag{8}$$

This expression shows that the isotherm under these conditions is an S-shaped curve although for f-values in the range commonly found for electrochemical processes[2,10,11] ($f \sim 10$) the departure from linearity for intermediate coverages is not great. The slope of the apparently linear portion approximates that given by (8) at $\theta = 0.5$, *viz.*,

$$\frac{d\theta}{d\phi} = \frac{F}{RT}\left(\frac{1}{f+4}\right) \tag{9}$$

The simplified isotherm, (4), for the Temkin model,

$$\exp f\theta = (k_1/k_{-1})a_A \exp (F\phi/RT) \tag{10}$$

gives a slope of

$$\frac{d\theta}{d\phi} = \frac{F}{RT}\cdot\frac{1}{f} \tag{11}$$

This means that, if coverages actually obey (7), analysis ignoring the pre-exponential term (*i.e.*, according to (10)) yields an f-value which is 4 higher than the true value.

By inserting numerical values into eqns. (7) and (10), CONWAY AND GILEADI[12] constructed isotherms which clearly show different slopes for all values of θ and they concluded that in this case the pre-exponential term cannot be neglected although it can be ignored in rate equations. They later derived[1] an expression similar to our eqn. (9) for the maximum adsorption pseudo-capacitance for the quasi-equilibrium case but seem not to have related this result back to the isotherm.

It should be noted that (9) leads to a much better approximation than (10) for the complete isotherm (7) at intermediate coverages, *viz.*,

$$\exp [(f+4)\theta] = (k_1/k_{-1})a_A \exp 2 \exp (F\phi/RT) \tag{12}$$

where f retains its original significance and the term, exp 2, is included so that (7) and (12) are equal at $\theta = \frac{1}{2}$.

TAFEL BEHAVIOUR

This discussion will be restricted to a reaction where the quasi-equilibrium assumption can be applied to reaction I which is followed by a rate-determining combination step

$$B\text{–}M + B\text{–}M \rightarrow C + 2\,M \qquad II$$

The rate of the overall reaction is given by the rate of reaction II which, for activated adsorption, is written as[1]:

$$i_2 = k_2\theta^2 \exp\left[2\alpha g(\theta)\right] \tag{13}$$

Once again, it is usual to disregard the pre-exponential term, θ^2, in treatments where $g(\theta) \neq 0$ and $0.2 < \theta < 0.8$. The exponential term is then substituted from (4) leading to

$$i_2 = (k_1/k_{-1})k_2 a_A \exp\left(2\alpha F\phi/RT\right) \tag{14}$$

for which the Tafel slope is[13]

$$\frac{\mathrm{d}\phi}{\mathrm{d}\ln i_2} = \frac{RT}{2\alpha F} \tag{15}$$

On the other hand, if the θ^2-term is not ignored in (13) and the term $\exp g(\theta)$ substituted from the complete isotherm (3), then

$$i_2 = k_2(k_1 a_A/k_{-1})^{2\alpha}\,\theta^2\{(1-\theta)/\theta\}^{2\alpha} \exp\left(2\alpha F\phi/RT\right) \tag{16}$$

The Tafel slope can be obtained as a function of θ from

$$\frac{\mathrm{d}\ln i}{\mathrm{d}\phi} = \left(\frac{\partial \ln i}{\partial \phi}\right)_\theta + \left(\frac{\partial \ln i}{\partial \theta}\right)_\phi \frac{\mathrm{d}\theta}{\mathrm{d}\phi}$$

which leads to

$$\frac{\mathrm{d}\phi}{\mathrm{d}\ln i_2} = \frac{RT}{2F}\left[\frac{1+\theta(1-\theta)g'(\theta)}{(1-\theta)(1+\alpha\theta g'(\theta))}\right] \tag{17}$$

For the Temkin model

$$\frac{\mathrm{d}\phi}{\mathrm{d}\ln i_2} = \frac{RT}{2F}\left[\frac{1+f\theta(1-\theta)}{(1-\theta)(1+\alpha f\theta)}\right] \tag{18}$$

Comparing (15) with (17) or (18), it is found that the Tafel slopes are equal

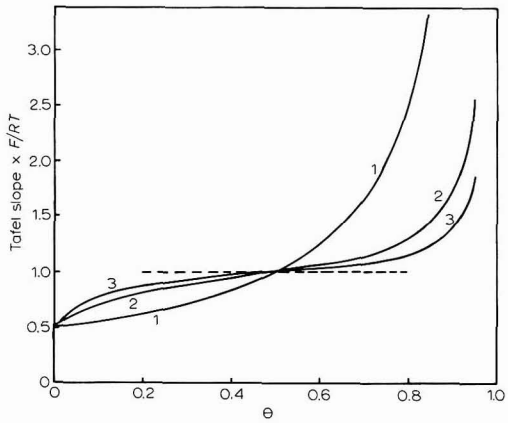

Fig. 1. Variation of Tafel slope with surface coverage under Temkin conditions for $\alpha = 0.5$ and f-values: (1), 0 (Langmuir); (2), 10; (3), 20. Broken line is the Tafel slope calcd. without pre-exponential terms.

only when $\theta = 1-\alpha$, *i.e.*, the effect of neglecting the pre-exponential terms is zero only at this value of θ. Tafel slopes for $\alpha = 0.5$ and $f = 0$ (Langmuir), 10 or 20 are plotted against θ in Fig. 1. It can be seen that the Tafel slope is independent of f at $\theta = 0.5$ (in general, at $\theta = 1-\alpha$). For the usual range of θ considered (0.2–0.8), eqn. (15) is a good approximation of (18) *only* for large values of f; eqn. (15) is the limiting case as $f \to \infty$. For common values of f, the approximation is rather inaccurate, *e.g.*, for $\alpha = 0.5$ and $f = 10$, the slope changes from 0.81 RT/F to 1.30 RT/F between $\theta = 0.2$ and $\theta = 0.8$. Note that the variation between given values of θ depends on both α and f.

REACTION ORDER

For the same mechanism as considered in the previous section, an analogous derivation yields the reaction order

$$\frac{\mathrm{d} \ln i_2}{\mathrm{d} \ln a_A} = 2\left[\frac{(1-\theta)(1+\alpha\theta g'(\theta))}{1+\theta(1-\theta)g'(\theta)}\right] \tag{19}$$

This expression is simply related to (17) as Tafel slope $\times$ reaction order $= RT/F$. Accordingly, for Temkin conditions with $\alpha = 0.5$, the ordinate scale of Fig. 1 is the reciprocal of the reaction order. Therefore, the error involved in neglecting the pre-exponential terms is of the same order as for Tafel slopes.

INDIVIDUAL RATE EQUATIONS

In the foregoing treatments we have considered only steady-state conditions for a particular mechanism. Consideration of the non-steady state by introducing a further variable, *viz.*, time, enables one to examine the individual rate equations for simple adsorption and desorption steps such as given in eqns. (1) and (2). The following treatment will be restricted to an irreversible step

$$\mathrm{A} + \mathrm{M} \rightarrow \mathrm{B\text{–}M} + e \qquad \text{III}$$

i.e., conditions are such that only reaction III contributes to changes in θ. Similarly to the reversible case I, the rate is usually formulated as

$$i_3 = k_3 a_A (1-\theta) \exp(\beta F\phi/RT) \exp -\alpha g(\theta) \tag{20}$$

In order to investigate this relation, it is necessary to change either a_A or ϕ and measure the current passed in approaching the new steady state. The simplest method is to make one of these variables a step function of time so that after the step the current refers to the new constant values of a_A and θ. Both experimental approaches have been used in the past, a_A being varied by rapid addition of reactant[10,14] and ϕ being stepped by suitable programming of a potentiostat[11,15–18]. The initial conditions are usually chosen so that $\theta \to 0$ although the treatment need not be restricted to this case.

As before, we wish to examine the effects of the common assumption that the pre-exponential term $(1-\theta)$ in (20) can be ignored, giving

$$i_3 = k_3 a_A \exp(\beta F\phi/RT) \exp -\alpha g(\theta) \tag{21}$$

For constant a_A and ϕ, eqns. (20) and (21) yield, respectively

$$\frac{\mathrm{d} \ln i_3}{\mathrm{d}\theta} = -\left(\alpha g'(\theta) + \frac{1}{1-\theta}\right) \tag{22}$$

and

$$\frac{\mathrm{d} \ln i_3}{\mathrm{d}\theta} = -\alpha g'(\theta) \tag{23}$$

Since in an actual experiment current will normally be measured directly as a function of time, it is more convenient to derive relationships between these quantities. Current, coverage and time are related by

$$i_3 = \frac{\mathrm{d}q_t}{\mathrm{d}t} = q_m \frac{\mathrm{d}\theta}{\mathrm{d}t}$$

where q_t is the charge passed to time t *via* reaction III and q_m is the charge needed to give $\theta = 1$. Using these relations it has been shown[11,19] that i_3^{-1} is a linear function of time for the particular case where a Temkin model is assumed and the pre-exponential term $(1-\theta)$ ignored:

$$i_3^{-1} = \{k_3 a_A \exp(\beta F\phi/RT)\}^{-1} + \alpha f t/q_m \tag{24}$$

This equation is simply (21) under Temkin conditions expressed in terms of current and time rather than current and coverage. For other cases, an explicit relationship between current and time cannot be derived but slopes of i_3^{-1} *vs.* t plots can be obtained as functions of θ using

$$\frac{\mathrm{d}i^{-1}}{\mathrm{d}t} = \frac{\mathrm{d}i^{-1}}{\mathrm{d}\theta} \cdot \frac{\mathrm{d}\theta}{\mathrm{d}t}$$

These slopes are as follows:

(a) Pre-exponential term included (20),

$$\frac{\mathrm{d}i_3^{-1}}{\mathrm{d}t} = \frac{1}{q_m}\left(\alpha g'(\theta) + \frac{1}{1-\theta}\right) \tag{25}$$

which under Temkin conditions becomes

$$\frac{\mathrm{d}i_3^{-1}}{\mathrm{d}t} = \frac{1}{q_m}\left(\alpha f + \frac{1}{1-\theta}\right) \tag{26}$$

(b) Pre-exponential term excluded (21),

$$\frac{\mathrm{d}i_3^{-1}}{\mathrm{d}t} = \frac{\alpha g'(\theta)}{q_m} \tag{27}$$

which under Temkin conditions is

$$\frac{\mathrm{d}i_3^{-1}}{\mathrm{d}t} = \frac{\alpha f}{q_m} \tag{28}$$

Comparing (22) and (23) with (25) and (27) it can be seen that the slopes of the two kinds of plots are closely related, *viz.*,

$$\frac{\mathrm{d} \ln i_3}{\mathrm{d}\theta} = -q_m \frac{\mathrm{d}i_3^{-1}}{\mathrm{d}t} \tag{29}$$

Therefore, the coverage-dependences of the two slopes will be discussed together.

The variation of slope with coverage is shown in Fig. 2 for $\alpha f=0$, 5 and 10. The case of $\alpha f=0$ corresponds to Langmuir conditions; in general, the slope can be considered as the sum of terms arising from the exponential and pre-exponential terms of (20)**. However, *relative* changes of slope in going from, say, $\theta=0$ to $\theta=0.8$*, and, therefore, the curvature of the ln i_3 *vs.* θ or i_3^{-1} *vs.* t plots, depend markedly on αf. For example, with $\alpha f=5$ it can be seen that the slope changes by a factor of 1.67 between $\theta=0$ and $\theta=0.8$. This curvature should be detectable if measurements are extended to sufficiently high coverages.

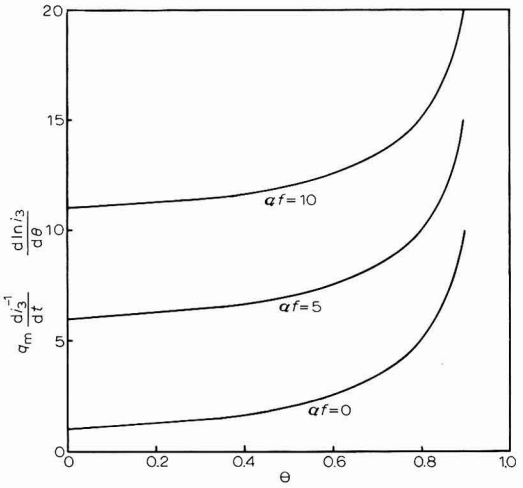

Fig. 2. Coverage-dependence of the slopes of kinetic plots for an irreversible adsorption step with charge transfer.

Even at low coverages, it is important to note that, for reactions obeying (20) under Temkin conditions, the slope approaches $(\alpha f+1)$ and not αf as predicted by the analysis based on neglect of the pre-exponential term.

For the case of desorption,

$$\text{B–M}+e \rightarrow \text{A}+\text{M} \qquad \text{IV}$$

the rate of which is written as

$$i_4=k_4\theta \exp\left[-(1-\beta)F\phi/RT\right] \exp\left[(1-\alpha)g(\theta)\right], \qquad (30)$$

a corresponding analysis gives slopes of the ln i_4 *vs.* θ and i_4^{-1} *vs.* t plots, which have the same form as (22), (23) and (25)–(28) except that the signs are reversed: α is replaced by $1-\alpha$ and the term $1/(1-\theta)$ is replaced by $1/\theta$.

DISCUSSION

The foregoing derivations for the particular mechanisms assumed are sum-

* If one considers 0.2–0.8 as the range of θ for which the pre-exponential term in the isotherm is negligible, then the corresponding range is 0–0.8 for the adsorption and 0.2–1.0 for the desorption steps. GILMAN[19] incorrectly regards eqn. (20) as being inapplicable at low coverages.
** *i.e.*, the shapes of curves in Fig. 2 are independent of αf.

marised in Table 1 for a Temkin model, *i.e.*, $g(\theta)=f\theta$. For the general case, f in these relations is replaced by $g'(\theta)$. The expressions given by (A) including, and (B) neglecting, the pre-exponential terms are seen to approach each other only at large values of f. For values of f commonly found in electrochemistry, *viz.* $f\sim 10$, significant differences between the tabulated slopes exist over the range $0.2<\theta<0.8$ for which it has been claimed repeatedly that the effects of the pre-exponential terms in θ are quite negligible.

TABLE 1

	A *Pre-exponential included*	*B* *Pre-exponential neglected*
Isotherm	$\frac{\mathrm{d}\theta}{\mathrm{d}\phi}=\frac{F}{RT}\left[\frac{\theta(1-\theta)}{1+f\theta(1-\theta)}\right]$	$\frac{F}{fRT}$
Tafel slope	$\frac{\mathrm{d}\phi}{\mathrm{d}\ln i}=\frac{RT}{2F}\left[\frac{1+f\theta(1-\theta)}{(1-\theta)(1+\alpha f\theta)}\right]$	$\frac{RT}{2\alpha F}$
Reaction order	$\frac{\mathrm{d}\ln i}{\mathrm{d}\ln a_{\mathrm{A}}}=\frac{2(1-\theta)(1+\alpha f\theta)}{1+f\theta(1-\theta)}$	2α
Adsorption	$\frac{\mathrm{d}\ln i}{\mathrm{d}\theta}=-\left(\alpha f+\frac{1}{1-\theta}\right)$	$-\alpha f$
	$\frac{\mathrm{d}i^{-1}}{\mathrm{d}t}=\frac{1}{q_{\mathrm{m}}}\left(\alpha f+\frac{1}{1-\theta}\right)$	$\frac{\alpha f}{q_{\mathrm{m}}}$
Desorption	$\frac{\mathrm{d}\ln i}{\mathrm{d}\theta}=(1-\alpha)f+\frac{1}{\theta}$	$(1-\alpha)f$
	$\frac{\mathrm{d}i^{-1}}{\mathrm{d}t}=\frac{-1}{q_{\mathrm{m}}}\left[(1-\alpha)f+\frac{1}{\theta}\right]$	$\frac{-(1-\alpha)f}{q_{\mathrm{m}}}$

For the Tafel slope and reaction order, the slopes from A and B are the same at $\theta=1-\alpha$ and the coverage-dependence of the slope is least in the middle range of coverages (Fig. 1). On the other hand, in the range $0.2<\theta<0.8$ the slopes from A and B can be significantly different, *e.g.*, for $\alpha=0.5$, $f=10$ the Tafel slope from A changes in this range from $\sim 4RT/5F$ to $\sim 4RT/3F$.

In the case of the isotherm, adsorption and desorption plots, not only are the slopes from A dependent on θ but also, even over the range of θ where the curvature of these plots is least, the slopes from A and B are never equal. In fact, in these ranges the f in column B becomes $f+4$ for the isotherm, $f+1/\alpha$ for the adsorption and $f+1/(1-\alpha)$ for the desorption plots in column A. Therefore, the slopes in column B do not yield correct f-values if the system obeys equations involving pre-exponential terms.

It is of interest at this point to compare the intrinsic heterogeneity model with the induced heterogeneity model discussed above. As already noted, general

rate equations cannot be obtained for this model but the isotherm can be derived for a uniformly heterogeneous surface[6,7]. For the usual case of chemisorption from the gas phase, this is written as

$$\theta = f'^{-1} \ln [(1 + A_0 P)/\{1 + A_0 P \exp(-f')\}] \quad (31)$$

where f' is now defined in terms of the rate of change of standard free energy of adsorption between patches, A_0 is the Langmuir adsorption constant for the highest energy patch and P is the pressure. At intermediate coverages and not too small values of f', this isotherm reduces to

$$\theta = f'^{-1} \ln A_0 P \quad (32)$$

an expression commonly known as the logarithmic Temkin isotherm. The electrochemical equivalent of this expression is eqn. (10) which is also the simplified isotherm from the induced heterogeneity model.

The identity of the simplified isotherms from the two models could be taken to imply that the complete isotherms from which they originate are equivalent. That this is not so has already been shown numerically by GILEADI AND CONWAY[1]. The reason is that for usual values of f' and f, the approximation made in the intrinsic heterogeneity model is a good one while the approximation made for the induced heterogeneity model suffers from the defects that we have discussed above. Thus, when the complete equations are considered, the isotherm slopes, $\mathrm{d}\theta/\mathrm{d} \ln P$ at $\theta = 0.5$, are $1/f'$ and $1/(f+4)$ for the intrinsic and induced heterogeneity models, respectively.

We have been able to show that for an induced heterogeneity model, the pre-exponential terms involving θ lead to a significant dependence of electrochemical kinetic relations on coverage. However, it should be pointed out that the use of terms such as θ and $1-\theta$ to represent reactant activities for the adsorbed species and electrode surface is presumably a simplification, and information about the true form of the activity terms is of interest. It is possible that the linearity reported in experimental kinetic plots, both for electrode processes and for chemisorption from the gas phase, could be due to the variation of the true activity with coverage being considerably less than given by the simple linear terms. For example, the empirical Elovich equation[3,4]

$$\frac{\mathrm{d}q}{\mathrm{d}t} = a \exp(-bq)$$

which contains *no* pre-exponential term in coverage* is obeyed in many gas phase chemisorptions[3,4] and in the few electrochemical systems to which it has been applied[10,11,15–18]. Note that electrochemical kinetic studies have the advantage that $\mathrm{d}q/\mathrm{d}t$ (current) is measured directly, whereas in conventional chemisorption studies q is measured as a function of time and the integrated form of the Elovich equation, which contains an adjustable parameter[3,4], must be applied. This introduces difficulties in assessing the effects of inserting a coverage-dependent pre-exponential term into the Elovich equation.

We suggest, therefore, that coverage-dependent pre-exponential terms should

* This form of equation has been derived[6] as an approximate solution for the case of a uniformly heterogeneous surface at intermediate coverages. Equation (21) under Temkin conditions is the electrochemical analogue of the Elovich equation.

not be summarily dismissed in electrochemical kinetic derivations since, in principle, information about the actual form of such terms can be obtained from accurate electrochemical measurements.

SUMMARY

The consequences of excluding coverage-dependent pre-exponential terms from rate equations involving chemisorbed species are examined. Expressions are derived for: (1) the slope of the isotherm for a reversible adsorption step with charge transfer, (2) the Tafel slope and reaction order when such a step is followed by a rate-determining combination step, and (3) the slopes of kinetic plots for irreversible adsorption steps with charge transfer. Comparisons are made between the expressions obtained including and neglecting the pre-exponential terms. It is shown that significant differences between these expressions can exist in the range of coverages where it is commonly assumed that the pre-exponential terms can be ignored.

REFERENCES

1 E. GILEADI AND B. E. CONWAY, *Modern Aspects of Electrochemistry*, No. 3, edited by J. O'M. BOCKRIS AND B. E. CONWAY, Butterworths, London, 1964, chap. 5.
2 B. E. CONWAY, *Theory and Principles of Electrode Processes*, Ronald, New York, 1965, chap. 6.
3 G. C. BOND, *Catalysis by Metals*, Academic Press, London, 1962.
4 D. O. HAYWARD AND B. M. W. TRAPNELL, *Chemisorption*, Butterworths, London, 1964.
5 M. BOUDART, *J. Am. Chem. Soc.*, 72 (1952) 3556.
6 M. I. TEMKIN, *Zh. Fiz. Khim.*, 15 (1941) 296.
7 S. BRUNAUER, K. S. LOVE AND R. G. KEENAN, *J. Am. Chem. Soc.*, 64 (1942) 751.
8 S. SRINIVASAN, H. WROBLOWA AND J. O'M. BOCKRIS, *Advan. Catalysis*, (1967) 352–418.
9 J. M. HALE AND R. GREEF, *Electrochim. Acta*, 12 (1967) 1409.
10 V. S. BAGOTSKY AND YU. B. VASSILIEV, *Electrochim. Acta*, 11 (1966) 1439.
11 T. BIEGLER AND D. F. A. KOCH, *J. Electrochem. Soc.*, 114 (1967) 904.
12 B. E. CONWAY AND E. GILEADI, *Trans. Faraday Soc.*, 58 (1962) 2493.
13 R. PARSONS, *Trans. Faraday Soc.*, (1958) 1053.
14 M. W. BREITER, *Electrochim. Acta*, 10 (1965) 503.
15 S. GILMAN, *Electrochim. Acta*, 9 (1964) 1025.
16 S. S. BESKOROVAINAYA, YU. B. VASIL'EV AND V. S. BAGOTSKII, *Elektrokhimiya*, 1 (1965) 1029.
17 J. WEBER, YU. B. VASIL'EV AND V. S. BAGOTSKII, *Elektrokhimiya*, 2 (1966) 515.
18 S. TRASATTI AND L. FORMARO, *J. Electroanal. Chem.*, 17 (1968) 343.
19 S. GILMAN, *Electroanalytical Chemistry*, Vol. 2, edited by A. J. BARD, Arnold, London, 1967, p. 159.

ELECTROANALYTICAL CHEMISTRY AND INTERFACIAL ELECTROCHEMISTRY
Elsevier Sequoia S.A., Lausanne – Printed in The Netherlands

DETERMINATION OF THE CHARGE ON THE REACTING SPECIES IN THE ELECTROREDUCTION OF ANIONS

W. R. FAWCETT, J. E. KENT AND Y. C. KUO LEE
Department of Chemistry, University of Guelph, Guelph, Ontario (Canada)
(Received September 23rd, 1968)

INTRODUCTION

In studies of the kinetics and mechanism of the reduction of anions at an electrode, it is generally considered necessary to determine the charge, z, on the species being reduced[1]. GIERST[2] has devised a method of determining z which is based on consideration of the rate of reaction k, and outer Helmholtz plane potential, ϕ_2, as functions of both electrode potential, ϕ_m, and base electrolyte concentration. It was pointed out by FRUMKIN *et al.*[3] that this method involves assumptions about the structure of the double layer and about the position of the reacting particle with respect to the outer Helmholtz plane. They proposed an alternative method in which z is determined from the dependence of the reaction rate on the base electrolyte concentration for constant charge density on the electrode; however, the method is only applicable to data obtained far from the electrocapillary maximum where the electrode charge density is high. In both the above methods, reaction rates are compared at different base electrolyte concentrations, so that it is assumed that the concentration of the reducible species and the reaction mechanism do not change with ionic strength. In this paper a simple differential method for determining z from kinetic data at a single base electrolyte concentration is described; the results of its application to data for the reduction of peroxydisulphate and periodate anions are presented.

THEORY

When electron transfer is the rate-determining step in an electrode reaction, and the reacting particle is at the outer Helmholtz plane (O.H.P.) in the transition state, then the reaction rate with consideration of the double layer effect is given by the Frumkin equation,

$$(\ln k)/f = (\ln k_0)/f + (\alpha n - z)(\phi_2 - \phi_2^\circ) - \alpha n \phi_m \qquad (1)$$

α is the transfer coefficient, n the number of electrons involved in the reduction, k_0 and ϕ_2°, the values of k and ϕ_2 for $\phi_m = 0$ (potential of the electrocapillary maximum (e.c.m.) in a non-specifically adsorbed electrolyte on the rational scale), and $f = F/RT$. If the particle is in the inner layer in the transition state, αn is replaced by $\alpha n - \lambda(\alpha n - z)$ where λ is the ratio of the distance between the O.H.P. and the centre of the particle, to the distance between the O.H.P. and the electrode[3]. The latter

equation is only valid in the absence of specific adsorption at the electrode when it is assumed, to a first approximation, that the potential drop in the inner layer is a linear function of distance.

The kinetic equations with inclusion of the double layer effect for the case that the slow step is a preceding chemical reaction have been given by MATSUDA[4]. Two types of reaction are considered for the reduction of anions at potentials cathodic of the e.c.m. In the reaction,

$$A \rightleftharpoons O + X \tag{2}$$

anion, A, with charge, z_A, dissociates to give the reducible anion, O, which has a lower charge, z_0, and a non-reducible anion, X. When the thickness of the reaction layer is much less than that of the diffuse double layer the rate of charge transfer in a simple 1–1 electrolyte is given by

$$(\ln k)/f = (\ln k_0)/f - \tfrac{1}{2}(z_A + z_0)\phi_2 \tag{3}$$

The second type of reaction

$$B + Y \rightleftharpoons O \tag{4}$$

is one of association of anion, B, with cation, Y, to give the reducible anion, O. The rate of charge transfer for the same conditions is

$$(\ln k)/f = (\ln k_0)/f - z_0\phi_2 \tag{5}$$

For both reactions, when the thickness of the reaction layer is much greater than that of the diffuse layer, the rate is not affected by the double layer. For intermediate situations, the rate expressions are complex.

If the above expressions are to be used in the determination of z, then a model for the diffuse double layer must be chosen. The simplest, and that commonly used, is the Gouy–Chapman model from which ϕ_2 in a simple 1–1 electrolyte which is not specifically adsorbed is related to the charge on the electrode by the equation,

$$q_m = 2(RT\varepsilon_0 C_0/2\pi)^{\frac{1}{2}} \sinh(\tfrac{1}{2}f\phi_2) \tag{6}$$

Here, q_m is the electrode charge density, ε_0 the dielectric constant of the pure solvent, and C_0 the concentration of the electrolyte. More recently, HURWITZ *et al.*[5] have presented a more detailed model in which the effects of polarization of the system by the ions, ionic electrostriction and specific molar volume, dielectric saturation of the solvent, and the stabilizing influence of the ionic atmospheres, are considered. The relation between q_m and ϕ_2 for the same type of electrolyte is:

$$q_m^2 = (2RT\varepsilon_0 C_0/\pi) \sinh^2(\tfrac{1}{2}f\phi_2) - (RTC_0/2\pi)[I_1 + I_2] \tag{7}$$

where

$$I_1 = \int_0^{f\phi_2} 2(\varepsilon_0 - \varepsilon) \sinh y \, dy$$

and

$$I_2 = \int_0^{f\phi_2} \varepsilon(e^{-y}\Delta_+ - e^{y}\Delta_-)dy$$

ε, Δ_+ and Δ_- are functions of y at a given electrolyte concentration and include constants for the specific ions and solvent related to the electrostriction effect, ionic

volume, and the effect of ionic strength on the dielectric constant. By calculating ϕ_2 from both models, the influence of the choice of model on the charge determination may be ascertained.

The technique of data analysis described here makes use of the method of finite differences. ϕ_m, ϕ_2, $\phi_2-\phi_m$, and ln k/f are tabulated for equal increments in ϕ_m. First differences between adjacent values of each quantity are then calculated. From eqns. (1), (3) and (5), the relationship between first differences may be generalized as follows:

$$\Delta\{(\ln k)/f\}=\zeta\Delta\phi_2+\beta\Delta(\phi_2-\phi_m) \quad (8)$$

ζ is a constant related to the charge on the species involved in the electron transfer step. β is equal to αn or $\alpha n-\lambda(\alpha n-z)$ when charge transfer is the slow step; otherwise it is zero.

When ζ and β remain constant over the potential range considered, a plot of

$$\Delta\{(\ln k)/f\}/\Delta(\phi_2-\phi_m) \textit{ vs. } \Delta\phi_2/\Delta(\phi_2-\phi_m)$$

yields a straight line with slope, ζ and intercept on the ordinate, β. Thus, the charge may be determined from kinetic data at constant base electrolyte concentration.

There are at least two cases where the above plot will not be linear. If the position of the anion with respect to the O.H.P. in the transition state changes with potential, then λ, and thus β, will change with ϕ_m. A non-linear plot is also expected if the reduction mechanism is complex. For anions it is quite possible that parallel reaction pathways exist, one path involving direct reduction of the anion, and the other reduction of an anion of lower charge formed by a preceding chemical reaction (eqns. (2) and (4)). The current resulting from the first path will predominate at low values of ϕ_2 and that due to the second at high values. Thus, the slope of the differential plot should be linear in the region where either mechanism is predominant.

EXPERIMENTAL

The reduction reactions were studied at a dropping mercury electrode the potential of which with respect to a saturated calomel reference electrode was controlled by an operational amplifier (Philbrick P25AU), the counter electrode being a coil of Pt wire[6]. The current was recorded on a Radiometer PO4 Polariter which also supplied a slow linear voltage ramp. The three electrodes were fitted into a simple all-glass cell *via* ground glass joints so that when they were in place, the contents were isolated from the atmosphere. Dropping mercury electrodes were prepared by drawing fine capillaries from 1-mm Pyrex capillary tubing; their characteristics were typically, $m=0.6$ mg sec^{-1}, $t=4$ sec for a mercury reservoir height of 80 cm. For flow rates above 1 mg sec^{-1}, polarographic maxima of the second kind[7] were observed. The junction between the SCE and the solution was made in a ground-glass joint.

Aqueous sodium hydroxide and sodium hydroxide–sodium fluoride solutions in the concentration range, 0.01–0.2 M, were used as base electrolytes, the depolarizer concentration being $5\cdot10^{-4}$ M. Equilibrium water prepared by distilling deionized water from alkaline permanganate was used in all operations. AnalaR-grade sodium hydroxide pellets were washed in a stream of water to dissolve the outer carbonate-

contaminated layers and then used directly to prepare a concentrated solution; solutions of required concentration were prepared by accurate dilution of the above solution after its concentration had been determined by titration. AnalaR-grade sodium fluoride was recrystallized from equilibrium water in Pt vessels. The depolarizers, sodium periodate and potassium peroxydisulphate were also of AnalaR-grade and were used without further purification. Mercury was purified by double distillation *in vacuo*.

Prior to all measurements, the solutions were degassed for 15 min with purified N_2. After recording the current voltage curves, drop times were measured at 100-mV intervals. The flow rate of mercury was found by collecting a sample of mercury in a glass cup in the cell for an accurately known period of time. In addition to determining the charging current curve in the various base electrolyte solutions, the potential of the electrocapillary maximum was measured with respect to the SCE using a streaming mercury electrode[8]. All measurements were carried out with the cell in a water bath thermostatted to $25.0 \pm 0.1°$.

RESULTS AND DISCUSSION

The rate of charge transfer was calculated from the measured current and drop time at 50-mV intervals using Koutecký's theory for irreversible electrode processes[9] with inclusion of the corrections for electrode sphericity in the determination of the diffusion coefficient from the diffusion limited current[10] and in the calculation of the function, χ[11]. The necessary double layer data, namely values of q_m as a function of ϕ_m, were obtained from PAYNE'S capacity data for NaOH[12] and GRAHAME'S data for NaF as tabulated by RUSSELL[13]. It was noted that q_m *vs.* ϕ_m plots for these two electrolytes at the same concentration were virtually superimposable at potentials cathodic of the e.c.m.; thus, q_m *vs.* ϕ_m values for mixed base electrolytes were taken from either source. Values of ϕ_2 were estimated according to the Gouy–Chapman theory and, in the case of NaOH, from the revised theory of HURWITZ *et al.* The necessary constants required in the latter case were taken from ref. 5. Both this calculation and the Koutecky calculation were carried out on a digital computer*.

The differential plot of kinetic data for the reduction of peroxydisulphate in NaOH is shown in Fig. 1. Its slope increases continuously as ϕ_m becomes more cathodic, but is approximately constant with a value of 2 for potentials close to the e.c.m. The shape of the plot is not substantially changed when ϕ_2 is calculated by the revised diffuse layer theory. It does not seem reasonable to attribute the increase in slope to an increase in particle charge, but it can be attributed to a change in β (*i.e.*, λ) with potential. One process which could account for this change is contraction of the inner layer due to electrostriction[14]. Thus, if the equilibrium position of the particle in the transition state is in the inner layer, its average distance to the O.H.P. decreases with cathodic increase in ϕ_m. This would also explain the non-linearity of the corrected Tafel plots for reduction of peroxydisulphate[3]. FRUMKIN and co-workers attributed the non-linearity to specific adsorption of the reacting particle at low cathodic potentials. This does not seem to be substantiated by the present method of examining the data, since, if the peroxydisulphate is specifically adsorbed

* Copies of the Fortran IV Programmes used for these calculations may be obtained from the authors.

to an appreciable extent, an approximately linear region in the differential plot would not be expected because of the change in the amount adsorbed with potential. The above workers found that the charge on the anion was -2 at high cathodic potentials; this result is confirmed here for low potentials as well. It is noted that the model used to calculate the O.H.P. potential is not important in the determination of z, at least in the potential range considered.

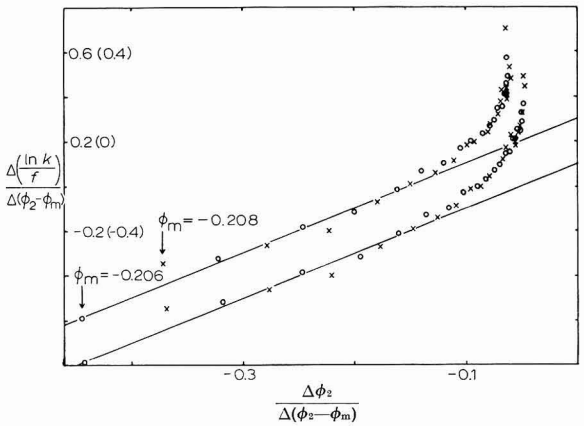

Fig. 1. Differential plot of kinetic data for the reduction of $5 \cdot 10^{-4}$ M peroxydisulphate anion on mercury with 0.01 M (×) and 0.02 M (O) NaOH as base electrolytes. Outer Helmholtz plane potential, φ_2, calcd. by the Gouy–Chapman theory in the lower curve, and by the revised theory of HURWITZ *et al.* in the upper (ordinate scale in brackets).

The periodate system is more complicated in that this anion is involved in several types of equilibria in aqueous solution[15–17]. In the pH range, 11–14, the most important equilibria are:

$$H_3IO_6^{2-} + OH^- \rightleftharpoons H_2IO_6^{3-} + H_2O \qquad (9)$$

and

$$2\,H_3IO_6^{2-} \rightleftharpoons I_2O_9^{4-} + 3\,H_2O \qquad (10)$$

Thus, the charge on the predominate species in solution will vary with pH; some variation with ionic strength is also expected, especially since the equilibria involve highly charged ions. In order that results could be examined at constant ionic strength with varying pH, and at constant pH with varying ionic strength, kinetic data were obtained using aqueous sodium hydroxide–sodium fluoride solutions as base electrolyte. The differential plot of data obtained at an ionic strength of 0.1 M is shown in Fig. 2. It is obvious that electron transfer is the rate-controlling step and that the charge on the species being reduced is -2. In a similar study of this system, LAMY[18] concluded that the charge was -1 by examining the dependence of $\ln k/f$ on ϕ_2 at constant ϕ_m for kinetic data obtained at constant pH (12) and varying ionic strength ($\mu = 0.01$–0.8 M). Differentiated data for these conditions are presented in Fig. 3. At ionic strengths of 0.01 and 0.02 M, the slope of the plot indicates that the charge on the species being reduced is -1 whereas at higher ionic strengths, the charge is -2. This is interpreted as evidence that periodate is reduced by parallel reaction mechanisms, one involving direct reduction of the divalent species, $H_3IO_6^{2-}$,

and the other involving reduction of the monovalent ion, $H_4IO_6^-$, produced from $H_3IO_6^{2-}$ in a preceding protonation reaction. At low ionic strength where ϕ_2 is more negative, the effect of the double layer is such that the current due to reduction of the monovalent ion is much greater than that due to reduction of the divalent form, whereas at higher ionic strength and smaller values of ϕ_2, the opposite is true. It is also noted that the slopes of the differential plots in the region where $\Delta\phi_2/\Delta(\phi_2-\phi_m)$ equals -0.1 are lower in the periodate system than in the peroxydisulphate system. This is probably due to the fact that the contribution to the total current from reduction of the monovalent form becomes more important as ϕ_2 and ϕ_m increase cathodically. Since the predominant mechanism changes with ionic strength and

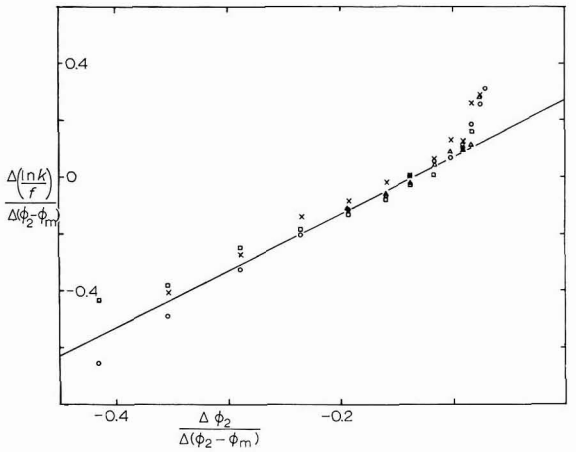

Fig. 2. Differential plot of kinetic data for the reduction of $5\cdot10^{-4}$ M periodate anion on mercury at constant ionic strength with varying pH: (△), 0.001 M NaOH + 0.099 M NaF; (×), 0.01 M NaOH + 0.09 M NaF; (○), 0.1 M NaOH; (□), LAMY's data for 0.01 M NaOH + 0.1 M NaF.

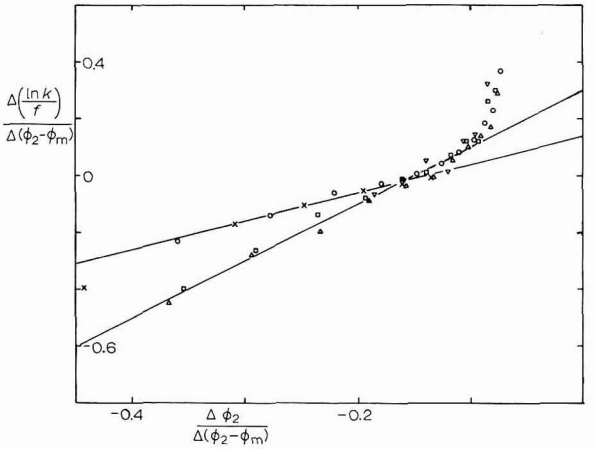

Fig. 3. Differential plot of kinetic data for the reduction of $5\cdot10^{-4}$ M periodate anion on mercury at constant pH with varying ionic strength: (×), 0.01 M NaOH; (○), 0.01 M NaOH + 0.01 M NaF; (△), 0.01 M NaOH + 0.04 M NaF; (□), 0.01 M NaOH + 0.09 M NaF; (▽), 0.01 M NaOH + 0.19 M NaF.

potential, the method of determining charge used by LAMY is not valid in this case. Further details of the kinetics of periodate reduction in basic media will be published elsewhere[19].

ACKNOWLEDGEMENTS

The authors wish to express their gratitude to the National Research Council of Canada for financial support and to the Institute of Computer Science of the University of Guelph for use of their facilities.

SUMMARY

A simple differential method for determining the charge on the reacting species from kinetic data for the reduction of anions at an electrode is described. Data for the reduction of peroxydisulphate and periodate anions are examined by this technique. It is found that the charge on the peroxydisulphate anion is -2, in agreement with the conclusion of FRUMKIN and co-workers based on a different method. The reduction of periodate anion follows a complex mechanism with the charge on the reacting species dependent on ionic strength at high pH.

REFERENCES

1 L. GIERST, L. VANDENBERGHEN, E. NICOLAS AND A. FRABONI, *J. Electrochem. Soc.*, 113 (1966) 1025.
2 L. GIERST, *Transactions Symposium on Electrode Processes, Philadelphia, 1959*, edited by E. YEAGER, Wiley, New York, 1961, p. 109.
3 A. N. FRUMKIN, O. A. PETRY AND N. V. NIKOLAEVA-FEDOROVICH, *Electrochim. Acta*, 8 (1963) 177.
4 H. MATSUDA, *J. Phys. Chem.*, 64 (1960) 336.
5 H. D. HURWITZ, A. SANFELD AND A. STEINCHEN-SANFELD, *Electrochim. Acta*, 9 (1964) 929.
6 W. M. SCHWARZ AND I. SHAIN, *Anal. Chem.*, 35 (1963) 1770.
7 J. HEYROVSKÝ AND J. KŮTA, *Principles of Polarography*, Academic Press, New York, 1966, p. 450.
8 D. C. GRAHAME, E. M. COFFIN, J. I. CUMMINGS AND M. A. POTH, *J. Am. Chem. Soc.*, 74 (1952) 1207.
9 J. HEYROVSKÝ AND J. KŮTA, *Principles of Polarography*, Academic Press, New York, 1966, p. 209.
10 J. HEYROVSKÝ AND J. KŮTA, *Principles of Polarography*, Academic Press, New York, 1966, p. 91.
11 J. KOUTECKÝ AND J. ČIŽEK, *Collection Czech. Chem. Commun.*, 21 (1956) 836.
12 R. PAYNE, *J. Electroanal. Chem.*, 7 (1964) 343.
13 C. D. RUSSELL, *J. Electroanal. Chem.*, 6 (1963) 486.
14 J. R. MACDONALD, *J. Chem. Phys.*, 22 (1954) 1857.
15 C. E. CROUTHAMEL, H. V. MEEK, D. S. MARTIN AND C. V. BANKS, *J. Am. Chem. Soc.*, 71 (1949) 3031.
16 P. SOUCHAY AND A. HESSABY, *Bull. Soc. Chim. France*, (1953) 599.
17 G. J. BUIST AND J. D. LEWIS, *Chem. Commun. (London)*, (1965) 66.
18 F. LAMY, Mémoire de Licence, Université Libre de Bruxelles, 1962.
19 W. R. FAWCETT AND Y. C. KUO LEE, *Can. J. Chem.*, in preparation.

ELECTROANALYTICAL CHEMISTRY AND INTERFACIAL ELECTROCHEMISTRY
Elsevier Sequoia S.A., Lausanne – Printed in The Netherlands

POLAROGRAPHISCHE UNTERSUCHUNGEN BEI REGULIERUNG DER TROPFZEIT DURCH ABSCHLAGEN DES TROPFENS

III. DER EINFLUSS GRENZFLÄCHENAKTIVER STOFFE AUF DIE KINETIK DER ELEKTRODENREAKTION

J. SIMÃO*, D. WOLF UND M. VON STACKELBERG
*Institut für Physikalische Chemie der Universität Bonn (Deutschland)***
(Eingegangen am 30 August 1968)

THEORETISCHE GRUNDLAGEN

Für die Stromdichte, i, einer irreversiblen elektrochemischen Durchtrittsreaktion gilt, wenn wir die für Reduktionsreaktionen übliche Schreibweise benutzen

$$i = -nFCk_0 \cdot \exp[-(1-\alpha)nFE/RT]$$

Der Durchtrittsfaktor, α, ergibt sich aus der Abhängigkeit der Stromdichte, i, vom Potential, E, der Elektrode. Beim Elektrodenpotential $E=0$, wofür wir hier das Potential der Wasserstoffnormalelektrode einsetzen, ist $i=-nFCk_0$. Die Geschwindigkeitskonstante, k_0, ergibt sich also, wenn die Konzentration C des reduzierbaren Stoffes an der Elektrodenoberfläche bekannt ist. Unsere Untersuchungen betreffen die Frage der Bestimmung von k_0 und α mit der Quecksilbertropfelektrode. Bei dieser lassen sich Angaben über C machen, wobei allerdings Schwierigkeiten infolge der Beweglichkeit der Elektrodenoberfläche auftreten.

Nach KOUTECKÝ[2] gilt mit guter Näherung***

$$I = I_d(K\sqrt{\vartheta})/(1+K\sqrt{\vartheta})$$

mit

$$K = 0.886\, D^{-\frac{1}{2}}k_0 \exp\left[-(1-\alpha)\frac{nFE}{RT}\right] = \frac{I\sqrt{\vartheta}}{I_d - I} \qquad (1)$$

Hierbei ist I die über die Tropfzeit, ϑ, gemittelte Stromstärke. $I_d = 607\, nCD^{\frac{1}{2}}m^{\frac{2}{3}}\vartheta^{\frac{1}{6}}$ ist also die über ϑ gemittelte diffusionsbedingte Grenzstromstärke nach ILKOVIČ. Die hier angegebene vereinfachte Form der Gl. (1) von KOUTECKÝ gilt, wenn die Gegenreaktion (die Rückoxydation des Reduktionsproduktes) vernachlässigt werden kann, also bei genügend negativen Potentialen gemessen wird. Andererseits muss man I beim Anstieg der polarographischen Stufe messen. Diese muss also negativer liegen als das reversible Redoxpotential. Die Reduktionsreaktion muss also irreversibel sein.

---

* Universität Coimbra, Portugal.
** Aus der Dissertation, Bonn, 1966 von JOÃO SIMÃO.
*** Bei einer exakten theoretischen Analyse zeigt sich nach KOUTECKÝ[2], dass der Faktor 0.886 in Gl. (1) nicht konstant ist. In dem bei unseren Versuchen vorkommenden Bereich von I/I_d = 0.20–0.78 steigt der Faktor von f = 0.836 auf 0.933. Die Variation von f könnte in Gl. (2) und den Abb. 4–6 entsprechenden Darstellungen dadurch berücksichtigt werden, dass man $K'f$ anstelle von K einsetzt mit $K' = D^{-\frac{1}{2}}k_0 \exp[-(1-\alpha)\, nFE/RT]$

Dividieren wir Zähler und Nenner des bei Gl. (1) gegebenen Ausdrucks für K durch $\vartheta^{\frac{1}{6}}$, so ergibt sich

$$K=(I/\vartheta^{\frac{2}{3}})/\{(I_d-I)/\vartheta^{\frac{1}{6}}\} \tag{2}$$

Eine Umformung ergibt

$$I/\vartheta^{\frac{1}{6}}=I_d/\vartheta^{\frac{1}{6}}-(1/K)I/\vartheta^{\frac{2}{3}};\quad y=y_0-(1/K)x \tag{2a}$$

Da $I_d/\vartheta^{\frac{1}{6}}$ nach der Ilkovič-Gleichung eine von der Tropfzeit unabhängige, experimentell bestimmbare Grösse(y_0) ist, so ergibt sich

$$K=x/(y_0-y)=-\mathrm{d}(I/\vartheta^{\frac{2}{3}})/\mathrm{d}(I/\vartheta^{\frac{1}{6}}) \tag{2b}$$

Bei Variation der Tropfzeit, ϑ, mit einer Abklopfvorrichtung, also bei konstantem m und E ergibt also eine Auftragung von $I/\vartheta^{\frac{1}{6}}$ gegen $I/\vartheta^{\frac{2}{3}}$ Gerade, deren Neigung $1/K$ entsprechen sollte. Bei bekanntem α liesse sich dann nach Gl. (1) auch k_0 bestimmen, wenn keine Störungen vorliegen.

Eine erhebliche Störung tritt durch den "Spüleffekt" auf: Das der Elektrode zuströmende Quecksilber verursacht eine tangentiale Bewegung der Tropfenoberfläche, die den Antransport des Depolarisators durch Konvektion beschleunigt und die Stromstärke erhöht. Zusatz eines Maximadämpfers zu der Lösung ist daher unerlässlich. Dann hängt aber k_0 von der Belegungsdichte des Dämpfers auf der Tropfenoberfläche ab. Und die Belegungsdichte hängt von der Tropfzeit und vom Potential ab. Man muss daher eine kleine aber ausreichende Dämpferkonzentration finden. Hierfür hat sich die Tropfelektrode als geeignet erwiesen.

Ferner ist bereits von WOLF[1] festgestellt worden, dass die Quecksilberausflussgeschwindigkeit m (und damit auch I_d) von der Tropfzeit abhängt, da bei kurzen Tropfzeiten der im Zeitmittel grössere Rückdruck den Ausfluss verlangsamt. Diese Störung ist nicht erheblich und kann durch Messungen von m eliminiert werden. Im Bereich $\vartheta=0.18$–1 sec nimmt m in Gegenwart von Dämpfern um etwa 3% zu, wodurch i_d und tg φ (hierzu Abb. 1) um etwa 2% vergrössert werden. Von den aus Abb. 1 ermittelten tg φ-Werten wären daher etwa 2%, d.h. etwa 0.003 abzuziehen.

EXPERIMENTELLE ANGABEN

Als Abklopfvorrichtung wurde der Rapidpolarographiestand E 354 der Firma Metrohm AG, Herisau, Schweiz, benutzt. Das Instrument ermöglichte die Einstellung der 6 Tropfzeiten von 1.00, 0.53, 0.33, 0.28, 0.21 und 0.18 sec.

Ohne Abklopfen betrug die Tropfzeit der Kapillare mit 52 μ Öffnungsdurchmesser bei 70 cm Hg-Druck etwa 5.0 sec. Die ausfliessende Quecksilbermenge betrug $m=1.37$ mg/sec, bei stark abgekürzten Tropfzeiten wegen des erhöhten mittleren Rückdruckes etwas weniger (vgl. WOLF[1]).

Das Potential der Tropfelektrode wurde gegen eine Ag/AgCl-Elektrode gemessen. Die nachfolgenden Angaben sind aber auf das Potential gegen eine n-Wasserstoffelektrode (0.23 V positiver) umgerechnet. Die Temperatur der Messlösung (stets entlüftet) betrug $25\pm0.1°$.

Untersucht wurden die Reduktionen $H^+/\frac{1}{2}\,H_2$, Cr^{3+}/Cr^{2+}, Zn^{2+}/Zn und zwar in Lösungen folgender Zusammensetzung:

1. H^+: $1.25 \cdot 10^{-3}$ *M* H_2SO_4 in 0.5 *M* KCl (H^+-Konzentration $= 2.5 \cdot 10^{-3}$ *M*).

2. Cr^{3+}: $2 \cdot 10^{-3}$ *M* Cr(III) in 1 *M* KCl–0.02 *M* HCl.

Die Vorratslösung wurde mit dem grünen Salz $[Cr(H_2O)_4Cl_2]Cl$ hergestellt, jedoch zeigte der Umschlag in die violette Farbe bereits nach einem Tage die Umwandlung des Chlorokomplexes in den Aquokomplex $[Cr(H_2O)_6]^{3+}$ an.

3. Zn^{2+}: $1 \cdot 10^{-3}$ *M* $ZnSO_4$ in 1 *M* NH_4Cl–1 *M* NH_3.

Die Messung der Reduktionsstromstärken erfolgte stets gegen die Stromstärke einer depolarisatorfreien Leitsalzlösung. Die Konzentrationen aller Leitsalzlösungen sind genügend hoch, um eine Berücksichtigung des ψ_1-Potentials überflüssig zu machen. Auch ist das durch Grenzflächenspannungs-Unterschiede bedingte "Maximum erster Art" bereits weitgehend unterdrückt. Jedoch ist der "Spüleffekt", d.h. die Stromstärkeerhöhung infolge der durch den Hg-Zufluss in den Tropfen bedingten Grenzflächenbewegung, durch die gute Leitfähigkeit der Lösung sehr begünstigt. Daher ist ein Zusatz von Maximadämpfern unerlässlich.

Als Dämpfer wurden benutzt:

1. Triton X-305 der Firma Rohm und Haas Co., Philadelphia: *Iso*-octylphenoxypolyäthoxyäthanol mit einer Kette von im Mittel 30.5 Äthoxygruppen, Molgewicht also 1550.

2. Polyglykol 10000 $HO\text{-}(CH_2\text{–}CH_2\text{–}O\text{–})_nH$ mit etwa 220 Äthoxygruppen, Molgewicht etwa 10000.

3. Gelatine.

ERGEBNISSE

1. *Einfluss von Dämpferzusätzten auf den polarographischen Grenzstrom*

Abbildung 1 zeigt den Einfluss von Dämpferzusätzen auf den polarographischen Diffusionsgrenzstrom, I_d, bei der Cr^{3+}- und H^+-Reduktion bei Variation der Tropfzeit, ϑ. Aufgetragen ist log I_d gegen log ϑ. Nach der Gleichung von Ilkovič ist I_d proportional $\vartheta^{\frac{1}{6}} = \vartheta^{0.167}$. Hiernach sollte in Abb. 1 die Neigung der Geraden tg $\varphi = 0.167$ betragen. Berücksichtigen wir die Verbesserung durch Koutecký:

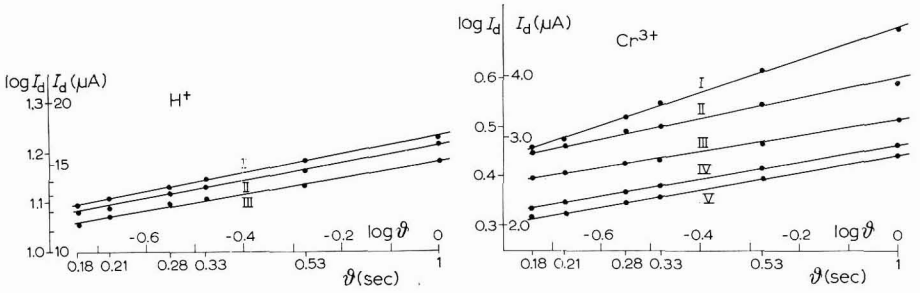

Abb. 1. Abhängigkeit des Grenzstromes, I_d, von der Tropfzeit, ϑ: log I_d als Funktion von log ϑ.
Links für H^+-Reduktion ($1.25 \cdot 10^{-3}$ *M* H_2SO_4–0.5 *M* KCl) (I), ohne Zusatz, tg φ = d log I_d/d log $\vartheta = 0.18$; (II), mit $1.0 \cdot 10^{-3}$% Triton, tg $\varphi = 0.17$; (III), mit $2.7 \cdot 10^{-3}$% Triton, tg $\varphi = 0.16$.
Rechts für Cr^{3+}-Reduktion ($2 \cdot 10^{-3}$ *M* Cr^{3+}–0.02 *M* HCl–1 *M* KCl). (I), mit Aktivkohle gereinigte Grundlösung, tg $\varphi = 0.32$; (II), mit $0.88 \cdot 10^{-3}$% Gelatine, tg $\varphi = 0.20$; (III), mit $3.3 \cdot 10^{-3}$% Gelatine, tg $\varphi = 0.16$; (IV), mit $0.4 \cdot 10^{-3}$% Triton, tg $\varphi = 0.18$; (V), mit $1.2 \cdot 10^{-3}$% Triton, tg $\varphi = 0.18$.

$$I_d = 607\, nCD^{\frac{1}{2}} m^{\frac{2}{3}} \vartheta^{\frac{1}{6}} (1 + 34\, D^{\frac{1}{2}} m^{-\frac{1}{3}} \vartheta^{\frac{1}{6}})$$

so wird

$$\operatorname{tg} \varphi = 0.1667 + 5.7 D^{\frac{1}{2}} m^{-\frac{1}{3}} \vartheta^{\frac{1}{6}}.$$

Mit $m^{-\frac{1}{3}} = 0.90$ erhält man im Bereich $\vartheta = 0.18$–1.0 sec:

für Cr^{3+} $(D = 4 \cdot 10^{-6})$: $\operatorname{tg} \varphi = 0.176$

für H^+ $(D = 60 \cdot 10^{-6})$: $\operatorname{tg} \varphi = 0.202$

Bei der H^+-Reduktion ist infolge der Dicke der Diffusionsschicht der Verarmungseffekt sehr gross, insbesondere bei grösseren ϑ. Daher ist tg φ nach Abb. 1 erheblich kleiner als hier berechnet.

Die hohe Lage und Steilheit der obersten Cr^{3+}-Kurve in Abb. 1 zeigt, dass bei der mit Aktivkohle gereinigten Lösung ein Rühreffekt auftritt. Merkwürdigerweise ist die Stromstärke bei langen Tropfzeiten besonders stark erhöht (tg $\vartheta = 0.32$!). Der Spüleffekt durch den Quecksilberzufluss sollte bei kleinen Tropfen, also bei kurzer Tropfzeit, besonders wirksam sein. Dies hat WOLF[1] bei der Cd^{2+}-Reduktion auch gefunden. Diese Reduktion erfolgt in der Nähe des elektrokapillaren Nullpotentials, also dort, wo der Spüleffekt besonders wirksam ist (LEVICH[3]). Bei der Cr^{3+}- Reduktion ist vielleicht doch ein Maximum 1. Art wirksam, also eine Differenz der Grenzflächenspannung, die bei grossen Tropfen besonders wirksam ist.

Abbildung 1 zeigt ferner, dass der Grenzstrom mit zunehmender Dämpferkonzentration kleiner wird. Dies kann einerseits auf einer Anlagerung der reduzierbaren Ionen an die grossen Dämpfermoleküle beruhen, da hierdurch eine Hemmung der Beweglichkeit eintritt. Neben dieser Verminderung von I_d kann aber durch Dämpferadsorption auch eine Verminderung der Reaktionsgeschwindigkeit oder der für die Reaktion noch freien Oberfläche eintreten (s. Abb. 3). Daher ist es notwendig, durch eine Reihe von Versuchen die geeignete, möglichst geringe Dämpferkonzentration zu finden.

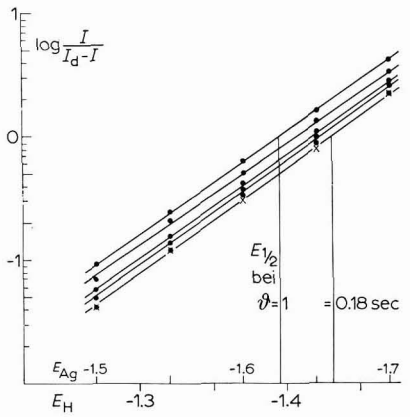

Abb. 2. Log $I/(I_d - I)$ in Abhängigkeit von E für $1.25 \cdot 10^{-3}$ M H_2SO_4– 0.5 M KCl mit $3.8 \cdot 10^{-3}$% Polyglykol 10 000. Oberste Kurve bei ϑ = 1 sec, dann ϑ = 0.53, 0.33, 0.28, 0.21 und 0.18 (Kreuze) sec.

2. Der Durchtrittsfaktor

Nach Gl. (1) ist

$$I/(I_d - I) = K\sqrt{\vartheta}, \text{ also}$$

$$\log [I/I(I_d - I)] = \text{const.} - (1-\alpha)\, nE/0.059$$

$$(1-\alpha)n = -0.059\, \mathrm{d} \log [I/(I_d - I)]/\mathrm{d}E = 0.059 \log (K_1/K_2)/(E_2 - E_1) \qquad (3)$$

wenn nur E geändert wird. Abbildung 2 zeigt die Auftragung der gemessenen Werte von $\log [I/(I_d - I)]$ gegen E bei der H^+-Reduktion in einer Lösung mit $3.8 \cdot 10^{-3}$% Polyglykol. Die Geraden verbinden Punkte mit gleichem ϑ, von $\vartheta = 1$ sec oben bis $\vartheta = 0.18$ sec unten, die Neigung der Geraden ergibt $1-\alpha = 0.491 \pm 0.005$. Der Durchtrittsfaktor ist von der Gegenwart grenzflächenaktiver Stoffe meist nur wenig abhängig, wie auch aus Literaturangaben[4] hervorgeht. Tabelle 1 enthält die nach Gl. (3) aus allen Versuchen erhaltenen Mittelwerte, auch für Cr^{3+} und Zn^{2+}.

TABELLE 1

	$(1-\alpha)n$	$\log k_0$	$E_{\frac{1}{2}}$
H^+	0.49 ± 0.01	-13.4 ± 0.1*	-1.38
Cr^{3+}	0.51	-8.6**	-0.70
Zn^{2+}	1.34	-24.2***	-0.96

* Dieser Wert und die Fehlergrenze gelten für alle Punkte der Abb. 5, also für alle ϑ- und E-Werte.
** Nach Abb. 4 für die Lösungen mit Gelatine (nach Abb. 1 ist $I_d/\vartheta^{\frac{1}{6}} = 3.8$, also $D = 5.8 \cdot 10^{-6}$) und ohne Dämpferzusatz.
*** Aus den Ergebnissen der potentiostatischen Messungen von VIELSTICH UND GERISCHER[5] lassen sich die Werte $\log K_0 = -24.4$ und $1-\alpha = 0.70$ berechnen.

3. Die Geschwindigkeitskonstante

k_0 sollte sich nach Gl. (2b) auch aus der Abhängigkeit der Stromstärke von der Tropfzeit, ϑ, ermitteln lassen, da sich hieraus die Grösse K ergibt, aus der man k_0 erhält, wenn D, α und E in Gl. (1) bekannt sind. Da jedoch die Lösung Maximadämpfer enthalten muss, um unkontrollierbare Erhöhungen der Stromstärke durch den Spüleffekt zu vermeiden, treten Störungen auf. Eine Erhöhung der Tropfzeit bedingt

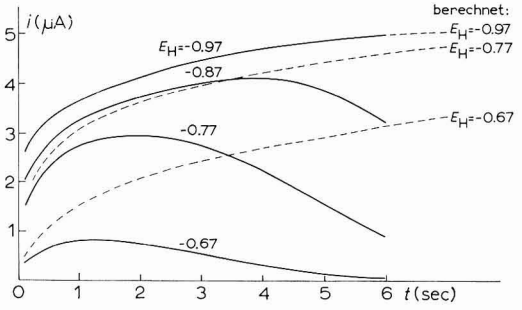

Abb. 3. Strom–Zeit-Kurven von "ersten Tropfen" (ohne Verarmung). Cr^{3+}-Reduktion in Gegenwart von Triton bei verschiedenen Potentialen. $2 \cdot 10^{-3}$ *M* Cr^{3+}–1 *M* NaCl–0.02 *M* HCl–$1.2 \cdot 10^{-3}$% Triton. Ausgezogene Kurven experimentell ermittelt, gestrichelte berechnet.

eine Verstärkung der Belegung der Elektrodenoberfläche mit der grenzflächenaktiven Substanz. Bei den hier untersuchten Systemen wird dadurch k_0 herabgesetzt, der Diffusionsgrenzstrom dagegen bei geringen Dämpferkonzentrationen nicht wesentlich beeinflusst. Er ist proportional $\vartheta^{\frac{1}{6}}$.

Abbildung 3 zeigt Stromstärke–Zeit-Kurven von Einzeltropfen* für die Cr^{3+}-Reduktion in Gegenwart von $1.2 \cdot 10^{-3}\%$ Triton bei 4 verschiedenen Elektrodenpotentialen ($E_H = -0.67, -0.77, -0.87, -0.97$ V von unten nach oben). Gestrichelt eingezeichnet sind berechnete Kurven für die Momentanstromstärke $i = i_d K \sqrt{t}/(1 + K\sqrt{t})$ mit $i_d = 3.64 t^{\frac{1}{6}}$ μA und mit $K = 1.22 \cdot 10^{-6} \cdot 10^{8.6(-E_H)}$ (berechnet nach Gl. (1) mit $D = 3.3 \cdot 10^{-6}$ nach Abb. 1 und mit $\log k_0 = -8.6$). Die 3 gestrichelten Kurven in Abb. 3 sind berechnet mit $E_H = -0.67, -0.77, -0.97$ V. Eine mit $E_H = -0.87$ V berechnete Kurve würde schon fast mit der für -0.97 V zusammenfallen. Da den 4 Potentialen die 4 K-Werte 0.69, 5.0, 36, 260 entsprechen, so ergeben die beiden letzten Werte schon annähernd $i = i_d$. Dementsprechend ist bei der gemessenen obersten Kurve i diffusionsbegrenzt und fast genau proportional $t^{\frac{1}{6}}$. Eine Hemmung von i_d durch den Dämpfer ist nicht feststellbar. Wenn aber das Potential weniger negativ und daher die Elektrodenreaktion weniger stark beschleunigt ist, so macht sich eine Hemmung um so mehr bemerkbar, je stärker die Bedeckung der Elektrode, je grösser t ist**, Schon bei $E_H = -0.87$ fällt i gegen Ende der Tropfzeit ab, noch mehr bei $E_H = -0.77$ und -0.67.

Infolge dieser kinetischen Hemmung durch Dämpferadsorption wird das Halbstufenpotential $E_{\frac{1}{2}}$ negativer bei Erhöhung der Dämpferkonzentration sofern die Tropfzeit gross ist (ohne Abklopfen). Bei $\vartheta = 0.18$ sec ist $E_{\frac{1}{2}}$ konstant, wenn die Dämpferkonzentration nicht sehr gross ist.

Abbildung 4 zeigt ebenfalls Ergebnisse der Cr^{3+}-Reduktion bei verschiedenen Potentialen jedoch unter Verwendung der Abklopfvorrichtung, also mit Variation der Tropfzeit. Hier handelt es sich um polarographisch registrierte, also über die Tropfzeit gemittelte Stromstärken, I. Aufgetragen ist $y = I/\vartheta^{\frac{1}{6}}$ gegen $x = I/\vartheta^{\frac{2}{3}}$. Die bei gleichem Potential, E, aber verschiedener Tropfzeit, ϑ, erhaltenen Punkte sind durch eine Gerade verbunden. Der Punkt mit der längsten Tropfzeit ($\vartheta = 1$ sec) liegt jeweils links, der mit der kürzesten Tropfzeit (0.18 sec) rechts. Nach Gl. (2b) sollten die Neigungen dieser Geraden gleich $-1/K$ sein und ihre Ordinate y_0 bei $x = 0$ für die Geraden bei allen Potentialen $y_0 = I_d/\vartheta^{\frac{1}{6}}$ betragen. In Abb. 4 sind die Ergebnisse von drei Versuchsreihen wiedergegeben.

1. Die punktierten Geraden und die durch Kreise wiedergegebenen experimentellen Punkte wurden erhalten bei einem Versuch, bei dem die Leitsalzlösung durch Behandlung mit Aktivkohle von grenzflächenaktiven Verunreinigungen befreit war. Hier ist y_0 annähernd gleich für alle Geraden, aber alle Stromstärken sind durch den Spüleffekt überhöht.

2. Die mit gestrichelten Geraden verbundenen Punkte ergab eine Lösung, die weder gereinigt noch mit Dämpfer versetzt war. y_0 ist hier merklich herabgesetzt, der Spüleffekt stark vermindert.

3. Die Kreuze und stark ausgezogenen Geraden wurden mit einer Lösung er-

* Hierbei wurde eine Apparatur benutzt, bei der die Spannung automatisch beim Abfallen eines Tropfens angelegt wird. Registriert wird die Stromstärke am hierauf folgenden "ersten" Tropfen, wodurch der "Verarmungseffekt" ausgeschaltet wird[6]. Die Kapillare dieser Apparatur unterschied sich von der in der vorliegenden Arbeit sonst benutzten. Die Tropfzeit betrug 6 sec.

** Siehe hierzu z.B. KŮTA UND SMOLER[7].

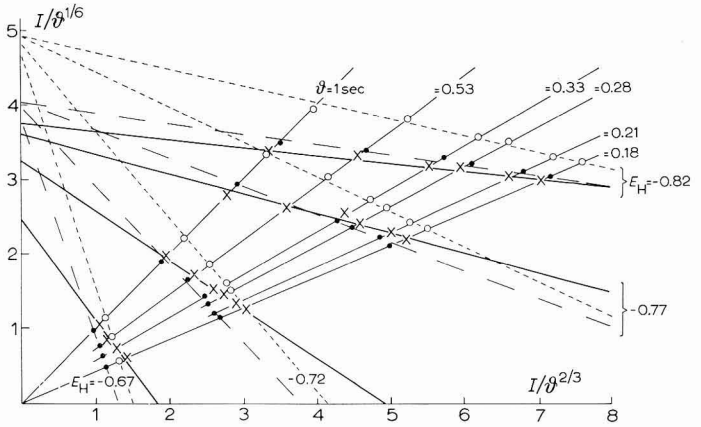

Abb. 4. Cr^{3+}-Reduktion mit der Abklopfvorrichtung: ϑ = 0.18–1.0 sec, $2 \cdot 10^{-3}$ *M* Cr^{3+}–1.0 *M* KCl–0.02 *M* HCl. Gl. (2) entsprechende Darstellung von 3 Versuchen:
(1) Kreise und punktierte Gerade: Leitsalzlösung mit Aktivkohle gereinigt.
(2) Punkte und gestrichelte Gerade: Lösung nicht gereinigt, ohne Dämpfer.
(3) Kreuze und ausgezogene Gerade: mit $0.88 \cdot 10^{-3}$% Gelatine. Jeweils 4 Gerade, entsprechend den 4 Potentialen E_H: −0.67; −0.72; −0.77; −0.82 V.

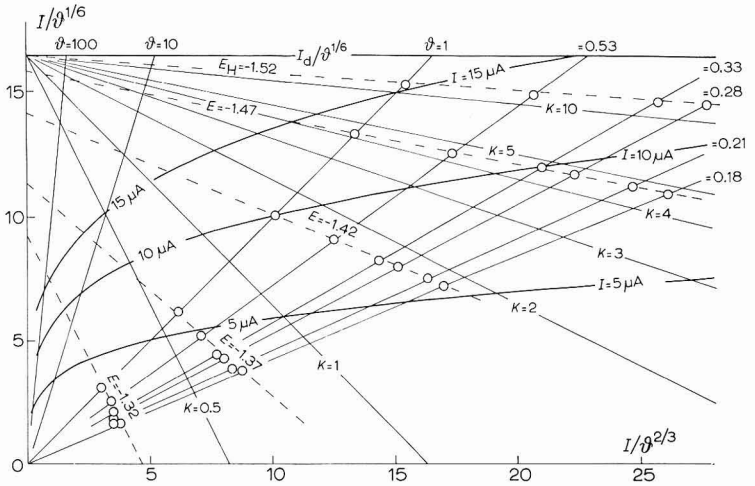

Abb. 5. H^+-Reduktion in Gegenwart von Triton. Darstellung wie in Abb. 4. $1.25 \cdot 10^{-3}$ *M* H_2SO_4–0.5 *M* KCl–$1 \cdot 10^{-3}$% Triton. $I_d/\vartheta^{\frac{1}{6}} = 16.5$. Eingezeichnet sind auch die Geraden, die ϑ = 0.18–1 (auch 10 und 100) und K = 0.5, 1, 2, 3, 4, 5 und 10 entsprechen und die Parabeln mit I = 5, 10 und 15 μA. (Bei ϑ = 1 ist $x = y = I$. Im allgemeinen ist $y_1 = x_1/\sqrt{\vartheta}$).

halten, die mit $8.8 \cdot 10^{-4}$% Gelatine versetzt war. Nunmehr haben alle Geraden sehr verschiedene Nullordinaten.

$y_0 = I_d/\vartheta^{\frac{1}{6}}$ ergibt sich nach Abb. 1 zu 3.8 (3.85 aus I_d bei $\vartheta = 1$ und 3.73 aus I_d bei $\vartheta = 0.18$). Tatsächlich ist aber y_0 nach Abb. 4 um so kleiner, je positiver E, je kleiner die Geschwindigkeit der Durchtrittsreaktion ist. Diese wird bei der längsten Tropfzeit durch die stärkere Belegung am stärksten gehemmt, wodurch dieser Punkt

am stärksten in Richtung des Nullpunktes des Koordinatensystems verschoben wird. Dadurch wird die Neigung der Geraden mit dem positivsten E am stärksten vermindert. K ist daher nicht aus der Neigung dieser Geraden zu ermitteln. K muss für jeden Punkt aus seinen Koordinaten nach Gl. (2), also

$$K = x/(y_0 - y) \tag{4}$$

ermittelt werden. Dies entspricht der Neigung einer Geraden, die durch den Messpunkt und die richtige Nullordinate $y_0 = I_d/\vartheta^{\frac{1}{6}}$ ($=3.8$ in Abb. 4) gezogen ist*.

Die mit Gelatine enthaltenden Lösungen gewonnenen Punkte der Abb. 4 ergeben für $\vartheta = 1$ sec, $\log k_0 = -8.64 \pm 0.01$ (für alle benutzten Potentiale) und für $\vartheta = 0.18$ sec, $\log k_0 = -8.59 \pm 0.01$. Für die Gelatine enthaltende Lösung ist also k_0 bei $\vartheta = 1$ um etwa 10% kleiner als bei $\vartheta = 0.18$.

Abbildung 5 zeigt Ergebnisse bei der H^+-Reduktion in Gegenwart von Triton. Auch hier ist die Neigung der Geraden, die Punkte mit verschiedener Tropfzeit aber gleichem Potential verbinden, bei positivem Potential viel zu gering. Aber Gerade, die die Punkte mit der richtigen Nullordinate $y_0 = I_d/\vartheta^{\frac{1}{6}}$ verbinden ergeben brauchbare Werte für k_0. Tabelle 1 enthält Messergebnisse. Auch hier ist k_0 bei $\vartheta = 1$ um etwa 10% kleiner als bei $\vartheta = 0.18$ sec.

Die Bedeckung einer Elektrodenoberfläche mit grenzflächenaktiven Stoffen ist auch vom Potential abhängig. Doch spielt dies innerhalb der kleinen Potentialberei-

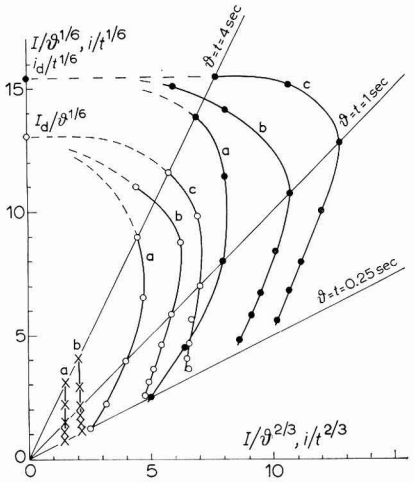

Abb. 6. In^{3+}-Reduktion, $8 \cdot 10^{-4}$ M $In(ClO_4)_3$–$8 \cdot 10^{-4}$ M $HClO_4$–$8 \cdot 10^{-2}$ M $LiClO_4$.
Kreuze: Lösung ohne Dämpfer. (a), bei $E_H = -0.47$; (b) -0.57 V.
Kreise: Mit Tritonzusatz. (a, b), $4 \cdot 10^{-4}$%, $E_H = 0.47$ bzw. -0.57 V; (c), $8 \cdot 10^{-4}$% Triton, $E_H = -0.57$. Kreuze und Kreise stellen über die Tropfzeit, ϑ, gemittelte Stromstärken, I, dar.
Punkte: Mit i–t-Kurven an "ersten Tropfen" erhaltene Momentanstromstärken i. (a,b), $4 \cdot 10^{-4}$% Triton, $E_H = -0.47$, bzw. -0.57 V; (c), $8 \cdot 10^{-4}$% Triton, -0.57 V. Also entsprechend den Bedingungen bei den Kreisen.

* Bei positiven Potentialen (-0.67 V) und kleinen Tropfzeiten ist die Stromstärke bei Gegenwart des Dämpfers auffallenderweise grösser als bei Abwesenheit. Dies kann darauf beruhen, dass der Rückdruck des Quecksilbertropfens durch die Grenzflächenspannung beim Fehlen grenzflächenaktiver Stoffe grösser ist, wodurch das Wachsen des Tropfens verlangsamt, m verkleinert ist

che einer Versuchsserie (z.B. -1.3 bis -1.5 V) bei Abb. 5 im allgemeinen nur eine untergeordnete Rolle.

Abbildung 6 zeigt ein Beispiel, bei dem der adsorbierte Maximadämpfer die Elektrodenreaktion beschleunigt. Es handelt sich allerdings hierbei nicht um die Durchtrittsreaktion, sondern um eine vorgelagerte Reaktion bei der In^{3+}-Reduktion, wahrscheinlich um die Abspaltung einer Wassermolekul aus dem Aquokomplex des Ions. Über die Untersuchung dieser Reaktion wird an anderer Stelle berichtet werden. Die beiden senkrechten Geraden links unten in Abb. 6 zeigen, dass in einer Lösung ohne Dämpferzusatz $I/\vartheta^{\frac{2}{3}}$ (also auch $i/t^{\frac{2}{3}}$) konstant ist. i wächst also proportional der Tropfenoberfläche. Auch bei $t=4$ sec ist i noch ausschliesslich kinetisch begrenzt und liegt noch weit unterhalb der diffusionsbegrenzten Werte. Bei Zusatz von Triton zu der Lösung nimmt $I/\vartheta^{\frac{2}{3}}$ und auch $i/t^{\frac{2}{3}}$ (Kurven mit Punkten, rechts) mit steigendem ϑ, bzw. t zunächst zu. Die Strom*dichte* steigt also mit zunehmendem Alter des Tropfens infolge der zunehmenden Belegung mit Triton. Aber etwa ab $t=1$ sec bewirkt die Diffusionshemmung ein Abbiegen der Kurven nach links bis schliesslich $i/t^{\frac{1}{6}}$ konstant wird. Die Belegung der Elektrodenoberfläche mit dem Katalysator ist so gross geworden, dass die Elektrodenreaktion nur noch diffusionsbegrenzt ist. Besonders früh tritt dies bei dem negativeren Potential, $E_H=-0.57$ V ein.

Die Belegungsdichte der Tropfenoberfläche mit dem Dämpfer in Abhängigkeit vom Tropfenalter lässt sich nicht mit den Diffusionsgesetzen berechnen. Insbesondere zu Beginn des Tropfenwachstums erfolgt ein verstärkter Antransport durch Rührung, und zwar einerseits durch den abfallenden vorherigen Tropfen, andererseits durch den Quecksilberzufluss.

Zusammenfassend lässt sich also sagen, dass die Berechnung von k_0 aus $K=-\mathrm{d}(I/\vartheta^{\frac{2}{3}})/\mathrm{d}(I/\vartheta^{\frac{1}{6}})$ also nach Gl. (2) aus der Neigung der Geraden, die in Abb. 4 und 5 Punkte mit verschiedener Tropfzeit aber gleichem Potential verbinden, nicht möglich ist. Trotzdem hat die Verwendung einer Abklopfvorrichtung, also die Variation von ϑ bei praktisch konstantem m den grossen Vorteil, dass man den Einfluss grenzflächenaktiver Substanzen auf die Geschwindigkeit der Elektrodenreaktion besser übersieht und dadurch zu brauchbaren Werten für k_0 gelangt. Der Bereich der Tropfzeiten von etwa 0.2–1 sec ist günstig, da sowohl bei kürzeren als auch bei längeren Tropfzeiten Störungen auftreten.

Der Deutschen Forschungsgemeinschaft und dem Landesamt für Forschung des Landes Nordrhein-Westfalen danken wir für die Beihilfen zur Beschaffung der Apparate. Einer von uns (J.S.) dankt der Comissão Coordenadora da Investigação Para A Otan, Lissabon, Portugal, für die Unterstützung der Arbeit durch Gewährung von Stipendien.

ZUSAMMENFASSUNG

Die von WOLF[1] begonnenen Untersuchungen über den Einfluss einer Beschleunigung der Tropfenfolge durch Abklopfen der Tropfen auf die Vorgänge an einer Tropfelektrode wurden in der vorliegenden Arbeit fortgesetzt. Dabei wurden die Bedingungen für die Bestimmung der Geschwindigkeitskonstante und des Durchtrittsfaktors der Elektrodenreaktion untersucht. Insbesondere wurde der Einfluss grenzflächenaktiver Stoffe, die als Maximadämpfer zugesetzt werden müssen, geprüft.

SUMMARY

This paper continues the investigation started by WOLF[1] on the effect of acceleration of the drop sequence (by knocking off drops) on the reactions at a dropping electrode. Here the conditions for the determination of rate constants and transfer coefficients are investigated. Particular attention is given to the effect of surface-active substances used as maximum suppressors.

LITERATUR

1 D. WOLF, *J. Electroanal. Chem.*, 5 (1963) 186; H. SCHMIDT UND R. V. SCHORLEMER, *J. Electroanal. Chem.*, 5 (1963) 345.
2 J. KOUTECKÝ, *Collection Czech. Chem. Commun.*, 18 (1953) 597; J. WEBER UND J. KOUTECKÝ, *Collection Czech. Chem. Commun.*, 20 (1955) 980.
3 V. G. LEVICH, *Physicochemical Hydrodynamics*, Prentice Hall, Englewood Cliffs, N.J., 1962, S. 582 ff.
4 Zum Beispiel: A. ARAMATA UND P. DELAHAY, *J. Phys. Chem.*, 68 (1964) 880; S. SATHYANARAYANA, *J. Electroanal. Chem.*, 10 (1965) 119.
5 W. VIELSTICH UND H. GERISCHER, *Z. Physik. Chem. N.F.*, 4 (1955) 10.
6 W. HANS, W. HENNE UND E. MEURER, *Z. Elektrochem.*, 58 (1954) 856.
7 J. KŮTA UND J. SMOLER, *Z. Elektrochem.*, 64 (1960) 285.

ELECTROANALYTICAL CHEMISTRY AND INTERFACIAL ELECTROCHEMISTRY
Elsevier Sequoia S.A., Lausanne – Printed in The Netherlands

ZUR RÜHRABHÄNGIGKEIT DES GRENZSTROMES AN TEILWEISE BEDECKTEN ROTIERENDEN SCHEIBENELEKTRODEN BEI RELATIV GROSSEN UMDREHUNGSZAHLEN

F. SCHELLER, R. LANDSBERG UND S. MÜLLER
Physikalisch-Chemisches-Institut der Humboldt-Universität, Berlin (DDR)
(Eingegangen am 7. September 1968)

EINLEITUNG

In einer früheren Arbeit[1] (im folgenden mit I bezeichnet) berichteten wir über die Rührabhängigkeit des Diffusionsgrenzstromes an teilweise blockierten rotierenden Scheibenelektroden. Durch Übertragung des elektrischen Analogons wurde dieser Zusammenhang durch folgende Gleichung angegeben:

$$\frac{1}{I_{gr}} = \frac{1.61\,\nu^{\frac{1}{6}}}{nFD^{\frac{2}{3}}\,c_L(2\pi)^{\frac{1}{2}}\,q_{geo}}u^{-\frac{1}{2}} + \frac{|\Sigma A_n \operatorname{tgh}(x_n\delta/r_2)|}{nFDc_L\,q_{geo}} \tag{1}$$

I_{gr}, Grenzstrom; ν, kinematische Viskosität; n, Reaktionsladungszahl; F, Faraday-Konstante; D, Diffusionskoeffizient; c_L, Konzentration im Lösungsinneren; q_{geo}, geometrische Elektrodenoberfläche; A_n, Koeffizienten für die SMYTHE[4] eine Bestimmungsgleichung angibt; x_n, Nullstelle der Besselfunktion erster Ordnung; δ, Diffusionsschichtdicke; r_2, Radius des Diffusionszylinders; r_1, Radius der aktiven Stelle; u, Umdrehungszahl der Elektrode.

In der vorliegenden Arbeit wird nun die Gültigkeit von Gl. (1) bei hohen Umdrehungszahlen diskutiert.

EXPERIMENTE

Die Modellelektroden wurden mit Hilfe der Photoresisttechnik hergestellt. Das Elektrodenmetall war Platin.

Für die Modellelektroden mit aktiven Stellen von 1 mm und 0.1 mm Durchmesser wurden in Kunststoff eingeklebte Platindrähte verwendet.

Es wurde der Diffusionsgrenzstrom der Reduktion von $K_3[Fe(CN)_6]$ in 1 *M* KCl bei 20° untersucht. Weitere Angaben über die experimentelle Durchführung befinden sich in I.

THEORETISCHE GRUNDLAGEN

Gleichung (1) geht für sehr kleine Werte von δ in

$$\frac{1}{I_{gr}} = \frac{1.61\,\nu^{\frac{1}{6}}}{nFD^{\frac{2}{3}}\,c_L(2\pi)^{\frac{1}{2}}q_{geo}}\left(1 + \frac{|\Sigma A_n x_n|}{r_2}\right)u^{-\frac{1}{2}} \tag{2}$$

über, da der tgh x für kleine x durch das Argument selbst ersetzt werden kann. Das entspricht einer Geraden, die durch den Koordinatenursprung verläuft. Der Anstieg soll dabei nach Gl. (2) nur vom Blockierungsgrad und nicht von der Zahl der aktiven Stellen abhängen, da $|\Sigma A_n x_n/r_2|$ nur eine Funktion von r_1/r_2 ist, es folgt also keine Lewitsch-Beziehung bezogen auf die aktive Fläche. Weil bei kleinen Werten von δ der Grenzstrom der Konzentration und der Wurzel aus der Umdrehungszahl proportional ist, nannten wir dieses Gebiet "Quasi-Lewitsch-Bereich".

Für die Anwendung von Gl. (2) muss man den Stofftransport zur rotierenden Scheibenelektrode durch die Konvektionsdiffusion untersuchen.

Die Diffusionsstromdichte, j, an der homogenen rotierenden Scheibenelektrode ergibt sich zu[2]:

$$j = DnF\left(\frac{\partial c}{\partial y}\right)_{y=0} = \frac{nFDc_L}{\delta} \tag{3}$$

Dabei wird bei der Berechnung der Konzentrationsverteilung vor der Scheibe der Stofftransport durch Diffusion und Konvektion in senkrechter Richtung zur Scheibenoberfläche (y-Richtung) berücksichtigt, während die Konzentration nicht von den Koordinaten r und φ abhängen soll. Die Diffusionsschicht nach Lewitsch beträgt

$$\Delta c/\left(\frac{\partial c}{\partial y}\right)_{y=0} = \delta \tag{4}$$

und der Stofftransport zur Scheibenoberfläche entspricht alleiniger Diffusion durch eine solche Schichtdicke.

Δc ist dabei die Konzentrationsdifferenz zwischen dem Lösungsinneren und der Elektrodenoberfläche. Formal berücksichtigt man hierbei den Stofftransport durch Konvektion, indem man im ersten Fickschen Gesetz eine Diffusionsschichtdicke einsetzt, die kleiner ist als das Gebiet, in dem in Wirklichkeit ein Konzentrationsgradient vorliegt.

Bei der Übertragung des Zylindermodells (siehe I) auf die teilweise blockierte rotierende Scheibenelektrode wird nun die Länge des Zylinders durch die Diffusionsschichtdicke der homogenen Elektrode nach Gl. (4) ersetzt, d.h., es wird mit der Nernstschen Vorstellung gearbeitet. Bei inhomogenen Elektroden ist die Konzentration in der Diffusionsschicht nicht nur eine Funktion des Abstandes y von der Elektrodenoberfläche, sondern sie muss durch den unterschiedlichen Stoffverbrauch an der Oberfläche auch in radialer Richtung ortsabhängig sein. D.h. aber, dass der Stofftransport durch die Flüssigkeitsströmung mit den Geschwindigkeitskomponenten v_r und v_φ nicht wie bei der homogen Elektrode vernachlässigt werden kann, sondern er muss in Abhängigkeit von der Umdrehungszahl berücksichtigt werden. Für die beiden Geschwindigkeitskomponenten der Flüssigkeitsströmung gilt nach Lewitsch:

$$v_r = ruF(y)2\pi \qquad v_\varphi = ruG(y)2\pi \tag{5}$$

(Die Bestimmungsgleichungen für F und G sind von LEWITSCH angegeben[2].)

Während der Stofftransport in y-Richtung der Wurzel der Umdrehungszahl proportional ist, sind v_r und v_φ direkt der Umdrehungszahl u proportional. Der Stofftransport durch die radiale Strömung wird so bei hohen Umdrehungszahlen einen relativ grossen Anteil liefern, während der Anteil bei sehr kleinen Umdrehungszahlen zu vernachlässigen ist. So ist es auch zu erklären, dass für kleine Umdrehungs-

zahlen (Frumkin-Gebiet) Gl. (1) mit den Experimenten innerhalb der Messgenauigkeit übereinstimmt.

Wird die Diffusionsschichtdicke sehr klein, so ist es wahrscheinlich, dass die nichtlineare Diffusion nicht mehr von der gesamten geometrischen Fläche erfolgen wird und damit die Definitionsgleichung für r_2 (siehe I)

$$N\pi r_2^2 = 1 \tag{6}$$

N, Anzahl der aktiven Stellen pro cm^2
ihre Gültigkeit verliert. Da r_2 nicht als Funktion von δ/r_1 bekannt ist, kann Gl. (2) nicht mehr angewandt werden.

Der Anteil der Konvektion am Stofftransport bei Elektroden mit inaktiven Bereichen zeigt sich darin, dass die Stromdichte an einer Ringelektrode höher ist als die an einer homogenen Scheibenelektrode im Zentrum. Überträgt man die Beziehung der Ringelektrode[3] auf eine grosse, azentrische, kreisförmige Stelle, so sollte analog gelten:

$$f_L = I_{gr(a)}/I_{gr(0)} = [(a-r_1)^3 - a^3]^{\frac{2}{3}}/[(a+r_1)^2 - a^2] \tag{7}$$

f_L = Überhöhungsfaktor; r_1 = Radius der aktiven Stelle
$I_{gr(0)}$ ist dabei der Strom nach der üblichen Lewitsch-Beziehung, wenn sich die aktive Stelle im Scheibenzentrum befindet. $I_{gr(a)}$ stellt den gemessenen Strom dar, wenn der Abstand der aktiven Stelle vom Scheibenzentrum a beträgt. Bei Elektroden mit vielen aktiven Stellen erhält man f_L, indem man in Gl. (7) jeweils die Ströme $I_{gr(a)}$ und $I_{gr(0)}$ der einzelnen aktiven Stellen summiert, d.h. f_L ergibt sich durch Mittelwertbildung aus den einzelnen Überhöhungsfaktoren.

Für grosse aktive azentrische Stellen mit dem Abstand vom Scheibenmittelpunkt a wird die Quasi-Lewitsch-Beziehung nach Gl. (7) erfüllt. Bei kleinen aktiven Stellen ist am Stofftransport bei hohen Umdrehungszahlen neben der linearen und nichtlinearen Diffusion auch die Zentrifugalströmung der Flüssigkeit beteiligt. Dabei hängt die Stromdichte ebenfalls linear von der Wurzel der Umdrehungszahl ab.

Für kleine Blockierungsgrade geht das Korrekturglied in Gl. (2) gegen Null (vgl. I, Abb. 3), d.h., man findet die Lewitsch-Beziehung. Da der Stofftransport durch die stromdichteerhöhende Konvektion in Gl. (2) nicht berücksichtigt ist, wird die Lewitsch-Beziehung experimentell schon bei Blockierungsgraden gefunden, für die die Abweichungen nach Gl. (2) noch ausserhalb der Messgenauigkeit liegen. Dieser Übergang zur Lewitsch-Beziehung sollte besonders früh bei Elektroden mit sehr vielen kleinen aktiven Stellen erfolgen, da hier der Konvektionsanteil besonders hoch ist.

MESSERGEBNISSE UND DISKUSSION

Um die Messwerte mit den nach Gl (2) zu erwartenden Werten zu vergleichen, wurde $|\Sigma A_n \operatorname{tgh}(x_n\delta/r_2)|$ programmiert und auf dem ZRA 1 für die 20 Radienverhältnisse, $r_1/r_2 = 0.05; 0.10; \ldots 1.00$ berechnet. Für die einzelnen Radienverhältnisse wurden jeweils 20 Werte für δ/r_2 (0.05; 0.10; ... 1.00) ermittelt, d.h., die Rührabhängigkeit für die verschiedenen Blockierungsgrade bestimmt.

In Abb. 1 ist die Rührabhängigkeit des Diffusionsgrenzstromes einer teilweise blockierten Modellelektrode dargestellt und die durch Gl. (1) bestimmte Kurve (d)

angegeben. Im Quasi-Lewitsch-Gebiet ist der gemessene reziproke Grenzstrom (Kurve c) kleiner als der nach Gl. (1) bestimmte, d.h., neben der Diffusion muss auch die in Gl. (1) nicht berücksichtigte zusätzliche Konvektion am Stofftransport zur Elektrodenoberfläche beteiligt sein. Durch diesen zusätzlichen Stofftransport wird auch der Übergang zwischen dem Quasi-Lewitsch- und Frumkin-Gebiet zu grösseren $u^{-\frac{1}{2}}$ verschoben, und das Frumkin-Gebiet beginnt erst bei $\delta > r_2$, was im Widerspruch zu Gl. (1) steht. Erst bei grossen δ-Werten kann der Stofftransport nur der linearen und nichtlinearen Diffusion zugeschrieben werden, da hier die Messwerte der Gl. (1) genügen.

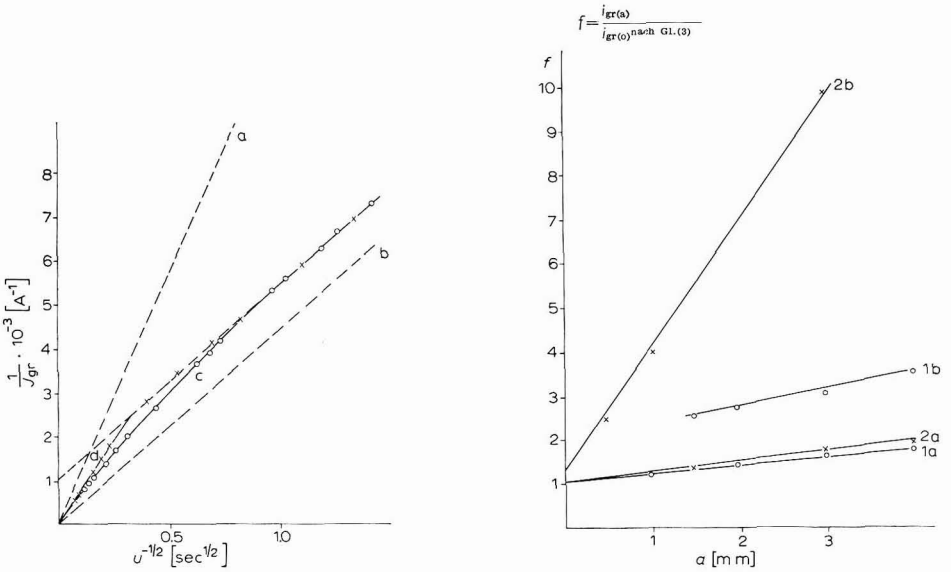

Abb. 1. Rührabhängigkeit des Grenzstromes. $r_1 = 2.5 \cdot 10^{-3}$ cm, $\psi = 62\%$, $c_L = 1 \cdot 10^{-2}$ M $K_3[Fe(CN)_6]$, 1 M KCl, 20°. (a), Lewitsch-Beziehung mit q_{akt}; (b), Lewitsch-Beziehung mit q_{geo}; (c), Messkurve; (d), Kurve nach Gl. (1).

Abb. 2. Abhängigkeit der Stromdichteüberhöhung von der Azentrizität einer aktiven Stelle. $c_L = 1 \cdot 10^{-2}$ M $K_3[Fe(CN)_6]$, 1 M KCl, 20°. (a), $r_1 = 5 \cdot 10^{-2}$ cm; (b), $r_1 = 5 \cdot 10^{-3}$ cm. (1), Kurve nach Gl. (7); (2), Messwerte von $i_{gr(a)}/i_{gr(0)}$.

Der Einfluss der Zentrifugalströmung auf den Stofftransport wird durch die Abhängigkeit der Grenzstromdichte einer aktiven Stelle von der Azentrizität nachgewiesen. Wie Abb. 2 zeigt, wächst der Grenzstrom (Kurve 2a) fast linear mit der Azentrizität der aktiven Stelle an und stimmt mit dem nach Gl. (7) berechneten Wert (Kurve 1a) bei einem Durchmesser der aktiven Stelle von 1 mm etwa überein. Sind mehrere aktive Stellen auf der Elektrode vorhanden, so kann man durch Summation der nach Gl. (7) für jede Stelle berechneten Ströme den Gesamtstrom bestimmen. Der Abstand zwischen den Stellen muss dabei gross sein. Tabelle 1 zeigt die Gegenüberstellung der mit Gl. (7) berechneten und der gemessenen Werte des Grenzstroms für verschiedene Modellelektroden.

Wie Tabelle 1 zeigt, stimmen die berechneten und die gemessenen Werte relativ gut überein.

Für Elektroden mit einer aktiven Stelle mit dem Durchmesser von 0.1 mm

ergibt Gl. (7) kleinere Grenzströme als experimentell bestimmt wurden (Abb. 2, Kurven 1b und 2b). Hier muss neben der zusätzlichen Konvektion und linearen Diffusion auch die nichtlineare Diffusion berücksichtigt werden.

Die mathematische Erfassung dieses Problemes ist nicht gelungen, ausserdem ist bei realen Elektroden mit kleineren Abständen zwischen den aktiven Stellen mit einer gegenseitigen Beeinflussung zu rechnen, was die quantitative Erfassung des Stofftransports noch weiter kompliziert.

Das Verhältnis von gemessenem und dem nach der Lewitsch-Beziehung mit der aktiven Elektrodenoberfläche berechneten Strom bezeichnen wir als f_M, den Überhöhungsfaktor. Diese Überhöhung resultiert aus dem Stofftransport durch nichtlineare Diffusion und die Zentrifugalströmung. Da durch Gl. (2) die lineare und nichtlineare Diffusion erfasst werden, kann man formal den Unterschied zwischen dem gemessenen und dem nach Gl. (2) berechneten Strom der zusätzlichen Konvektion zuschreiben. Wir bezeichnen deshalb das Verhältnis von gemessenem und nach Gl. (2) berechneten Strom als Überhöhungsfaktor der Konvektion, f_K. Unter der Bedingung, dass sich die aktiven Stellen nicht gegenseitig beeinflussen, sollte f_K gleich

TABELLE 1

VERGLEICH DER NACH GL. (7) BERECHNETEN UND GEMESSENEN GRENZSTROMDICHTEN i_{gr} FÜR MODELLELEKTRODEN MIT $r_1 = 5 \cdot 10^{-2}$ CM

Zahl der aktiven Stellen (Platindrähte)	$i_{gr} \cdot 10^3 (A)$ *nach Gl. (7)*	$i_{gr} \cdot 10^3 (A)$ *(Messwerte)*
4	7.50	7.95
13	7.98	8.43
19	8.03	8.05
25	8.05	8.16

TABELLE 2

ÜBERHÖHUNGSFAKTOREN FÜR VERSCHIEDENE MODELLELEKTRODEN

ψ (%)	N (1/cm²)	$r_1 \cdot 10^3$(cm)	f_M	f_L	f_K
94	10,000	1.40	3.66	4.13	1.71
84	32,400	1.25	3.02	4.14	1.68
80	40,000	1.25	2.70	4.13	1.52
73	48,400	1.35	2.30	4.15	1.42
70	57,600	1.25	2.20	4.13	1.38
62	19,600	2.50	1.81	3.29	1.17
45	25,600	2.60	1.51	3.30	1.08
80	6,400	3.30	2.28	2.99	1.33

dem nach Gl. (7) berechneten f_L sein, wobei $I_{gr(0)}$ hier den Grenzstrom darstellt, den man mit Hilfe von Gl. (2) berechnet. Damit sind die lineare, die nichtlineare Diffusion sowie die Zentrifugalströmung berücksichtigt worden. Tabelle 2 zeigt aber, dass stets $f_K < f_L$ ist, d.h., die aktiven Stellen beeinflussen sich gegenseitig. Bei konstantem r_1 steigt f_K mit wachsendem Abstand zwischen den aktiven Stellen an, die Wechselwirkung nimmt ab. So haben Elektroden mit gleichem Blockierungsgrad aber unterschiedlicher Stellenzahl auch verschiedene Grenzströme.

Wie Tabelle 2 zeigt, sind die gemessenen Ströme immer grösser als Gl. (2)

angibt ($f_K > 1$). Da die Berechnung des Anteils der Konvektion nicht gelang, ist es nicht möglich, den Blockierungsgrad ψ aus dem Anfangsanstieg der I_{gr}^{-1}–$u^{-\frac{1}{2}}$-Kurve zu bestimmen. Abbildung 3 zeigt die Konzentrationsabhängigkeit des Grenzstromes im Quasi-Lewitsch-Gebiet. In Abb. 4 ist die Rührabhängigkeit des Grenzstromes für Elektroden mit relativ grossen Stellen dargestellt, bei denen nur das Quasi-Lewitsch-Gebiet auftritt.

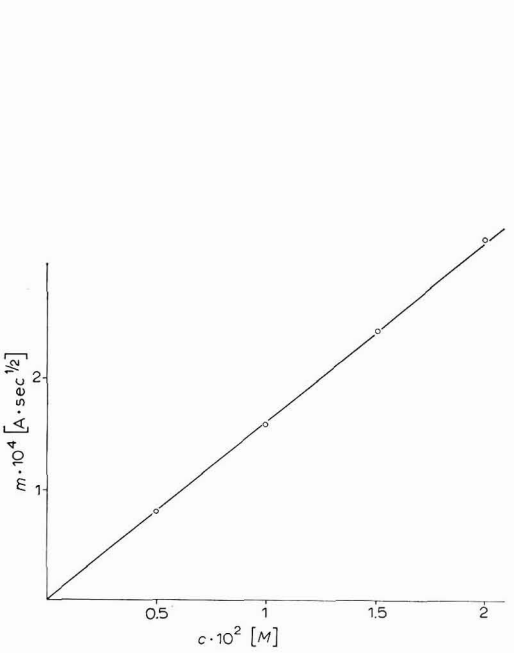

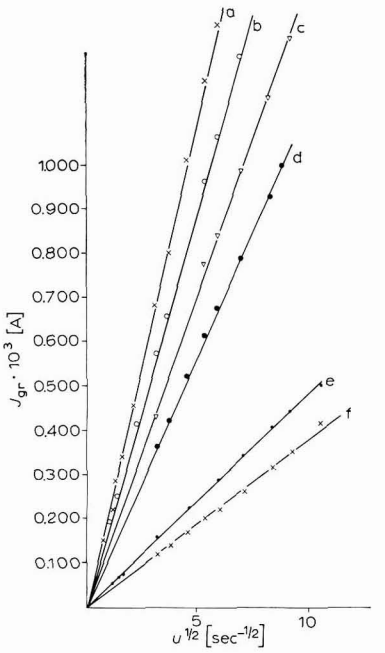

Abb. 3. Konzentrationsabhängigkeit des Anstieges m im Quasi-Lewitsch-Gebiet. 1 M KCl, 20°. $r_1 = 1.25 \cdot 10^{-3}$ cm, $\psi = 70.5\%$.

Abb. 4. Rührabhängigkeit des Grenzstromes. $c_L = 1 \cdot 10^{-2}$ M $K_3[Fe(CN)_6]$, 1 M KCl, 20°. (a), Pt-Elektrode, $\varnothing = 5$ mm; (b), $r_1 = 3.1 \cdot 10^{-3}$ cm, $\psi = 30\%$, $q_{geo} = 0.2$ cm^2; (c), $r_1 = 7.3 \cdot 10^{-3}$ cm, $\psi = 77\%$, $q_{geo} = 0.2$ cm^2; (d), $r_1 = 7.0 \cdot 10^{-3}$ cm, $\psi = 80\%$, $q_{geo} = 0.2$ cm^2; (e), $r_1 = 5.0 \cdot 10^{-3}$ cm, $\psi = 99\%$, $q_{geo} = 0.8$ cm^2; (f), $r_1 = 8.7 \cdot 10^{-3}$ cm, $\psi = 90\%$, $q_{geo} = 0.2$ cm^2.

Da bei der galvanostatischen Messanordnung die zusätzliche Konvektion nicht auftritt, sollte hier Gl. (2) anwendbar sein, deshalb erscheint das galvanostatische Verfahren zur Bestimmung des Blockierungsgrades und von r_1 geeigneter als die rotierende Scheibenelektrode.

Für die Bearbeitung einiger mit der Arbeit zusammenhängender mathematischer Fragen sind wir Herrn H. J. SPITZER sehr dankbar.

ZUSAMMENFASSUNG

Mit Hilfe von Modellelektroden, die eine definierte Zahl aktiver Bereiche besitzen, wird die Rührabhängigkeit des Grenzstroms bei relativ hohen Umdrehungszahlen untersucht. Bei genügend grossen (Ø, 1 mm) und genügend weit entfernten

Stellen ist der Grenzstrom mit der Gleichung für die Ringelektrode berechenbar, werden die Stellen kleiner (Ø, 0.1 mm), so ist der gemessene Strom grösser als der auf obige Weise berechnete. D.h., der Strom ergibt sich durch Überlagerung von Konvektion, linearer und nichtlinearer Diffusion. Der Anteil der nichtlinearen Diffusion lässt sich nicht quantitativ erfassen. Bei einer grösseren Zahl von aktiven Stellen tritt gegenseitige Beeinflussung auf, so dass der Strom zwischen den beiden Werten liegt, die sich bei Berücksichtigung von linearer und nichtlinearer Diffusion einerseits und von linearer und nichtlinearer Diffusion und Konvektion andererseits berechnen.

SUMMARY

Model electrodes having a known number of active circular sites were used to obtain the dependence of the limiting current on the rate of rotation of disk electrodes. The limiting current may be calculated by means of the formula for the ring electrode if the sites are sufficiently large and sufficiently far apart. For smaller sites, the current is larger than that given by this equation because non-linear as well as linear diffusion and convection contribute to it.

The current to each site is influenced by that to neighbouring sites if they are not sufficiently far apart. In this case it was not possible to calculate the contribution of non-linear diffusion to the limiting current. It lay between the value calculated considering linear and non-linear diffusion and that calculated taking into account convection in addition to the two types of diffusion.

LITERATUR

1 F. SCHELLER, S. MÜLLER, R. LANDSBERG UND H. J. SPITZER, *J. Electroanal. Chem.*, 19 (1968) 187.
2 W. G. LEWITSCH, *Physikalisch Chemische Hydrodynamik*, Verlag der Akad. Nauk, Moskau, 1959, Kap. 2.
3 J. IWANOW UND W. G. LEWITSCH, *Dokl. Akad. Nauk SSSR*, 126 (1959) 1029.
4 W. SMYTHE, *J. Appl. Phys.*, 24 (1953) 70.

ELECTROANALYTICAL CHEMISTRY AND INTERFACIAL ELECTROCHEMISTRY
Elsevier Sequoia S.A., Lausanne – Printed in The Netherlands

POUDRES MÉTALLIQUES FORMÉES PAR ÉLECTROLYSE SUR L'ÉLECTRODE À GOUTTE DE MERCURE

A. CĂLUȘARU
Institut de Physique Atomique, Bucarest (Roumanie)
J. KŮTA
Institut de Polarographie "J. Heyrovský", Prague (Tchécoslovaquie)
(Reçu le 15 août 1968; en forme revisée le 1 octobre 1968)

INTRODUCTION

Le processus de formation des poudres métalliques par électrolyse a été etudié dans le cas de la déposition sur les électrodes solides[1]. Le besoin croissant de poudres métalliques pour diverses applications pratiques a fait naître des techniques électrolytiques qui permettent l'obtention des métaux dispersés sous formes diverses. En ce qui concerne le mécanisme de déposition il faut distinguer trois cas: (1) dépôts pulvérulents, obtenus lors de petites densités de courant; (2) dépôts rugueux; (3) dépôts finement dispersés, formés aux hautes densités de courant. Une étude approfondie sur le mécanisme de formation de poudres lors de petites densités de courant a été faite par KUDRIATZEV[2]. Le processus de formation des dépôts rugueux a été étudié récemment par IBL ET SCHADEG[3], qui ont mis en évidence l'influence des processus de transport. Pour la troisième catégorie de dépôts, formés lors de grandes densités de courant, on a formulé diverses hypothèses. Une étude critique sur ces hypothèses peut être trouvée dans les revues consacrées à ce sujet[1,4].

La formation de poudres sur l'électrode à goutte de mercure[5] appartient à la troisième catégorie de dépôts. A ce point de vue l'électrode à goutte est particulièrement favorable pour la détermination des potentiels de formation des poudres, en raison de sa surface très propre et reproductible.

Dans le présent travail, nous étudions le processus de formation des poudres de plusieurs métaux sur l'électrode à goutte de mercure prenant comme point de départ les résultats obtenus pour l'explication du mécanisme de formation de poudres pour des grandes densités de courant. Nous déduisons ensuite l'expression du potentiel de formation des poudres sur l'électrode à goutte de mercure.

PARTIE EXPÉRIMENTALE

Pour l'observation microscopique de la goutte de mercure nous avons utilisé une cellule polarographique de type Šerak. L'une des faces de cette cellule est une paroie plane; l'anode est une électrode saturée de calomel. La séparation entre les compartiments anodique et cathodique est effectuée au moyen d'un diaphragme de cellophane. L'observation a été faite à un grossissement microscopique de (30×).

Pour photographier la goutte et les dendrites nous avons utilisé la lentille objectif (5×) seulement. Le film a été ensuite copié à un grossissement d'environ 3–4×. La polarisation de l'électrode et l'enregistrement des courbes ont été effectués avec un polarographe du type LP 55. Nous avons utilisé deux capillaires: (1) $m = 2.73$ mg sec^{-1}, $t_1 = 3$ sec, $h = 85$ cm; (2) $m = 0.45$ mg sec^{-1}, $t_1 = 90$ sec, $h = 56$ cm, dans une solution de KNO_3 2 M, en circuit ouvert.

RÉSULTATS EXPÉRIMENTAUX

Il est possible d'observer au moyen d'un microscope les dendrites métalliques qui se forment dans le voisinage de la surface de la goutte qui croît[6]. On peut balayer les potentiels de la vague polarographique et déterminer le potentiel qui correspond à la formation des dendrites en fixant successivement le curseur sur divers points du fil potentiométrique et en observant la chute de plusieurs gouttes. Nous avons obtenu des résultats reproductibles en polarisant l'électrode à des potentiels successifs, séparés par un intervalle de 25 mV; cette valeur représente ainsi la précision avec laquelle nous avons déterminé les potentiels de formation des poudres.

Conditions de formation de dendrites

Cuivre. Nous avons étudié la formation de dendrites de cuivre dans une solution de $CuCl_2$, KNO_3 2 M comme électrolyte support. Nous avons constaté que la poudre de cuivre se forme à des potentiels plus négatifs que −0.8 V et dans des solutions cuivriques de concentrations supérieures à 0.05 M (Fig. 1). A la valeur du

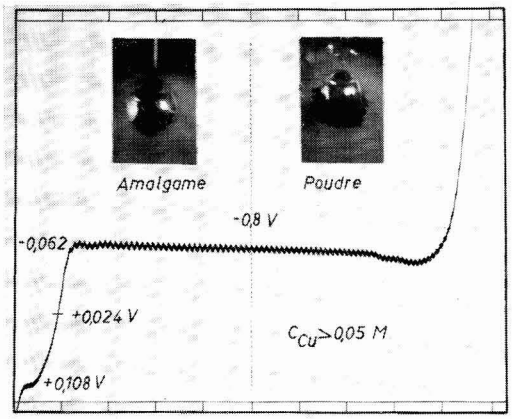

Fig. 1. Domaines de formation d'amalgame et de poudre dans le cas de la décharge d'ions cuivriques ($CuCl_2$) sur l'électrode à goutte de mercure en milieu KNO_3 2 M et en présence de gélatine (0.05%). Potentiel de départ 0.000 V; −200 mV/absc.; anode, E.C.S.

potentiel de −0.80 V les dendrites se forment nettement, mais elles se dissolvent rapidement dans la goutte qui croît. A −0.85 V une partie des dendrites formées reste dans le voisinage de la surface. Il est intéressant de remarquer que la poudre de cuivre ne se forme ni dans la période initiale, ni dans la période finale de la croissance de la goutte. L'apparition des dendrites de cuivre est conditionnée par une certaine vitesse de croissance de la surface de l'électrode. En général, les particules

métalliques se forment dans la portion médiane et inférieure de la goutte. L'aspect de la poudre de cuivre formée sur l'électrode liquide est analogue à l'aspect de la poudre obtenue sur les électrodes solides[7,8]. On observe dans les deux cas la forme caractéristique de la poudre de cuivre et la couleur rouge du cuivre. A la valeur de 1.00 V il est possible d'observer nettement l'apparition de l'hydroxyde de cuivre.

Bismuth. Dans le cas du bismuth nous avons utilisé une solution de $Bi(NO_3)_3$, HCl 4 *M*. Le potentiel de formation de la poudre est −0.575 V et la concentration limite 0.0098 *M* (Fig. 2). A −0.60 V on observe quelques dendrites qui restent longtemps à la surface de la goutte. Pour les valeurs légèrement inférieures à −0.60 V, les particules sont groupées à la surface sous la forme de cercles noirs. Aux potentiels plus grands la goutte est couverte par une masse spongeuse noire qui se meut à la surface de la goutte et se dissout partiellement dans le mercure. Le volume apparent de la poudre dépasse plusieurs fois le volume de la goutte.La croissance lente de la surface de l'électrode favorise la formation de la poudre de bismuth.

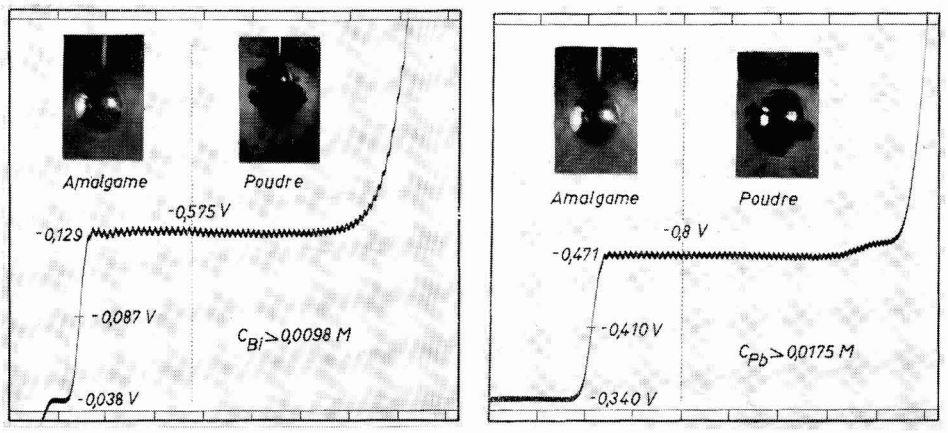

Fig. 2. Comme Fig. 1 pour ions de bismuth ($Bi(NO_3)_3$) excepté le milieu —HCl 4 *M*.

Fig. 3. Comme Fig. 1 pour ions de plomb ($Pb(NO_3)_2$).

Plomb. Nous avons utilisé une solution de $Pb(NO_3)_2$, KNO_3 2 *M*. Sur la Fig. 3 on peut voir que le potentiel de formation est situé à −0.80 V et la limite inférieure de la concentration à 0.0175 *M*. Dans le cas du plomb, le processus de dissolution des dendrites dans la goutte est très caractéristique. La taille des particules augmente rapidement, mais même les particules de grandes dimensions ne se détachent pas de l'électrode. Très souvent quelques dendrites se dissolvent dans le mercure; elles entraînent alors parfois la totalité de la poudre et, en une fraction de seconde, la goutte se trouve parfaitement nettoyée. En ce qui concerne l'influence de la vitesse de croissance de la goutte le phénomène est analogue au cas du cuivre: les particules se forment à des certaines vitesses de croissance; au début et à la fin de la formation de la goutte il n'y a aucune apparition de poudre.

Thallium. Nous avons étudié la formation des dendrites de thallium dans une solution de $TlNO_3$, KNO_3 2 *M*. Les dendrites se forment à des potentiels supérieurs à −1.30 V et à des concentrations dépassant 0.0175 *M* (Fig. 4). Dans le cas du

thallium, les particules ont la forme dendritique la plus caractéristique et sont très luisantes. En général, la poudre se détache de la goutte et tombe dans la solution. Parfois, pendant le mouvement de la surface de la goutte, des particules se dissolvent très rapidement dans le mercure, donnant l'impression d'une disparition instantanée. Les poudres se forment toujours sous la forme de rameaux isolés, spécialement dans la période finale de la formation de la goutte.

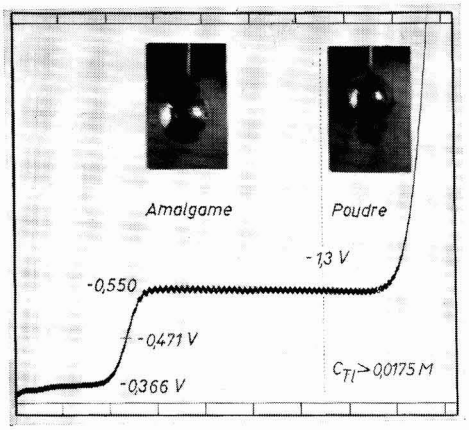

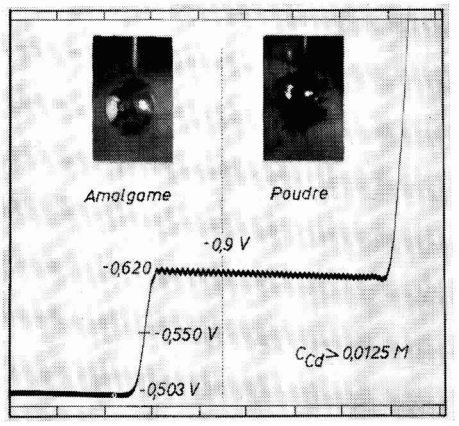

Fig. 4. Comme Fig. 1 pour ions de thallium ($TlNO_3$).

Fig. 5. Comme Fig. 1 pour ions de cadmium ($CdCl_2$).

Cadmium. Nous avons utilisé des solutions de $CdCl_2$, KNO_3 2 *M*. Le potentiel de formation de la poudre est situé à −0.90 V, la limite de la concentration à 0.0125 *M* (Fig. 5). L'aspect de la poudre de cadmium est semblable à celui de la poudre de plomb. Par rapport aux autres métaux la formation des dendrites de cadmium présente les phénomènes les plus caractéristiques. Dans l'intervalle de concentration de 0.1–0.4 *M* il n'y a pas formation des dendrites avec le capillaire lent (2). Par contre si on utilise le capillaire rapide (1) les dendrites se forment en grande quantité à partir du potentiel limite de −0.90 V. A la concentration de 0.05 *M* on n'observe plus la formation de dendrites sur la goutte avec le capillaire (2), mais l'apparition de la poudre est nette avec le capillaire (1) jusqu'à la concentration en $CdCl_2$ de 0.025 *M*. A cette valeur de la concentration, les dendrites se forment en général sur la première goutte (capillaire droite, en position verticale) à −0.90 V, mais elles ne se forment plus sur les autres gouttes. Si on utilise des solutions saturées en KNO_3, assez concentrées en cadmium (~0.5 *M*) et en présence de gélatine (~0.06%) on constate l'apparition des dendrites en forme d'aiguilles avec le capillaire lent au commencement de la formation de la goutte. Ces dendrites se dissolvent dans le mercure avec une vitesse relativement petite et on peut constater un dégagement intense d'hydrogène sur les portions non dissoutes.

Argent. Dans le cas de l'argent nous avons utilisé une solution de $AgNO_3$, H_2SO_4 3 *M*. Le potentiel de formation des dendrites est situé à −0.30 V et la concentration minimale est de 0.016 *M*. Des cristaux luisants se forment en grande quantité à la partie inférieure de la goutte et se dissolvent rapidement dans le mercure. Les

dendrites se forment particulièrement dans la période initiale de la croissance de la goutte. L'observation du phénomène au microscope est rapidement gênée par la précipitation de AgCl: le précipité apparait rapidement au voisinage du diaphragme de cellophane et diffuse dans l'espace cathodique.

Influence du pH et de substances étrangères

La concentration en ions d'hydrogène influence la formation des poudres en favorisant ou en empêchant la formation des dendrites. Dans les solutions ammoniacales contenant des ions cuivriques il n'a pas été possible d'observer la formation de dendrites sur l'électrode à goutte, alors que, sur les électrodes solides, la poudre de cuivre se forme facilement dans ces conditions[1]. En milieu neutre et acide on observe toujours la formation de poudre de cuivre sur l'électrode à goutte. Il est à remarquer qu'une croissance considérable de la concentration en acide ne modifie pas visiblement la valeur du potentiel de formation de la poudre (Fig. 6). Un comportement analogue a été observé dans le cas du thallium. La croissance de l'alcalinité ne modifie pas le potentiel de formation de la poudre (Fig. 6) mais, à un potentiel donné, elle augmente la quantité de poudre formée.

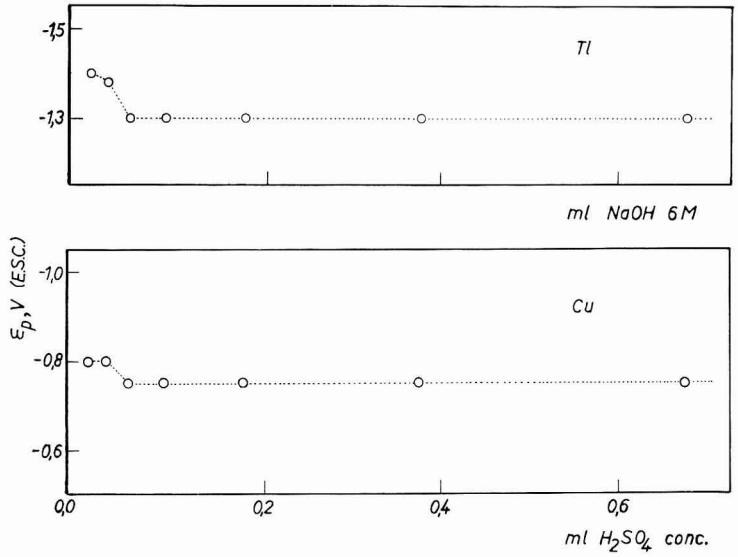

Fig. 6. Influence de la présence d'hydroxyde de sodium sur le potentiel de formation de la poudre de thallium et d'acide sulfurique sur le potentiel de formation de la poudre de cuivre.

La formation des poudres est favorisée en général par la présence de l'ion nitrate. L'apport d'autres ions, même en quantité relativement grande n'a pas d'influence visible sur le processus.

La présence de gélatine favorise la formation des dendrites: la quantité de poudre formée augmente et le seuil de la concentration diminue.

Série des potentiels de formation des poudres métalliques sur l'électrode à goutte de mercure

La Fig. 7 donne les potentiels de formation des poudres en fonction de la

concentration en ions métalliques pour plusieurs métaux. On remarque que ces potentiels ne dépendent pas de la concentration en ions métalliques dans les limites de la précision des déterminations expérimentales. Il semble difficile de faire une corrélation entre la valeur du potentiel de formation des poudres et une propriété du métal considéré. Les conditions de totale irréversibilité qui semblent caractériser le processus de formation des poudres métalliques rend encore plus difficile cette corrélation.

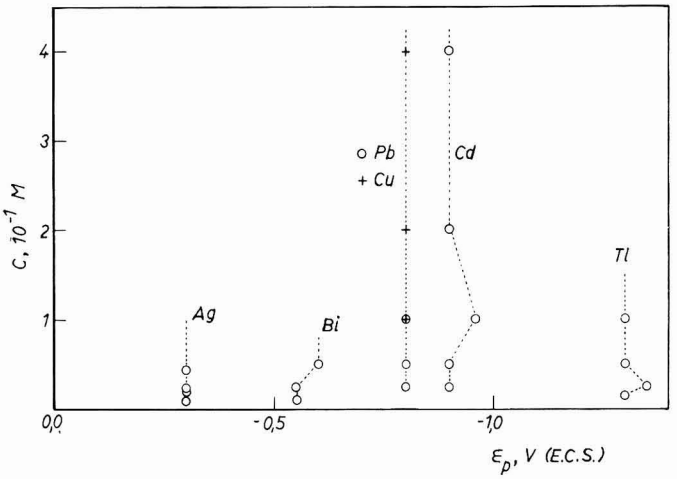

Fig. 7. Série des potentiels de formation de poudre (ε_p) sur l'électrode à goutte de mercure en fonction de la concentration en ion métallique. $AgNO_3$, H_2SO_4 3 M; $Bi(NO_3)_3$, HCl 4 M; $Pb(NO_3)_2$, $CuCl_2$, $CdCl_2$ et $TlNO_3$ en KNO_3 2 M; gélatine 0.05%.

INTERPRÉTATION ET DISCUSSION DES RÉSULTATS

Mécanisme de formation des poudres métalliques sur l'électrode à goutte de mercure

La formation des dendrites sur l'électrode à goutte de mercure apporte des données supplémentaires pour l'élucidation du problème de la formation de poudre métallique par électrolyse. Dans ce cas il faut tenir compte des deux conditions particulières suivantes: (1) la surface de la goutte, continuellement renouvelée, exclue l'influence spécifique d'une surface irrégulière; (2) tous les métaux étudiés dans le présent travail forment facilement un amalgame avec le mercure, de sorte que le métal qui est en contact avec l'électrode est immédiatement dissous.

L'explication la plus simple de la formation des dendrites serait de considérer que, sur la surface de la goutte, dans la zone du courant limite, des combinaisons intermétalliques se forment et subsistent un certain temps à la surface; sur ces combinaisons intermétalliques se produit ensuite la croissance des dendrites métalliques lorsqu'on applique à l'électrode un certain potentiel.

Toutes les observations expérimentales faites lors de la formation des dendrites sur l'électrode à goutte de mercure démentent cette explication. Nous donnons dans ce qui suit les preuves de cette infirmation:

(1) Il semble difficile d'accepter que, sur une surface qui augmente conti-

nuellement, des centres de dimensions très petites et qui sont très solubles peuvent rester dans cet état pendant plusieurs secondes, surtout dans le cas du thallium qui forme un amalgame liquide même à une teneur de 40% en Tl; il faut encore mentionner que la concentration en ions métalliques est très faible, de l'ordre de 0.01 M[9].

(2) Les dendrites se meuvent sur la surface de la goutte.

(3) Lorsque le déplacement de la surface de la goutte en expansion, ou le mouvement des courants liquides assure un contact réel de la goutte avec la particule métallique, celle-ci se dissout rapidement dans le mercure.

(4) En général on n'observe pas de dégagement d'hydrogène sur les dendrites; ce dégagement devrait se produire dans le cas où il y aurait réellement contact entre le mercure et la particule métallique, puisque la surtension de l'hydrogène est plus petite sur les métaux étudiés que sur le mercure. Sur les particules de cadmium cependant il est possible parfois d'observer le dégagement d'hydrogène, mais seulement après le commencement de la dissolution des dendrites; il est donc nécessaire qu'un bon contact soit réalisé avec la goutte.

(5) La formation des dendrites dépend de la vitesse de croissance de la goutte. En général les dendrites ne se forment pas dans la période finale, lorsque en raison du volume appréciable de la goutte le déplacement de la surface de celle ci est lent. Dans le cas du cadmium ($c=0.1$–0.4 M) les dendrites ne se forment pas avec les capillaires lents ($t_1=90$ sec), mais leur apparition est intense sur les capillaires rapides ($t_1=3$ sec).

(6) Les substances adsorbantes, comme la gélatine, favorisent la formation des dendrites.

Ces résultats expérimentaux que nous venons de présenter semblent indiquer qu'il n'y a pas de contact direct entre la particule métallique et l'électrode. Mais il n'est pas possible de fournir une preuve directe, basée sur la mesure de la distance de séparation. A cet égard il est à remarquer que cette distance a un sens statistique et qu'il faut considérer sa valeur moyenne[10,11].

La formation des particules métalliques dans le voisinage de l'électrode à des potentiels très négatifs, a été considérée par la théorie quantique de la formation des poudres métalliques[1,4,10,11]. Dans le cas des potentiels négatifs il y a une probabilité assez grande pour la neutralisation de l'ion métallique à une certaine distance de l'électrode. De cette façon des particules métalliques peuvent se former dans le voisinage immédiat de la surface de la goutte. Les substances adsorbantes, telles que la gélatine ou les hydroxydes qui se forment dans la zone du courant limite isolent, et en même temps jouent le rôle d'adhésif et "collent" à la surface les particules qui ne se dissolvent plus dans le mercure (Fig. 8-1). En raison de la très petite distance qui existe entre la particule métallique et l'électrode, un certain contact électrique imparfait peut assurer la croissance des dendrites collées (Fig. 8-2). Lors du mouvement de la surface de la goutte ou du déplacement de la dendrite métallique la couche adsorbante adhésive peut être rompue et la dendrite se dissout immédiatement dans la goutte de mercure (Fig. 8-3), comme on peut l'observer expérimentalement. Il est donc possible d'expliquer l'action favorable de la gélatine par la formation de couches isolantes qui "collent" les particules formées à la surface. L'influence de la vitesse de déplacement de la surface de la goutte s'interprète également: la vitesse est optimale, lorsque, par l'avancement de la surface, les couches adsorbées deviennent assez minces, de sorte que le courant peut passer entre l'électrode et la particule

formée à distance; si la vitesse de mouvement est trop grande, la couche adsorbée est rompue, les particules formées à distance sont immédiatement assemblées par la surface mouvante qui les dissout; si la vitesse est trop petite, la couche adsorbée n'est pas assez mince pour rendre possible le passage du courant et la dendrite ne peut plus croître.

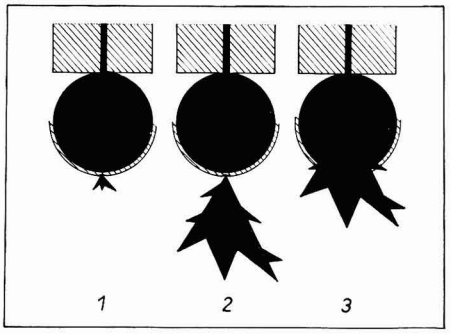

Fig. 8. Formation (1), croissance (2) et dissolution (3) d'une dendrite métallique sur l'électrode à goutte de mercure.

Expression du potentiel de formation de poudres métalliques sur l'électrode à goutte de mercure

Dans un travail antérieur[11] nous avons montré que, du fait de la surtension de diffusion très grande atteinte dans le domaine du courant limite il existe une certaine probabilité de neutralisation des ions dans la solution. De cette manière les atomes métalliques hydratés peuvent se former dans la solution. On peut donc considérer le système rédox:

$$Me_{aq.}^{z+} \cdot Me_{aq.}^{0}$$

qui existe dans une zone près de la surface de l'électrode. Les atomes hydratés, $Me_{aq.}^{0}$, formés à une distance finie de la surface de l'électrode de mercure ne forment plus d'amalgame et peuvent créer des noyaux isolés de cristallisation. D'une manière analogue au traitement appliqué dans le cas des électrodes solides[11], nous déduirons l'expression du potentiel de formation de poudre sur l'électrode à goutte de mercure.

Pour la réaction:

$$Hg + Me_{aq.}^{0} \rightarrow Me^{0}(Hg) \qquad (1)$$

on peut écrire la différence entre les enthalpies qui correspondent à l'atome solvaté et à l'atome à l'état d'amalgame. Cette différence, ΔH^0, est égale à l'enthalpie de sublimation, L, augmentée de l'enthalpie de formation d'amalgame à partir du métal solide A, et diminuée de la chaleur d'hydratation du métal, H_{Me}:

$$\Delta H^0 = L + A - H_{Me} \qquad (2)$$

Afin d'écrire la différence des potentiels chimiques il faut prendre en considération les différences d'entropie liées à l'éqn. (1). On note avec $-T\Delta S_2$ la chaleur qui correspond à l'effet Peltier du métal sous forme d'amalgame. Une énergie analogue

doit être prise en considération pour la variation d'entropie correspondant à l'atome métallique solvaté, ΔS_1[11].

La différence des potentiels chimiques est représentée par l'équation suivante:

$$\Delta\mu^0 = L + A - H_{Me} - T(\Delta S_1 + \Delta S_2) \quad (3)$$

A partir du potentiel chimique il est possible d'écrire la différence de deux potentiels absolus d'électrode. A la place de celle-ci on peut écrire la différence de tensions des cellules[11] et de cette manière nous arrivons à la relation suivante, liant le potentiel standard, $\varepsilon_p{}^0$, qui correspond à la réduction d'un ion à l'atome solvaté et le potentiel de demi-vague, $\varepsilon_{Me^{\frac{1}{2}}}$:

$$\varepsilon_p{}^0 = \varepsilon_{Me^{\frac{1}{2}}} + \{L + A - H_{Me} - T(\Delta S_1 + \Delta S_2)\}/zF \quad (4)$$

Pratiquement les réactions à l'électrode dans le cas de la formation de poudre sont irréversibles; il faut donc tenir compte de l'inégalité:

$$\varepsilon_p \geqslant \varepsilon_{Me^{\frac{1}{2}}} + \{L + A - H_{Me} - T(\Delta S_1 - \Delta S_2)\}/zF \quad (5)$$

La différence de forme entre l'inégalité (5) qui correspond au potentiel de formation de poudre sur l'électrode à goutte, par rapport à l'inégalité, qui correspond aux électrodes solides, est que dans le cas de l'électrode de mercure il faut aussi prendre en considération la chaleur de formation d'amalgame.

Notons enfin que les éqns. (4) et (5) ne tiennent pas compte de l'existence de pellicules adsorbées.

RÉSUMÉ

Sur l'électrode à goutte de mercure les poudres métalliques se forment à une valeur caractéristique du potentiel, située dans le domaine du courant limite. L'apparition et la croissance des dendrites sont conditionnées par une certaine vitesse de déplacement de la surface de la goutte. L'apport de gélatine et de nitrate favorise la formation des dendrites. Le seuil inférieur de la concentration en ions métalliques pour lequel on peut observer la formation des dendrites est en général situé à environ 0.01 *M*.

Nous avons déterminé les potentiels de formation des poudres pour quelques métaux qui forment un amalgame avec le mercure.

Nous avons déduit finalement une expression qui montre la signification des potentiels de formation des poudres sur l'électrode à goutte de mercure.

SUMMARY

On the dropping mercury electrode metal powders are formed at a characteristic value of potential, situated in the limiting current region. The formation and growth of the dendrites are conditioned by a certain rate of displacement of the drop surface. The addition of gelatine and of nitrate favours dendrite formation. The lower threshold of metal ion concentration for which it is possible to observe dendrite formation, is about 0.01 *M*.

The potentials of powder formation for some metals forming an amalgam with mercury have been determined.

Finally, an expression showing the significance of potentials of powder formation on the dropping mercury electrode has been deduced.

BIBLIOGRAPHIE

1 A. CĂLUȘARU, *Depunerea electrolitica a metalelor în formă dispersă*, Editura Academiei Române, București, 1962.
2 N. KUDRIATZEV, *Tr. Soveshch. Elektrokhim., Akad. Nauk SSSR, Otd. Khim. Nauk*, 1950 (1953) 258.
3 N. IBL ET K. SCHADEG, *J. Electrochem. Soc.*, 114 (1967) 54.
4 N. IBL, *Advan. Electrochem. Electrochem. Eng.*, 2 (1962) 49–143.
5 A. CĂLUȘARU ET J. KŮTA, *Nature*, 211 (1966) 1080.
6 J. KŮTA ET I. SMOLER, *Collection Czech. Chem. Commun.*, 26 (1961) 224.
7 A. CĂLUȘARU, *Rev. Chim. (Bucharest)*, 8 (1957) 369.
8 I. ATANASIU ET A. CĂLUȘARU, *Rev. Roumaine Met. Acad. Rep. Populaire Roumaine*, 3 (1958) 109.
9 J. KORYTA, *Advan. Electrochem. Electrochem. Eng.*, 6 (1967) 289.
10 A. CĂLUȘARU ET I. ATANASIU, *Rev. Roumaine Met. Acad. Rep. Populaire Roumaine*, 5 (1960) 291.
11 A. CĂLUȘARU, *Electrochim. Acta*, 12 (1967) 1507.

ELECTROANALYTICAL CHEMISTRY AND INTERFACIAL ELECTROCHEMISTRY
Elsevier Sequoia S.A., Lausanne – Printed in The Netherlands

EQUATIONS OF THE POLAROGRAPHIC WAVES OF SIMPLE OR COMPLEXED METAL IONS

IV. THE METAL ION IS REDUCED WITH AMALGAM FORMATION FROM A SERIES OF COMPLEXES FORMED WITH A NON-HYDROLYSABLE LIGAND

MIHAIL E. MACOVSCHI
Institute of Physical Chemistry of Roumanian Academy of Sciences, Bucharest (Roumania)
(Received August 28th, 1968)

In previous work[1-3], equations of the polarographic waves were studied for complexes for the reduction step of the metal ion:

$$Me^{n+} \rightarrow Me^0(Hg) \tag{1}$$

with the assumption that only the ions, M, X and the complex MX_q (and of course the supporting electrolyte) exist in solution.

The results obtained are of interest for those cases when, apart from a given complex, all other complexes in solution, being in very low proportion, can be neglected. They are also a comparison basis for the following results.

The present paper begins the study of the reduction step (1) for a series of complexes and deals with the case of a non-hydrolysable ligand.

The notations used are as in the previous work[1-3].

The complexes formed are MX_0 (or M), MX, MX_2, ... MX_{q_m} (where q_m is the number of ligands in the last complex that can be formed). Their dissociation constants, both at the dropping electrode surface and in the bulk solution are:

$$\beta_0 = C_M f_M / C_M f_M = C^0_M f_M / C^0_M f_M = 1 \tag{2a}$$

$$\beta_q = C_M f_M (C_X f_X)^q / C_{MX_q} f_{MX_q} = C^0_M f_M (C^0_X f_X)^q / C^0_{MX_q} f_{MX_q} \tag{2b}$$

$$\beta_{q_m} = C_M f_M (C_X f_X)^{q_m} / C_{MX_{q_m}} f_{MX_{q_m}} = C^0_M f_M (C^0_X f_X)^{q_m} / C^0_{MX_{q_m}} f_{MX_{q_m}} \tag{2c}$$

For the concentrations of species M and X, the following relations are also valid.

$$\left.\begin{aligned} C_X^{tot} &= C_X + \sum_0^{q_m} q C_{MX_q} \\ (C^0_X)^{tot} &= C^0_X + \sum_0^{q_m} q C^0_{MX_q} \end{aligned}\right\} \tag{3a, 3b}$$

$$\left.\begin{aligned} C_M^{tot} &= \sum_0^{q_m} C_{MX_q} \\ (C^0_M)^{tot} &= \sum_0^{q_m} C^0_{MX_q} \end{aligned}\right\} \tag{4a, 4b}$$

I. EQUATION OF THE POLAROGRAPHIC WAVE

The transport phenomena, in the neighbourhood of the dropping mercury electrode, that accompany the passing of the electric current through the solution, are illustrated in Fig. 1.

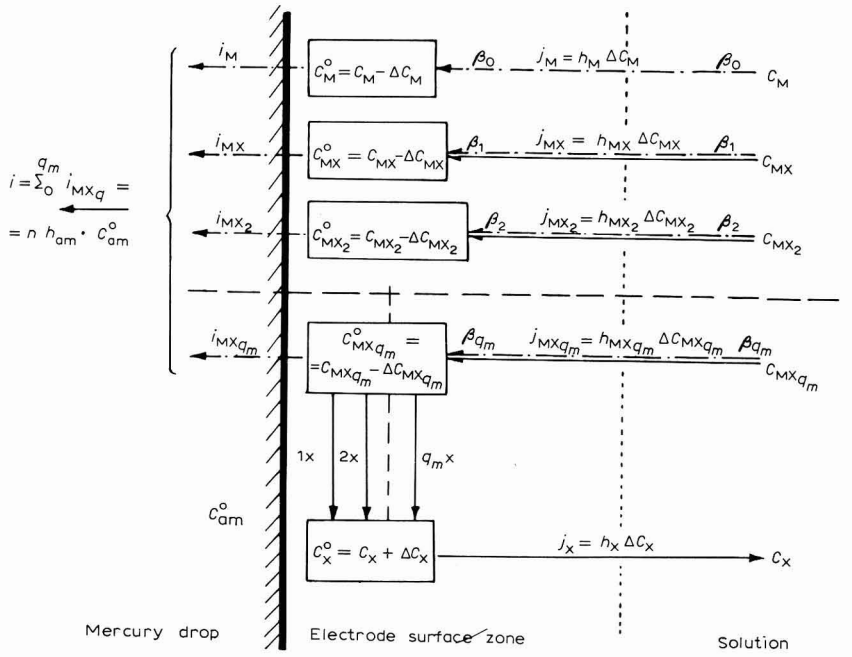

Fig. 1. Distribution of concentrations, diffusion and ionic equilibrium near the dropping electrode surface. (– · –), Mass circuit of species M; (———), mass circuit of species X.

In quasi-stationary conditions the following relations are valid for the mass currents[2] into the system:

$$j_{am} = h_{am} C^0_{am} = \sum_0^{q_m} j_{MX_q} = \sum_0^{q_m} h_{MX_q} \Delta C_{MX_q} = \sum_0^{q_m} h_{MX_q} (C_{MX_q} - C^0_{MX_q}) \tag{5}$$

$$j_X = h_X \Delta C_X = h_X (C^0_X - C_X) = \sum_0^{q_m} q j_{MX_q} = \sum_0^{q_m} q h_{MX_q} \Delta C_{MX_q} = \sum_0^{q_m} q h_{MX_q} (C_{MX_q} - C^0_{MX_q}) \tag{6}$$

At the same time, we have for the electric current:

$$i = nF j_{am} \tag{7}$$

It follows from relations (5) and (7):

$$i_d - i = nF \sum_0^{q_m} h_{MX_q} C^0_{MX_q} \tag{8}$$

where

$$i_d = nF \sum_0^{q_m} h_{MX_q} C_{MX_q} \tag{9}$$

The dropping electrode potential is given by the thermodynamic relation:

$$E = \varepsilon - (RT/nF) \ln (C^0_{am} f_{am} / C^0_M f_M) \tag{10}$$

Taking into account (5) and (7) and the expression for the half-wave potential of the simple metal ion (written in terms of the mass current):

$$E^M_{\frac{1}{2}} = \varepsilon - (RT/nF) \ln (f_{am} h_M / f_M h_{am}) \tag{11}$$

relation (10) becomes:

$$E = E^M_{\frac{1}{2}} - (RT/nF) \ln (i/nF h_M C^0_M) \tag{12}$$

C^0_M in (12) is replaced by the value obtained from (8) and (2):

$$C^0_M = (i_d - i) \Big/ nF \sum_0^{q_m} \{h_{MX_q} f_M (C^0_X f_X)^q / f_{MX_q} \beta_q\} \tag{13}$$

to give:

$$E = E^M_{\frac{1}{2}} - \frac{RT}{nF} \ln \left\{ \frac{i}{i_d - i} \sum_0^{q_m} \frac{h_{MX_q} f_M (C^0_X f_X)^q}{h_M f_{MX_q} \beta_q} \right\} \tag{14}$$

C^0_X is calculated by means of relations (6), (2) and (13):

$$h_X (C^0_X - C_X) = \sum_0^{q_m} q h_{MX_q} C_{MX_q} - \sum_0^{q_m} q h_{MX_q} C^0_M f_M (C^0_X f_X)^q / f_{MX_q} \beta_q =$$

$$= \sum_0^{q_m} q h_{MX_q} C_{MX_q} - \frac{i_d - i}{nF} \sum_0^{q_m} \frac{q h_{MX_q} (C^0_X f_X)^q}{f_{MX_q} \beta_q} \Big/ \sum_0^{q_m} \frac{h_{MX_q} (C^0_X f_X)^q}{f_{MX_q} \beta_q} \tag{15}$$

Rearrangement of the terms in the relation (15) gives:

$$\Psi_q \equiv \sum_0^{q_m} (h_{MX_q} f_M / h_M f_{MX_q} \beta_q) \left\{ (C^0_X f_X)^{q+1} / f_X \right.$$

$$\left. + \left[q(i_d - i)/nF h_X - C_X - \sum_0^{q_m} p h_{MX_p} C_{MX_p} / h_X \right] (C^0_X f_X)^q \right\} = 0 \tag{16a}$$

or in another form:

$$\Psi_q \equiv \frac{h_{MX_{q_m}} f_M}{h_M f_{MX_{q_m}} f_X B_{q_m}} (C^0_X f_X)^{q_m+1} + \sum_0^{q_m} \left(q \frac{i_d - i}{nF h_X} - C_X - \sum_1^{q_m} p \cdot \frac{h_{MX_p}}{h_X} C_{MX_p} \right.$$

$$\left. + \frac{\beta_q h_{MX_{q-1}} f_{MX_q}}{\beta_{q-1} h_{MX_q} f_{MX_{q-1}} f_X} \right) \frac{h_{MX_q} f_M}{h_M f_{MX_q} \beta_q} (C^0_X f_X)^q - C_X - \sum_1^{q_m} p \cdot \frac{h_{MX_p}}{h_X} C_{MX_p} = 0 \tag{16b}$$

The solution ψ

$$\psi \equiv C^0_X f_X \geqslant C_X f_X \tag{17}$$

of the function Ψ_q (relation (16)) introduced in (14) gives the polarographic wave equation:

$$E = E^{M}_{\frac{1}{2}} - \frac{RT}{nF} \ln \left\{ \frac{i}{i_d - i} \sum_{0}^{q_m} \frac{h_{MX_q} f_M \psi^q}{h_M f_{MX_q} \beta_q} \right\} \tag{18}$$

II. THE EQUATION OF THE POLAROGRAPHIC WAVE OF THE SIMPLE METAL ION

The condition that no complex be formed may be expressed in three ways: (a) $q_m = 0$; (b) $\beta_0 = 1$, $\beta_1 = \ldots = \beta_{q_m} = 0$ and (c) $C_X^{tot} = 0$ (*i.e.*, $C_X = 0$, $C_{MX} = 0, \ldots C_{MX_{q_m}} = 0$). In cases (a) and (b), $\psi = C_X f_X$ and in case (c) $\psi = 0$. Consequently in all the three cases eqn. (18) is transformed into the polarographic wave equation of the simple metal ion[4].

III. DISCUSSION OF EQUATION (18) FOR THE CASE OF A SINGLE COMPLEX ($q = 0$ and $q = q$)

A. In the previous papers[1-3] the inferred equation of the polarographic wave had a different form from that of relation (18), *i.e.*,

$$E = E^{M}_{\frac{1}{2}} - (RT/nF) \ln (i/\varphi) \tag{19}$$

The difference is explained as follows:

To write the polarographic wave equation, the value of C_M^0 must be known (see relation (12)). As has been shown, this value is calculated from a system with two unknowns: C_M^0 and C_X^0, a system that results from the combination of eqn. (2) and the mathematical relation describing the transport phenomena in the neighbourhood of the dropping electrode, (5), (6) and (7).

In the case of a single complex, the equality:

$$j_{MX_q} = j_{am} - j_M \tag{20}$$

makes the elimination of C_X^0 more convenient than the elimination of C_M^0, in solving the equation system obtained. Therefore, an equation in C_M^0, $\Phi = 0$ results, the solution, φ, of which when introduced in relation (12) gives the form (19) of the polarographic wave equation.

In the case of a complex series, as

$$j_{am} = \sum_{0}^{q_m} j_{MX_q} \tag{5}$$

the elimination of C_X^0 is no longer possible, and it is necessary to eliminate C_M^0. Thus, the calculation leads to function Ψ_q (relation (16)) instead of Φ and eqn. (18) has not the same form as eqn. (19).

Otherwise, if in the case of a single complex (ref. 1) we eliminate C_M^0 instead of C_X^0, we obtain the following result:

$$E = E^{M}_{\frac{1}{2}} - (RT/nF) \ln \{[1 + h_{MX_q} f_M (C_X^0 f_X)^q / h_M f_{MX_q} \beta_q] \cdot (i/i_d - i)\} \tag{21}$$

and

$$\Psi_{0,q} \equiv (h_{MX_q} f_M / h_M f_{MX_q} \beta_q) \{(C_X^0 f_X)^{q+1}/f_X + [q(i_d - i)/nFh_X - C_X - q h_{MX_q} C_{MX_q}/h_X](C_X^0 f_X)^q\} + C_X^0 - C_X - q h_{MX_q} C_{MX_q}/h_X = 0 \tag{22}$$

It can be seen that relations (21) and (22) are special cases of relations (14) and (16) and are obtained if the summations from (14) and (16) are reduced to the terms for $q = 0$ and $q = q$.

B. Equation (22) (eqn. (16) specified for a single complex) may be solved with corresponding limiting conditions, to produce the special cases discussed in a former paper[1]:

—for C_X very high ($C_X \approx C_X^{tot}$), the equation of Buck[5] (if β_q is high) or of Lingane[6] (if β_q is low) are obtained.

— for C_X equal to 0 or very low, it is necessary to have β_q very low for eqn. (22) to be solved, *i.e.*,

$$(C_X^0)^q/\beta_q \gg C_X^0 \tag{23}$$

(equivalent to $i \approx i_{MX_q}$); in these conditions (21) transforms, if $C_X = 0$, in the Butler and Kaye[7] equation, or in eqn. (64) ref. 1, if $C_X \neq 0$.

C. The ratio

$$\sum_0^{q_m} q h_{MX_q}(C_X^0 f_X)^q/f_{MX_q}\beta_q \Big/ \sum_0^{q_m} h_{MX_q}(C_X^0 f_X)^q/f_{MX_q}\beta_q$$

from relation (15) represents, in fact, the average value of the ligand number in the complexes formed at the dropping electrode and under the given conditions[8], *i.e.*,

$$\sum_0^{q_m} q \frac{h_{MX_q}(C_X^0 f_X)^q}{f_{MX_q}\beta_q} \Big/ \sum_0^{q_m} \frac{h_{MX_q}(C_X^0 f_X)^q}{f_{MX_q}\beta_q} = \overline{q^0} \tag{24}$$

As a result, C_X^0 can be expressed in terms of $\overline{q^0}$ (see relation (15)):

$$C_X^0 = C_X + \overline{q_i^0}/nFh_X + \sum_0^{q_m}(h_{MX_q}/h_X)C_{MX_q}(q - \overline{q^0}) \tag{25}$$

For a single complex ($q = 0$ and $q = q$) $\overline{q^0}$ takes the form:

$$\overline{q^0} = q/\{1 + [h_M f_{MX_q}\beta_q]/[h_{MX_q} f_M (C_X^0 f_X)^q]\} \tag{26}$$

Relation (26) shows that the ratio of the concentration of ions M and MX_q is different at the dropping electrode surface from that in the solution; this is quite normal and is due to the passage of the electric current through the solution.

IV. DISCUSSION OF EQUATIONS (16) AND (18) FOR THE COMPLEX SERIES

A. Possibilities of eqn. (18) solving in limiting conditions

Equation (16a) can be written:

$$\Psi_q \equiv \sum_0^{q_m}(h_{MX_q} f_M/h_M f_{MX_q}\beta_q)(C_X^0 f_X)^q \times \left[C_X^0 + q(i_d - i)/nFh_X - C_X - \sum_0^{q_m} p(h_{MX_p}/h_X)C_{MX_p}\right] = 0 \tag{27}$$

If the term $q(i_d - i)/nFh_X$ in the parenthesis can be neglected in comparison with the other terms, then eqn. (27) may be split in two equations:

$$C_X^0 - \psi = 0 \tag{28a}$$

$$\sum_0^{q_m}(h_{MX_q} f_M/h_M f_{MX_q}\beta_q)(C_X^0 f_X)^q = 0 \tag{28b}$$

of which only eqn. (28a) has a positive solution. But it must be shown that terms, $q(i_d - i)/nFh_X$ and $\Sigma_0^{q_m} p(h_{MX_p}/h_X)C_{MX_p}$, in the parenthesis are of the same order of magnitude and therefore cannot be neglected in relation to one another*. We have therefore the following cases:

(a), $q(i_d - i)/nFh_X$ and $\Sigma_0^{q_m} p(h_{MX_p}/h_X)C_{MX_p}$ are neglected in comparison with C_X^0 and C_X; the case of DeFord and Hume[9], that will be discussed further below, is found.

(b), Neglecting $q(i_d - i)/nFh_X$, $\Sigma_0^{q_m} p(h_{MX_p}/h_X)C_{MX_p}$ and C_X, gives $\psi = 0$ and the case of the simple metal ion is found (§2).

(c), If we neglect only C_X (approximation of Butler and Kaye type) then eqn. (27) is no longer split into the two equations (28a) and (28b), because the parenthesis depends on the summation index q, in other words, eqn. (27) is no longer solvable in the general case. This contrasts with the case of a single complex when the equation of Butler and Kaye[7] or eqn. (64) of ref. 1 are found.

This shows that in the case of a complex series, DeFord and Hume's relation represents the single possibility of simplification of the general relations.

B. DeFord and Hume[9] case

We have shown that eqn. (16) can be solved in the general case only if C_X is very high (approximation of Lingane type) or in other words, $C_X = C_X^{tot}$. Then from (28a)

$$C_X^0 f_X = C_X^{tot} f_X \tag{29}$$

As a consequence, (18) transforms into:

$$E = E_{\frac{1}{2}}^M - (RT/nF) \ln (i/i_d - i) - (RT/nF) \ln \sum_0^{q_m} h_{MX_q} f_M (C_X^{tot} f_X)^q / h_M f_{MXq} \beta_q \tag{30}$$

Relation (30) shows that in the DeFord and Hume case, as in all cases deriving from Lingane-type approximations, the shape of the polarographic wave is normal, the dropping electrode potential depending upon $\ln \{i/(i_d - i)\}$.

To find the equation given by DeFord and Hume, the average constant of the mass current, $\overline{h_{MX_q}}$, is used (written as a function of C_X^{tot} because the discussion is carried out in a Lingane-type approximation):

$$\overline{h_{MX_q}} = \sum_0^{q_m} h_{MX_q} \frac{f_M (C_X^{tot} f_X)^q}{f_{MX_q} \beta_q} \Bigg/ \sum_0^{q_m} \frac{f_M (C_X^{tot} f_X)^q}{f_{MX_q} \beta_q} \tag{31}$$

Taking into account (31), for $i = i_d/2$, (30) becomes**:

$$E_{\frac{1}{2}}^C = E_{\frac{1}{2}}^M - (RT/nF) \ln \left\{ (\overline{h_{MX_q}}/h_M) \sum_0^{q_m} f_M (C_X^{tot} f_X)^q / f_{MX_q} \beta_q \right\} \tag{32}$$

C. The shape of the polarographic waves in the general case

Taking into account (25), (18) becomes:

---

* In the special case when $C_X^{tot} = 0$, then $\Sigma_0^{q_m} p(h_{MX_p}/h_X)C_{MX_p} = 0$ and $i_d/nFh_X = (h_M/h_X)C_M > 0$; as soon as a small quantity of ligand is added (C_X^{tot} comparable with C_M^{tot}) the values of the terms $q(i_d - i)/nFh_X$ and $\Sigma_0^{q_m} p(h_{MX_p}/h_X)C_{MX_p}$ become comparable.

** DeFord and Hume gave relation (32) in the terms of "Ilkovič constants" k (and not in the terms of the mass current); therefore in the original paper (relations (14) and (15) from ref. 9) $\overline{I_C}/I_M$ appears instead of $\overline{h_{MX_q}}/h_M$ ($\overline{h_{MX_q}}/h_M = nF\overline{h_{MX_q}}/nFh_M = \overline{I_C}/I_M$).

$$E = E^{M}_{\frac{1}{2}} - \frac{RT}{nF} \ln \left\{ \frac{i}{i_d - i} \sum_{0}^{q_m} \frac{h_{MX_q} f_M f_X^q \left[C_X + \overline{q^0}\, i/nFh_X + \sum_{0}^{q_m} h_{MX_p} C_{MX_p} (q - \overline{q^0})/h_X \right]}{f_{MX_q} h_M \beta_q} \right\} \tag{33}$$

Noting:

$$\sum_{0}^{q_m} \frac{h_{MX_q} f_M f_X^q \left[C_X + (i/nFh_X)\overline{q^0} + \sum_{0}^{q_m} h_{MX_p} C_{MX_p} (q - \overline{q^0})/h_X \right]^q}{h_M f_{MX_q} \beta_q} = \sum_{0}^{q_m} P_q \cdot i^q \tag{34}$$

the equation of the polarographic wave can be written:

$$E = E^{M}_{\frac{1}{2}} - (RT/nF) \ln \left\{ \sum_{0}^{q_m} P_q \cdot i^{q+1})/(i_d - i) \right\} \tag{35}$$

Relation (35) shows that in the general case the potential of the dropping electrode depends on the sum of the i powers (the maximum power being $q_m + 1$) as compared with the classical dependence on the 1st power of i. Therefore, the shape of the polarographic wave can be modified in that: (i) the wave is no longer symmetrical about the half-wave potential and (ii) the slope of the wave decreases, it no longer corresponds to the number of electrons involved in the electrode process.

Let us analyse the conditions necessary for the appearance of this phenomenon. A study of relation (16b) leads to the conclusion that the coefficient with which $C^0_X f_X$ appears at different powers (except the maximum power q_{+1}) has the general form:

$$T_q \equiv \left[q(i_d - i)/nFh_X - C_X - \sum_{1}^{q_m} (ph_{MX_p} C_{MX_p}/h_X) + (\beta_q f_{MX_q} h_{MX_{q-1}}/\beta_{q-1} f_{MX_{q-1}} h_{MX_q} f_X) \right] (h_{MX_q} f_M / h_M f_{MX_q} \beta_q) \tag{36}$$

or approximating for all h equal to each other and all f equal to unity:

$$T_q \equiv [q(i_d - i)/nFh - C^{tot}_X + \beta_q/\beta_{q-1}] (1/\beta_q) \tag{37}$$

where $i_d/nFh \approx C^{tot}_M$. For the value of the T_q coefficient to be influenced by the parameter i, the following relations must hold:

$$q(i_d - i)/nFh \text{ comparable or } \gg \text{ as } C^{tot}_X \tag{38a}$$

$$q(i_d - i)/nFh \text{ comparable or } \gg \text{ as } \beta_q/\beta_{q-1} \tag{38b}$$

If one of these relations (or both) are not fulfilled, then the value of the coefficient T_q does not depend on i.

The form of the polarographic wave is modified only if C^0_X is dependent on i (see relations (17) and (18)), that is if both relations (38) are fulfilled for at least one of the T_q coefficients ($1 \leqslant q \leqslant q_m$): otherwise the form of the polarographic wave is the classical one.

The Lingane-type approximation assumes:

$$C^{tot}_X \gg q(i_d - i)/nFh \tag{39}$$

which is the opposite of relation (38a); this explains why in the case of the Lingane-type approximations the polarographic wave is always classical in form.

Relation (38b) shows that also in the general case when relation (39) is not fulfilled, unmodified polarographic waves can exist only if the consecutive dissociation constants:

$$\beta_{q,q-1} = C_X f_X C_{MX_{q-1}} f_{MX_{q-1}} / C_{MX_q} f_{MX_q} = \beta_q / \beta_{q-1} \tag{40}$$

of all complexes are high enough compared to $q(i_d - i)nFh$. As a result, for complexes that are not very stable, the undesirable effect of deformation of polarographic waves can be eliminated by lowering the metal ion concentration (so that $q(i_d - i)/nFh$ is 2–3 orders of magnitude lower than β_q/β_{q-1}).

D. Ringbom and Eriksson relation[10]

Ringbom and Erikson[10] found a particular form of relation (14) (but not relation (16)) which is relation (7) (ref. 10):

$$E = E^C_{\frac{1}{2}} - E^M_{\frac{1}{2}} = -(RT/nF) \ln [1 + C^0_X/\beta_1 + (C^0_X)^2/\beta_2 + \ldots + (C^0_X)^{q_m}/\beta_{q_m}] \tag{41}$$

They propose a method for calculating the dissociation constants of the complexes for the case of slight ligand excesses. Relation (41) results from relation (14) if all activity coefficients are assumed to be equal to 1, all diffusion coefficients (respective h) are equal to each other and $i = i_d/2$.

E. Particular case of solving eqn. (16)

Considering the frequent occurrence of complexes of forms, MX_2 and MX_3, the general solving of eqn. (16) for $q = 2$ and $q = 3$ would be of special interest. Theoretically this is possible because equations of the 3rd and 4th degree have to be solved. The calculations, however, are especially difficult because of the radicals and the impossibility of simplifying the equations (in the general case).

For the simplest case, when $q = 1$ (and therefore eqn. (16) is only of 2nd degree) the polarographic wave equation is:

$$\begin{aligned} E = {} & E^M_{\frac{1}{2}} - (RT/nF) \ln \{i/(i_d - i)\} \\ & - (RT/nF) \ln \left\{ 1 + (h_{MX} f_M f_X / 2\beta_1 h_M h_X f_{MX}) \left[h_X C_X + h_{MX} C_{MX} - (i_d - i)/nF \right.\right. \\ & \left.\left. - \beta_1 h_M h_X f_{MX} / h_{MX} f_M f_X \right.\right. \\ & \left.\left. + \left\{ \left(h_X C_X + h_M C_M - \frac{i_d - i}{nF} - \frac{\beta_1 h_M h_X f_{MX}}{h_{MX} f_M f_X} \right)^2 + 4 \frac{\beta_1 h_M h_X f_{MX}}{h_{MX} f_M f_X} (h_X C_X + h_{MX} C_{MX}) \right\}^{\frac{1}{2}} \right] \right\} \end{aligned}$$

V. CONCLUSIONS

The following conclusions can be drawn from the data presented above:

(a) Equation (18) contains the equation of the simple metal ion, the general equation (and therefore all the particular equations) for the case of a single complex and the known equations for the case of a complex series.

(b) In the case of a complex series there is a single equation (besides the equation of the simple metal ion) obtained in limiting conditions (DeFord and Hume equation) compared with 4 special equations in the case of a single complex[1]. Figure 2 gives a comparative illustration for the case of a complex series and for the case of a single complex and shows the fields of application of the different equations.

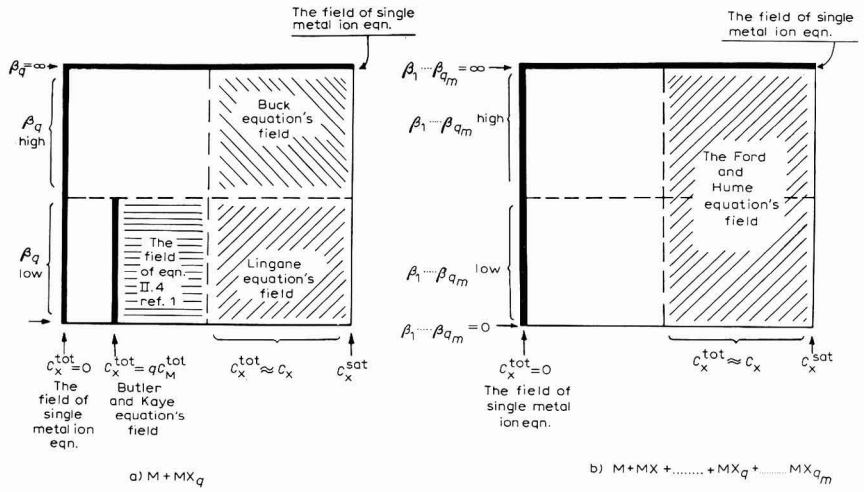

Fig. 2. Schematic representation of the field of application of the limiting equations. (a), For a single complex; (b), for a series of complexes. C_X^{sat}, satd. ligand concn.

(c) It is demonstrated that in the case of Lingane-type approximations, the polarographic waves are always classical in shape; in this case the potential of the dropping electrode depends on $\ln\{i/(i_d-i)\}$ and the slope of the waves corresponds to the number of electrons involved in the electrode process.

(d) In the general case the potential of the dropping electrode depends on the logarithm of the sum of the i powers from 1 to q_m+1. Consequently the shape of the polarographic waves will be modified as shown by a decrease of the slope compared with the value determined by the number of electrons changed at the electrode; at the same time, the wave is no longer symmetrical about the half-wave potential. The change will be smaller than in the case of a single complex because of the sum of the i powers (for a single complex it was $\ln\{i^{q+1}/(i_d-i)\}$).

(e) Theoretically, eqn. (16) can be solved exactly, with literal coefficients, until $q_m = 3$ (eqn. (16) of the 4th degree) but the results obtained would be of an especially complicated form. It is preferable therefore to work with numerical coefficients, and to solve eqn. (16) for each particular case.

SUMMARY

The present paper is the first on the study of a series of complexes for the reduction step, $Me^{n+} \rightarrow Me^0(Hg)$, and treats the case of a non-hydrolysable ligand. The polarographic wave equation has the form:

$$E = E_{\frac{1}{2}}^{M} - (RT/nF)\ln\left[\{i/(i_d-i)\}\cdot\sum_{0}^{q_m} h_{MX_q} f_M \psi^q / h_M f_{MX_q} \beta_q\right]$$

where ψ is the solution of an equation, $\Psi_{q_m} = 0$ and ψ/f_X represents the free ligand concentration at the mercury drop surface. The DeFord and Hume equation is obtained as a limiting case.

The conditions in which the shape of the polarographic wave is, or is not modified are discussed; it is demonstrated that in cases of Lingane approximations the polarographic waves are always of classical shape, and an explanation for this is given.

REFERENCES

1 M. MACOVSCHI, *J. Electroanal. Chem.*, 16 (1968) 457.
2 M. MACOVSCHI, *J. Electroanal. Chem.*, 18 (1968) 47.
3 M. MACOVSCHI, *J. Electroanal. Chem.*, 19 (1968) 219.
4 J. HEYROVSKY AND J. KUTA, *Tratat de Polarografie*, Academy R.P.R., 1959, p. 118.
5 R. P. BUCK, *J. Electroanal. Chem.*, 5 (1963) 295.
6 J. J. LINGANE, *Chem. Rev.*, 29 (1941) 1.
7 C. G. BUTLER AND R. C. KAYE, *J. Electroanal. Chem.*, 8 (1964) 463.
8 J. BJERRUM, Thesis, Copenhagen, 1941.
9 D. D. DEFORD AND N. D. HUME, *J. Am. Chem. Soc.*, 73 (1951) 5321.
10 A. RINGBOM AND L. ERIKSSON, *Acta Chem. Scand.*, 7 (1953) 1105.

ELECTROANALYTICAL CHEMISTRY AND INTERFACIAL ELECTROCHEMISTRY
Elsevier Sequoia S.A., Lausanne – Printed in The Netherlands

IONIC COMPONENTS AT THE REVERSIBLE AgI–AQUEOUS ELECTROLYTE INTERFACE

S. LEVINE
Department of Mathematics, University of Manchester, Manchester (England)
(Received April 17th, 1968; in final form, August 20th, 1968)

In an analysis of the surface excess of ions at a plane AgI–aqueous electrolyte interface, LYKLEMA[1,2] obtained the relations (in somewhat different notation)

$$e_0\Gamma_{\pm} = \pm e_0 \int \left(\frac{\partial \sigma_0}{\partial \mu}\right)_{\psi_0} \mathrm{d}\psi_0 - \tfrac{1}{2}\sigma_0 \pm K \tag{1}$$

by introducing certain assumptions. Here e_0 is the proton charge, $\Gamma_{\pm}$ are the surface excesses of cations and anions of an added uni–univalent electrolyte, σ_0 the surface charge density due to potential-determining ions (Ag^+, I^-), μ the chemical potential of the salt of the added electrolyte, ψ_0 the potential drop across the interface and K an integration constant. We wish to obtain the generalisation of (1), which is based on thermodynamics. The derivation of an electrocapillary equation for a reversible electrode, from which (1) is derived, was first given by GRAHAME AND WHITNEY[3] and generalised by MOHILNER[4] who modelled his treatment on the theory of ideal polarised electrodes by PARSONS AND DEVANATHAN[5–7]. Here we shall adapt the theory to the AgI–electrolyte interface. The analysis leading to the well-known equations, (8) and (9) below, differs from that of GRAHAME[8,9] for the mercury–solution interface, only in the way that the charge density, σ_0, is introduced. It will be assumed throughout that the temperature, T, and pressure, p, are fixed.

For a plane interface, with the dividing surface chosen to make the surface excess of water zero, and with H^+ and OH^- ions ignored when they are not species of the added electrolyte, the Gibbs adsorption equation reads

$$\mathrm{d}\gamma = -\Gamma_{Ag^+}\mathrm{d}\mu_{Ag^+} - \Gamma_{I^-}\mathrm{d}\mu_{I^-} - \Gamma_{+}\mathrm{d}\mu_{+} - \Gamma_{-}\mathrm{d}\mu_{-} \tag{2}$$

where γ is the interfacial tension, Γ_{Ag^+}, Γ_{I^-} are the surface excesses of Ag^+ and I^- ions, μ_{Ag^+}, μ_{I^-} the corresponding chemical potentials and μ_+, μ_- the chemical potentials of the added cations and anions. We now *define*

$$\sigma_0 = e_0(\Gamma_{Ag^+} - \Gamma_{I^-}) = e_0(\Gamma_{-} - \Gamma_{+}) \tag{3}$$

where the second relation follows from the condition of electrical neutrality. If ψ_0 is the inner (Galvani) potential of the solid AgI phase relative to the aqueous phase, then

$$e_0\mathrm{d}\psi_0 = \mathrm{d}\mu_{Ag^+} = -\mathrm{d}\mu_{I^-} \tag{4}$$

The second equation is obtained when we assume that the interior of the solid AgI is unaffected by any changes in composition of the aqueous phase. Also

$$\mathrm{d}\mu = \mathrm{d}\mu_{+} + \mathrm{d}\mu_{-} \tag{5}$$

We imagine the AgI–electrolyte interface as part of one electrode of a galvanic cell, of which the other (reference) electrode is reversible to one of the ion species of the added electrolyte. When the reference electrode is reversible to the anion of the added electrolyte, its Galvani potential, $-\phi_-$, satisfies the relation:

$$e_0 \mathrm{d}\phi_- = \mathrm{d}\mu_- \tag{6}$$

and the e.m.f. of the cell is

$$E_- = \psi_0 + \phi_- \tag{7}$$

By making use of eqns. (3)–(7), we can write (2) as

$$\mathrm{d}\gamma = -\sigma_0 \mathrm{d}E_- - \Gamma_+ \mathrm{d}\mu \tag{8}$$

from which

$$(\partial\sigma_0/\partial\mu)_{E^-} = (\partial\Gamma_+/\partial E_-)_\mu \tag{9}$$

At fixed T and p, σ_0 depends on two intensive variables which may be taken as μ and ψ_0, or μ and E_-. Thus we have

$$\sigma_0 = \sigma_0(\mu,\psi_0) = \sigma_0(\mu, E_- - \phi_-(\mu,E_-)) \tag{10}$$

making use of (7). It follows that (9) can be expressed as

$$\left(\frac{\partial\Gamma_+}{\partial E_-}\right)_\mu = \left(\frac{\partial\sigma_0}{\partial\mu}\right)_{\psi_0} - \left(\frac{\partial\sigma_0}{\partial\psi_0}\right)_\mu \left(\frac{\partial\phi_-}{\partial\mu}\right)_{E_-} = \left(\frac{\partial\sigma_0}{\partial\mu}\right)_{\psi_0} - \frac{1}{e_0}\left(\frac{\partial\sigma_0}{\partial\psi_0}\right)_\mu \left(\frac{\partial\mu_-}{\partial\mu}\right)_{E_-} \tag{11}$$

where we have substituted (6). Integrating this relation with respect to ψ_0 at constant μ, we derive the surface charge excess of cations

$$\sigma_+ = e_0\Gamma_+ = e_0 \int_\chi^{\psi_0} \left[\left(\frac{\partial\sigma_0}{\partial\mu}\right)_{\psi_0} - \frac{1}{e_0}\left(\frac{\partial\sigma_0}{\partial\psi_0}\right)_\mu \left(\frac{\partial\mu_-}{\partial\mu}\right)_{E_-}\right] \mathrm{d}\psi_0 + K_+(\mu) \tag{12}$$

where χ (the so-called Lange chi-potential) is the value of ψ_0 at the point of zero charge (p.z.c. where $\sigma_0 = 0$), and the integration constant, K_+ (a function of μ), is the value of σ_+ at the p.z.c. In a similar manner, by assuming that the reference electrode is reversible to the cation of the added electrolyte, we obtain the surface charge excess of anions

$$\sigma_- = -e_0\Gamma_- = -e_0 \int_\chi^{\psi_0} \left[\left(\frac{\partial\sigma_0}{\partial\mu}\right)_{\psi_0} + \frac{1}{e_0}\left(\frac{\partial\sigma_0}{\partial\psi_0}\right)_\mu \left(\frac{\partial\mu_+}{\partial\mu}\right)_{E_+}\right] \mathrm{d}\psi_0 + K_-(\mu) \tag{13}$$

where the e.m.f. of the cell is now E_+. It is observed that for a given electrolyte in the aqueous phase, the function, $\sigma_0(\mu,\psi_0)$, does not depend on the nature of the reference electrode. On making use of (3) and (4)

$$K_+(\mu) = -K_-(\mu) = K(\mu) \qquad \text{say} \tag{14}$$

which is simply the condition of electrical neutrality, $\sigma_+ = -\sigma_- = K_+(\mu)$ at the p.z.c. Apart from the neglect of H^+ and OH^- ions, the formulae (12)–(14) are thermodynamically exact. We wish to discuss the nature of the approximations made when the relations (12)–(14) are replaced by the formulae (1) of LYKLEMA.

In choosing μ and $E_\mp$ as the independent variables, it is understood that $E_\mp$ can be changed at constant μ by altering the AgI concentration in the aqueous phase. If the latter is much smaller than the concentration of added electrolyte,

then the dependence of $\phi_{\mp}(\mu,E_{\mp})$ on $E_{\mp}$ can be ignored, implying that $\mu_{\mp}$ are functions of μ only. Equations (12)–(14) then simplify to

$$\sigma_+ = e_0\int_{\chi}^{\psi_0}\left(\frac{\partial\sigma_0}{\partial\mu}\right)_{\psi_0}\mathrm{d}\psi_0 - \sigma_0\left(\frac{\mathrm{d}\mu_-}{\mathrm{d}\mu}\right)+K(\mu),\quad \sigma_- = -e_0\int_{\chi}^{\psi_0}\left(\frac{\partial\sigma_0}{\partial\mu}\right)_{\psi_0}\mathrm{d}\psi_0 - \sigma_0\left(\frac{\mathrm{d}\mu_+}{\mathrm{d}\mu}\right)-K(\mu) \tag{15}$$

The chemical potentials, $\mu_{\mp}$, can be expressed as:

$$\mu_{\mp} = \mu_{\mp}{}^0(T,p)+kT\ln nf_{\mp} \tag{16}$$

where the standard chemical potentials, $\mu_{\mp}{}^0$, depend only on T and p, k is Boltzmann's constant, n the bulk number density of cations or anions of the added electrolyte and $f_{\mp}$ are the corresponding activities. From (5) and (16) we may derive

$$\frac{\mathrm{d}\mu}{\mathrm{d}\mu_-} = 1+\frac{\mathrm{d}\mu_+}{\mathrm{d}\mu_-} = 2+\frac{\mathrm{d}\ln(f_+/f_-)/\mathrm{d}\ln n}{1+\mathrm{d}\ln f_-/\mathrm{d}\ln n} \tag{17}$$

and $\mathrm{d}\mu/\mathrm{d}\mu_+$ is obtained from (17) by interchanging the suffixes + and −. LYKLEMA assumed that $\mathrm{d}\mu_+=\mathrm{d}\mu_-=\frac{1}{2}\mathrm{d}\mu$, equivalent to ignoring the second term in the right-hand member of (17), in which case the second term in formulae (15) for σ_+ and σ_- reduces to $-\sigma_0/2$. Because of this approximation, LYKLEMA confined his analysis to 1–1 electrolyte concentrations $\lesssim 0.1\ M$. To examine the conditions under which his assumption is valid, we imagine that the 1–1 electrolyte medium is a continuous solvent containing ions with interaction energies for the three types of ion-pairs given by U_{2+}, U_{2-} and U_{+-}, which consist of the usual Coulomb term and a short-range contribution. If $U_{2+}=U_{2-}$ regardless of the form of U_{+-}, then the cations and anions are distinguishable only in respect to sign of the charge, and from physical considerations $f_+=f_-$. In particular, for the hard-sphere model with distances of nearest approach, a_{2+}, a_{2-} and a_{+-}, $f_+=f_-$ if $a_{2+}=a_{2-}$. The last term in (17) will now vanish and this result does not depend on any additional approximation, such as the Debye–Huckel theory, as suggested by LYKLEMA. By using cluster theory, MEERON[10] has shown that the activity coefficient of an ion species in a 1–1 electrolyte is insensitive to the values of a_{2+} and a_{2-}, except possibly at high concentrations ($\gtrsim 0.5\ M$). This implies that the effect of differences between a_{2+} and a_{2-} on the ratio f_+/f_- will be small and consequently it seems likely that the term neglected by LYKLEMA remains small well beyond the limit of the Debye–Huckel theory. Apparently, it is not possible to determine f_+/f_- experimentally.

In order to calculate ionic components from (15), one must find $K(\mu)$ which measures specific adsorption of added electrolyte at the p.z.c. LYKLEMA simply assumed $K(\mu)=0$. One simple method of estimating $K(\mu)$ is based on the small observed shift in the p.z.c. with change in electrolyte concentration. The Stern–Grahame model is introduced for the inner region, which is treated as a uniform dielectric medium and the Gouy–Chapman theory is applied to the diffuse layer (so that the method is limited to electrolyte concentrations $\lesssim 0.1\ M$). Let Ψ_0 and ψ_d, respectively, be the potentials at the AgI surface and the outer Helmholtz plane (o.h.p.) due to the true charge distribution, K_i the integral capacity and d the thickness of the inner region, γ the distance between the inner Helmholtz plane (i.h.p.) and the o.h.p. and σ_β the charge density of adsorbed ions on the i.h.p. Then from the electrostatic relations for the inner region

$$\Psi_0 - \psi_d = \sigma_0/K_i + (\gamma/d)(\sigma_\beta/K_i) \tag{18}$$

At the lowest concentration of added electrolyte, we assume no specific adsorption at the p.z.c., where, therefore, $\sigma_0 = 0$, $K(\mu) = 0$, $\psi_0' = \psi_0 - \chi = 0$ and also $\Psi_0 = \psi_d = 0$. Let us now consider the case where, with addition of electrolyte, specific adsorption of cations occurs at the p.z.c., which consequently shifts ψ_0 by a positive amount, ϕ. The charge density of adsorbed cations at the p.z.c. is then $\sigma_\beta = K(\mu)$ and, on identifying Ψ_0 with ϕ, it follows from (18) that

$$\phi = [\psi_d + (\gamma/d)K(\mu)/K_i]_{p.z.c.} \tag{19}$$

(Because $\sigma_0 = 0$, $\phi = \psi_\beta$, the potential at the i.h.p.). The net charge per unit cross-sectional area in the diffuse layer is $-K(\mu)$, so that on applying the Gouy–Chapman theory

$$K(\mu) = a \sinh \tfrac{1}{2} \frac{e_0 \psi_d}{kT} \approx \frac{\kappa \varepsilon \psi_d}{4\pi} ; \qquad a = \frac{\kappa \varepsilon kT}{2\pi e_0} \tag{20}$$

where ε is the dielectric constant of the electrolyte medium, K is the Debye–Huckel parameter given by $K^2 = 8\pi n e_0^2/\varepsilon kT$ and we have assumed $K(\mu)$ sufficiently small to justify linearisation with respect to ψ_d. From (19) and (20)

$$K(\mu) = (\kappa \varepsilon \phi/4\pi)/(1 + \kappa \varepsilon \gamma/4\pi d K_i) \tag{21}$$

For 0.1 M 1–1 electrolyte, $K_i = 30\ \mu$F cm^{-2}, $\gamma/d = \frac{1}{4}$ and a typical potential shift $\phi = 10$ mV at $T = 25°$ ($\varepsilon = 78$), we find $K(\mu) = 0.26\ \mu$C cm^{-2}. We observe that the formula (21) depends on knowing the quantity, $K_2 = dK_i/\gamma$, which is the capacity of that part of the inner region situated between the i.h.p. and o.h.p. If $\gamma = 0$, $K(\mu) = 0.72$ μC cm^{-2} at $\phi = 10$ mV and 0.1 M.

The difficulty of determining K_2 can be partly resolved by using the discreteness-of-charge theory[11–13], according to which, in the presence of specific adsorption of cations, a maximum occurs in the charge excess of anions, σ_-, at larger (negative) values of ψ_0. At the p.z.c. the potential $\psi_0 = \chi$ or $\psi_0' = 0$, whereas adsorption of cations produces a potential difference due to the true charge, given by $\Psi_0 = \phi$. On identifying Ψ_0 with $\psi_0' + \phi$ at a general potential ψ_0, it follows from (18) that at the maximum in σ_-,

$$\phi = [-\psi_0' + \psi_d + \sigma_0/K_i + (\gamma/d)(\sigma_\beta/K_i)]_{\max \text{ in } \sigma_-} \tag{22}$$

where ϕ will have the same value in (19) and (22) at a given concentration of added electrolyte. The integral capacity, however, takes different values in (19) and (22), because it depends on ψ_0 and we shall assume that this is described by a variation coefficient, $t = (kT/e_0)\mathrm{d} \ln K_i/\mathrm{d}\psi_0$, where $t \sim 0.02$–0.04 in 1–1 electrolytes. The discreteness-of-charge theory provides an expression for K_i at the maximum in σ_-, namely[13]

$$K_i = \frac{\beta\gamma}{d^2} \frac{e_0}{kT} g\sigma_\beta \left[1 - \frac{\sigma_\beta/N_s e_0}{(1 - \sigma_\beta/N_s e_0)} + \frac{e_0}{kT} \frac{\beta}{d} \frac{\sigma_\beta}{K_i} t - \frac{\kappa \varepsilon t}{2\pi g K_i} \sinh \tfrac{1}{2} \frac{e_0 \psi_d}{kT}\right] \tag{23}$$

where $\beta = d - \gamma$, N_s is the density of Langmuir-type adsorption sites on the AgI surface and g is a factor somewhat greater than 1 in the self-atmosphere potential at an adsorbed ion, defined by, $\phi_\beta = -(\beta\gamma\sigma_\beta/d^2 K_i)g$ which characterizes the discreteness-of-charge effect. The corresponding value of K_i in (19) at the p.z.c. can then

be calculated, given t. We also require the charge excesses, σ_+, σ_-, at the maximum in σ_-. At the p.z.c., (15) becomes $\sigma_\pm = \pm K(\mu)$ but since LYKLEMA assumes $K(\mu) = 0$ when he uses the equations (15) to find σ_+ and σ_-, his charge excesses are actually, $\sigma_\pm' = \sigma_\pm \pm K(\mu)$. On applying the Gouy–Chapman theory to the diffuse layer, we have the relations

$$\sigma_- = \sigma_-' + K(\mu) = \tfrac{1}{2}a[1 - \exp(e_0\psi_d/2kT)] \tag{24}$$

$$\sigma_d{}^+ = \sigma_+ - \sigma_\beta = \sigma_+' - K(\mu) - \sigma_\beta = \tfrac{1}{2}a[\exp(-e_0\psi_d/2kT) - 1] \tag{25}$$

where $\sigma_d{}^+$ is the charge excess of cations in the diffuse layer.

The method consists in choosing $K(\mu)$ such that (19) and (22) give the same value of ϕ, assuming that ψ_0' is known at the maximum in σ_-. For any $K(\mu)$, having obtained σ_+' and σ_-' from (15), σ_β and ψ_d at the maximum in σ_- can be calculated from eqns. (24) and (25). Also, ψ_d is determined from (20) at the p.z.c. For given values of t, g, γ/d and N_s, all quantities on the right-hand sides of (19) and (22) are known, and $K(\mu)$ is adjusted until the two values of ϕ are equal. A limitation on the choice of the above parameters is provided by a relation between the total differential and integral capacities, $C = \mathrm{d}\sigma_0/\mathrm{d}\psi_0$ and $K_t = \sigma_0/\psi_0$. The discreteness-of-charge theory predicts a maximum in the potential $|\psi_\beta|$ at the i.h.p. where, if K_i' is given by (23) when the last term in the square brackets is omitted[13],

$$C = (d/\beta)K_i' + (e_0/kT)t\sigma_0 \tag{26}$$

and if the (σ_0,ψ_0) plots are convex to the ψ_0-axis, as for 0.1 M KNO_3, then $C < K_t$. As an example, if we choose $t = 0.03$, $g = 5/4$, $\gamma/d = 1/5$, $N_s = 5 \cdot 10^{14}$ cm^{-2}, $\psi_0' = -250$ mV, $\sigma_-' = 0.85$ μC cm^{-2} and $\sigma_+' = 3.0$ μC cm^{-2} at the maximum in σ_-, then $\phi \approx 2$ mV, $K(\mu) \approx 0.04$ μC cm^{-2}, and $K_i \approx 16$ μF cm^{-2} at this maximum. Also, at the maximum in $|\psi_\beta|$, $C \approx 10$ μF cm^{-2} and $K_t \approx 15$ μF cm^{-2}. These were calculated by choosing LYKLEMA's curve for σ_+ in 0.1 M KNO_3 in his Fig. 4 (ref. 2).

While the discreteness-of-charge theory involves certain quantities such as g and γ/d, which require further investigation, the above application illustrates its potentialities in providing useful information about the inner region.

The following alternative method of finding $K(\mu)$, the basis of which was suggested to the author by PARSONS[15,16], does not use a model of the structure of the inner region. From (8), we can write

$$\mathrm{d}(\gamma + \sigma_0 E_-) = E_- \mathrm{d}\sigma_0 - \Gamma_+ \mathrm{d}\mu \tag{27}$$

leading to the relation

$$(\partial E_-/\partial\mu)_{\sigma_0} = -(\partial\Gamma_+/\partial\sigma_0)_{E_-} \tag{28}$$

in which the left-hand member is determined from experiment. Integrating with respect to σ_0 at fixed E_-, we have

$$\sigma_+ = e_0\Gamma_+ = -e_0\int_0^{\sigma_0} (\partial E_-/\partial\mu)_{\sigma_0}\mathrm{d}\sigma_0 + K_+(E_-) \tag{29}$$

where $K_+(E_-)$ is the value of σ_+ at the p.z.c. and given E_-. Figure (1a) shows a schematic plot of σ_0 *vs.* E_- at two concentrations, c_1 and c_2 ($c_1 > c_2$) of added electrolyte. We assume that specific adsorption of cations occurs at point A which represents the p.z.c. with the higher concentration c_1, but not at the point 0, the p.z.c. with the

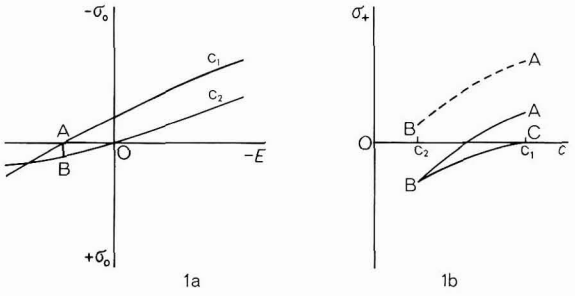

Fig. 1. Schematic diagrams illustrating use of eqn. (29) to determine $K(\mu)$. (a) Plots of σ_0 *vs.* E_-. (b) Plots of σ_+ *vs.* c. Dotted line AB represents integration of (29) with arbitrary value for constant $K_+(E_-)$.

concentration c_2. We now choose the value of E_- at point A and carry out the integration in (29) along the vertical line AB from c_1 to c_2 concentrations (it should be observed here that the range of E_- where σ_0 can be zero and therefore, where (29) has a meaning is in general very limited). This integration yields σ_+ as a function of electrolyte concentration, c, (or σ_0) (illustrated by curve AB in Fig. (1b)), apart from the unknown additive constant, $K_+(E_-)$, which is identical with $K_+(\mu)$ in eqn. (12) for the value of μ corresponding to concentration c_1. Suppose now we assume no specific adsorption at all concentrations from c_1 to c_2 and use the Gouy–Chapman theory of the diffuse layer. If $v = -\sigma_0/a$, we can write[9]

$$\sigma_+ = a(v - 1 + \sqrt{1+v^2}) \tag{30}$$

so that, corresponding to each point on curve AB in Fig. 1b, where both σ_0 and c are specified, we can calculate σ_+, thereby obtaining curve CB in Fig. 1b. At end B, (and in its vicinity) the two curves, AB and CB, should coincide since we have postulated no specific adsorption at the electrolyte concentration, c_2. The experimental curve AB must be shifted vertically until it coincides with the theoretical curve CB at the end B, and the height CA is the required value of $K_+(E_-)$. Although this method has the merit of being independent of any inner region model, one possible drawback is its poor accuracy when the path AB in Fig. (1a) is very short.

A simpler way of using (28), without introducing an inner region model, is due to PARSONS[15,16]. We assume that along a constant concentration (constant μ) curve in the (ψ_0,σ_0) plane, there exists a point, say (Ψ_0,Σ_0), where no specific adsorption takes place. At this point, the surface charge excess of cations, say σ_+^0, will be given by (30) with $\sigma_0 = \Sigma_0$. The position of this point is specified by the condition that the *experimentally*-determined left-hand member of (28) be equal to the theoretical right-hand member of (28), which is *calculated* by differentiating (30) with respect to σ_0. If in (15) we put $d\mu_-/d\mu = 1/2$ and replace the limits of integration (χ,ψ_0) by (χ,Ψ_0), then we obtain

$$\sigma_+^0 = e_0 \int_{\chi}^{\Psi_0} \left(\frac{\partial\sigma_0}{\partial\mu}\right)_{\psi_0} d\psi_0 - \tfrac{1}{2}\Sigma_0 + K(\mu) \tag{31}$$

in which the only unknown is $K(\mu)$. The above two methods of finding $K(\mu)$ without a model constitute a useful check for self-consistency.

A fifth method of finding $K(\mu)$, proposed by LYKLEMA[2,14], involves the D.L.V.O. theory of colloid stability at two temperatures. Comparison of the various methods described should be useful in testing theories of the inner region.

REFERENCES

1 J. LYKLEMA, *Trans. Faraday Soc.*, 59 (1963) 418.
2 J. LYKLEMA, *Discussions Faraday Soc.*, 42 (1966) 81.
3 D. C. GRAHAME AND R. B. WHITNEY, *J. Am. Chem. Soc.*, 64 (1942) 1548.
4 D. M. MOHILNER, *J. Phys. Chem.*, 66 (1962) 724.
5 R. PARSONS AND M. A. V. DEVANATHAN, *Trans. Faraday Soc.*, 49 (1953) 404.
6 R. PARSONS, *Modern Aspects of Electrochemistry*, edited by J. O'M. BOCKRIS AND B. E. CONWAY, Butterworths, London, 1954, pp. 103–179.
7 P. DELAHAY, *Double Layer and Electrode Kinetics*, Interscience, New York, 1965.
8 D. C. GRAHAME, *Chem. Rev.*, 41 (1947) 441.
9 D. C. GRAHAME AND B. A. SODERBERG, *J. Chem. Phys.*, 22 (1954) 449.
10 E. MEERON, *J. Chem. Phys.*, 26 (1957) 804.
11 S. LEVINE, J. MINGINS AND G. M. BELL, *J. Electroanal. Chem.*, 13 (1967) 280.
12 S. LEVINE AND A. L. SMITH, *Discussions Faraday Soc.*, 42 (1966) 97.
13 S. LEVINE, A. L. SMITH, J. MINGINS AND G. M. BELL, *Proc. Intern. Congr. Surface Active Substances, 4th, Brussels*, II/B (1964) 101, Gordon and Breach, New York, 1967.
14 J. LYKLEMA, *III Int. Vortragstagung über grenzflachenaktive Stoffe, Abhandl. Deut. Akad. Wiss. Berlin*, (1967) 542.
15 R. PARSONS, private communication.
16 R. PARSONS, *Proc. Intern. Congr. Surface Activity, 2nd, London, 1957*, Butterworths, London, 1957, p. 38.

ELECTROANALYTICAL CHEMISTRY AND INTERFACIAL ELECTROCHEMISTRY
Elsevier Sequoia S.A., Lausanne – Printed in The Netherlands

THERMODYNAMICS OF THE $Cl_2/Cl^-/Cl_3^-$ SYSTEM IN AQUEOUS SOLUTION

A. CERQUETTI, P. LONGHI, T. MUSSINI AND G. NATTA
Laboratory of Electrochemistry and Metallurgy, University of Milan, Milan (Italy)
(Received September 4th, 1968)

INTRODUCTION

From solubility measurements, SHERRILL AND IZARD[1] found the equilibrium constant for the reaction

$$Cl_2\,(gas) + Cl^-\,(aq.) \rightleftharpoons Cl_3^-\,(aq.) \qquad (1)$$

to be $K_1 = 0.010$ at 25°, and that for the reaction

$$Cl_2\,(aq.) + Cl^-\,(aq.) \rightleftharpoons Cl_3^-\,(aq.) \qquad (2)$$

to be $K_2 = 0.176$ at 25°.

Using the spectrophotometric method, ZIMMERMANN AND STRONG[2] found $K_2 = 0.191$ at 25°.

The e.m.f.-based method described in the present work enables K_1 and $E_G°$—the standard potential of the chlorine electrode—to be determined simultaneously at any temperature. Thus, K_1 and $E_G°$ have been determined over the range 25–80°, and used to obtain the previously unknown values of $H°$ and $S°$ for the aqueous Cl_3^- ion. Measurements of chlorine solubility were run parallel to the e.m.f. measurements, in order to determine K_2 and thus the thermodynamic functions for all relevant species of the $Cl_2/Cl^-/Cl_3^-$ system have now been derived.

The method described here is essentially based on e.m.f. measurements of the cell.

$$H_2,\ 1\ atm \mid HCl,\ 1\ M \mid Cl_2,\ p\ atm \qquad (3)$$

at various chlorine pressures and temperatures, with constant HCl molality, the chlorine solubility in HCl being measured at any chlorine pressure and temperature.

Owing to the occurrence of reaction (1) in the compartment of the chlorine electrode, the molality of the Cl^- ion, m_{Cl^-}* (the asterisk will be used throughout the paper to denote m_{Cl^-} in the chlorine electrode compartment), is different from m_{HCl} as some Cl^- ions are converted into Cl_3^- ions; in the hydrogen electrode compartment, $m_{H^+} = m_{Cl^-} = m_{HCl}$. As reaction (1) does not change the ionic strength of the solution, the activity coefficient for the Cl^- ion, γ_{Cl^-}, remains unchanged in the two half-cell compartments.

The equilibrium constant for reaction (1) can be expressed as

$$K_1 = m_{Cl_3^-}\gamma_{Cl_3^-}/(p_{Cl_2} m_{Cl^-}{}^* \gamma_{Cl^-}) \qquad (4)$$

where m_{Cl^-}* is defined by

$$m_{HCl} = m_{Cl^-}{}^* + m_{Cl_3^-} \tag{5}$$

Substituting the value of $m_{Cl_3^-}$ obtained from eqn. (4) into eqn. (5) we get

$$m_{Cl^-}{}^* = m_{HCl}/(1 + K_1 p_{Cl_2} \gamma_{Cl^-}/\gamma_{Cl_3^-}) \tag{6}$$

It is difficult to assess whether, and to what extent, the individual ionic activity coefficients, γ_{Cl^-} and $\gamma_{Cl_3^-}$, are different from each other. Cl^- and Cl_3^- are influenced by the same ionic strength and should not be much different in the solvated-ion size and therefore it is reasonable to assume $\gamma_{Cl^-} = \gamma_{Cl_3^-}$. The uncertainty introduced in the calculated K_1-values by this assumption is probably of the order of 2–3%, working with unit HCl molality.

Taking into account eqn. (6) and the above assumption, the e.m.f. of cell (3) with $p_{H_2} = 1$ atm is given by:

$$\begin{aligned} E &= E_G^\circ + (RT/2F) \ln p_{Cl_2} - (RT/F) \ln (m_{H^+} \gamma_{H^+} m_{Cl^-}{}^* \gamma_{Cl^-}) \\ &= E_G^\circ + (RT/2F) \ln p_{Cl_2} - (2RT/F) \ln (m\gamma_\pm)_{HCl} + (RT/F) \ln(1 + K_1 p_{Cl_2}) \end{aligned} \tag{7}$$

where $\gamma_\pm = (\gamma_{H^+}\gamma_{Cl^-})^{\frac{1}{2}}$ is the mean molal activity coefficient of HCl and E_G° is the standard molal potential of the chlorine electrode referred to the reaction:

$$\tfrac{1}{2}Cl_2(gas) + e = Cl^-(aq.) \tag{8}$$

As K_1 is of the order of $1.0 \cdot 10^{-2}$ and $p_{Cl_2} \leq 1$ atm, the last logarithmic term in eqn. (7) can be linearized according to $\ln(1 + K_1 p_{Cl_2}) = K_1 p_{Cl_2}$ without introducing any appreciable error. Thus, the rearrangement of eqn. (8) yields

$$(EF/RT) + 2\ln(m\gamma_\pm)_{HCl} - \tfrac{1}{2} \ln p_{Cl_2} = (FE_G^\circ/RT) + K_1 p_{Cl_2} = \Psi \tag{9}$$

Equation (9) requires that a plot of Ψ *vs.* p_{Cl_2} should produce a straight line the slope of which gives K_1 and the intercept of which gives $FE_G^\circ/(RT)$, *i.e.*, K_1 and E_G° are determined simultaneously. The results obtained conform to the predicted behaviour (see below); 1 *M* HCl was used throughout and the relevant $\gamma_\pm$-values over the range 25–80° were obtained from a recent work[4].

Once K_1 is known, K_2 can be determined provided that the total chlorine in solution, viz.,

$$m_{Cl_2}{}^{tot} = m_{Cl_3^-} + m_{Cl_2} \tag{10}$$

is known at any p_{Cl_2} used.

The expression for K_2 is:

$$K_2 = m_{Cl_3^-}\gamma_{Cl_3^-}/(m_{Cl_2}\gamma_{Cl_2} m_{Cl^-}{}^* \gamma_{Cl^-}) \tag{11}$$

If the value for $m_{Cl_3^-}$ obtained from eqn. (11) is substituted in eqn. (10) with the assumption $\gamma_{Cl^-} = \gamma_{Cl_3^-}$,

$$m_{Cl_2} = m_{Cl_2}{}^{tot}/(1 + K_2 m_{Cl^-}{}^* \gamma_{Cl_2}) \tag{12}$$

where m_{Cl_2} is the molality of free chlorine in solution and γ_{Cl_2} is the corresponding activity coefficient. Equations (5), (10) and (12) give

$$m_{Cl_2} = m_{Cl_2}{}^{tot} + m_{Cl^-}{}^* - m_{HCl} = m_{Cl_2}{}^{tot}/(1 + K_2 m_{Cl^-}{}^* \gamma_{Cl_2}) \tag{13}$$

Substituting eqn. (6) into (13) and solving for K_2 gives

$$K_2 = (1 + K_1 p_{Cl_2})/\gamma_{Cl_2}[(m_{Cl_2}{}^{tot} + m_{Cl_2}{}^{tot}/(K_1 p_{Cl_2}) - m_{HCl})] \quad (14)$$

As K_1, K_2 and $E_G°$ are known as functions of temperature, the standard thermodynamic functions, $H°$, $G°$, $S°$ of the species that characterize the $Cl_2/Cl^-/Cl_3^-$ system are all determinable quantities (see below).

EXPERIMENTAL

The hydrogen electrode in cell (3) was of the capillary-imbibition type, as recently described by BIANCHI[5–7]. The chlorine electrode was prepared and operated as described by FAITA *et al.*[3] and gave a bias potential of 0.01 mV. Chlorine–nitrogen mixtures of appropriate chlorine percentages were used to obtain chlorine pressures in the range $5 \cdot 10^{-2}$–1 atm. The values of chlorine pressures were known to $\pm 0.1\%$.

The e.m.f.-values were measured by means of a K-3 Leeds and Northrup potentiometer. The null-point detector, a 610-B Keithley electrometer, had an input impedance greater than 10^{14} Ω, thus enabling work to be carried out with stopcocks continuously closed between the half-cells in order to prevent inter-diffusion. The e.m.f.-values were read after an appropriate time of equilibration, after which they remained constant within $\pm$ 0.01 mV for 1 h. A large single stock of 1 *M* HCl solution, enough for all measurements carried out, was prepared with triply-distilled water and certified Carlo Erba hydrochloric acid. The HCl titration was carried out potentiometrically[8,9]. To determine the molality of chlorine ($Cl_2 + Cl_3^-$) in the HCl solution, in each experiment the iodine liberated from excess KI by chlorine was titrated with thiosulphate. The cell temperatures were regulated to $\pm$ 0.02° by means of a specially designed air-thermostat.

RESULTS AND DISCUSSION

Standard potentials, and equilibrium constants

Table 1 shows the e.m.f.-values of cell (3) measured in 1 *M* HCl and corrected to 760 mm Hg pressure of hydrogen, at various pressures of chlorine, with the corresponding molality values of chlorine ($Cl_2 + Cl_3^-$) in solution, over the temperature range, 25–80°. A plot of Ψ *vs.* p_{Cl_2}, according to eqn. (9), was made at each experimental temperature producing in each case a straight line (see Fig. 1) from the slope and intercept of which (determined by the least-squares method) the equilibrium constant, K_1, and the standard potential, $E_G°$, were obtained. The $E_G°$- and K_1-values as a function of temperature together with the standard errors, and the $E_A°$- and K_2-values with the uncertainties derived therefrom are shown in Table 2.

The value of K_2 was calculated (K_1 being known from eqn. (14)) using all values of $m_{Cl_2}{}^{tot}$ in Table 1 (see Table 2). Regarding the value to be assigned to γ_{Cl_2} when $m_{HCl} = 1$ (eqn. (14)) it is seen from SHERRILL AND IZARD's work at 25° that such a γ_{Cl_2} is very close to unity. In this paper, a value, $\gamma_{Cl_2} = 1.00$, at unit m_{HCl} has been used over all the range, 25–80°. This would probably introduce an uncertainty of the order of 3% for K_2.

The $E_G°$-values in Table 2 can be reproduced with a maximum deviation of 4 μV—in practice, with all the significant figures—by the least-squares polynomial:

TABLE 1

E.M.F.-VALUES, E, OF CELL (3), AND MOLALITIES OF TOTAL DISSOLVED CHLORINE, $m_{Cl_2}^{tot}$, AS FUNCTIONS OF CHLORINE PRESSURES, AT VARIOUS TEMPERATURES, IN 1 M HCl

t (°C)	E (V)	p_{Cl_2} (atm)	$m_{Cl_2}^{tot} \cdot 10^3$
25	1.33907	0.0946	6.354
	1.34417	0.1403	9.418
	1.35109	0.2406	16.16
	1.36370	0.6366	42.75
	1.36787	0.8719	58.55
	1.36924	0.9718	65.38
	1.36933	0.9758	65.40
40	1.31976	0.0905	3.807
	1.32524	0.1353	5.705
	1.33254	0.2331	9.968
	1.34573	0.6152	25.14
	1.34986	0.8327	35.16
	1.35132	0.9288	39.35
60	1.29116	0.0784	2.136
	—	0.1109	2.888
	1.29704	0.1180	—
	1.29723	0.1195	3.112
	1.30486	0.2037	4.775
	1.31888	0.5394	14.05
	—	0.7234	18.84
	1.32471	0.8076	21.03
80	1.25668	0.0544	1.025
	—	0.1017	1.917
	1.27087	0.1382	2.419
	1.28580	0.3681	6.636
	—	0.4598	8.668
	1.29166	0.5416	10.21

$$E_G^\circ = 1.3873947 - (1.0939812 \cdot 10^{-3})T - (2.8370370 \cdot 10^{-6})T^2 \quad (15)$$

where T is absolute temperature.

With the E_G°-, K_1- and K_2-values known at each experimental temperature, it is possible to determine the standard potentials, E_A°, of the chlorine electrode referred to the reaction[10]:

$$\tfrac{1}{2}Cl_2(aq.) + e = Cl^-(aq.) \quad (16)$$

The actual potential of the chlorine electrode, E_{Cl_2/Cl^-}, can be expressed in terms of either E_G° or E_A°:

$$\begin{aligned} E_{Cl_2/Cl^-} &= E_G^\circ + (RT/2F)\ln p_{Cl_2} - (RT/F)\ln(m_{Cl^-}{}^*\gamma_{Cl^-}) \\ &= E_A^\circ + (RT/2F)\ln(m_{Cl_2}\gamma_{Cl_2}) - (RT/F)\ln(m_{Cl^-}{}^*\gamma_{Cl^-}) \end{aligned} \quad (17)$$

so that, taking into account eqns. (4) and (11), we obtain

$$E_A^\circ = E_G^\circ + \frac{RT}{2F}\ln\frac{K_2}{K_1} \quad (18)$$

The values of E_A° obtained from eqn. (18) are given in Table 2, and can be reproduced

with a maximum deviation of 0.6 mV by the least-squares polynomial:

$$E_A^\circ = 1.40922 - (4.30504 \cdot 10^{-4})T - (4.87922 \cdot 10^{-6})T^2 \quad (19)$$

A comparison is made in Table 2 with the literature data for the variables cited. The agreement is good, particularly for the E_G°-values, in view of the limits of uncertainty quoted in previous works[4].

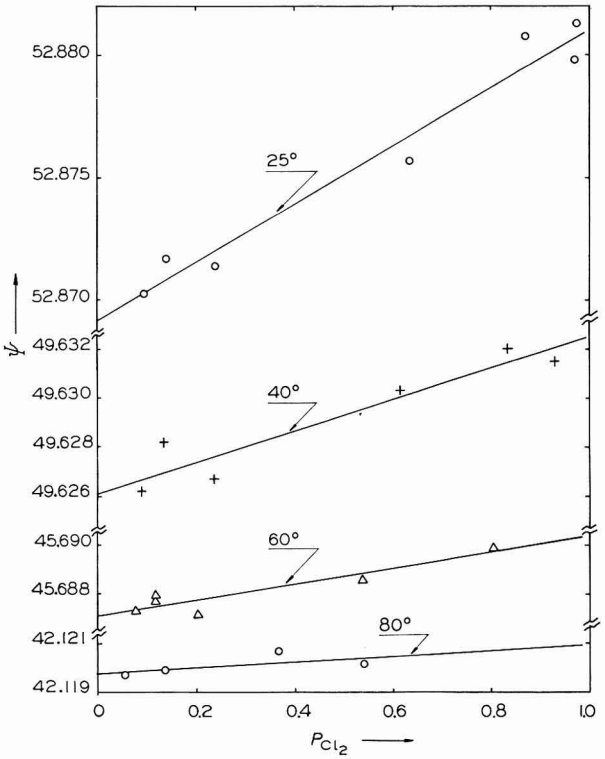

Fig. 1. Plots of Ψ *vs.* p_{Cl_2} (atm) according to eqn. (9), at various temps. Slopes of straight lines give K_1; intercepts at $p_{Cl_2} = 0$ give $FE_G^0/(RT)$.

TABLE 2

STANDARD POTENTIALS FOR THE CHLORINE ELECTRODE, AND EQUILIBRIUM CONSTANTS (*cf.* REACTIONS (1) AND (2)), AT VARIOUS TEMPERATURES

Literature values in italics

t (°C)	E_G° (V)	E_A° (V)	K_1	K_2
25	1.35827±0.00002	1.396±0.002	0.0119±0.0009	0.215±0.022
	1.35852[4]	*1.39*[10]	*0.010*[1]	*0.176*[1]
				0.191[2]
40	1.33910±0.00002	1.384±0.004	0.0064±0.0009	0.18±0.03
	1.33919[4]	—	—	—
60	1.31154±0.00001	1.366±0.006	0.0032±0.0007	0.14±0.03
	1.31144[4]	—	—	—
80	1.28172±0.00001	1.344±0.036	0.0012±0.0010	0.07±006
	1.28153[4]	—	—	—

Thermodynamic functions

The standard thermodynamic functions, $\Delta H°$, $\Delta G°$, $\Delta S°$, for reaction (8) were determined from the values of $E_G°$ and $dE_G°/dT$ at 25° (see Table 3), the $dE_G°/dT$-value having been obtained from the first derivative of eqn. (15). Only three significant figures have been retained for the $dE_G°/dT$-value, owing to the fact that the $E_G°$-values were obtained at temperature intervals of 15–20°, thereby limitating the accuracy of the evaluation of $dE_G°/dT$ at the extreme temperature, 25°. The standard thermodynamic functions were also obtained for reactions (1) and (2) from the K_1- and K_2-values by using the relations, $\Delta G° = -RT\ln K$ and

$$\Delta H° = -R\frac{d(\ln K)}{d(1/T)} ,$$

TABLE 3

THERMODYNAMIC FUNCTIONS AT 25° FOR SOME REACTIONS OF THE $Cl_2/Cl^-/Cl_3^-$ SYSTEM

Literature values in italics

Reactions	$\Delta H°$ *(kcal mole^{-1})*	$\Delta G°$ *(kcal mole^{-1})*	$\Delta S°$ *(cal deg^{-1}mole^{-1})*
(8) $\frac{1}{2}Cl_2$ (gas) + $e \rightleftharpoons Cl^-$ (aq.)	−39.85	−31.325	−28.6
	−39.895[4]	*−31.331*[4]	*−28.713*[4]
	−39.952[11]	*−31.372*[11]	
(1) Cl_2 (gas) + Cl^- (aq.) $\rightleftharpoons Cl_3^-$ (aq.)	− 7.44	+ 2.63	−33.8
	—	*+ 2.729*[1]	—
(2) Cl_2 (aq.) + Cl^- (aq.) $\rightleftharpoons Cl_3^-$ (aq.)	− 2.40	+ 0.91	−11.1
	—	*+ 1.03* [1]	—
		+ 0.981[2]	

TABLE 4

COMPARISON OF THERMODYNAMIC FUNCTIONS AT 25° OF THE $Cl_2/Cl^-/Cl_3^-$ SYSTEM

Literature values in italics. Data for the homologous systems, $Br_2/Br^-/Br_3^-$ and $I_2/I^-/I_3^-$, in parentheses, all from ref. 12

Species	$\Delta H°$ *(kcal mole^{-1})*	$\Delta G°$ *(kcal mole^{-1})*	$S°$ *(cal mole^{-1}deg^{-1})*
Cl^- (aq.)	−39.85	−31.325	− 2.0
	−39.895[4]	*−31.331*[4]	*− 2.079*[4]
	−39.952[11]	*−31.372*[11]	*− 2.1*[11]
Br^- (aq.)	*(−29.05)*	*(−24.85)*	*(+ 4.11)*
I^- (aq.)	*(−13.19)*	*(−12.33)*	*(+11.0)*
Cl_2 (aq.)	− 5.04	+ 1.72	+30.5
	− 5.6[11]	*+ 1.65*[11]	*+29*[11]
Br_2 (aq.)	*(− 0.62)*	*(+ 0.94)*	*(+31.2)*
I_2 (aq.)	*(+ 5.4)*	*(+ 3.92)*	*(+32.8)*
Cl_3^- (aq.)	−47.26	−28.70	+17.6
	—	*−20*[11]	—
Br_3^- (aq.)	*(−31.17)*	*(−25.59)*	*(+35.9)*
I_3^- (aq.)	*(−12.3)*	*(−12.3)*	*(+41.6)*

as both $\ln K_1$ and $\ln K_2$ varied linearly with T^{-1} in the interval 25–60° thus permitting an easy evaluation of $\Delta H°$ at 25°.

The values of the standard thermodynamic functions for reactions (1), (2), and (8) having been determined, those for the species, Cl^- aq., Cl_2 aq., Cl_3^- aq., were finally derived by obvious combinations of these values, and are collected in Table 4 for comparison with literature data. N.B.S. data[12] for the homologous species, Br^-, Br_2, Br_3^- and I^-, I_2, I_3^-, have also been included, for comparison purposes. Table 4 shows that there is good agreement between the literature data and the values from the present work for the $Cl^-/Cl_2/Cl_3^-$ system. Moreover, all the above functions follow a regular trend towards more positive values as the size of the halogen concerned increases, in the order: chlorine < bromine < iodine, with $\Delta G°$ for Br_2 aq. the only discrepancy. It seems reasonable to assume that the G^0-value for the Cl_3^- ion given in ref. 11, which is equally against the above trend, is due to a misprint. In fact, SHERRILL AND IZARD's value[1] for K_1 combined with earlier accurate values of $E_G°$ for the chlorine electrode[10,13,14] gives values of $\Delta G°$ of Cl_3^- such as -28.6 kcal mole^{-1}, not -20 kcal mole^{-1}.

The ionic entropy values quoted in Table 4 are all referred to

$$S_{H^+}° = \tfrac{1}{2} S_{H_2}° \text{ (at all temperatures)} \qquad (20)$$

a relation which comes directly from the convention of taking the standard potential of the hydrogen electrode as zero at all temperatures[15]. In particular, $S_{H^+}° = \frac{1}{2} S_{H_2}° =$ 15.604 cal deg^{-1} mole^{-1} at 25°[12]. If, however, the independent convention: $S_{H}° =$ 0.000 cal deg^{-1} mole^{-1} at 25° is used, 15.604 should be added to all values of ionic entropies quoted in Table 4. This, for example, would yield $S_{Cl^-}° = 13.6$ and $S_{Cl_3^-} =$ 33.2 cal deg^{-1} mole^{-1}.

ACKNOWLEDGEMENT

This investigation has been sponsored by the Consiglio Nazionale delle Ricerche, Rome, Italy.

SUMMARY

A new method using e.m.f. measurements of the cell, H_2, 1 atm | HCl, 1 M | Cl_2, p atm, combined with measurements of chlorine solubility in 1 M HCl is described for determining the standard potentials of the chlorine electrode and the equilibrium constants for the reactions, $Cl_2(gas) + Cl^-(aq.) = Cl_3^-(aq.)$ and $Cl_2(aq.) + Cl^-(aq.) = Cl_3^-(aq.)$ over the range 25–80°. The standard thermodynamic functions for the species relevant to the $Cl_2/Cl^-/Cl_3^-$ system have been derived from the results.

REFERENCES

1 M. S. SHERRILL AND E. F. IZARD, *J. Am. Chem. Soc.*, 53 (1931) 1667.
2 G. ZIMMERMANN AND F. C. STRONG, *J. Am. Chem. Soc.*, 79 (1957) 2063.
3 G. FAITA, P. LONGHI AND T. MUSSINI, *J. Electrochem. Soc.*, 114 (1967) 340.
4 A. CERQUETTI, P. LONGHI AND T. MUSSINI, *J. Chem. Eng. Data*, 13 (1968) 458.
5 G. BIANCHI, *J. Electrochem. Soc.*, 112 (1965) 233.
6 G. BIANCHI, A. BAROSI, G. FAITA AND T. MUSSINI, *J. Electrochem. Soc.*, 112 (1965) 921.
7 G. BIANCHI, G. FAITA AND T. MUSSINI, *J. Sci. Instr.*, 42 (1965) 693.

8 J. J. LINGANE, *Electroanalytical Chemistry*, 2nd rev. ed., Interscience, New York, 1958, p. 91.
9 D. A. MACINNES AND I. A. COWPERTHWAITE, *J. Am. Chem. Soc.*, 53 (1931) 555.
10 G. CHARLOT, *Oxidation–Reduction Potentials*, Pergamon, Paris, 1958, p. 25.
11 *Selected Values of Chemical Thermodynamic Properties, Nat. Bur. Std. (U.S.), Technical Note* 270–1, pp. 25–27, 1965.
12 *Selected Values of Chemical Thermodynamic Properties, Nat. Bur. Std. (U.S.), Technical Note* 270–3, pp. 31–37, 1968.
13 W. M. LATIMER, *Oxidation Potentials*, 2nd ed., Prentice-Hall, Englewood Cliffs, N.J., 1952, p. 53.
14 R. PARSONS, *Handbook of Electrochemical Constants*, Butterworths, London, 1959, p. 71.
15 D. J. G. IVES AND G. J. JANZ, *Reference Electrodes*, Academic Press, New York, 1961, pp. 11–14.

ELECTROANALYTICAL CHEMISTRY AND INTERFACIAL ELECTROCHEMISTRY
Elsevier Sequoia S.A., Lausanne – Printed in The Netherlands

VOLTAMMETRIC BEHAVIOUR OF CHLORITES AND CHLORINE DIOXIDE ON A PLATINIZED-PLATINUM MICROELECTRODE WITH PERIODICAL RENEWAL OF THE DIFFUSION LAYER AND ITS ANALYTICAL APPLICATIONS

GIORGIO RASPI AND FRANCESCO PERGOLA
Istituto di Chimica Analitica, Università di Pisa (Italy)
(Received September 27th, 1968)

The reduction of chlorites on a dropping mercury electrode has been the subject of several studies. Thus, RIUS AND GARRITZ[1] noted that chlorite gives a polarographic wave due to its irreversible reduction to chloride in a solution of 1 *M* KCl and 0.05 *M* $LaCl_3$. KONOPIK[2], and later KONOPIK AND BERGER[3], investigated the polarographic behaviour of chlorite in 1 *N* NaOH; under these conditions the height of the reduction wave is a non-linear, but reproducible, function of the chlorite concentration down to 10^{-6} *M*. HARTLEY AND ADAMS[4] suggest the determination of chlorite in solutions of pH 4.2–4.5 because in this pH-range the limiting current is proportional to the chlorite concentration.

Chlorite solutions can be reduced as well as oxidized. However, the study of the electrochemical oxidation of chlorite is not possible at a dropping mercury electrode because the process occurs at more positive potentials than that of mercury anodic dissolution. SCHWARZER AND LANDSBERG[5] studied the oxidation of chlorite on a graphite disk electrode in buffered solutions at various pH. In the pH-range 5–9, the oxidation process gives rise to a well-defined wave (barely reproducible data are obtained above pH 9) which allows the quantitative determination of chlorite. Chlorite and chlorine dioxide mixtures, in solutions of pH 5–5.5, give cathanodic waves characterized by a transfer coefficient, $\alpha = 0.5$, for both the anodic and the cathodic branch. Similar measurements carried out by the same authors at a platinum electrode, did not give satisfactory results; this was attributed to the presence of platinum oxides on the electrode surface and to a lower oxygen overvoltage.

The methods suggested so far consider the cathodic or the anodic behaviour of chlorites, within narrow pH-ranges. The present study of chlorite reduction and oxidation, in solutions of pH 0–14, makes use of the electrode with periodical renewal of the diffusion layer as suggested by COZZI *et al.*[6]. The results obtained have enabled us to set up a general method for the determination of chlorite and chlorine dioxide, separately or in mixture, and to establish the limits of its applicability in the presence of other species that are electroactive in the same potential range. The method gives a good reproducibility over a wide concentration range, is sensitive and easy to work.

The measurements were carried out at $25 \pm 0.1°$ with a three-electrode system using a Polarecord E261 Metrohm, modified to allow a slow change of the applied

potential, and an IR compensator, type E446 Metrohm. The microelectrode was platinized for 5 sec by a procedure described previously[7]. A saturated mercurous sulphate reference electrode, joined to the polarographic cell by a bridge of gelified silicic acid or by a solid mixture of silica gel and K_2SO_4 (3:2), was used. Buffer solutions of ionic strength, $\mu = 1$, were used as supporting electrolytes. Oxygen was removed by nitrogen scrubbing. The sodium chlorite solutions were prepared by the method suggested by FOERSTER AND DOLCH[8], and the chlorine dioxide solutions were prepared according to BRAY[9]. All potentials reported in the present work are referred to the SCE.

EXPERIMENTAL

By applying decreasing positive voltages to the electrode, a $1 \cdot 10^{-3}$ M chlorite solution, buffered at pH = 7.0 and deaerated, yields a current/voltage curve (curve a, Fig. 1) characterized by the presence of two distinct waves. The height of the anodic wave ($E_{\frac{1}{2}} = +0.705$ V) is one-quarter of that of the cathodic wave ($E_{\frac{1}{2}} = +0.080$ V).

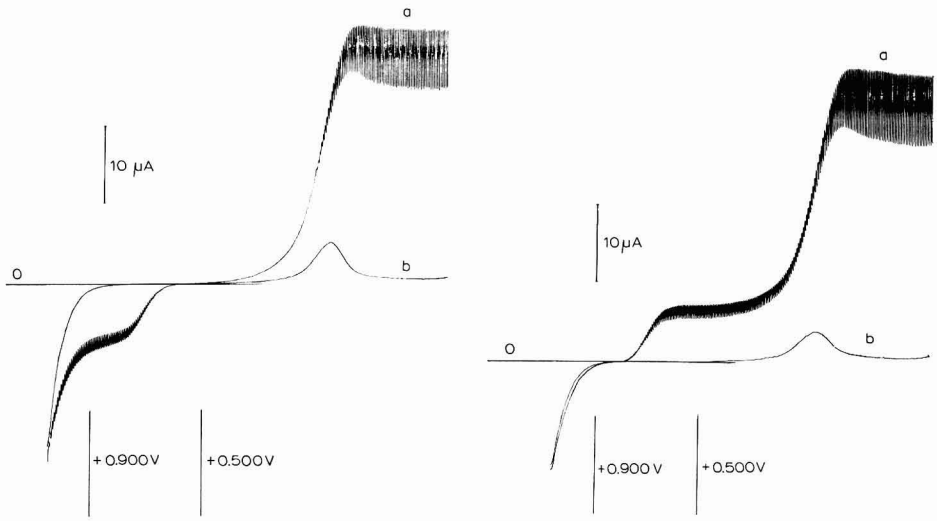

Figs. 1–2. Voltammetric curves of: (1) $1 \cdot 10^{-3}$ M chlorite; (2) $8 \cdot 10^{-4}$ M ClO_2. (a), in buffer soln. pH 7.0; (b), supporting electrolyte alone.

The current/voltage curve given by chlorine dioxide under the same experimental conditions shows two cathodic waves (Fig. 2): the $E_{\frac{1}{2}}$ of the first wave is +0.705 V and that of the second, +0.080 V. The second step is four times higher than the first. A comparison of Figs. 1 and 2, shows that the responses given by chlorite and chlorine dioxide solutions are substantially identical, when the different positions of the two curves with respect to the zero current line are taken into account. As ClO_2 and ClO_2^- behave analogously also under different conditions of acidity, only the results obtained with chlorite solutions will be described in detail.

In solutions of pH 5–9, the anodic wave is well formed and its limiting current is proportional to the chlorite concentration. The results of the coulometric meas-

urements (Table 1) show that the anodic electrode process is characterized by the transfer of one electron per molecule, according to the equation:

$$ClO_2^- \rightleftharpoons ClO_2 + e \qquad (1)$$

The charge transfer process (1), which has a high degree of irreversibility on smooth platinum, occurs reversibly on platinized-platinum. Thus, the log $[i/(i_d - i)]$ *vs.* E plot derived from the voltammetric curves of ClO_2^- (Fig. 1), ClO_2 (Fig. 2) and mixtures of the two is a straight line with a slope of about 60 mV, in accordance with the

TABLE 1

COULOMETRY OF 0.164 MMOLES OF $NaClO_2$ IN SOLUTION BUFFERED AT pH 7.0 AT A PLATINIZED-PLATINUM ANODE (7.5 cm^2) POLARIZED AT + 0.85 V

$C_{ClO_2^-}$ (mM)	Coulombs		
	Calcd. for 1 electron	*Exptl.*	*Difference*
2.60	—	—	—
2.27	2.01	2.10	+0.09
2.12	2.92	2.95	+0.03
1.96	3.90	4.00	+0.10
1.77	5.05	4.95	−0.10
1.60	6.09	6.00	−0.09
1.40	7.30	7.40	+0.10
1.22	8.40	8.40	—
0.99	9.80	9.75	−0.05
0.81	10.90	11.00	+0.10
0.58	12.30	12.25	−0.05

TABLE 2

COULOMETRY OF 0.164 MMOLES OF $NaClO_2$ IN SOLUTION BUFFERED AT pH 7.0 AT A PLATINIZED-PLATINUM CATHODE (7.5 cm^2) POLARIZED AT −0.25 V

$C_{ClO_2^-}$ (mM)	Coulombs		
	Calcd. for 4 electrons	*Exptl.*	*Difference*
2.60	—	—	—
2.44	3.90	4.00	+0.10
2.25	8.50	8.40	−0.10
2.11	11.92	12.00	+0.08
1.93	16.30	16.40	+0.10
1.75	20.70	20.70	—
1.57	25.00	25.10	+0.10
1.32	31.10	31.25	+0.15
1.10	36.50	36.40	−0.10
0.95	40.20	40.20	—
0.67	48.00	48.05	+0.05

reversible exchange of one electron. The value of the half-wave potential (+0.705 V) agrees with the value of the standard potential reported[10-12] for the ClO_2/ClO_2^- couple. The $E_{\frac{1}{2}}$-value does not vary with changes in the pH of the solution, according to eqn. (1). At constant chlorite concentration, for pH values above 10.5 the wave is doubled. The value of the ratio, $\Delta E/\Delta \log [i/(i_d - i)]$, remains at 60 mV. This shows that, also in alkaline solutions the electrode process takes place with the transfer of only one electron and not two as the amperometric measurements suggest. The above results indicate that the electrode reaction in strong alkaline media is still expressed by eqn. (1). However, as a result of the instability of ClO_2 in alkaline solutions, this electrode reaction is coupled with the purely chemical reaction:

$$2\,ClO_2 + 2\,OH^- \rightarrow ClO_2^- + ClO_3^- + H_2O$$

This disproportionation reaction yields chlorate and regenerates chlorite, which can then be further oxidized at the electrode, according to eqn. (1).

In solutions of pH 9–10.5, the limiting current is not well defined: this particular behaviour is being further investigated.

With chlorite solutions below pH 5, a composite cathanodic wave is observed. The cathodic limiting current of the above wave increases with increase in the acidity of the solution, reaching a limiting value corresponding to four times the anodic limiting current at pH < 2. Figure 3 shows the cathanodic wave obtained in

1 N $HClO_4$; the value for the ratio, $\Delta E/\Delta \log \{[(i_d)_c - i]/[i - (i_d)_a]\}$ derived from the logarithmic analysis of this wave is still equal to 60 mV. When ClO_2 is polarographed under the same experimental conditions, a cathodic wave with the same slope and half-wave potential as the cathanodic wave of Fig. 3 is obtained. In acid solutions

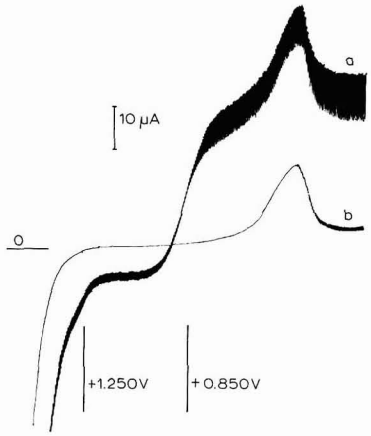

Fig. 3. Cathanodic wave of: (a), $1 \cdot 10^{-3}$ M chlorous acid in 1 N $HClO_4$ soln.; (b), supporting electrolyte alone.

(pH < 2) chlorous acid is not very stable tending to disproportionate according to the equation:

$$5\ HClO_2 \rightarrow 4\ ClO_2 + Cl^- + H^+ + 2\ H_2O$$

and if this is taken into account an examination of the results obtained leads to the following conclusions:

(a) The anodic zone of the composite wave corresponds to the oxidation of chlorous acid at the platinized-platinum electrode according to the following scheme:

$$HClO_2 \rightleftharpoons ClO_2 + H^+ + e$$

(b) The cathodic zone is due to the reduction of chlorine dioxide, produced by disproportionation of $HClO_2$ on the electrode:

$$ClO_2 + H^+ + e \rightleftharpoons HClO_2$$

Obviously, the above electrode process regenerates chlorous acid.

The cathodic wave ($E_{\frac{1}{2}} = +0.080$ V) shown in Fig. 1 (curve a) is not detectable (for the reasons already given) at pH < 2. It appears distorted at pH 2–5, and it is well formed only above pH 5. The limiting current of such a wave is proportional to the chlorite concentration. The current peak observed in the limiting current zone (curve a, Fig. 1) is due to the platinum oxide reduction, as can be seen from a comparison with the voltammetric curve of the supporting electrolyte (curve b, Fig. 1). The results of the coulometric measurements show that the reduction of chlorite takes place with participation of four electrons per molecule, in accordance with the electrode reaction:

$$ClO_2^- + 4\ H^+ + 4\ e \rightarrow Cl^- + 2\ H_2O \qquad (2)$$

The process occurs irreversibly on platinized-platinum, although with a lower overvoltage than that on smooth platinum. The logarithmic analysis of the wave shows that the ratio, $\Delta E/\Delta\log[(i_d-i)/i]$, is equal to 110 mV. As shown by eqn. (2), the process is influenced by the pH: a decrease in the acidity causes a displacement of $E_{\frac{1}{2}}$ of about 70 mV per pH unit towards more negative potentials.

ANALYTICAL APPLICATIONS

The determination of chlorite and chlorine dioxide is based on their different oxidizing powers in solution and how this is affected by the pH. The methods proposed make use of: (a) classic volumetric processes[13–15]; spectrophotometric measurements of either the optical density of the CCl_4 extract[16] or of the colour changes of the solution as a consequence of the oxidation of some organic substances[17]; (c) electroanalytical procedures for the detection of the equivalence point[3–5,18,19].

Methods (a) are laborious and their sensitivity is clearly lower than that reached by polarographic techniques; also, their specificity is unsatisfactory.

Methods (b), although giving appreciable sensitivity, are not very specific as many oxidizing substances react in the same way as chlorite and chlorine dioxide.

The electro-reduction of chlorite to chloride and its electro-oxidation to chlorine dioxide on the electrode with periodical renewal of the diffusion layer, occur at well-defined potentials for each pH-value, allowing the qualitative determination of ClO_2^-. Furthermore, the presence of two independent waves allows the chlorite concentration to be determined (by measuring the height of the anodic or the cathodic step) when the solution under examination contains compounds that interfere in the cathodic or anodic zone, respectively. Chlorates and chlorides do not interfere as the former is not electroactive and the latter may be oxidized only at voltages much more positive than the redox potential of the ClO_2/ClO_2^- couple. The hypochlorite ion is reduced to chloride at more positive potential than those at which chlorite is reduced. In 1 *N* NaOH solution, the reaction between ClO^- and ClO_2^- is very slow[20] and the determination of chlorite in the presence of hypochlorite is possible provided the molar ratio, ClO^-/ClO_2^-, is not greater than 15.

TABLE 3
POLAROGRAPHIC DETERMINATION OF $NaClO_2$ IN BUFFER SOLUTION PH 7.00

$NaClO_2$ added (mg/l)	*Anodic wave*		*Cathodic wave*	
	$NaClO_2$ found (mg/l)	*Error (%)*	*$NaClO_2$ found (mg/l)*	*Error (%)*
1.8	—	—	1.65	−8.5
3.6	3.37	−6.4	3.35	−7.0
5.2	5.42	+4.2	4.88	−6.2
10.4	10.12	−2.7	10.97	+5.5
20.8	20.14	−3.2	20.47	−1.6
30.0	30.75	+2.5	30.93	+3.1
41.6	42.00	−1.0	41.23	−0.9
55.0	54.56	−0.8	54.67	−0.6
68.0	68.60	+0.9	68.34	+0.5
83.2	83.86	+0.8	83.95	+0.9
100.0	99.05	−0.5	100.90	+0.9

Chlorine dioxide should be determined in a relatively acid solution ($HClO_4$, 1 N) in order to attain a greater sensitivity. Fe(III) and O_2 do not interfere. Chlorine dioxide can be determined in the presence of chlorine when the Cl_2/ClO_2 molar ratio is below 20.

This method, which is of general applicability, is particularly suitable for the determination of chlorite (Table 3) and chlorine dioxide (Table 4), even when present in $2 \cdot 10^{-5}$ M concentration.

TABLE 4

POLAROGRAPHIC DETERMINATION OF ClO_2 IN 1 N $HClO_4$ SOLUTION

ClO_2 added (mg/l)	*ClO_2 found (mg/l)*	*Error (%)*	*ClO_2 added (mg/l)*	*ClO_2 found (mg/l)*	*Error (%)*
1.34	1.24	−7.3	45.20	45.42	+0.5
2.68	2.54	−5.2	56.40	57.05	+1.2
5.40	5.72	+5.9	68.30	67.75	−0.8
10.70	10.26	−4.1	79.60	79.45	−0.2
21.50	21.03	−2.2	90.00	90.27	+0.3
33.00	33.45	+1.4			

ACKNOWLEDGEMENT

The authors are grateful to the Consiglio Nazionale delle Ricerche of Italy for financial support.

SUMMARY

Chlorite and chlorine dioxide solutions show an analogous voltammetric behaviour on a platinized-platinum micro-electrode with periodical renewal of the diffusion layer.

Dilute chlorite solutions at pH > 5 shows two distinct waves, one in the anodic and the other in the cathodic range. The anodic wave is due to the oxidation of chlorite to chlorine dioxide and the cathodic to its reduction to chloride. At pH ≥ 10.5, the anodic wave is influenced by the disproportionation of chlorine dioxide produced at the electrode. Thus its height is doubled and the final oxidation product is chlorate. At pH < 2 the disproportionation of $HClO_2$ takes place very rapidly on platinized-platinum producing a cathanodic wave due to the system, $ClO_2/HClO_2$. The charge transfer process is reversible under the above conditions.

A new polarographic method is reported for the determination of chlorites and chlorine dioxide, based on the measurements of the height of the waves given by these species.

REFERENCES

1 A. RIUS AND A. M. GARRITZ, *Anales Real Soc. Espan. Fis. Quim. Madrid*, 46B (1950) 683.
2 N. KONOPIK, *Monatsh. Chem.*, 83 (1952) 255.
3 N. KONOPIK AND E. BERGER, *Monatsh. Chem.*, 84 (1953) 666.
4 A. H. HARTLEY AND A. C. ADAMS, *J. Electroanal. Chem.*, 6 (1963) 460.
5 O. SCHWARZER AND R. LANDSBERG, *J. Electroanal. Chem.*, 14 (1967) 339.

6 D. COZZI, G. RASPI AND L. NUCCI, *J. Electroanal. Chem.*, 12 (1966) 36.
7 G. RASPI AND G. CIANTELLI, *Chim. Ind. Milan*, 47 (1965) 1325.
8 F. FOERSTER AND P. DOLCH, *Z. Elektrochem.*, 23 (1917) 138.
9 W. BRAY, *Z. Physik. Chem.*, 54 (1906) 569.
10 G. HOLST, *Svensk Papperstid.*, 48 (1945) 23.
11 I. E. FLIS, *Zh. Fiz. Khim.*, 32 (1958) 573.
12 T. NAITO, *Kogyo Kagaku Zasshi*, 65 (1962) 749.
13 I. M. KOLTHOFF AND R. BELCHER, *Volumetric Analysis*, Vol. III, Interscience, New York, 1958.
14 E. SCHULEK AND P. ENDVOI, *Anal. Chim. Acta*, 5 (1951) 245.
15 E. SCHULEK AND P. ENDVOI, *Anal. Chim. Acta*, 5 (1951) 368.
16 M. I. SHERMAN AND J. D. H. STRICKLAND, *Anal. Chem.*, 27 (1955) 1778.
17 H. W. HODGEN AND R. S. INGOLS, *Anal. Chem.*, 26 (1954) 1224.
18 F. HALLER AND S. S. LISTEK, *Anal. Chem.*, 20 (1948) 639.
19 J. KEPIŃSKI AND G. BLASZKIEWICZ, *Talanta*, 13 (1966) 357.
20 H. TAUBE AND H. DODGEN, *J. Am. Chem. Soc.*, 71 (1949) 3330.

ELECTROANALYTICAL CHEMISTRY AND INTERFACIAL ELECTROCHEMISTRY
Elsevier Sequoia S.A., Lausanne – Printed in The Netherlands

DEPENDENCE OF ELECTRODE KINETICS ON MOLECULAR STRUCTURE. NITRO-COMPOUNDS IN DIMETHYLFORMAMIDE

M. E. PEOVER AND J. S. POWELL
Division of Molecular Science, National Physical Laboratory, Teddington, Middlesex (U.K.)
(Received September 28th, 1968)

INTRODUCTION

There has been little systematic study of the factors influencing the electrode kinetics of organic compounds in relation to the structure of the organic. In part, this is due to the complications introduced by the ready adsorption of organic compounds on the electrode from aqueous solutions. However, in non-aqueous solvents it is possible to find conditions under which the electrode behaviour of many organics shows little or no specific adsorption phenomena. ATEN AND HOYTINK showed that the reduction of polycyclic aromatic hydrocarbons can be investigated by conventional impedance bridge methods in dimethylformamide[1]. Recently DIETZ *et al.*[2] studied electron transfer in a series of stilbenes in the same solvent, in which changes in both heterogeneous and homogenous electron exchange rates could be correlated with change in structure of the molecule. In the stilbene series, the charge in the resulting anion-radicals is delocalised over the whole molecule and changes in rate with structure were attributed to effects of non-planarity in the initial state–transition state–final state sequence, leading to lower rates of reaction in the non-planar compounds. By contrast, we have now investigated a series of nitro-compounds in which the charge in the anion-radical is more or less localised on the nitro-group. The spin density on the nitro-group is known from electron-spin-resonance studies and can be changed easily by suitable structural changes in the remainder of the molecule. Thus, in the anion-radical of an aliphatic nitro-compound the charge on the nitro-group is virtually unity, while in that of a nitrobenzene, charge can be delocalised into the aromatic system. The degree of localisation in the aromatic ring can be varied particularly by twisting the nitro-group out of the plane of the ring, using suitable substituents. In this way, the fraction of spin on the nitro-group has been varied from unity to about 0.15 electron. We shall adopt the working hypothesis that spin and charge densities are similar and change in a similar fashion. Under these conditions it can be expected that the changes in solvation energy resulting from charge distributions will predominate in the kinetic picture, as the nitro-group is small compared with the benzene ring.

As in the work on stilbenes, a series of compounds has been chosen covering a small range of reduction potential to minimise effects arising from the dependence of electrical double layer effects on electrode charge. Despite attendant problems, quaternary ammonium salts have been used as base electrolytes. The great advantage in the use of quaternary ammonium salts is that ion-association with the aromatic

anions is minimised. Such associations are important with alkali metal cations and nitro-aromatic anions in dimethylformamide as shown by ADAMS *et al.*[3] through perturbations of the ESR spectra and by polarographic studies[4]. These authors also provided good evidence that the quaternary ammonium salts are essentially free ions in dimethylformamide[3]. The solvent used, dimethylformamide, gives little specific solvation of the nitro-group as shown from studies of solvent-dependence of the nitrogen coupling constant in the ESR spectra[5].

EXPERIMENTAL

Impedance measurements were made on a conventional Wien bridge (Fig. 1). A Wagner earth was used to cancel stray capacitance to earth, and it also ensures that one side of the cell (the dropping mercury electrode) is at virtual earth potential. This minimises noise pick-up and also places one side of the bias-measuring voltmeter at earth potential. The Wagner earth was adjusted by switching the detection amplifier between earth and one of the detection points on the bridge. Noise was also minimised by eliminating transformer input and using a directly coupled detector amplifier instead. The whole apparatus was placed in a Faraday cage. The bias potential was applied across the bridge avoiding shunting the cell and the need to correct for this. The balance point was detected by passing the amplifier output to the Y plates and the reference signal from the oscillator to the X plates of an oscilloscope. When off balance, an inclined ellipse is formed, at the balance point a horizontal straight line is formed; measurements were made at the end of drop life using free-fall; in this connection a long persistence phosphor is useful.

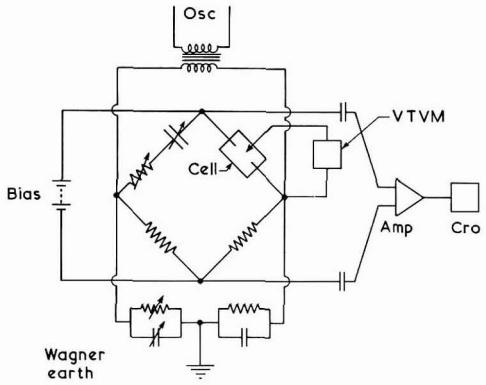

Fig. 1. Schematic diagram of the impedance bridge.

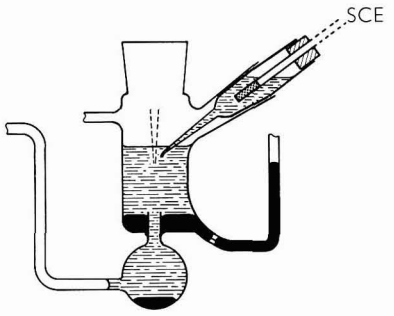

Fig. 2. The cell.

The cell is shown in Fig. 2. The annular mercury pool working anode avoids change in level with accumulation of mercury drops and also avoids electrical noise as the drop strikes the pool. An additional opening for introduction of material without affecting cell geometry is omitted from Fig. 2. Solutions were de-oxygenated with "oxygen-free" nitrogen (Air Products) through the lower tube. The electrode assembly is shown in Fig. 3. The capillary and whisker tip are of lead glass. The tip

reduced dispersion of the capacity from that with a blunt end capillary, 6–10% to 0.5–1% in the region 400–10,000 Hz. Using free-fall drops, reproducibility was ±0.1%.

Dimethylformamide was distilled under reduced pressure with a N_2 bleed, passed through a column of 4A molecular sieve and stored over molecular sieve for a few days. Decomposition of solvent is readily detected by liberation of free iodine from iodide solutions; the solvent could usually be kept for one week before re-purification was necessary. Tetrabutylammonium iodide was purified as described previously[2]. The nitro-compounds were either purified commercial samples or were synthesised according to literature methods, and had reported physical constants. Purity was checked by gas–liquid chromatography and polarography. The concentration of nitro-compound was $2 \cdot 10^{-4}$ M except for the nitroalkanes which were $5 \cdot 10^{-4}$ M.

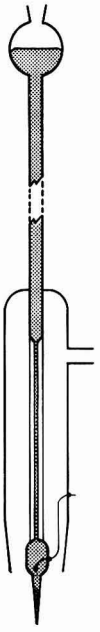

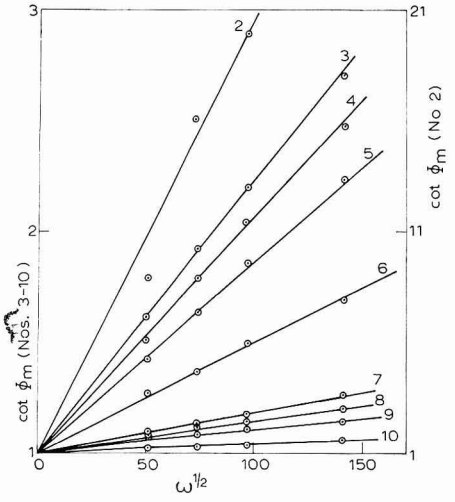

Fig. 3. The dropping mercury electrode.

Fig. 4. Frequency-dependence of the cotangent of the phase angle minimum in reduction of nitro-compounds in dimethylformamide containing 0.1 M NBu_4I at 30°. Key as in Table 1.

RESULTS

The bridge measurements were evaluated by computation of the phase angle, Φ, which has the advantage that adsorption phenomena are readily revealed by anomalous phase angles; also, Φ is independent of electrode geometry, concentration of electroactive species and, in certain circumstances, of coupled chemical reactions[6]. The maximum value of cot Φ occurs near the redox potential and is given by[6]:

$$\cot \Phi_m = 1 + (2D\omega)^{\frac{1}{2}} / \{k_{app}([\alpha/(1-\alpha)]^{-\alpha} + [\alpha/(1-\alpha)]^{1-\alpha})\} \quad (1)$$

and the potential at cot Φ_m is given by

$$E_{\cot\Phi_m} = E_{\frac{1}{2}} + (RT/F) \ln (\alpha/(1-\alpha)) \quad (2)$$

where k_{app} and α are the measured rate constant and transfer coefficient, respectively. The diffusion coefficient is obtained from the frequency-dependence of the minimum in the diffusion polarisation resistance

$$q_m\omega = \sigma_m\omega^{\frac{1}{2}}(4RT\omega^{\frac{1}{2}}/n^2F^2(2D)^{\frac{1}{2}}C_bA) \qquad (0.6>\alpha>0.4) \quad (3)$$

The dependence of cot Φ_m on frequency, eqn. (1), is shown in Fig. 4 and is normal. At higher concentrations of nitro-compounds, slightly higher rate constants are obtained (by about 10%). It is believed that relative rate constants should be meaningful, while absolute values are probably less reliable than those reported recently for the stilbenes in which no concentration variation was found. A further reservation must be applied to the results for nitropropane and nitrobutane since a coupled chemical reaction (presumably protonation by the solvent) is involved, comparable in rate with drop life but slow compared with a.c. frequency. Under those conditions, the phase angle is predicted to be unaffected by the chemical reaction, although the magnitude of the alternating current is affected[6]. However, in our case the chemical reaction leads to further electron transfer

$$R + e \rightleftharpoons R^- \text{ (at electrode)}$$

$$R^- + HS \rightleftharpoons RH^\circ + S^- \text{(in diffusion layer)}$$

$$RH^\circ + R^- \rightarrow RH^- + R \text{ (in diffusion layer)}$$

$$(RH^\circ + e \rightarrow RH^-) \text{ (at electrode)}$$

Provided reduction of RH° occurs *via* R^- and not at the electrode, *i.e.*, in the diffusion layer, the phase angle should still remain unaffected for moderate excursions into charge-transfer control[7]. This is likely to be true for the slow chemical reactions involved here (reaction ~ 80–90% complete in 5 sec). Since coupled chemical reactions affect the diffusion polarization term, diffusion coefficients for the nitroalkanes were obtained from d.c. polarographic measurements.

The rate constants obtained from eqns. (1)–(3) are apparent values, uncorrected for retardation of electron transfer by the electric field in the diffuse layer. The range of electrode charge covered by the nitro-compounds is -7 to -11.5 μC/cm^2 and this will not lead to large variations in the rate inhibition. Although tetrabutylammonium cations are much less surface active in dimethylformamide than in water, some specific adsorption probably occurs at high negative values of electrode charge[8]. There is the further problem of the location of the electroactive molecule in the pre-electrode state. By analogy with the results for stilbenes[2], neither of these factors appears to be of overwhelming significance and application of simple diffuse layer theory taking into account ion-association of the supporting electrolyte probably gives a better estimate of the absolute magnitude of the true rate constants and the effects of double-layer inhibition than with no correction applied. A factor of about ten is involved, which may be too large if there is specific adsorption of quaternary ammonium ions or if the molecule is located further from the electrode than the outer Helmholtz plane. In addition, potassium iodide base electrolyte was used for nitromesitylene, and the lower rate found, 0.18 cm/sec compared with 0.31 cm/sec,

is consistent with the higher value of electrode charge, 11.4 μC/cm^2 compared with 10.4 μC/cm^2, and may also reflect less retardation in the quaternary ammonium solution through some specific adsorption of that ion. However, the important point is that the effect of change in cation is fairly small, much smaller than the double-layer corrections. The results are collected in Table 1.

TABLE 1

ELECTROCHEMICAL PARAMETERS FOR REDUCTION OF NITRO-COMPOUNDS IN DIMETHYLFORMAMIDE CONTAINING 0.1 M NBu_4I AT 30°

	$-E_{\frac{1}{2}}$ (V vs. SCE)	q^M (μC/cm^2)	a_N	$D^{\frac{1}{2}} \cdot 10^3$ (cm/sec$^{\frac{1}{2}}$)	α	k_{app} (cm/sec)
1. *tert*-Nitrobutane	1.64	11.5	26 [a]	3.6	0.5	0.009
2. *tert*-Nitropropane	1.64	11.5	26 [a]	3.6	0.5	0.0125
3. Aminonitrodurene	1.52	11.0	20.65 [b]	2.3	0.51	0.128
4. Nitrodurene	1.42	10.5	19.13 [b]	2.9	0.50	0.145
5. Nitromesitylene	1.38	10.4	15.95 [b]	2.9	0.50	0.28
6. *o-tert*-Butylnitrobenzene	1.30	10.0	14.9 [c]	3.2	0.49	0.45
7. *p*-Nitroaniline	1.37	10.4	11.49 [b]	3.1	0.51	1.21
8. *o*-Nitrotoluene	1.28	9.8	11.0 [c]	3.4	0.50	1.65
9. *p*-Nitrotoluene	1.14	9.5	10.06 [d]	3.4	0.54	2.7
10. *m*-Dinitrobenzene	0.80	7	3.97 [e]	3.5	0.50	5

[a] in CH_3CN, from ref. 10. [b] in DMF, from ref. 16. [c] in CH_3CN, from ref. 11. [d] in DMF, from ref. 17. [e] in DMF, from ref. 5.

DISCUSSION

The rate constants for anion-radical formation at a mercury electrode for the series of nitro-compounds are inversely related to the values of the coupling constant at the nitrogen atom, a_N, determined by electron spin resonance, Table 1. We shall now attempt to put this relation on a quantitative basis.

The value of a_N is a measure of the unpaired spin density on the nitro-group and we shall assume it to be directly proportional to the charge density excess over that in the neutral molecule. This is certainly only approximately correct. Since for the nitroalkanes the charge density on the alkyl groups is very small, $\sim 1\%$, the average experimental value of $a_N = 26$ corresponds closely to unit charge[9,10]. In nitrobenzenes the hybridisation state of the carbon atom bearing the nitro-group is sp^2 while in nitroalkanes it is sp^3. However, the spin density on that carbon is negligible in 2-nitropropane and has been estimated to be so in nitrobenzenes also. Thus the proportionality between spin density and charge density in the nitro-group should be the same in both cases:

$$e(NO_2) = a_N Q_N \qquad (Q_N = 1/26) \tag{4}$$

Thus, reference to Table 1 shows that the charge density on the nitro-group on our assumptions varies from unity to 0.15 electron in the series considered. The solvation energy of the anion radical will be considered on the basis of a model consisting of two or more spheres, one representing the nitro-group of radius $r_{NO_2} = 2.75$ Å, and one representing the remainder of the molecule, in the case of nitrobenzenes of average radius, $r_{ring} = 3.5$ Å. For dinitrobenzene, a third sphere is considered. Also,

for the aliphatic compounds the solvent cavity is determined by the size of the molecule as a whole, $r = 3$ Å. This type of model gives good agreement with experimental solvation energies[12] and in our opinion is preferred to a summation over excess charge at each atom localised at the centre of its own solvent sphere since, in fact, that model departs further from the physical reality—it is not possible for each atom to be surrounded by a solvent sphere.

The values for the radii were chosen from models. According to the theories of MARCUS[13] and HUSH[14], the chief contribution to the free energy of activation for electron transfer comes from the reorientation of solvent molecules and is given on a dielectric continuum model by

$$\Delta F_{sol}^{*} = \tfrac{1}{2} m^2 (ne)^2 \, (1/a_1 - 1/2\delta)(1/D_{op} - 1/D_s) \qquad (5)$$

where $m = -\alpha$, a_1 is the radius of the reactant in the transition state (assumed spherical), δ is the distance from the centre of the reactant to the electrode surface and D_{op} and D_s are the local optical and static dielectric constants, respectively.

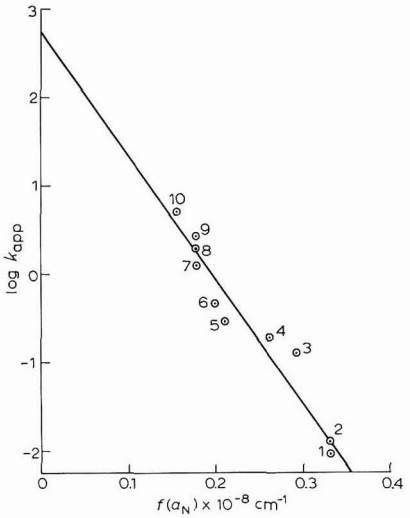

Fig. 5. Dependence of experimental rate constant for electro-reduction of nitro-compounds on spin density at the nitrogen atom in nitroanion radicals in dimethylformamide at a mercury electrode (eqns. (6) and (7)). The line is of theoretical slope (eqn. (7)). Key as in Table 1.

Assuming for our series of compounds the same location of the pre-electrode state, then δ, D_{op} and D_s are constant, and since experimentally, α varies little from 0.5, we have, replacing a_1 by our model

$$\Delta F_{sol}^{*} = \frac{e^2}{8}\left[\sum (a_N Q_N)^2 / r_{NO_2} + (1 - \sum a_N Q_N)^2 / r_{ring}\right](1/D_{op} - 1/D_s) - e^2(1/D_{op} - 1/D_s)/16\delta \qquad (6)$$

Here we neglect solvation of the neutral molecule and also suppose that the transition state radii are the same as in the neutral molecule. Also from the Arrhenius–Marcus equation we have for an adiabatic reaction:

$$\ln k \cong \ln Z - \Delta F_{sol}^{*}/RT$$
$$= \ln Z - Ne^2(1/D_{op} - 1/D_s) f(a_N)/8\,RT + Ne^2(1/D_{op} - 1/D_s)/16\,RT\delta \qquad (7)$$

where N is Avogadro's number, Z is the collision frequency, $\approx 10^4$ cm/sec, and $f(a_N)$ is the term in a_N in eqn. (6). The test of eqn. (7) is shown in Fig. 5 where the slope of the line has the theoretical value of:

$$-Ne^2(1/D_{op} - 1/D_s)/(2.303\,RT \cdot 8)$$

D_s being taken as the bulk value. A fair prediction of the variation in experimental rate constant with structure is found.

ACKNOWLEDGEMENT

The authors thank Dr. R. DIETZ for helpful discussions and Mr. B. E. LARCOMBE for preparation of some of the compounds.

SUMMARY

The kinetic parameters for the one-electron reduction of a series of nitro-compounds in dimethylformamide covering three orders of magnitude have been determined by the impedance bridge. The rate constants are correlated with spin localisation in the resulting anion-radical. Marcus theory, using a dielectric continuum model taking into account charge distribution, gives a reasonably satisfactory description of the behaviour.

REFERENCES

1 A. C. ATEN AND G. J. HOYTINK, *Advances in Polarography*, Pergamon, Oxford, 1961, p. 777.
2 R. DIETZ AND M. E. PEOVER, *Discussions Faraday Soc.*, 45 (1968).
3 T. KITAGAWA, T. LAYLOFF AND R. N. ADAMS, *Anal. Chem.*, 36 (1964) 925.
4 L. HOLLECK AND D. BECHER, *J. Electroanal. Chem.*, 4 (1962) 321.
5 P. H. RIEGER AND G. K. FRAENKEL, *J. Chem. Phys.*, 39 (1963) 609.
6 D. E. SMITH, *Electroanalytical Chemistry*, Dekker, New York, 1966, chap. 1.
7 D. E. SMITH, personal communication, 1968.
8 V. D. BEZUGLYI AND L. A. KORSHIKOV, *Sov. Electrochem.*, 1 (1965) 1279.
9 L. H. PIETTE, P. LUDWIG AND R. N. ADAMS, *J. Am. Chem. Soc.*, 83 (1961) 3909; 84 (1962) 4212; *Anal. Chem.*, 34 (1962) 916.
10 A. K. HOFFMANN, W. G. HODGSON, D. L. MARICLE AND W. H. JURA, *J. Am. Chem. Soc.*, 86 (1964) 631.
11 D. H. GESKE, J. L. RAGLE, M. A. BAMBENEK AND A. L. BALCH, *J. Am. Chem. Soc.*, 86 (1964) 987.
12 M. E. PEOVER, *Electrochim. Acta*, 13 (1968) 1083.
13 R. A. MARCUS, *J. Chem. Phys.*, 43 (1965) 679.
14 N. S. HUSH, *Trans. Faraday Soc.*, 57 (1961) 557.
15 J. M. HALE, personal communication, 1968.
16 R. D. ALLENDOEFER AND P. H. RIEGER, *J. Am. Chem. Soc.*, 88 (1966) 3711.
17 J. M. FRITSCH, T. P. LAYLOFF AND R. N. ADAMS, *J. Am. Chem. Soc.*, 87 (1965) 1724.

NOTE ADDED IN PROOF

HALE has suggested[15] that $f(a_N)$ contains an additional term $2a_N Q_N(1 - a_N Q_N)/R$, where R is the distance between the spheres in the above model, representing in effect the repulsion energy between the two spheres. The variation in k_{app} with $f(a_N)$ remains essentially unchanged by this addition, but the intercept in Fig. 5 becomes closer to the theoretical value of log Z. This may imply that the image term in δ, eqn.(7), is negligible, providing the double-layer corrections are small.

ELECTROANALYTICAL CHEMISTRY AND INTERFACIAL ELECTROCHEMISTRY
Elsevier Sequoia S.A., Lausanne – Printed in The Netherlands

SOLUBILITY PRODUCTS AND RELATED THERMODYNAMIC QUANTITIES OF SILVER HALIDES IN MOLTEN (Li,K)NO_3 FROM E.M.F. MEASUREMENTS

GIUSEPPE ALBERTO SACCHETTO, GIAN ANTONIO MAZZOCCHIN AND G. GIORGIO BOMBI

Istituto di Chimica Analitica dell'Università, Padova (Italy)

(Received September 28th, 1968)

INTRODUCTION

The solubility products of silver halides in molten (Li,K)NO_3 eutectic have been determined by TIEN AND HARRINGTON[1], at temperatures ranging between 420 and 485°K, from potentiometric titration data. Their data are in approximate agreement with the result obtained with the same technique, at 423°K, by BOMBI *et al.*[2] in the case of AgCl, but disagree with analogous results for AgBr and AgI. On the other hand, the solubility product for AgI by BOMBI *et al.* is confirmed by the values calculated by SACCHETTO *et al.*[3] from standard potential values for the $I_{2(g)}/I^-$ electrode and from thermodynamic data for the formation of AgI.

JORDAN *et al.*[4] determined the values of $\Delta H°$ for the precipitation of silver halides in the same solvent at 431°K, by the thermometric titration technique; they also obtained a value of $\Delta G°$ for the precipitation of AgCl, which appears to be too negative when compared with the data reported by TIEN AND HARRINGTON and by BOMBI *et al.*

In order to clarify these discrepancies and to improve the reliability of the solubility products and related thermodynamic quantities, measurements in a wide temperature range, by the e.m.f. method, have been undertaken for the three silver halides in the same alkali nitrate mixture.

The e.m.f. of the cell:

$$\begin{array}{ccc|c|c|c|c|c|c} & & (\text{Li,K})NO_3 & & (\text{Li,K})NO_3 & & & & \\ \text{Pt} & \text{Ag} & & \| & & \text{AgX} & \text{Ag} & \text{Pt} & \text{(I)} \\ & & AgNO_3 & & KX & & & & \end{array}$$

has been determined for KX (X = Cl, Br, I) concentrations ranging between $5 \cdot 10^{-4}$ and $1 \cdot 10^{-1}$ mole kg^{-1}, in the temperature intervals 410–560°K for AgCl and AgBr, and 410–500°K for AgI. No measurement was taken at higher temperatures for AgI, owing to the oxidizability of the iodide ion in the (Li,K)NO_3 melt already ascertained[2,3].

EXPERIMENTAL

Details on the preparation of the (Li,K)NO_3 (43 mole% $LiNO_3$) solvent have

been given elsewhere[5]. All other chemicals employed were reagent-grade (C. Erba, Milano).

E.m.f. measurements were carried out in a multiple-neck cell similar to that previously described[3]. Silver–silver halides electrodes (wires, 1 cm^2 area) were prepared according to the electrolytic procedure described by IVES AND JANZ[6]. For other details on apparatus, see ref. 3. The reference compartment was separated from the main solution (150 g) by means of a fine sintered glass disk and contained about 10 g of a silver nitrate solution of known concentration (about 10^{-2} mole kg^{-1}).

To test the validity of the Nernst equation for the silver–silver ion electrode, the e.m.f. of silver nitrate concentration cells was measured over the temperature range, 410–570°K. After proper correction for the bias potentials (see below), the Nernst equation was found to be obeyed within 0.2 mV at concentrations above about 10^{-2} mole kg^{-1}, and within 1 mV at concentrations down to $5 \cdot 10^{-4}$ mole kg^{-1}.

For measurements on cell (1), about $5 \cdot 10^{-3}$ mole kg^{-1} $AgNO_3$ and an equivalent amount of KX were added to the main compartment, to ensure saturation of the solution before introducing the electrodes. Weighed amounts of KX were successively introduced and the e.m.f. was measured after each addition at different increasing or decreasing temperatures; the additions were always made at the highest or lowest temperature of the run. In some cases, the additions were made after a complete temperature cycle. Agreement within 0.1–0.2 mV was found between the values obtained with increasing and decreasing temperature. Occasionally, the solution in the reference compartment was changed for a solution of different concentration. If the concentration difference is taken into account, the agreement between the measured e.m.f. values was again within a few tenths of a millivolt.

Duplicate e.m.f.-values were obtained by using four electrodes, two in each half-cell. The potential differences (biases) between the electrodes in the same compartments were monitored; these biases were generally lower than 0.4 mV (typical value, 0.2 mV) and remained constant within ± 0.2 mV during a run. At the end of each experiment, the biases between the electrodes from different compartments were measured by immersing all four electrodes in the main solution. The latter biases were of the same order of magnitude as those above and were algebraically added to the measured e.m.f.-values. After this correction, the duplicate e.m.f.-values agreed within the bias uncertainty (± 0.2 mV); their mean value was used in the calculations.

RESULTS AND DISCUSSION

The formation of soluble complexes between silver and halide ions must be taken into account in calculating the solubility products from e.m.f. data. The relevant equations are reported in ref. 7; from these, considering only the species, AgX, AgX_2^- and Ag_2X^+, the following equation can be obtained:

$$K_{s0} = [Ag^+](C_X + [Ag^+])/(1 + \beta_{2,1} K_{s0} - \beta_{1,2}[Ag^+]^2) \quad (2)$$

C_X is the total concentration of halide added, $\beta_{2,1}$ and $\beta_{1,2}$ are the overall stability constants for AgX_2^- and Ag_2X^+, respectively, and $[Ag^+]$ is the free silver ion concentration, obtained from the e.m.f. of cell (1), regarded as a silver ion concentration cell.

The only available stability constants for silver–halide complexes in the

eutectic (Li,K)NO_3 mixture are those by TIEN AND HARRINGTON[8,9] ($\beta_{1,1}=96$ mole^{-1} kg; $\beta_{2,1}=16$ mole^{-2} kg^2 for $AgCl$ and $AgCl_2^-$, respectively, at 498°K) and by GAL *et al.*[10] ($\beta_{1,1}=310$ mole^{-1} kg and $\beta_{2,1}=38800$ mole^{-2}kg^2 for the same complexes at 423°K).

From a thorough investigation of the existing data for various nitrate melts (for a detailed bibliography see the review by HSU *et al.*[11]), some general features can however be assumed. The values of $\beta_{1,2}$ and $\beta_{2,1}$ for a given halide in a particular solvent mixture are of the same order of magnitude and do not vary greatly from one mixture to another, while $\beta_{1,2}$- and $\beta_{2,1}$-values for different halides in the same solvent increase by about an order of magnitude when going from chloride to bromide and from bromide to iodide. Furthermore, the $\Delta H°$-values for the formation of AgX_2^- and Ag_2X^+ vary from about -8 to -16 kcal mole^{-1} and are always smaller, as can be easily anticipated, than the $\Delta H°$-values for the precipitation of the corresponding solid halides (from about -18 to -32 kcal mole^{-1}). From these facts and from the existing data, the values of $\beta_{2,1}$ and of $\beta_{1,2}$ for the three halides in (Li,K)NO_3 can be roughly estimated at various temperatures; their order of magnitude is such that the denominator in eqn. (2) cannot differ significantly from unity for bromide and iodide in our experimental temperature range, while a small effect can be expected for chloride. The β-values can therefore be put equal to zero for bromide and iodide, while in the case of chloride, reliable β-values are needed. To supplement the data quoted above, approximate formation constants for the silver–chloride complexes in our solvent mixture were obtained by e.m.f. measurements at 560°K in the concentration range of silver and chloride ions where no precipitation occurs. Using the computing method proposed by BRAUNSTEIN *et al.*[12] and assuming $\beta_{1,2}=\beta_{2,1}$, we obtained $\beta_{1,1}=65$ mole^{-1}kg and $\beta_{1,2}=\beta_{2,1}=1200$ mole^{-2}kg^2. β-values at other temperatures were obtained by linear interpolation in a log $\beta_{2,1}$ *vs.* $1/T$ plot between our datum and that of GAL *et al.* (the $\beta_{2,1}$-value by TIEN AND HARRINGTON is probably wrong) and by assuming, as before, $\beta_{1,2}=\beta_{2,1}$. These values were introduced into eqn. (2) to compute K_{s0}-values. If the formation of $AgCl_2^-$ and Ag_2Cl^+ were neglected, the values of K_{s0} would be higher by about 0.2% at the lowest, and by about 1.5% at the highest, experimental temperature. On the other hand, in view of the small effect of these complexes, the relatively large inaccuracy in the β-data and the simplifying assumption that $\beta_{1,2}=\beta_{2,1}$ cannot affect appreciably the calculated K_{s0}-values.

The right-hand half-cell of cell (1) can be also considered as a silver–silver halide second-kind electrode, the standard potential of which is given by

$$E°_{Ag/AgX/X^-}=E°_{Ag/Ag^+}+(RT/F)\ln K_{s0}$$

or, assuming the Ag/Ag^+ (1 mole kg^{-1}) electrode as the standard reference, by

$$E°_{Ag/AgX/X^-}=(RT/F)\ln K_{s0} \qquad (3)$$

As a consequence of our choice of the standard reference electrode, all the thermodynamic quantities for the silver–silver halide electrode reaction are equal to the corresponding quantities for the dissolution reaction of the corresponding silver halide. The values of $\Delta G°(=-RT\ln K_{s0})$ for the dissolution reactions can be expressed as a function of the absolute temperature by means of the linear equation:

$$\Delta G° = \Delta G°_{450}-\Delta S°(T-450) \qquad (4)$$

under the assumption that $\Delta S°$ (and $\Delta H°$) is constant in the experimental temperature range (equivalent to assuming $\Delta C_P° = 0$). The parameters, $\Delta G°_{450}$ and $\Delta S°$, have been determined for the three silver halides by the least-squares method, attaching equal statistical weight to all measurements[5].

In Figs. 1a, 2a and 3a, the differences between experimental and calculated $\Delta G°$- (and $E°$-) values (residuals) are plotted *versus* the absolute temperature.

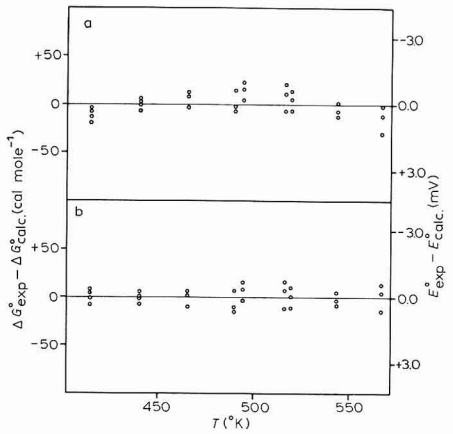

Fig. 1. Differences between exptl. and calcd. $\Delta G°$- (and $E°$-) values (residuals) for AgCl. (a), according to eqn. (4); (b), according to eqn. (7).

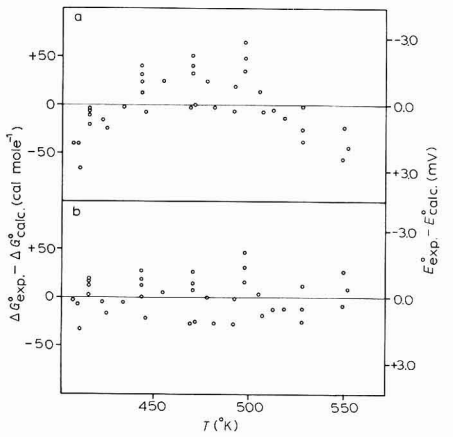

Fig. 2. As in Fig. 1, for AgBr.

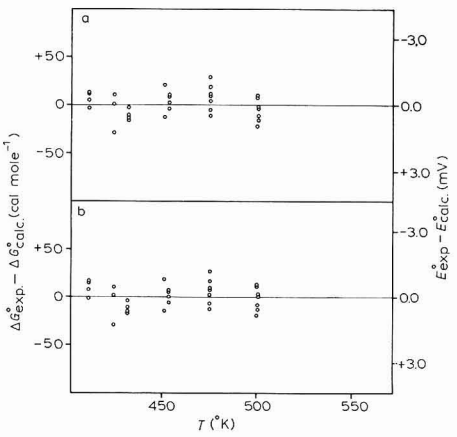

Fig. 3. As in Fig. 1, for AgI.

It can be seen that the linear equation for AgCl and AgBr is unsatisfactory, because the above residuals are not random but show a definite distribution with temperature, indicating that $\Delta H°$ and $\Delta S°$ for the dissolution reactions are not strictly constant in the experimental temperature range. For AgI, a linear equation seems satisfactory, due also to the smaller temperature interval.

The simplest further assumption that can be made to express the experimental

TABLE 1

STANDARD THERMODYNAMIC QUANTITIES FOR THE REACTIONS: (a) $AgX_{(s)} + e \rightleftharpoons Ag_{(s)} + X^-$; (b) $AgX_{(s)} \rightleftharpoons Ag^+ + X^-$ (X = Cl,Br,I) (Uncertainties are expressed as standard deviations)

Halide	$\Delta G°_{450}$ *(kcal mole^{-1}) (a) (b)*	$\Delta H°_{450}$ *(kcal mole^{-1}) (a) (b)*	$\Delta S°_{450}$ *(cal mole^{-1} deg^{-1}) (a) (b)*	$\Delta C_P°$ *(cal mole^{-1} deg^{-1}) (a) (b)*	$E°_{450}$ *(mV) (a)*	$pK_{s0\,450}$ *(K_{s0} in mole^2 kg^{-2}) (b)*
Cl	13.8039 ± 0.0023	18.377 ± 0.031	10.162 ± 0.069	3.56 ± 0.77	− 598.58 ± 0.10	6.7041 ± 0.0011
Br	18.5623 ± 0.0044	23.416 ± 0.052	10.787 ± 0.118	12.78 ± 1.74	− 804.92 ± 0.19	9.0150 ± 0.0021
I	25.0484 ± 0.0025	28.315 ± 0.035	7.260 ± 0.076		−1086.18 ± 0.11	12.1651 ± 0.0012

$\Delta G°$ results is that $\Delta C_P°$ for the dissolution reaction is constant in the temperature range investigated. Consequently, $\Delta H°$, $\Delta S°$ and $\Delta G°$ are given by the equations:

$$\Delta H° = \Delta H°_{450} + \Delta C_P°(T - 450) \quad (5)$$

$$\Delta S° = \Delta S°_{450} + \Delta C_P° \ln (T/450) \quad (6)$$

$$\Delta G° = \Delta G°_{450} + (\Delta C_P° - \Delta S°_{450})(T - 450) - \Delta C_P° T \ln (T/450) \quad (7)$$

The three parameters in the last equation, namely $\Delta G°_{450}$, $(\Delta C_P° - \Delta S°_{450})$, and $-\Delta C_P°$, were calculated, again by the least-squares method.

The use of the three-parameters eqn. (7) eliminates the non-randomness of the residuals for AgCl and AgBr (see Figs. 1b and 2b) and markedly reduces the sum of the squares of the residuals [from 4.05 to $2.22 \cdot 10^3$ cal^{2}mole^{-2} for AgCl (29 experimental points) and from 35.2 to $13.8 \cdot 10^3$ cal^{2}mole^{-2} for AgBr (38 points)], while in the case of AgI (31 points) the sum of the squares of the residuals remains practically constant (from 5.11 to $4.99 \cdot 10^3$ cal^2 mole^{-2}). A variance analysis according to the F test shows that the hypothesis that $\Delta C_P°$ is different from zero is significant at least to the 1% level in the case of chloride and bromide, while the linear eqn. (4) is sufficient to represent the data for AgI.

The thermodynamic quantities at 450°K for the three dissolution reactions (and for the electrode reactions), calculated from the parameters of the equations for $\Delta G°$, are given in Table 1, together with their standard deviations. It must be pointed out that the $\Delta C_P°$-values reported for AgCl and AgBr are to be considered with some caution, although their random errors are relatively small, since the presence of small temperature-dependent errors in the measured quantities (*i.e.*, E- or ΔG-values) could introduce significant systematic errors in $\Delta C_P°$.

The values of the thermodynamic quantities at temperatures other than 450°K can be calculated from the following equations.

AgCl(410–560°K)

$$\Delta G°(\text{cal mole}^{-1}) = 13803.9 - 6.607(T - 450) - 8.19 T \log (T/450)$$

$$\Delta H°(\text{cal mole}^{-1}) = 18377 + 3.56(T - 450)$$

$$\Delta S°(\text{cal mole}^{-1}\,\text{deg}^{-1}) = 10.162 + 8.19 \log (T/450)$$

$$E°(\text{mV}) = -598.58 + 0.2865(T - 450) + 0.355 T \log (T/450)$$

$$pK_{s0} = -1.444 + 3666.6/T - 1.789 \log (T/450)$$

AgBr(410–560°K)

$$\Delta G°(\text{cal mole}^{-1}) = 18562.3 + 1.992(T - 450) - 29.43 T \log (T/450)$$

$\Delta H°(\text{cal mole}^{-1}) = 23416 + 12.78(T-450)$

$\Delta S°(\text{cal mole}^{-1}\,\text{deg}^{-1}) = 10.787 + 29.43 \log (T/450)$

$E°(\text{mV}) = -804.92 - 0.0864(T-450) + 1.276T \log (T/450)$

$pK_{s0} = 0.435 + (3861.0/T) - 6.431 \log (T/450)$

AgI(410–500°K)

$\Delta G°(\text{cal mole}^{-1}) = 25048.4 - 7.260(T-450)$

$\Delta H°(\text{cal mole}^{-1}) = 28315$

$\Delta S°(\text{cal mole}^{-1}\,\text{deg}^{-1}) = 7.260$

$E°(\text{mV}) = -1086.18 + 0.3148(T-450)$

$pK_{s0} = -1.587 + (6188.4/T)$

The solubility product values obtained in the present study for the three silver halides, substantially confirm the previous data by BOMBI *et al.*[2] and by SACCHETTO *et al.*[3], as it can be seen from the comparison in Table 2.

TABLE 2

COMPARISON OF pK_{s0}-VALUES OF THE THREE SILVER HALIDES IN MOLTEN (Li,K)NO_3

(K_{s0}-values are in molality units)

T (°K)	*AgCl*			*AgBr*			*AgI*			
	Ref. 1	*Ref. 2*	*This work*	*Ref. 1*	*Ref. 2*	*This work*	*Ref. 1*	*Ref. 2*	*This work*	*Calcd.*[3]
421.7	7.22		7.30	9.3		9.77	11.7		13.09	13.01
423.2		7.4	7.27		9.7	9.73		13.0	13.04	12.96
445.2	6.72		6.80	8.8		9.14	11.0		12.31	12.26
467.7	6.22		6.37	8.2		8.58	10.3		11.64	11.62
484.7	5.91		6.06	8.1		8.19				

TABLE 3

COMPARISON OF STANDARD DISSOLUTION ENTHALPIES IN MOLTEN (Li,K)NO_3 AT 431°K (kcal mole^{-1})

	AgCl	*AgBr*	*AgI*
JORDAN *et al.*[4]	18.9	26.1	32.1
This work	18.31	23.17	28.31
Calculated*	—	—	27.28

* From calcd. pK_{s0} data reported in Table 2, last column.

The disagreement with the reports of TIEN AND HARRINGTON[1], which corresponds to differences in e.m.f. up to 40 mV for the bromide and up to 120 mV for the iodide, cannot be accounted for in any reasonable way, as already pointed out[3]. A comparison with the $\Delta H°$- and the $\Delta S°$-values given by TIEN AND HARRINGTON would be of little meaning in view of the discrepancies in the solubility products; it is worth noting that the data in Tables II and III in their paper are inconsistent between themselves.

In Table 3 dissolution enthalpies obtained in the present work are compared with the calorimetric values of JORDAN *et al.*[4]. The agreement is reasonably good for

silver chloride, but large discrepancies are observed for bromide and iodide which are difficult to explain, since the direct calorimetric measurements should give good enthalpy data. On the other hand, the reasonable agreement between the $\Delta H°$-value for AgI from this study and the completely independent value obtained from the calculated solubility products (Table 3, third row) gives confidence that the present enthalpies, although indirectly derived, are free from large systematic errors.

The rather large difference between the $\Delta G°$-values for AgCl given by JORDAN *et al.* (14.9 kcal mole^{-1} at 431°K) and ours (14.0 kcal mole^{-1} at the same temperature) can, on the other hand, be explained by the inherently poor reliability of the calorimetric titration method when applied to free energy measurements.

ACKNOWLEDGEMENT

The authors thank Professor L. RICCOBONI for his interest in this work. All the numerical calculations were performed on an Olivetti Elea 6001 computer at the Centro Elettronico di Calcolo Scientifico of the University of Padova. This work was supported by the Italian National Research Council (C.N.R.).

SUMMARY

The solubility products of silver halides in molten (Li,K)NO_3 and the related thermodynamic quantities have been determined from e.m.f. measurements, and are compared with previous data. The standard electrode potentials of the silver–silver halide second-kind electrodes have also been computed.

REFERENCES

1 H. T. TIEN AND G. W. HARRINGTON, *Inorg. Chem.*, 2 (1963) 369.
2 G. G. BOMBI, M. FIORANI AND G. A. MAZZOCCHIN, *J. Electroanal. Chem.*, 9 (1965) 457.
3 G. A. SACCHETTO, G. G. BOMBI AND M. FIORANI, *J. Electroanal. Chem.*, 20 (1969) 89.
4 J. JORDAN, J. MEIER, E. J. BILLINGHAM, JR. AND J. PENDERGRAST, *Nature*, 187 (1960) 318.
5 G. A. MAZZOCCHIN, G. G. BOMBI AND M. FIORANI, *J. Electroanal. Chem.*, 17 (1968) 95.
6 D. J. G. IVES AND G. J. JANZ, *Reference Electrodes*, Academic Press, New York—London, 1961, pp. 206 *et seq.*
7 M. FIORANI, G. G. BOMBI AND G. A. MAZZOCCHIN, *J. Electroanal. Chem.*, 13 (1967) 167.
8 H. T. TIEN AND G. W. HARRINGTON, *Inorg. Chem.*, 3 (1964) 215.
9 G. W. HARRINGTON AND H. T. TIEN, *Inorg. Chem.*, 3 (1964) 1333.
10 I. J. GAL, J. MÉNDEZ AND J. W. IRVINE, JR., *Inorg. Chem.*, 7 (1968) 985.
11 Y. T. HSU, R. B. ESCUE AND T. H. TIDWELL, JR., *J. Electroanal. Chem.*, 15 (1967) 245.
12 J. BRAUNSTEIN, M. BLANDER AND R. M. LINDGREN, *J. Am. Chem. Soc.*, 84 (1962) 1529.

ELECTROANALYTICAL CHEMISTRY AND INTERFACIAL ELECTROCHEMISTRY
Elsevier Sequoia S.A., Lausanne – Printed in The Netherlands

THE DETERMINATION OF TRACES OF INDIUM IN COBALT BY PULSE POLAROGRAPHY

A. LAGROU AND F. VERBEEK
Laboratory for Analytical Chemistry, University of Ghent (Belgium)
(Received September 25th, 1968)

The determination of traces of indium in cobalt and its compounds has not yet been reported in the literature, probably because the quantities present are extremely low and usually beyond the detection limit of the analytical techniques applied. In this investigation a pulse polarographic method has been developed for determining traces of indium in a cobalt matrix. This very sensitive polarograph with its high resolution capacity has already been used for the determination of bismuth[1], copper, lead, cadmium[2], nickel[3], zinc and manganese[4] in the same matrix.

The problem involved the study of the techniques for the quantitative separation of indium from excess cobalt and minor quantities of lead and cadmium, respectively. The procedure finally preferred can also be applied to the determination of traces of indium in other elements hydrolysing at relatively high pH–values such as cadmium[5], nickel and zinc[6].

EXPERIMENTAL

1. Apparatus and reagents

Pulse polarograph Southern type A 1700 mark II. The measurement of peak heights and working conditions of this instrument were described in a previous paper[7].

pH-meter Radiometer pH M 22; Radiometer glass electrode G 202 BH and calomel electrode K 4016 for high temperature.

Scaler ACEC type ANC 660 with a NaI(Tl) well-type crystal.

^{114}In-solution: 1 mC ^{114}In (γ-energy = 0.191, 0.552 and 0.722 MeV; $T_{\frac{1}{2}}$ = 49 days) in a volume of 1 ml and with a specific activity of 530 mC/g In was obtained from U.K.A.E.A. (Amersham, England).

^{210}Pb-solution: 1 mC of RaD (^{210}Pb; γ-energy = 47 keV; β-energy = 25 keV; $T_{\frac{1}{2}}$ = 22 years) with decay products in approximate equilibrium in 2.5 *M* nitric acid, and a total lead concentration of 0.2 mg in 0.5 ml was obtained from U.K.A.E.A. (Amersham, England).

Indium stock solution: prepared from the analytical-grade metal and standardised gravimetrically as In_2O_3.

Mercury, water, nitrogen, hydrochloric acid and ammonia were purified as previously described[7]. Analytical-grade sodium hypophosphite and potassium iodide were purified by a 24-h electrolysis at a cathode potential of -1.5 V *vs.* a saturated

calomel electrode (SCE); the electrolysis was performed in separate electrode compartments and under a nitrogen atmosphere.

All other reagents were analytical-grade and used without further purification.

2. Polarographic data

The polarographic behaviour of indium has been investigated by several authors[8]. In non-complexing media such as perchloric acid, an irreversible wave is observed with a half-wave potential of -0.95 V *vs.* SCE, due to the reduction of the indium(III)-ion. On the addition of chloride or iodide, the wave shifts to more positive values and the slope of the curve becomes steeper and better defined, due apparently to the chloro- or iodo-complex ions formed being reduced more reversibly. The half-wave potentials in 1 *M* and 0.1 *M* potassium chloride are -0.60 and -0.56 V *vs.* SCE, respectively, and the electrode reaction corresponds with a reversible three-electron reduction. As cobalt is reduced at -1.24 V in 1 *M* potassium chloride, it should be possible to determine indium polarographically in a cobalt matrix. However, in most electrolytes the indium wave partly coincides with the reduction of cadmium, also present as an impurity and usually to a higher degree. In 1 *M* hydrochloric acid the half-wave potentials of cadmium and indium differ by about 40 mV; it is possible to detect both elements by pulse polarography up to a molar concentration ratio, In/Cd = 1/10 owing to the less sensitive character of cadmium (peak current proportional to the square of the number of electrons involved in the electrode reaction). The ratio is usually much more unfavourable ($\leqslant 1/100$) and the medium is therefore unsuitable for a direct determination of both elements. The high resolution required implies the use of the 7-mV pulse amplitude and integration 3.

To enable more unfavourable molar concentration ratios of In/Cd to be determined the use of various complexing agents was investigated: tartrate, citrate, thiocyanate, hypophosphite and iodide. Tartrate gives a rather poor separation; higher pH-values result in the hydrolysis of indium and the reduction becomes more irreversible. Citrate and thiocyanate were of little interest. For a small excess of cadmium, a hypophosphite–hydrochloric acid mixture was most satisfactory. The effect of the hydrochloric acid concentration is very important. In 1 *M* hydrochloric acid, the waves almost coincide but the separation gradually improves on increasing the hydrochloric acid concentration (2, 4, 6 *M*). In high concentrations of hydrochloric acid (~ 6 *M*) the indium peak for low concentrations (10^{-7} *M*) is situated in the slope of the rising base line, rendering the measurement of the peak heights rather difficult. Finally, a mixture of 10% sodium hypophosphite–4 *M* hydrochloric acid was chosen as supporting electrolyte. A typical derivative pulse polarogram of indium and cadmium in this electrolyte is shown in Fig. 1. The medium enables indium to be determined in the presence of a forty-fold excess of cadmium. The linearity and reproducibility of the pulse polarographic determination was verified by a calibration graph in the concentration range, $2 \cdot 10^{-4}$–10^{-7} *M*. The sensitivity is limited to about $3 \cdot 10^{-8}$ *M* (giving a peak height of about 33 mm at maximum sensitivity of the apparatus; drop time 4 sec) as the unfavourable position of the indium peak with respect to the rising base line prevents the attainment of the maximum sensitivity.

In practice, for each of the electrolytes investigated an In/Cd separation is always required. After the separation, an electrolyte which gives more or less separated reduction waves should be used in order to avoid any interference caused by an in-

complete separation. This condition if fulfilled for a hypophosphite–hydrochloric acid mixture. Moreover, this electrolyte has the advantage that iron(III), added as collector for the co-precipitation, is partially reduced by the hypophosphite, resulting in a decrease of the reduction of iron(III) at the mercury pool and the DME. Pulse polarography has the advantage of tolerating up to 10^4 times greater concentration of ions reducing at lower potentials. The recorded polarograms, however, were less stable.

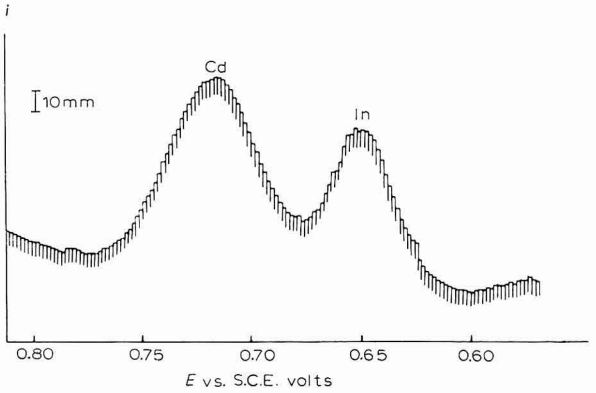

Fig. 1. Pulse polarogram of $2.5 \cdot 10^{-6}$ *M* In^{3+}, $5 \cdot 10^{-6}$ *M* Cd^{2+} and $2 \cdot 10^{-3}$ *M* Fe^{3+} in 4 *M* HCl–10% $NaH_2PO_2 \cdot 1H_2O$. Conditions: Sensitivity 1/10; ampl. 7 mV; 3 integrations; pol. rate 60 min/V, recorder 1 in/min.

An accurate quantitative determination in the presence of a large excess of cadmium is only possible in potassium iodide medium. In 1 *M* potassium iodide (pH = 2) the reduction peaks of indium and cadmium are separated by 160 mV, allowing a direct pulse polarographic determination even for very unfavourable Cd/In ratios. Other authors have already recommended the medium[9–12]. However, the electrolyte has the disadvantage that there is only a 50-mV difference between the half-wave potentials of lead and indium, allowing only a molar concentration ratio, In/Pb = 10/1, for very accurate measurements. As lead is more often present, and in much higher concentration, than indium (> 100-fold excess), this medium can only be used after a previous In/Pb separation.

The use of hydrobromic acid[13], phosphoric acid[14] and pyrophosphoric acid[15] was not investigated. In a paper recently published on the determination of traces of indium in cadmium[5], the possibilities of mixtures of hydrobromic acid–hydrochloric acid, potassium iodide–hydrochloric acid and ethylenediamine are discussed.

3. Separation techniques

For the determination of low indium concentrations in either chloride or iodide medium, a prior separation from cadmium or lead is necessary.

(a) Indium–lead separation. As in hydrochloric acid, the half-wave potentials of lead and indium ($E_{\frac{1}{2}}$, −0.44 and −0.60 V *vs.* SCE respectively in 1 *M* hydrochloric acid) are sufficiently different, for it to be theoretically possible to separate lead quantitatively from indium on a mercury electrode by a controlled cathode potential electrolysis. The assembly for the electrolysis, *i.e.*, cell and circuit, is the same as that

described in a previous paper[1]. The cathode potential was fixed at −0.55 V *vs.* the mercury pool.

The deposition was controlled pulse-polarographically. It was impossible to record a polarogram of the electrolysed solution as the reduction wave of indium was disturbed by a high wave probably due to the reduction of peroxides generated at the cathode during the electrolysis. An electrolysis in separate electrode compartments and under nitrogen atmosphere gave only a slight improvement. It was necessary to evaporate the solution to dryness on a hot plate at 200–250°. Higher temperatures had to be avoided owing to the volatility of $InCl_3$. After a 40-h electrolysis at −0.55 V, 0.1% of the original lead concentration was still present, even after regular renewal of the mercury cathode. The use of a cell, as described by CORIOU and coworkers[16,17], with a continuously renewed mercury electrode gave no improvement.

As the lead remaining still interfered to some extent with the indium determination (depending on the indium concentration to be determined) this time-consuming method was not further investigated.

(b) Indium–cadmium separation. Various separation techniques can be envisaged: separation on an ion exchange column[18,19], extraction with diethyl-[20–22] or isopropylether[5,23] and co-precipitation[24–26]. In this investigation the latter technique was preferred as indium can be readily hydrolysed. A quantitative recovery was obtained using iron as collector. This element does not interfere in the pulse polarographic determination of indium as it is reduced at a more positive potential.

In order to investigate the indium yield, various co-precipitations were performed on 1-g samples at pH 4.5–5 with the addition of known activities of ^{114}In. A comparison of the activity recovered in the precipitate and of the activity originally added gave the indium yield. The possible interference of sulphate or nitrate ion was checked by carrying out similar separations using $CoSO_4 \cdot 7H_2O$ and $Co(NO_3)_2 \cdot 6H_2O$, respectively. The results are summarised in Table 1. The average percentage yield was

TABLE I

RECOVERY OF INDIUM AFTER CO-PRECIPITATION WITH IRON(III) HYDROXIDE

(1-g sample; pH 4.5–5; 25 μg In; 5 mg Fe)

Product	*Activity added (counts/min)*	*Activity found (counts/min)*	*yield (%)*
1 g $CoCl_2 \cdot 6\,H_2O$	54 450	53 185	97.68
1 g $CoCl_2 \cdot 6\,H_2O$	54 505	52 455	96.24
1 g $CoCl_2 \cdot 6\,H_2O$	52 480	53 245	101.46
1 g $CoCl_2 \cdot 6\,H_2O$	54 465	53 400	98.04
1 g $CoSO_4 \cdot 7\,H_2O$	54 217	52 475	96.79
1 g $Co(NO_3)_2 \cdot 6\,H_2O$	55 185	54 100	98.03

98.04 ± 1.17%. To verify that no co-precipitation of cadmium occurred at pH 4.5–5, a series of co-precipitations was performed with the addition of increasing quantities of cadmium. The results are summarised in Table 2, and show that no co-precipitation of cadmium occurred in the concentration range investigated. Precipitation at pH > 5 was not investigated, as this could lead to co-precipitation of cadmium.

The pulse polarographic determination could not be carried out in iodide

TABLE II

CO-PRECIPITATION OF INDIUM WITH IRON(III) HYDROXIDE IN PRESENCE OF CADMIUM

(1-g sample; 1.43 μg In; pH 4.5–5; 5 mg Fe)

Cd added (μg)	*Cd/In ratio (g/g)*	*In found (μg)*	*Yield (%)*
0	0	1.38	96.50
1.12	0.78	1.38	96.50
11.24	7.80	1.35	94.41
112.4	78	1.34	93.71
1 124	780	1.45	101.40

TABLE III

DETERMINATION OF INDIUM IN COBALT

(1-g sample; final volume 25 ml)

In added (μg)	*In found (μg)*	*Yield (%)*	*In added (μg)*	*In found (μg)*	*Yield (%)*
0.72	0.75	104.17	5.74	5.37	93.55
0.72 (a)	0.69	95.83	7.17	6.89	96.09
1.43	1.45	101.40	14.35	14.14	98.54
1.43 (a)	1.38	96.50	28.69	28.49	99.30
2.87	2.73	95.12	57.38	56.22	97.98

(a) 10-g sample

medium as experiments with ^{210}Pb showed partial precipitation of $Pb(OH)_2$ and a supporting electrolyte of hypophosphite–hydrochloric acid was therefore used.

4. Procedure

Dissolve a suitable weight of cobalt metal (1–10 g) in a mixture of hydrochloric acid and nitric acid. Evaporate to about 20 ml or less. Add about 5 mg iron(III) as chloride, nitrate or sulphate and dilute to about 350 ml. Heat to $\pm 40°$ and neutralise slowly with 1 *M* ammonia to pH = 2, and with 0.1 *M* ammonia to pH 4.5–5. Keep the solution at 80°–90° for 15 min, filter through a fine porosity sintered glass filter and wash the precipitate several times with hot water. Dissolve the precipitate in 12.5 ml of 8 *M* hydrochloric acid, add 10 ml of 25% sodium hypophosphite and dilute to 25 ml in a calibrated flask. After de-aerating, record a pulse polarogram and determine indium by the standard addition method.

For cobalt compounds proceed in the same way after dissolving the salt in about 350 ml of 0.1 *M* hydrochloric acid.

RESULTS

To check the efficiency and the accuracy of the method a number of analyses are performed on synthetic samples, prepared by adding known quantities of indium to analytical-grade cobalt. The results are shown in Table 3. The percentage yield was $97.85 \pm 2.38\%$. Analyses of various commercially available cobalt samples showed that the amount of indium present was below the detection limit (< 0.004 p.p.m.).

The pulse polarographic sensitivity is $3 \cdot 10^{-8}$ M and the method enables as little as 0.01 p.p.m. of indium to be determined for a sample weight of 10 g and a final volume of 25 ml. The sensitivity can be increased by a factor of 2.5 (*i.e.*, 0.004 p.p.m.) by decreasing the final volume to 10 ml but it is then necessary to evaporate the solution with the dissolved precipitate nearly to dryness. It was shown experimentally that no losses occurred during this process.

Experiments on the homogeneous precipitation of $In(OH)_3$ with aluminium and urea[5] also gave good results.

SUMMARY

A pulse polarographic method is described for determining traces of indium in cobalt and its compounds. The interference due to the reduction of excess cadmium was eliminated by a prior precipitation of indium as the hydroxide with iron(III) as collector, at pH 4.5–5. The separation was quantitative and no co-precipitation of cadmium occurred. The pulse polarographic sensitivity was $3 \cdot 10^{-8}$ M in 4 M hydrochloric acid–10% sodium hypophosphite, allowing the determination of as little as 0.01 p.p.m. indium for a 10-g sample and a final volume of 25 ml.

REFERENCES

1 A. LAGROU AND F. VERBEEK, *J. Electroanal. Chem.*, 10 (1965) 68.
2 A. LAGROU AND F. VERBEEK, unpublished results.
3 A. LAGROU AND F. VERBEEK, *J. Electroanal. Chem.*, 19 (1968) 125.
4 A. LAGROU AND F. VERBEEK, *J. Electroanal. Chem.*, 19 (1968) 413.
5 E. TEMMERMAN AND F. VERBEEK, *Z. Anal. Chem.*, in press.
6 H. VANDEBROEK, unpublished results.
7 E. TEMMERMAN AND F. VERBEEK, *J. Electroanal. Chem.*, 12 (1966) 158.
8 I. M. KOLTHOFF AND J. J. LINGANE, *Polarography*, Vol. II, Interscience Publishers Inc., New York, London, 1952, p. 519.
9 T. MATSUMAE, *J. Electrochem. Soc. Japan*, 27 (1959) 10.
10 M. KASAGI AND C. V. BANKS, *Anal. Chim. Acta*, 30 (1964) 248.
11 S. L. PHILLIPS AND E. MORGAN, *Anal. Chem.*, 33 (1961) 1192.
12 R. J. HOFER, R. Z. BACHMAN AND C. V. BANKS, *Anal. Chim. Acta*, 29 (1963) 61.
13 P. G. PATS AND S. B. TSFASMAN, *Zavodsk. Lab.*, 27 (1961) 266.
14 H. SHIRAI, *Bunseki Kagaku*, 9 (1960) 206.
15 D. I. KURBATOV AND M. S. RUSAKOVA, *Izv. Sibirsk. Otdl. Akad. Nauk SSSR*, 7 (1960) 67.
16 H. CORIOU, J. DIRIAN AND H. HURE, *Anal. Chim. Acta*, 12 (1955) 368.
17 H. CORIOU, J. GUERON, H. HERING AND P. LEVEQUE, *J. Chim. Phys.*, 48 (1951) 55.
18 I. P. ALIMARIN, E. P. TSINTSEVICH AND V. P. BURLAKA, *Zavodsk. Lab.*, 25 (1959) 1287.
19 J. DOLEZAL, P. POVONDRA, K. STULIK AND Z. SULCEK, *Collection Czech. Chem. Commun.*, 29 (1964) 1538.
20 I. WADA AND R. ISHIL, *Sci. Papers Inst. Phys. Chem. Res. Tokyo*, 34 (1937–1938) 787.
21 J. E. HUDGENS AND L. C. NELSON, *Anal. Chem.*, 24 (1952) 1472.
22 S. NECIU, S. POPESCU, M. AURELIAN AND V. LUGURAN, *Rev. Chim. (Bucharest)*, 14 (1963) 528.
23 L. KOSTA AND J. HOSTE, *Mikrochim. Acta*, (1956) 790.
24 H. BLUMENTHAL, *Analyse der Metalle*, 2 Band, *Betriebsanalysen* 1. Teil, Berlin Springer, 1953, p. 345.
25 D. JENTZSCH, I. FROTSCHER, G. SCHWERDTFEGER AND F. SARFERT, *Z. Anal. Chem.*, 144 (1955) 8.
26 G. RIENACKER AND E. HOSCHEK, *Z. Anorg. Allgem. Chem.*, 268 (1952) 260.

ELECTROANALYTICAL CHEMISTRY AND INTERFACIAL ELECTROCHEMISTRY
Elsevier Sequoia S.A., Lausanne – Printed in The Netherlands

UNTERSUCHUNG DER OBERFLÄCHENAKTIVITÄT VON TRIÄTHYLPHOSPHAT AN DER Hg-ELEKTRODE IN VERSCHIEDENEN GRUNDLÖSUNGEN

H. SOHR UND KH. LOHS
Deutsche Akademie der Wissenschaften zu Berlin, Institut für Biophysik, Berlin-Buch
(Eingegangen am 25 Juni, 1968; revisioniert 23 September 1968)

Bei polarographischen Untersuchungen vor allem von Cu(II) in Gegenwart oberflächenaktiver Phosphorsäuretriester stellten wir fest, dass der Grundelektrolyt grossen Einfluss auf die Deformation der polarographischen Kurven hat. Während z.B. in 1 *N* $NaClO_4$ und 1 *N* $NaNO_3$ keine Inhibitionseffekte auftreten, sind sie in 1 *N* Na_2SO_4 in Abhängigkeit von der Grösse der Alkoxyreste z.T. in ausgeprägter Form messbar. Das gleiche gilt für 1 *N* KCl; hierbei ist allerdings die Deformation der polarographischen Kurven anderer Art als in 1 *N* Na_2SO_4[1,2].

Ausserdem stellten wir fest, dass die Inhibitionseffekte auch von der Konzentration und neben der Anionen- auch von der Kationenart abhängen[1].

Zu ähnlichen Ergebnissen gelangten einige Autoren bei anderen oberflächenaktiven Substanzen[3,4].

Für die Erklärung dieser Erscheinungen ist zunächst zu berücksichtigen, ob es zwischen dem Depolarisator und den Ionen des Grundelektrolyten chemische Wechselwirkungskräfte gibt, wie etwa Ionenpaar- oder Komplexbildung (z.B. Chlorokomplexe bei Anwesenheit von Cl^--Ionen in der Lösung). Weiterhin können Wechselwirkungskräfte zwischen den oberflächenaktiven Substanzen und den Grundelektrolyten sowohl in der Lösung, als auch infolge der geänderten Konzentrationsverhältnisse verstärkt in der Adsorptionsschicht wirksam werden, was zur Änderung der Assoziations- und Adsorptionsgleichgewichte führt. Desweiteren müssen Aussalz- und Einsalzeffekte und der Einfluss der spezifischen Adsorptionseigenschaften, vor allem der Anionen, an der Hg-Elektrode beachtet werden.

Um nähere Aussagen über die eingangs geschilderten Effekte machen zu können, wurden zunächst die Adsorptionseigenschaften des Triäthylphosphats untersucht. Diese Substanz eignet sich besonders gut für derartige Untersuchungen, weil sich das Adsorptions- und Assoziationsgleichgewicht sehr schnell einstellt. Die Einstellung dieser Gleichgewichte lässt sich leicht überprüfen, indem längere mit kürzeren Tropfzeiten verglichen werden. In unserem Fall ist dies sowohl mit der Tropfzeitmethode, als auch tensammetrisch erfolgt. Wir konnten eindeutig nachweisen, dass die Gleichgewichte bei den von uns gewählten Bedingungen eingestellt waren. Damit ist die wichtigste Voraussetzung für die Aufnahme von Elektrokapillarkurven nach der Tropfzeitmethode und von tensammetrischen Kurven erfüllt. Auch bei den Phosphaten (Tripropyl- und Tributylphosphat) mit grösseren Alkoxyresten erhält man derartige Ergebnisse.

EXPERIMENTELLES

Die Aufnahme der tensammetrischen Kurven erfolgte mit einem Gleichwechselstrompolarographen vom Typ GWP 563 der Akademiewerkstätten der Deutschen Akademie der Wissenschaften zu Berlin. Die Elektrokapillarkurven wurden nach der Tropfzeitmethode registriert, wobei speziell die von NÜRNBERG UND WOLF gewählten Bedingungen berücksichtigt wurden[5]. Das betrifft sowohl die Aufnahmetechnik, als auch die Auswertung der Kurven. In dieser Arbeit ist ausserdem eine Fehlerbetrachtung, einschliesslich einer Diskussion der Vor- und Nachteile der Tropfzeitmethode, enthalten. Bei unseren Messungen konnten wir bestätigen, dass bei genauer Versuchsdurchführung der angegebene Fehler ($\pm$ 0.5 dyn) nicht überschritten wird.

Die Temperatur betrug bei allen Versuchen 25 $\pm$ 0.1°. Die tensammetrischen Kurven wurden bei 6 und 10 mV Wechselspannung und 78 Hz aufgenommen. Der Durchmesser der Kapillare betrug $5.7 \cdot 10^{-3}$ cm, die Ausflussgeschwindigkeit $m = 1.39$ mg sec^{-1} in 1 N Na_2SO_4 bei 0 V, die Höhe des Hg-Gefässes 65 cm und die Tropfzeit bei 0 V in 1 N Na_2SO_4, 5.23 sec. Die tensammetrischen und Tropfzeit-Kurven sind mit derselben Tropfelektrode in einer geschlossenen Zelle aufgenommen worden. Entlüftet wurde 20 min mit nachgereinigtem Stickstoff. Das Quecksilber und das Triäthylphosphat wurden zweimal destilliert. Die übrigen Chemikalien hatten den Reinheitsgrad p.A. Die Potentiale wurden sämtlich gegen die gesättigte Kalomelelektrode gemessen.

ERGEBNISSE UND DISKUSSION

In Abb. 1 sind die tensammetrischen Kurven von $2 \cdot 10^{-3}$ M Triäthylphosphat in 6 verschiedenen Grundelektrolyten aufgezeichnet. Es ist klar erkennbar, dass sich

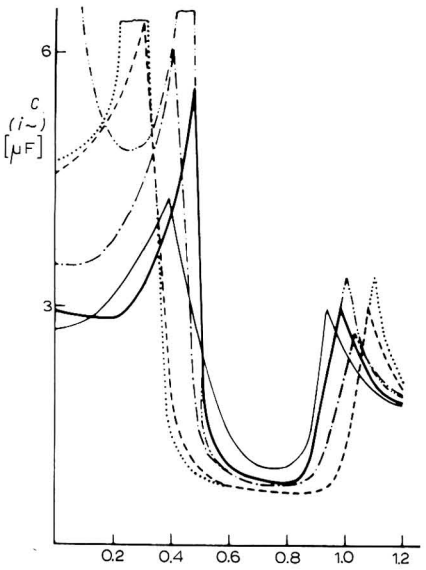

Abb. 1. Tensammetrische Polarogramme von $2 \cdot 10^{-3}$ M Triäthylphosphat in: (.....), 1 N Na_2SO_4; (— · · —), 1 N KCl; (— · —), 1 N H_2SO_4; (——), 1 N $NaNO_3$; (——), 1 N $NaClO_4$. Empfindlichkeit 6 μA; $E_\sim$ = 10 mV.

diese unter vergleichbaren Bedingungen aufgenommenen Kurven stark voneinander unterscheiden. Zunächst kann man schlussfolgern, dass diese Differenzen nicht durch die spezifischen Adsorptionseigenschaften der Anionen an der Hg-Oberfläche zu erklären sind. Obgleich sowohl Cl^--Ionen, als auch ClO_4^-- und NO_3^--Ionen im Gegensatz zu den SO_4^--Ionen spezifisch adsorbiert werden, sind die beträchtlichen Differenzen dieser Kurven damit nicht erklärbar[6,7]. Ausserdem sollten danach die tensammetrischen Kurven in 1 *N* KCl die stärksten Abweichungen zeigen, was jedoch nicht der Fall ist.

Aus der Abb. 1 geht hervor, dass die stärksten Differenzen zwischen den Kurven des Triäthylphosphats in 1 *N* Na_2SO_4 und 1 *N* $KClO_4$ vorliegen, daher wurden beide Systeme einer näheren Untersuchung unterzogen.

In Abb. 2 und 3 sind die tensammetrischen und Tropfzeit-Kurven in den beiden Grundlösungen in Abhängigkeit von der Triäthylphosphatkonzentration dargestellt und in Abb. 4 die dazugehörigen Θ,C-Adsorptionsisothermen. Obgleich die Tensammetrie gegenüber der Brückenmethode bestimmte Nachteile aufweist, ergeben sich im Prinzip keine unterschiedlichen Ergebnisse.

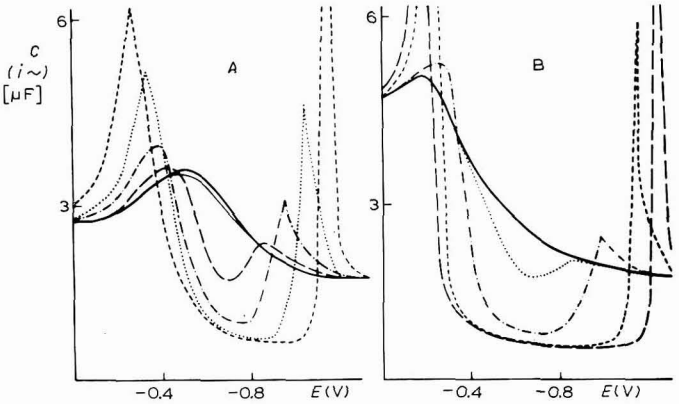

Abb. 2. Tensammetrische Polarogramme von Triätylphosphat verschiedener Konzentrationen in: (A), 1 *N* $NaClO_4$. (——), 1; (——), $6\cdot10^{-4}$; (— —), 10^{-3}; (— · —), $2\cdot10^{-3}$; (.....), $4\cdot10^{-3}$; (- - -), $8\cdot10^{-3}$ *M*. (B), 1 *N* Na_2SO_4. (——), 1; (.....), $4\cdot10^{-4}$; (— · —), 10^{-3}; (- - -), $4\cdot10^{-3}$; (— —), $8\cdot10^{-3}$ *M*.
Empfindlichkeit 10 μA; $E_\sim$ = 10 mV.

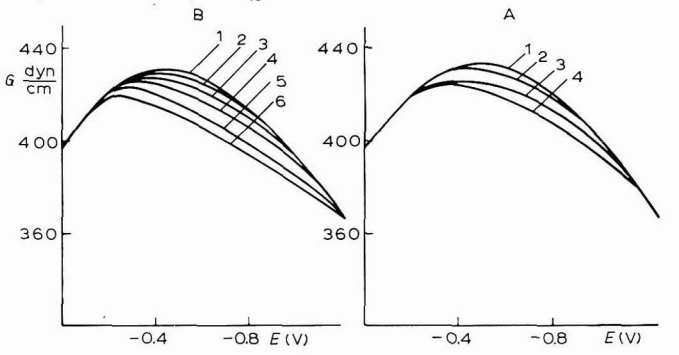

Abb. 3. Tropfzeitkurven von Triäthylphosphat verschiedener Konzentrationen in:
(A), 1 *N* $NaClO_4$. (1), 0; (2), $2\cdot10^{-3}$; (3), $4\cdot10^{-3}$; (4), $8\cdot10^{-3}$ *M*.
(B), 1 *N* Na_2SO_4. (1), 0; (2), $2\cdot10^{-4}$; (3), $4\cdot10^{-4}$; (4), 10^{-3}; (5), $2\cdot10^{-3}$; (6), $4\cdot10^{-3}$ *M*.

Von LORENZ und MÜLLER[8] wurde *tert*-Amylalkohol in verschiedenen Grundelektrolyten untersucht, wobei die Autoren gleichfalls eine solche Abhängigkeit der Adsorptionsisothermen vom Grundelektrolyten feststellten. Die gering kapillarinaktiven ClO_4^--Ionen bewirkten auch in diesem Fall eine Differenzierung der Adsorptionsisothermen analog dem Triäthylphosphat. Die kapillarinaktiven F^--Ionen zeigen dagegen die geringste Wirkung und die kapillaraktiven Cl-Ionen liegen dazwischen[8]. Im

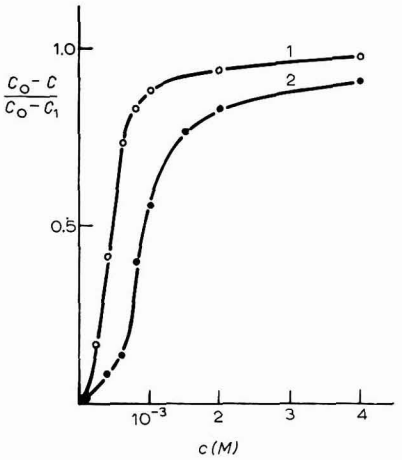

Abb. 4, Θ, C-Adsorptionsisothermen von Triäthylphosphat aus tensammetrischen Kurven ermittelt (1), 1 N Na_2SO_4; (2), 1 N $NaClO_4$.

Gegensatz hierzu fanden WATANABE und Mitarbeiter[9] bei der tensammetrischen Untersuchung von Kondensationsprodukten des Äthylenoxid mit einer Gliederzahl bis zu 30 die Adsorbierbarkeit in Gegenwart von KCl grösser, als in Sulfatlösungen gleicher Konzentration.

Hierin sehen wir einen erneuten Beweis dafür, dass die chemischen Wechselwirkungskräfte die dominierende Rolle spielen. In Abb. 4 sind die Adsorptionsisothermen von Triäthylphosphat in den beiden Grundelektrolyten dargestellt, die aus tensammetrischen Kurven abgeleitet wurden. Die Auswertung der tensammetrischen Kurven erfolgt bei verschiedenen Triäthylphosphatkonzentrationen jeweils beim Potential

$$\tfrac{1}{2}(E_2^{max} - E_1^{max}) = E_m \qquad (1)$$

E_1^{max}, E_2^{max} = Potentiale der Kapazitätsmaxima, E_m = mittleres Potential im Adsorptionsbereich wobei die von LORENZ begründete Formulierung

$$\Theta = [C_0 - C_{(c)}]_{E=Em} \qquad (2)$$

angewendet wurde[10].

Aus den Adsorptionsisothermen wurden nach der Frumkinschen Gleichung

$$\{\Theta/(1-\Theta)\}\exp(-2a\Theta) = \beta c \qquad (3)$$

die Adsorptionskoeffizienten β sowie die Wechselwirkungskoeffizienten a vom Triäthylphosphat für beide Grundelektrolyten ermittelt.

Dass diese Adsorptionsisothermen der Frumkin-Gleichung genügen, lässt sich nachweisen, indem Θ gegen $C_\Theta = 0.5$ dargestellt wird, wobei sich die Isothermen bei $\Theta = 0.5$ schneiden[11,12].

1 N Na_2SO_4; $\beta = 410$ l Mol^{-1}; $a = 1.70$

1 N $NaClO_4$; $\beta = 345$ l Mol^{-1}; $a = 1.07$

Von JEHRING wurde in anderem Zusammenhang für Triäthylphosphat in 1 N KCl $a = 1.57$ ermittelt; dieser Wert fügt sich gut in die von uns gemessenen ein[13]. (In Abb. 1 liegt die tensammetrische Kurve in 1 N KCl Grundelektrolyten zwischen den in 1 N Na_2SO_4 und 1 N $NaClO_4$.)

TABELLE 1

SÄTTIGUNGSKONZENTRATION (Γ_m) UND FLÄCHENBEDARF PRO ADSORBIERTES MOLEKÜL (S) VON TRIÄTHYLPHOSPHAT IN 1 N Na_2SO_4 UND 1 N $NaClO_4$ BEI VERSCHIEDENEN POTENTIALEN

E (v)	$\Gamma_m \cdot 10^{10}$ (Mol·cm^{-2})	S (Å^2)	E (V)	$\Gamma_m \cdot 10^{10}$ (Mol·cm^{-2})	S (Å^2)
1 N Na_2SO_4					
−0.4	3.0	55	−0.8	3.0	55
−0.5	3.1	53	−0.9	2.7	61
−0.6	3.3	50	−1.0	2.6	63
−0.7	3.2	52	−1.1	2.2	75
1 N $NaClO_4$					
−0.4	2.2	75	−0.7	2.9	57
−0.5	2.5	66	−0.8	3.2	52
−0.6	2.6	63	−0.9	3.4	46

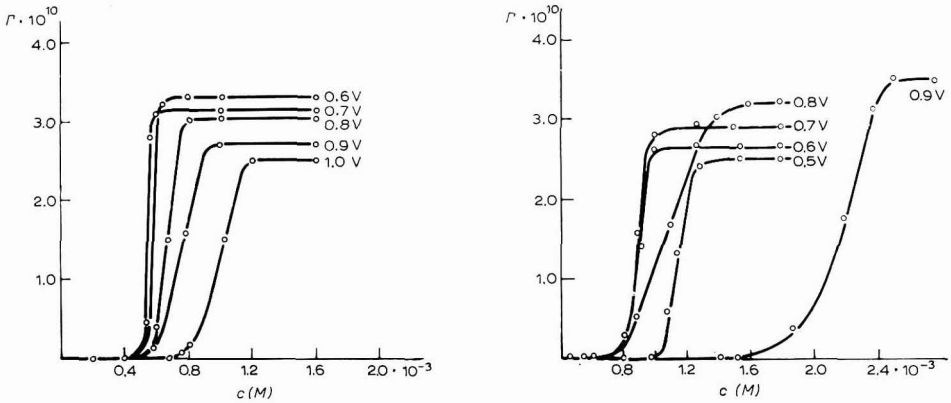

Abb. 5–6. Γ, c-Adsorptionsisothermen von Triäthylphosphat aus elektrokapillaren Kurven ermittelt, bei verschiedenen Potentialen in: (5) 1 N $NaSO_4$; (6) 1 N $NaClO_4$.

In Tab. 1 sind die elektrokapillarometrischen Kurven ausgewertet worden und zwar wurden aus den Elektrokapillarkurven die Gibbsisothermen berechnet und aus jenen wiederum die Frumkin-Isothermen.

Ein Vergleich dieser Werte in den beiden Grundelektrolyten zeigt, dass die Struktur der beiden Adsorptionsschichten unterschiedlich sein muss. Während in 1 N Na_2SO_4 (Abb. 5) die Werte für den Flächenbedarf im Bereich zwischen −0.4 bis

0.9 V ziemlich konstant sind und ihr Minimum bei −0.6 V liegt, nimmt in 1 N $NaClO_4$ dieser Wert immer mehr ab und strebt bei −0.9 V einem Miniumm zu, d.h. die Flächenkonzentration wird immer dichter. Was die Verschiebung der Frumkin-Isotherme bei −0.9 V in Abb. 6 anbetrifft, so entsteht die Differenz durch die Verschiebung des Adsorptionsbereiches. Das heisst, bei einer Konzentration von 10^{-3} M Triäthylphosphat ist beim Potential von −0.9 V noch keine Depression der Oberflächenspannung vorhanden, da die Desorption der Triäthylphosphatmoleküle von der Hg-Oberfläche bei positiveren Spannungswerten erfolgt.

Die Flächenkonzentrationen in beiden Grundelektrolyten können nur bei den Potentialen −0.7 V und −0.8 V verglichen werden, bei den übrigen Potentialwerten ist die Diskrepanz teilweise beträchtlich.

Diese Ergebnisse führen zu der Schlussfolgerung, dass derartige Unterschiede vor allem durch unterschiedliche chemische Wechselwirkungen zwischen den Ionen des Grundelektrolyten und den Triäthylphosphatmolekülen zustandekommen, wobei noch die unterschiedlichen Konzentrationen der einzelnen Komponenten an der Kathode bzw. in deren unmittelbarer Umgebung und in der Lösung zu berücksichtigen sind.

Aus Extraktionsuntersuchungen mit Tributylphosphat in elektrolytfreien Wasser geht hervor, dass in wässriger Lösung ein Monohydrat vorliegt (primäre Hydrathülle)[14,15].

$$(RO)_3PO + H_2O \leftrightarrows (RO)_3PO\cdots HOH \tag{4}$$

Dieses Monohydrat reagiert in Abhängigkeit von der Ionenart und deren Konzentration allgemein formuliert wie folgt:

$$[(RO)_3PO\cdots HOH]_x + [H_2O]_y + [MeX]_z \leftrightarrows \{[(RO)_3PO]_x[H_2O]_{(y+x)}(MeX)_z\} \tag{5}$$

(MeX = Salze oder Säuren).

Die Werte x, y und z können dabei vor allem je nach der Art von MeX sehr unterschiedlich sein; z ist jedoch in den meisten Fällen 1.

Für die meisten starken Säuren ist[16]:

$$x = 1; \quad y = 4; \quad z = 1$$

während schwächere Säuren meist unhydratisiert aus wässrigen Lösungen extrahiert werden. Die Assoziate können sowohl neutralen, als auch ionischen Charakter besitzen. Die Lage des Gleichgewichts ist von der Art und Konzentration des MeX abhängig.

Bei den Kationen der Alkalimetalle, einschliesslich der H-Ionen, steigt die Bildungstendenz wie folgt:

$$CsX < KX < NaX < LiX < HX$$

und in der Reihe der Anionen:

$$MeSO_4 < MeCl < MeBr < MeI < MeNO_3 \sim MeClO_4$$

wobei die Anionen bei Anwesenheit von Alkalikationen einen wesentlich stärkeren Einfluss haben. Von den Alkaliperchloraten und der Perchlorsäure ist bekannt, dass deren Wirkung hierbei ungefähr mit der der Nitrate und Salpetersäure vergleichbar ist. Nach unserer Auffassung sind diese Ergebnisse im Prinzip auch auf die chemischen Wechselwirkungen zwischen dem Triäthylphosphat und dem Grundelektrolyten zu übertragen; zumindest die Tendenz der Abstufung der chemischen Wechselwirkung

dürfte vergleichbar sein. Bei den Untersuchungen von Adsorptionsschichten an der Hg-Elektrode spielen naturgemäss die Potentialänderungen bzw. Ladungsänderungen eine Rolle. Bei den neutralen Molekülen scheint eine gesteigerte chemische Wechselwirkung mit den Ladungsträgern des Grundelektrolyten auch eine gesteigerte Potentialabhängigkeit der Assoziationskräfte hervorzurufen. Dies geht klar aus dem Vergleich unserer Ergebnisse in 1 *N* Na_2SO_4 und 1 *N* $NaClO_4$-Lösung hervor. Da die Anionen, wie schon erwähnt, im Vergleich zu den Alkalikationen eine wesentlich stärkere Wechselwirkungstendenz besitzen und die Konzentration an Anionen im positiven Potentialbereich der Adsorption, bezogen auf das Potential des elektrokapillaren Maximums an der Kathode besonders hoch ist, wird demzufolge die starke Differenz der tensammetrischen Kurven in diesem Bereich verständlich.

Normalerweise ist das Triäthylphosphat so adsorbiert, dass die hydrodisierte hydrophile Phosphorylgruppe der Lösung zugerichtet ist, während die 3 hydrophoben Äthoxigruppen an der Hg-Oberfläche anliegen. Offenbar sind, wie aus Abb. 3 hervorgeht, vor allem in Gegenwart von NO_3^-- und ClO_4-Ionen im positiven Potentialbereich die Verhältnisse dahingehend geändert, dass die Triäthylphosphat–Salz-Assoziate so auf der Hg-Oberfläche angeordnet sind, dass der hydrophobe und hydrophile Teil des Moleküls flach auf der Hg-Oberfläche angeordnet sind und sich hieraus ein erhöhter Flächenbedarf erklärt. Damit lassen sich diese Ergebnisse mit denen von GIERST und DAMASKIN vergleichen, die in Gegenwart von Pyridin erhalten wurden. Beim Pyridin ist jedoch zusätzlich noch der Einfluss der π-Elektronen zu berücksichtigen[17,12].

ZUSAMMENFASSUNG

Durch tensammetrische und elektrokapillarometrische Untersuchungen am Triäthylphosphat in verschiedenen Grundlösungen wurde der Einfluss des Grundelektrolyten auf das Adsorptions- und Assoziationsgleichgewicht sowie die Struktur der Adsorptionsschicht geprüft. Sowohl das Adsorptions-, als auch das Assoziationsgleichgewicht sind vom Grundelektrolyten abhängig, wobei vor allem die Anionen einen starken Einfluss im positiven Potentialbereich bezüglich des elektrokapillaren Maximums haben. Aus unseren Messungen und deren Vergleich mit Ergebnissen der Extraktion von Kationen und Anionen an wässriger Lösung mit Phosphorsäuretriestern ziehen wir die Schlussfolgerung, dass sich in der Adsorptionsschicht definiert Assoziate zwischen Triäthylphosphat, den Grundelektrolyten und Wasser bilden.

SUMMARY

Tensammetric and droptime measurements were made on triethylphosphate in different base solutions, and used to examine the influence of the base electrolyte on adsorption and association equilibria as well as the structure of the adsorption layer. Both the adsorption and the association equilibria depend on the base electrolyte; anions particularly have a strong effect on the region at potentials more positive than the electrocapillary maximum. From our measurements and comparison of them with results for the extraction of cations and anions from aqueous solution with phosphoric acid tri-esters, we conclude that definite associates are formed in the adsorbed layer between triethylphosphate, the base electrolyte and water.

LITERATUR

1 H. SOHR, bisher unveröffentlichte Ergebnisse.
2 H. SOHR UND KH. LOHS, *J. Electroanal. Chem.*, 13 (1967) 107.
3 L. GIERST, J. TONDEUR UND E. NICOLAS, *J. Electroanal. Chem.*, 10 (1965) 397.
4 A. P. MARTIROSYAN UND T. A. KRYUKOVA, *Zh. Fiz. Khim.*, 27 (1953) 851.
5 H. W. NÜRNBERG UND G. WOLF, *Collection Czech. Chem. Commun.*, 30 (1965) 3997.
6 R. PAYNE, *J. Phys. Chem.*, 70 (1966) 204.
7 R. PAYNE, *J. Phys. Chem.*, 69 (1965) 4113.
8 W. LORENZ UND W. MÜLLER, *Z. Physik. Chem. N. F.*, 25 (1960) 161.
9 A. WATANABE, F. TSUJI UND S. UEDA, *Kolloid-Z.*, 193 (1963) 39.
10 W. LORENZ, F. MÖCKEL UND W. MÜLLER, *Z. Physik. Chem. N. F.*, 25 (1960) 145.
11 A. N. FRUMKIN, *Z. Physik.*, 35 (1926) 792.
12 B. B. DAMASKIN, Vortrag auf der XIV. CITCE-Tagung, Moskau, 1963.
13 H. JEHRING, Vortrag auf der Tagung über oberflächenaktive Stoffe, Berlin, 1965.
14 K. ALCOCK, S. S. GRIMLEY, T. V. HEALY, J. KENNEDY UND H. A. C. MCKAY, *Trans. Faraday Soc.*, 52 (1956) 39.
15 D. G. TUCK, *J. Chem. Soc.*, (1958) 2783.
16 W. H. BALDWIN, C. E. HIGGENS UND B. A. SOLDANO, *J. Phys. Chem.*, 63 (1959) 118.
17 L. GIERST, *Trans. Symp. Electrode Processes, Philadelphia, Pa., 1959*, G. Wiley, New York, 1961, p. 294.

ELECTROANALYTICAL CHEMISTRY AND INTERFACIAL ELECTROCHEMISTRY
Elsevier Sequoia S.A., Lausanne – Printed in The Netherlands

POLAROGRAPHIC STUDY OF THE FORMATION OF METAL CHELATES OF EDTA TYPE

MILOSLAV KOPANICA AND TRAN CHUONG HUYEN
J. Heyrovský Polarographic Institute, Analytical Laboratory, Czechoslovak Academy of Sciences, Prague (Czechoslovakia)
(Received October 19th, 1968)

Polarography is a useful tool for the study of the formation of metal chelates and complexes. The application of polarography is mostly based on the measurement of the half-wave potential in the dependence on the concentration of the complex-forming reagent[1]; the utilization of the measurement of the limiting currents has been of lesser interest[2–4]. It is shown in the present paper that the formation of chelates of EDTA type may be studied *via* the measurement of the wave of the hydrogen ions released during the chelation reaction.

EXPERIMENTAL

Reagents

All solutions used were prepared from reagent-grade chemicals. All metal salts solutions were standardized by visual or, if possible, amperometric titration with EDTA as titrant. Similarly, the solutions of the chelate-forming reagents, ethylenediaminetetraacetic (EDTA), nitrilotriacetic acid (NTA), 1,2-diaminocyclohexanetetraacetic acid (DCTA), diethylenetriaminepentaacetic acid (DTPA) and triethylenetetraminehexaacetic acid (TTHA), were standardized by visual titration with zinc or lead solutions.

Apparatus

Polarographic measurements were performed with a Polarecord Metrohm, E 261 R, using a H-type polarographic cell with a separate saturated calomel electrode. Oxygen dissolved in the solutions analyzed was removed with nitrogen purified with the aid of the BTS catalyst (Badische Anilin und Sodafabrik, GFR). The catalyst was activated according to the manufacturer's recommendation by heating (approx. 130°) in a stream of hydrogen.

Procedure

Polarographic measurement was carried out as follows: First, the wave of a given concentration of metal ion was recorded in an unbuffered solution of sodium perchlorate (0.1 *M*) of approximately pH 5. The equivalent amount, or a fraction of the equivalent amount of the chelate-forming reagent was then added to the solution and the polarogram was recorded. This polarogram showed the wave of the chelate formed (if polarographically active) and the wave corresponding to the reduction of

hydrogen ions released on chelation. The exact recording of the hydrogen wave is possible only after complete removal of dissolved oxygen from the solution; this was achieved by a 10-min flow of nitrogen through a column filled with activated catalyst.

RESULTS AND DISCUSSION

After the addition of a complex-forming reagent to a solution of a metal ion, in the case of the formation of a complex, the corresponding polarographic wave of the cation decreases or is shifted to more negative potentials, or if the complex is polarographically active a new wave appears. In the polarographic study of the chelates of EDTA type it was found that after the addition of the reagent solution to the metal solution in unbuffered medium, a new polarographic wave appeared. In 0.1 *M* sodium perchlorate solution, the half-wave potential of this new wave was 1.60 V (SCE). The well-developed wave is of diffusion character and was found to be identical with the wave of the reduction of hydrogen ions from a solution of hydrochloric acid recorded under identical conditions. It was suggested therefore that this wave corresponded to the reduction of hydrogen ions released according to the reaction:

$$Me^{2+} + H_2Y^{2-} \rightleftharpoons MeY^{2-} + 2H^+ \qquad (1)$$

or

$$Me^{2+} + H_2Y^{2-} \rightleftharpoons MeHY^- + H^+ \qquad (2)$$

where H_4Y denotes the EDTA reagent. The prevailing dissociation forms of EDTA, DCTA and DTPA at approximately pH 5 are the H_2X^{n-} species, as follows from the values of the dissociation constants of these reagents.

The wave of the reduction of hydrogen ions from hydrochloric acid solution recorded in the 0.1 *M* sodium perchlorate solution was of diffusion character in the concentration range studied (1.10^{-4}–$5 \cdot 10^{-3}$ *M*). A comparison of this diffusion current with the diffusion current corresponding to the reduction of zinc(II) ions in the same medium, showed that the experimental value of the ratio of the diffusion current of zinc(II) ions to the diffusion current of hydrogen ions, i_{Zn}/i_H, is 1:1.5. The theoretical value of this ratio is 1:1.8, the value of i_H being calculated by means of the correction factor in the Ilkovič equation according to TAMAMUSHI[5]. The disagreement between the two values may be due to the limited validity of the Ilkovič equation in the case of the reduction of hydrogen ions or to an experimental error. It was found that the height of the hydrogen wave changed with the time of flow of nitrogen through the solution examined and that any impurity decreased the height of this wave.

The wave obtained in sodium perchlorate solution after the reaction of the reagent with the metal ion has the same slope and the same half-wave potential as the hydrogen wave yielded by hydrochloric acid. It is evident that the validity of either reaction (1) or reaction (2) may be distinguished by the determination of the hydrogen ion concentration. If the diffusion current, i_{Me}, of a divalent metal ion, Me^{2+}, is expressed by the Ilkovič equation:

$$i_{Me} = 607 n D_{Me}^{\frac{1}{2}} m^{\frac{2}{3}} t^{\frac{1}{6}} C_{Me} \qquad (3)$$

where n is the number of electrons involved in the electrode process, D_{Me} is the diffu-

sion coefficient of the metal ion, C_{Me} its concentration, m the flow rate of mercury and t the life-time of one drop. Because t and m are constants, eqn. (3) may be expressed as:

$$i_{Me} = KnD_{Me}^{\frac{1}{2}}C_{Me} \quad (4)$$

where K is a constant equal to 607 $m^{\frac{2}{3}}t^{\frac{1}{6}}$. Similarly, the diffusion current of hydrogen ions, i_H, is determined by the equation:

$$i_H = KnD_H^{\frac{1}{2}}C_H \quad (5)$$

where D_H is the diffusion coefficient of hydrogen ions and C_H is the hydrogen ion concentration. If the numerical values of n, D_{Me} and D_H are introduced into eqns. (4) and (5), the ratio i_{Zn}/i_H may be defined as

$$i_{Zn}/i_H = 1.68C_{Zn}/3.33C_H \quad (6)$$

where the value 1.09 was used for the n-value corresponding to the number of electrons involved in the reduction of hydrogen ions (according to TAMAMUSHI[5]). If the formation of the EDTA chelate proceeds according to reaction (1), then $C_{Zn} = 0.5C_H$ and the ratio i_{Zn}/i_H has the value, 1:3.9; if the chelate is formed according to reaction (2), then $C_{Zn} = C_H$ and the ratio is equal to 1:1.98. Table 1 summarizes the experimentally-obtained values of the ratio, i_{Me}/i_H, for various metal ions and various chelate-forming

TABLE 1

EXPERIMENTALLY-OBTAINED VALUES OF THE RATIO, $i_{Me^{2+}}/i_{H^+}$, FOR VARIOUS METAL CHELATES

Reagent	*Metal ion*	$i_{Me^{2+}}/i_{H^+}$	*Reagent*	*Metal ion*	$i_{Me^{2+}}/i_{H^+}$
EDTA	Cu^{2+}	1:1.90	DTPA	Zn^{2+}	1:1.70
	Cd^{2+}	1:1.85		Ni^{2+}	1:1.80
	Zn^{2+}	1:2.05		Ca^{2+}	1:1.60
	Ni^{2+}	1:2.10			
	Ca^{2+}	1:1.65	TTHA	$2Ni^{2+}$	1:1.75
				$2Zn^{2+}$	1:1.80
DCTA	Cu^{2+}	1:2.15		$2Cu^{2+}$	1:1.15
	Ni^{2+}	1:2.10		$Ni^{2+}+Zn^{2+}$	1:1.75
	Zn^{2+}	1:2.10		$Ca^{2+}+Zn^{2+}$	1:0.70
	Ca^{2+}	1:1.60			

reagents. These data were read from similar diagrams to those on Fig. 1. Data for Fig. 1 were obtained by polarographic measurement, according to the given procedure, with copper(II) ions and EDTA solution. Curve 1 on Fig. 1 shows the decrease of the wave corresponding to the reduction of free copper(II) ions with increasing concentration of added reagent (amperometric titration of copper with EDTA); curve 2 illustrates the change of height of the hydrogen wave during the addition of the reagent and curve 3 shows the appearance of the wave of the resulting Cu–EDTA chelate. In the case of a metal, the chelate of which is not polarographically active (nickel(II)), the diagram consisted only of curves 1 and 2; when the metal ion itself was polarographically inactive, only curve 2 was obtained.

The decrease of the i_{H^+}-values on curve 2, after the equivalence point is due to the recombination of released hydrogen ions with excess of the reagent (in the case of EDTA reagent this process illustrates the reaction, $H^+ + H_2X^{2-} \rightleftharpoons H_3X^-$). This reac-

tion was confirmed experimentally by the addition of hydrochloric acid solution to the sodium perchlorate solution and afterwards to the solution of sodium perchlorate and EDTA. In the latter case, a lower hydrogen wave was observed; the difference between the heights of the two waves corresponded to the amount of hydrogen ions removed by the reaction, $H^+ + H_2X^{2-}$.

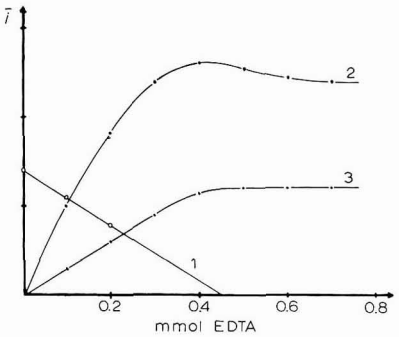

Fig. 1. Dependence of the diffusion current of free Cu(II), hydrogen ions and the Cu–EDTA chelate on the amount of added EDTA reagent. (1), diffusion current of free Cu(II) ions; (2), diffusion current of hydrogen ions; (3), limiting current of the Cu–EDTA chelate.

Figure 1 shows that EDTA, DCTA, and DTPA reagents formed with the metals investigated chelates of 1:1 metal/ligand ratios of general formula, $MeHX^-$ where H_nX denotes the reagent. This is in agreement with SCHWARZENBACH's[6] results obtained potentiometrically. In the case of calcium chelates, the measured hydrogen wave is lower than the corresponding waves observed on the formation of other chelates. The diffusion current of calcium ions cannot be determined experimentally; calcium ions yield no polarographic wave. For the determination of the ratio, $i_{Ca^{2+}}/i_{H^+}$, and "ideal" diffusion current, $i_{Ca^{2+}}$ was taken as the current corresponding to the reduction of zinc(II) ions under identical conditions. The theoretical $i_{Ca^{2+}}/i_{H^+}$ ratio for reaction (2) is 1:1.86. Table 1 shows that the experimental value differs from the theoretical one. The lowering of the hydrogen wave in comparison with the hydrogen waves observed on the formation of other chelates may be explained by the relatively low stability of calcium chelates compared with that of the chelates of divalent transition metals. At relatively low pH-values, calcium chelate may be dissociated to a higher degree than, for example, nickel chelate.

A similar effect was observed on the examination of NTA chelates of divalent transition metals where the height of the hydrogen wave was found to be lower then that observed on the reduction of the chelates of other reagents. The dependence of i_{H^+} *vs.* millilitres of added NTA solution gave, however, a similar curve with a definite equivalence point as in the case of other chelates studied. On the other hand, the value of the ratio, $i_{Me^{2+}}/i_{H^+}$, was found to be very small and cannot substantiate the release of one hydrogen ion as shown earlier by SCHWARZENBACH[2]. In the case of the reaction of calcium ions with NTA no hydrogen wave was observed.

TTHA reagent forms relatively stable chelates, with 1:1 or 2:1 metal/ligand ratios[7–9]. For the formation of 2:1 chelates, three types of reactions are possible:

$$2Me^{2+} + H_3X^{3-} \rightleftharpoons Me_2X + 3H^+ \quad (7)$$

$$2Me^{2+} + H_3X^{3-} \rightleftharpoons Me_2HX^- + 2H^+ \quad (8)$$

$$2Me^{2+} + H_3X^{3-} \rightleftharpoons Me_2H_2X + H^+ \quad (9)$$

The existence of H_3X^{3-} species at pH 5 follows from the distribution curve of the dissociated forms of TTHA *vs.* pH[10]. The theoretical value of the ratio, $i_{Me^{2+}}/i_{H^+}$, is 1:2.6 for reaction (7), 1:1.98 for reaction (8) and 1:0.99 for reaction (9). Table 1 shows that for the reaction of two millimoles of zinc(II) or nickel(II) ions with 1 millimole of TTHA reagent the resulting chelates were Zn_2HX^- and Ni_2HX^-, respectively. The results with copper(II) ions showed the more probable existence of the Cu_2X^{2-} chelate. The examination of 1:1 TTHA chelates by the described procedure did not give satisfactory results, the hydrogen wave was smaller than that corresponding to the release of one hydrogen ion. This effect may be explained as follows. In the case of 1:1 TTHA chelates, $MeHX^{3-}$ or MeH_2X^{2-} chelates must be assumed to be formed in the solution of pH 5. The stability constants of copper, cadmium, nickel and calcium 1:1 TTHA chelates are, however, relatively small (pK-values for these chelates lie in the range 7–10[11,12]).

As was found in the study of NTA and EDTA chelates, the procedure described cannot be used when less stable chelates are formed.

It has already been established[13] that TTHA also forms binuclear mixed chelates, e.g., $CaZnX^{2-}$ or $NiZnX^{2-}$; this was verified by the application of the method described. If an equimolar mixture of two metal ions reacts with TTHA reagent and a binuclear mixed chelate is formed, two possible reaction paths may be formulated:

$$Me_1^{2+} + Me_2^{2+} + H_3X^{3-} \rightleftharpoons Me_1Me_2HX^- + 2H^+ \quad (10)$$

$$Me_1^{2+} + Me_2^{2+} + H_3X^{3-} \rightleftharpoons Me_1Me_2H_2X + H^+ \quad (11)$$

The theoretical value of the ratio $(i_{Me_1^{2+}} + i_{Me_2^{2+}})/i_{H^+}$ for reaction (10) is 1:1.9 and for reaction (11) is 1:0.99. The value of this ratio obtained experimentally for the mixture $(Ni^{2+} + Zn^{2+})$ ions is very close to the theoretical value, 1:1.9 (see Table 1), which proved the existence of a binuclear mixed chelate, $NiZnXH^-$. The verification of the existence of the calcium–zinc chelate is more complicated, owing to the fact that calcium ions yield no polarographic wave. The theoretical value of the ratio, $(i_{Ca^{2+}} + i_{Zn^{2+}})/i_{H^+}$, was therefore calculated as for the calcium–EDTA chelate. The experimentally determined value was 1:0.9, which may prove the existence of the $CaZnH_2X$ chelate.

Such a proof is, however, not so conclusive as in the case where the diffusion currents of both metal ions involved can be measured.

CONCLUSION

The results described show that the measurement of the height of the hydrogen wave in the dependence on the amount of added reagent enables (a) the metal/ligand ratio of the resulting chelate, (b) the number of hydrogen ions released during the chelation reaction and (c) the formation of a mixed binuclear chelate, to be established. The determination of metal/ligand ratio is achieved by an amperometric titration where the indication parameter is the diffusion current corresponding to the reduction of hydrogen ions. In this way even those metal ions that are not polarographically

active, (*e.g.*, calcium ions) can be titrated. The course of the titration is not influenced by the stability of the resulting chelate. The measurement of the diffusion current of hydrogen ions at the end-point of the titration allows the determination of the ratio, $i_{Me^{a+}}/i_{H^+}$, and a comparison with the theoretical value enables the number of released hydrogen ions to be calculated. To obtain satisfactory results, the metal ion studied should be polarographically active, the corresponding current must be of diffusion nature and the resulting chelate must be moderately stable (pK-value >10). For the investigation of the formation of mixed binuclear chelates both metal ions involved should be polarographically active.

The measurement of the changes in heights of the two corresponding waves in the dependence on the concentration of added reagent and the simultaneous measurement of the hydrogen wave enables the existence of the binuclear chelate to be verified. In all cases, the method can be applied only in unbuffered solutions of neutral salts of approximately pH 5. The presence of nitrate anions interferes with the accurate measurement of the height of the hydrogen wave.

SUMMARY

The amount of hydrogen ions released on formation of a chelate in the reaction of a metal ion with a reagent of EDTA type

$$H_aX^{b-} + Me^{c+} \rightleftharpoons MeH_{(a-d)}X^{(b-d+c)-} + dH^+$$

may be determined by the polarographic measurement of the height of the hydrogen wave. The determination of hydrogen ion concentration enables the mechanism of the chelation reaction to be established. In the titration of a metal ion with the reagent, the diffusion current of the reduction of hydrogen ions may be used for the indication of the titration. This indication may be applied even for the titration of metal ions that are polarographically inactive. In the case of the formation of mixed binuclear chelates, MeMe'X, the existence of such chelates may be verified and their formulae may be determined on the basis of the measurement of the hydrogen wave.

REFERENCES

1 D. D. DEFORD AND D. N. HUME, *J. Am. Chem. Soc.*, 73 (1951) 5321.
2 G. SCHWARZENBACH AND H. ACKERMANN, *Helv. Chim. Acta*, 35 (1952) 485.
3 N. TANAKA AND K. KATO, *Bull. Chem. Soc. Japan*, 32 (1959) 516.
4 D. R. CROW, *J. Electroanal. Chem.*, 16 (1968) 137.
5 R. TAMAMUSHI, *Bull. Chem. Soc. Japan*, 25 (1952) 293.
6 G. SCHWARZENBACH AND H. FLASCHKA, *Die komplexometrische Titration*, F. Enke, Stuttgart, 1967.
7 G. CONRADI AND M. KOPANICA, *Collection Czech. Chem. Commun.*, 28 (1963) 1600.
8 T. A. BOHIGIAN AND A. E. MARTELL, *Inorg. Chem.*, 4 (1965) 1264.
9 K. H. SCHRØDER, *Acta Chem. Scand.*, 19 (1965) 1797; 20 (1966) 881.
10 K. STULÍK AND F. VYDRA, *J. Electroanal. Chem.*, 16 (1968) 385.
11 T. A. BOHIGIAN AND A. E. MARTELL, *J. Am. Chem. Soc.*, 89 (1967) 832.
12 G. CONRADI, M. KOPANICA AND J. KORYTA, *Collection Czech. Chem. Commun.*, 30 (1965) 2029.
13 M. KOPANICA, *Talanta*, 15 (1968) 1457.

ELECTROANALYTICAL CHEMISTRY AND INTERFACIAL ELECTROCHEMISTRY
Elsevier Sequoia S.A., Lausanne – Printed in The Netherlands

PRE-VAGUE CATALYTIQUE DU COBALT EN PRESENCE DE SELENOCYSTINE

A. CĂLUȘARU ET V. VOICU
Institut de Physique Atomique, Bucarest (Roumanie)
(Reçu le 29ième août, 1968)

La dénomination de "processus catalysés" est utilisée en polarographie pour le cas particulier des courants cinétiques, où la réaction chimique est parallèle au processus à l'électrode[1]. Mais l'expression de catalyse en polarographie se réfère le plus souvent à la décharge catalytique de l'hydrogène en l'absence[2] et en présence d'ions de cobalt ou de nickel[3]. Dans ce cas, la hauteur de la vague catalytique de l'hydrogène est de plusieurs fois supérieure à la vague de diffusion qui correspondrait à la réduction de la substance catalytique seule. Autrement dit, chaque molécule catalytique décharge à l'électrode un grand nombre de protons[4]. Le même processus se produit lors de la formation de pré-vagues catalytiques, mais dans ce cas, ce sont les ions métalliques qui se déchargent à l'électrode[3].

L'influence du pouvoir tampon sur la décharge catalytique de l'hydrogène montre que ce processus est influencé par la vitesse de protonisation. C'est donc un phénomène cinétique qui intervient dans ce cas et qui pourrait justifier le fait que l'on range les courants catalytiques dans le groupe des courants cinétiques. Il y a toutefois des systèmes[5] où le pouvoir tampon reste sans influence ou même diminue la hauteur de la vague catalytique. Dans ce cas, la molécule catalytique décharge un petit nombre de protons; le courant est alors influencé par la concentration et la vitesse de diffusion du complexe catalytique à l'électrode. C'est la raison pour laquelle aucun effet cinétique ne contrôle plus la hauteur de la vague catalytique[5]. Ce comportement justifie que l'on classe en polarographie les courants catalytiques dans un groupe séparé de courants, bien différent par rapport aux courants cinétiques. Grace à l'analogie qui existe entre la décharge catalytique de l'hydrogène et la décharge catalytique des ions métalliques, il est préférable d'utiliser l'expression de pré-vague catalytique pour caractériser ce dernier processus, bien que les effets cinétiques y soient présents[6,7].

La composition des systèmes où se produit la décharge catalytique de l'hydrogène en présence de cobalt ou de nickel est complexe. C'est la raison pour laquelle d'autre processus ont lieu parallèlement à la catalyse de l'hydrogène. Les pré-vagues catalytiques du cobalt[7–9] et du nickel[6] ont été souvent étudiées pour mieux comprendre le processus de décharge catalytique de l'hydrogène. Le déplacement d'environ 200 mV de la vague du cobalt vers les potentiels positifs, signalé par BRDIČKA[10] dans son premier mémoire sur les vagues catalytiques des protéines, suggérait une étroite liaison avec le processus de décharge catalytique de l'hydrogène. On a même suggéré qu'il était possible d'établir une corrélation entre la hauteur de la pré-vague du cobalt en présence de cystéine et la hauteur de la vague catalytique de l'hydro-

gène[8,9]. Ce parallèlisme n'existe plus dans le cas du nickel[6]; en outre, plusieurs substances forment des pré-vagues catalytiques sans produire la décharge catalytique de l'hydrogène[3]. On peut encore signaler qu'en présence de nitrohydroxylaminate de sodium[11] aucun déplacement de la vague n'est observé, bien que dans ce système se produise la décharge catalytique de l'hydrogène.

On peut donc conclure que malgré l'analogie des processus, il n'y a aucune liaison directe entre la pré-vague du cobalt ou du nickel et la vague catalytique de l'hydrogène, au moins dans un nombre important de systèmes. Le point commun entre ces deux processus est le fait qu'ils soient produits par des complexes faisant intervenir le même ion métallique et le même ligand. Un équilibre chimique existe entre ces complexes et des effets cinétiques peuvent se produire dans la couche de réaction lorsque les concentrations à l'équilibre sont modifiées par le passage de courant. Il est donc nécessaire de tenir compte de la formation des pré-vagues lorsqu'on étudie la décharge catalytique de l'hydrogène.

Le présent travail décrit les propriétés caractéristiques de la pré-vague catalytique dans le système cobalt–séléno-cystine. La séléno-cystine forme une pré-vague catalytique du cobalt bien définie, sans produire de vagues correspondant à la décharge catalytique de l'hydrogène. C'est la raison pour laquelle ce système est particulièrement favorable pour l'étude des pré-vagues catalytiques. Le tampon ammoniacal, malgré les désavantages justifiés signalés en réf. 7, représente le système tampon le mieux adapté, car il est le plus spécifique pour la catalyse de l'hydrogène et il permet une large variation des paramètres fondamentaux: concentration de l'ion métallique et pouvoir tampon. En outre, même dans le tampon au borate où la vague du cobalt n'est pas déformée par des maxima, on est obligé d'employer des substances adsorbantes, afin de supprimer les maxima de la pré-vague catalytique[7].

PARTIE EXPÉRIMENTALE

La séléno-cystine a été sythétisée selon la méthode décrite par PAINTER[12]. Prenant la sérine comme substance de départ nous avons synthétisé l'hydrochlorure de l'ester méthylique de la sérine. Cette dernière substance a réagi avec le benzyl-séléno-mercaptan pour produire la β-benzyl-séléno-alanine, qui a été ensuite réduite avec du sodium métallique dans l'ammoniaque liquide. Le produit formé a été dissous dans l'eau et oxydé en présence de l'oxygène de l'air en β, β'-diséléno-dialanine (séléno-cystine). Finalement, nous avons effectué la purification de cette substance par dissolution dans l'acide bromhydrique dilué et recristallisation, à pH controlé, à basse température. Toutes les autres substances ont été des reactifs *pro analysi*.

La dissolution de la séléno-cystine a été effectuée en présence d'acide bromhydrique, qui a été ensuite neutralisé par l'hydroxyde d'ammonium jusqu'à pH=7. De cette manière, nous avons évité l'utilisation de l'acool éthylique comme milieu de dissolution, recommandé en réf. 13. Les solutions de séléno-cystine ne sont pas complètement stables. A une concentration de 10^{-4} M en séléno-cystine, nous avons constaté que pendant 5 jours la solution n'a pas évolué. Dans le cas des concentrations de l'ordre 10^{-3} M, la décomposition devient appréciable après environ 2 jours. La stabilité diminue encore lorsque la concentration en séléno-cystine est augmentée.

Les solutions ont été étudiées avec un polarographe LP 60 dans une cellule

ayant comme anode une électrode saturée au calomel. Le capillaire a eu les constantes caractéristiques suivantes: $m = 2.64$ mg sec^{-1} et $t_1 = 3.56$ sec en solution NH_4Cl 0.1 M, NH_4OH 0.1 M, $CoCl_2$ 10^{-3} M, séléno-cystine $5 \cdot 10^{-6}$ M, gélatine 0.01%, circuit ouvert et $h = 56$ cm.

RESULTATS EXPÉRIMENTAUX

1. Influence de la gélatine

En l'absence de gélatine, la vague du cobalt est fortement déformée par l'apparition d'un maximum de premier ordre. Dans ce cas en présence de séléno-cystine, même à une concentration très faible (10^{-6} M) aucun dédoublement de la vague du cobalt ne se produit; on observe seulement un déplacement de la vague d'environ 85 mV dans la direction des potentiels positifs. A des concentrations plus grandes en séléno-cystine ($5 \cdot 10^{-6}$ M) la croissance de la concentration en gélatine produit la séparation progressive des vagues. On peut observer en outre la diminution de la hauteur de la première vague lorsqu'on augmente la quantité de gélatine (Fig. 1).

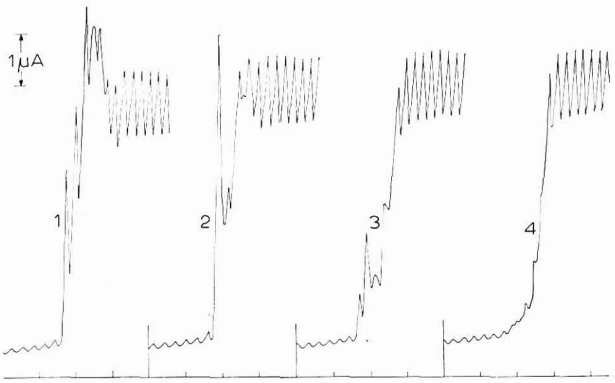

Fig. 1. Influence de la gélatine sur la pré-vague catalytique du cobalt en présence de séléno-cystine. Potentiel de départ, −0.6 V; −200 mV/absc.; anode E.S.C.; hauteur du reservoir de mercure h = 26 cm. Solution: Co^{2+}, 10^{-3} M; NH_4Cl/NH_4OH, 0.1 M; séléno-cystine, $5 \cdot 10^{-6}$ M. Gélatine: (1), 0.002; (2), 0.004; (3), 0.01; (4), 0.02%.

Pour une concentration de 0.004% en gélatine (courbe 2, Fig. 1), on peut remarquer que la pré-vague acquiert à peu près la moité de la hauteur de la vague du cobalt (10^{-3} M), bien que la concentration de la séléno-cystine soit seulement de $5 \cdot 10^{-6}$ M. Ce comportement démontre le caractère catalytique de la pré-vague du cobalt en présence de séléno-cystine.

Il est intéressant de remarquer l'influence de la gélatine sur la hauteur du maximum formé par la pré-vague. A une concentration en gélatine de 0.004%, le maximum du cobalt est pratiquement supprimé, tandis que le maximum de la pré-vague reste encore très fort. L'augmentation de la concentration en gélatine jusqu'à 0.01% ne supprime pas le maximum de la pré-vague. L'abaissement de ce dernier est accompagné par la diminution de la vague; le rapport entre le maximum et la vague reste encore grand.

La variation de la hauteur de la pré-vague du cobalt en fonction de la concentration en gélatine est montrée sur la Fig. 2 pour deux hauteurs différentes du

réservoir de mercure. On peut observer sur cette Figure l'existence de trois domaines séparés. Dans la première région, située entre 0.002 et 0.005%, la hauteur de la pré-vague varie, mais la limite de séparation des vagues est accentuée progressivement. Dans la seconde région, située entre 0.005 et 0.01%, les vagues sont bien séparées,

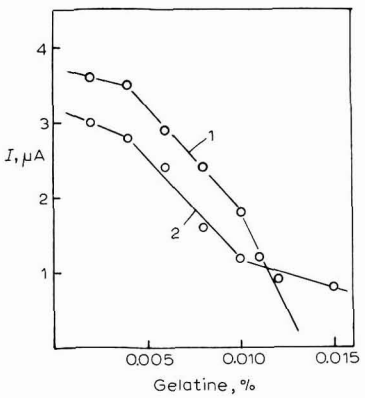

Fig. 2. Variation de la hauteur de la pré-vague en fonction de la concn. en gélatine. Solution: Co^{2+}, 10^{-3} M; NH_4Cl/NH_4OH, 0.1 M; séléno-cystine, $5 \cdot 10^{-6}$ M. h: (1), 65; (2), 26 cm.

mais la hauteur de la prévague diminue rapidement lorsque la concentration en gélatine augmente. Dans la troisième région corréspondant à des concentrations supérieures à 0.01%, la hauteur de la pré-vague diminue plus vite dans le cas des grandes hauteurs du réservoir de mercure et plus lentement dans le cas des petites hauteurs. Pratiquement à la concentration de $5 \cdot 10^{-6}$ M en séléno-cystine la pré-vague n'est plus visible pour une concentration de 0.05% en gélatine. L'intervalle le plus favorable est situé dans la seconde région. Il en résulte que la reproducibilité des résultats est fortement influencée par la quantité de gélatine.

2. Influence de la hauteur du réservoir de mercure

La non-corréspondance entre la hauteur de la pré-vague du cobalt et la concentration stoechiométrique en séléno-cystine est une preuve du caractère catalytique de la pré-vague. Une indication importante est obtenue en considérant la variation de la hauteur de la pré-vague en fonction de la hauteur du réservoir de mercure. Sur la Fig. 3 sont montrés les polarogrammes enregistrés dans le système cobalt–séléno-cystine à différentes hauteurs du réservoir de mercure et à une concentration de 0.005% en gélatine. On peut remarquer sur cette figure que la pré-vague présente un fort maximum, qui peut dépasser la vague totale du cobalt, dans le cas des petites hauteurs du réservoir de mercure (courbe 1, Fig. 3). Ce maximum diminue (courbes 2 et 3, Fig. 3) et disparaît complètement lorsque la hauteur du réservoir augmente (courbe 4, Fig. 3). Le maximum de premier ordre qui correspond à la vague du cobalt montre un comportement différent. A une concentration de 0.005% en gélatine, ce maximum est complètement supprimé lorsque la hauteur du réservoir de mercure est faible (courbe 1, Fig. 3), mais il devient plus grand lorsque la hauteur du réservoir augmente (courbe 4, Fig. 3).

KOLTHOFF *et al.*[7] signalent également l'apparition des maxima qui accom-

pagnent la pré-vague catalytique du cobalt en système tampon au borate et en présence de cystéine. Ils ont constaté que ce maximum est causé par l'agitation de l'électrolyte et peut être supprimé par apport de substances adsorbantes: perchlorate de tétrabutylammonium, gélatine, polyacrylamide, Triton X-114 et alcool polyvinylique.

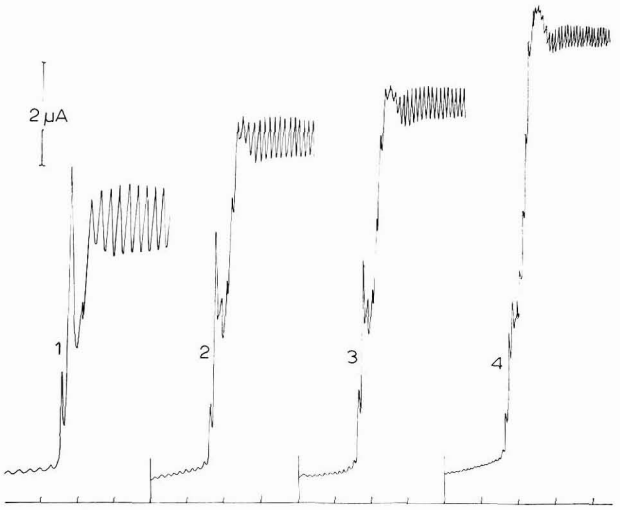

Fig. 3. Influence de la hauteur du reservoir de mercure sur la pré-vague catalytique. Potentiel de départ, −0.6 V; −200 mV/absc.; anode, E.C.S. Solution: Co^{2+}, 10^{-3} M; NH_4Cl/NH_4OH, 0.1 M; séléno-cystine, $5 \cdot 10^{-6}$ M; gélatine, 0.01%. Hauteur du reservoir: (1), 26; (2), 46; (3), 56; (4), 87 cm.

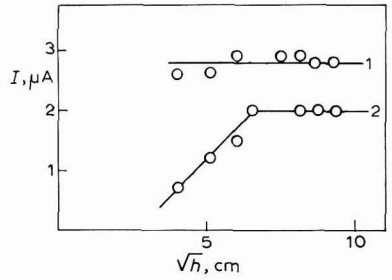

Fig. 4. Représentation graphique de la hauteur de la pré-vague en fonction du $\sqrt{h}$. Co^{2+}, 10^{-3} M; NH_4Cl/NH_4OH, 0.1 M; séléno-cystine, $5 \cdot 10^{-6}$ M. Gélatine: (1), $5 \cdot 10^{-3}$; (2), 10^{-2} %.

Bien qu'ils aient également constaté la diminution de la pré-vague en présence de ces substances ils ont tiré la conclusion, en se fondant sur ces données, que le maximum de la pré-vague représente un maximum de premier ordre. Dans le cas du maximum de la pré-vague en présence de séléno-cystine, il faut tenir compte des différences qu'on peut observer lorsqu'on examine les Figs. 1 et 3. Il en résulte que, par différence avec le maximum du cobalt, qui est sans doute un maximum de premier ordre, le maximum de la pré-vague est supprimé dans le cas des grandes hauteurs du réservoir, tandis que l'action suppréssive de la gélatine semble être réduite.

Si l'on considère la Fig. 4, courbe 2, lorsque la pré-vague arrive à la moité de la vague totale, on constate que la hauteur de la pré-vague varie en fonction de la hauteur du réservoir de mercure dans le cas des petites hauteurs du réservoir; la hauteur de la pré-vague tend vers une limite pour les grandes hauteurs du réservoir. Dans le cas d'une concentration plus grande en gélatine, Fig. 4, courbe 1, lorsque la pré-vague est beaucoup diminuée, sa hauteur ne varie plus en fonction de la hauteur du réservoir et ce comportement peut indiquer le caractère cinétique de la pré-vague catalytique.

3. Influence de la concentration en séléno-cystine

La pré-vague catalytique du cobalt est visiblement séparée même à une concentration de 10^{-6} *M* en séléno-cystine. Mais une séparation nette des vagues peut être remarquée pour les concentrations supérieures à $3 \cdot 10^{-6}$ *M* (Fig. 5). A la concentration de $2 \cdot 10^{-5}$ *M* en séléno-cystine on peut observer un déplacement total de la vague du cobalt dans la région de la pré-vague. Dans ces conditions ce déplacement est de 150 mV.

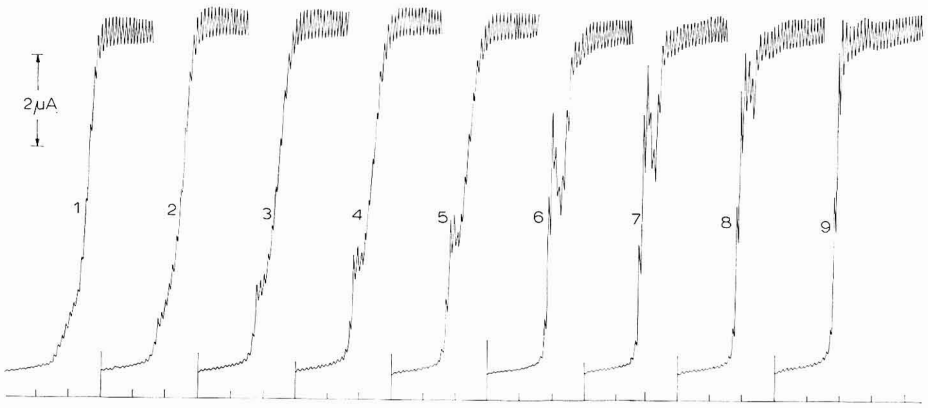

Fig. 5. Influence de la concn. en séléno-cystine sur la vague du cobalt. Potential de départ, −0.6 V; −200 mV/absc.; Co^{2+}, 10^{-3} *M*; NH_4Cl/NH_4OH, 0.1 *M*; gélatine, 0.01%. Séléno-cystine: (1), 1; (2), 2; (3), 3; (4), 4; (5), 5; (6), 8; (7), 9; (8), 10; (9), $20 \cdot 10^{-6}$ *M*.

Sur la Fig. 5, courbes 6 et 7, on voit que le maximum de la pré-vague qui est bien formé augmente lorsque la pré-vague croît. Mais ce maximum disparaît lorsque la vague du cobalt est entièrement déplacée.

Sur la Fig. 6 nous avons représenté la variation de la hauteur de la pré-vague en fonction de la concentration en séléno-cystine. Il est à remarquer que la courbe tend vers une limite, comme il a été constaté dans plusieurs autres cas[6-9]. Cette valeur limite est atteinte lentement.

Il n'a pas été possible d'étudier l'influence de la concentration en séléno-cystine sur la hauteur de la pré-vague en l'absence de gélatine, faute de séparation entre la pré-vague et la vague du cobalt.

4. Influence de la concentration du cobalt

Si on maintient constante la concentration en séléno-cystine et si on augmente

progressivement la concentration du cobalt, on constate une diminution de la pré-vague catalytique. Pour une concentration de la séléno-cystine de $5 \cdot 10^{-6}$ M et une concentration du cobalt de $2 \cdot 10^{-4}$ M, la vague est complètement déplacée dans la région de la pré-vague. Sur la Fig. 7 nous avons représenté la hauteur de la pré-vague en fonction de la concentration en cobalt. Il est important de remarquer la diminution de la hauteur de la pré-vague lorsque la concentration en cobalt croît. Ce comportement est différent du cas des vagues catalytique de l'hydrogène; ces vagues augmentent à des concentrations plus grandes du cobalt, ce qui indique le déplacement de l'équilibre en faveur de la formation des complexes catalytiques. Dans le cas des pré-vagues catalytiques du cobalt[7-9] et du nickel[6] en présence de cystéine on observe de même une croissance de la hauteur de la pré-vague lorsqu'on augmente la concentration en cobalt.

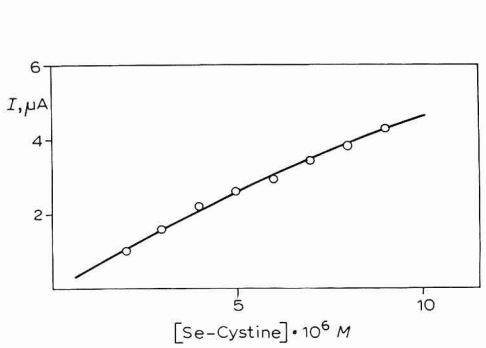

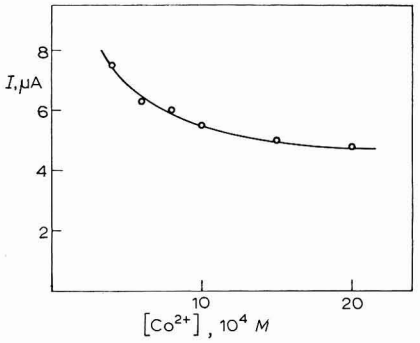

Fig. 6. Variation de la hauteur de la pré-vague en fonction de la concn. en séléno-cystine. Co^{2+}, 10^{-3} M; NH_4Cl/NH_4OH, 0.1 M; gélatine, 0.01%.

Fig. 7. Variation de la pré-vague en fonction de la concn. du cobalt. NH_4Cl/NH_4OH, 0.1 M; séléno-cystine, $5 \cdot 10^{-6}$ M; gélatine, 0.01%.

5. Influence du pouvoir tampon

Le pouvoir tampon augmente en général les vagues qui correspondent à la décharge catalytique de l'hydrogène, car le proton hydraté participe à ce processus. Le système tampon NH_4Cl–NH_4OH forme des complexes amminiques avec le cobalt. L'augmentation de la concentration de ces composants modifie les équilibres entre les complexes qui peuvent se former dans la solution. Lorsque le nombre des protons déchargés par chaque molécule de complexe est petit[4] la vague catalytique de l'hydrogène diminue si le pouvoir tampon est augmenté[5], puisque la hauteur de la vague est déterminée par la concentration du complexe. La concentration de ce dernier diminue pour les grandes concentrations du tampon qui déplacent l'équilibre vers la formation des complexes ammoniacaux. Un phénomène analogue a lieu également dans le cas de la pré-vague du cobalt. Cette pré-vague est produite par la formation d'un complexe du cobalt avec la séléno-cystéine et la concentration de ce complexe est diminuée par la croissance de la concentration de la substance complexante. La variation de la hauteur de la pré-vague catalytique en fonction du pouvoir tampon est représentée sur la Fig. 8. La courbe tend vers une limite pour les concentrations des composants du tampon supérieures à 0.5 M.

6. Influence de la concentration en chlorure d'ammonium

Dans le cas des petites hauteurs de la pré-vague du cobalt, la variation de la concentration en chlorure d'ammonium ne produit pas d'effet visible sur cette pré-vague, à des concentrations en chlorure supérieures à 0.05 M, comme il résulte de la Fig. 9. A des concentrations plus petites en chlorure d'ammonium (0.02 M), la stabilité des complexes ammoniacaux est très réduite et le cobalt a alors tendence à précipiter; la pré-vague catalytique croît brusquement dans ce cas (Fig. 9).

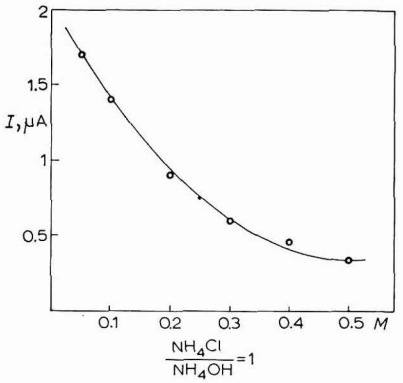

Fig. 8. Influence du pouvoir tampon sur la hauteur de la pré-vague catalytique. Co^{2+}, 10^{-3} M; NH_4Cl/NH_4OH = 1; séléno-cystine, $5 \cdot 10^{-6}$ M; gélatine, 0.01%.

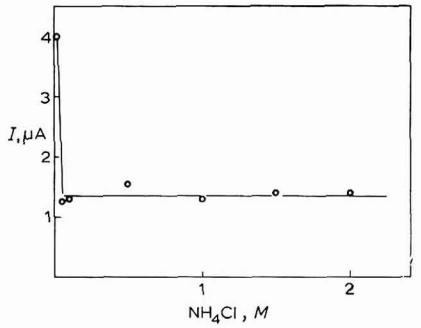

Fig. 9. Influence de la concn. en NH_4Cl sur la hauteur de la pré-vague catalytique. Co^{2+}, 10^{-3} M; NH_4OH, 0.1 M; séléno-cystine, $5 \cdot 10^{-6}$ M; gélatine, 0.01%.

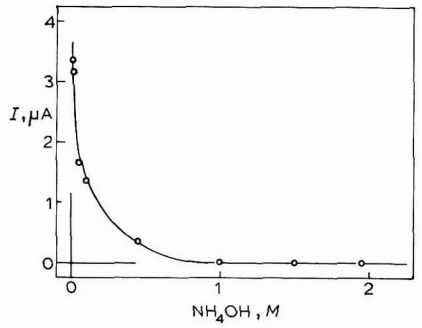

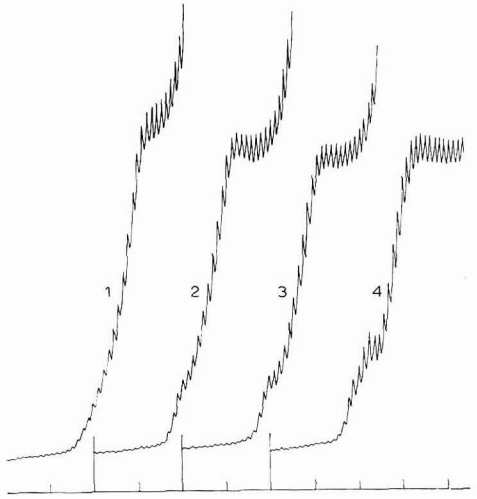

Fig. 10. Influence de la concn. en NH_4OH sur la hauteur de la pré-vague catalytique. Co^{2+}, 10^{-3} M; NH_4Cl, 0.1 M; séléno-cystine, $5 \cdot 10^{-6}$ M; gélatine, 0.01%.

Fig. 11. Influence du pH sur la pré-vague catalytique. Co^{2+}, 10^{-3} M; séléno-cystine, $5 \cdot 10^{-6}$ M; gélatine $5 \cdot 10^{-3}$%. Tampon acétate, pH: (1), 3.19; (2), 4.1; (3), 4.4; (4), 5.0. Potentiel de départ, −0.6 V; −200 mV/absc.; anode E.S.C.

7. Influence de la concentration en hydroxyde d'ammonium

La concentration de l'hydroxyde d'ammonium a une influence marquée sur la hauteur de la pré-vague catalytique dans le système cobalt–séléno-cystine. La courbe représentée sur la Fig. 10 montre que la hauteur de la pré-vague diminue rapidement lorsque la concentration de l'ammoniaque augmente. A une concentration de 1 M en ammoniaque la pré-vague disparaît entièrement.

8. Influence du pH

La variation du rapport entre NH_4Cl et NH_4OH, par le changement de la concentration de l'un des composants, conduit implicitement à la variation du pH de la solution. Mais dans le tampon ammoniacal, le cobalt forme des complexes; sur la pré-vague agissent donc simultanément la variation de la concentration des complexes et la variation du pH. Les données antérieurement présentées et qui se réfèrent à l'influence de la variation de la concentration de chacun des composants du tampon, montrent que la stabilité des complexes est le facteur principal qui agit sur la hauteur de la pré-vague. C'est la raison pour laquelle nous avons choisi le système tampon acide acétique–acétate de sodium. Dans l'intervalle de pH situé entre 3.19 et 4.1 la pré-vague est très faiblement définie (Fig. 11). Au delà de pH 4.7, les deux vagues sont bien séparées. On remarque une croissance de la hauteur de la pré-vague en fonction de la croissance de la valeur du pH (Fig. 12). L'allure des polarogrammes évolue peu même pour des grandes variations du pH (valeurs inférieures à 6).

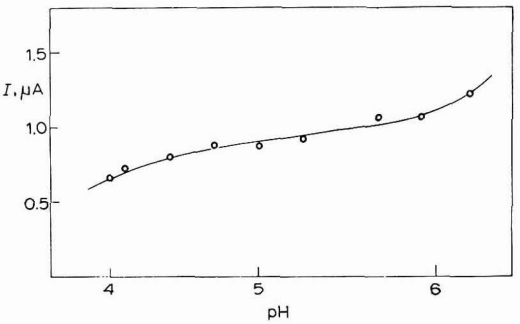

Fig. 12. Variation de la hauteur de la pré-vague en fonction de pH. Co^{2+}, 10^{-3} M; séléno-cystine, $5 \cdot 10^{-6}$ M; gélatine, $5 \cdot 10^{-3}$ %; tampon acétate.

9. Influence de la force ionique

La force ionique modifie le pH et influence les processus d'adsorption dans la couche double électrique[14,15]. Par son action électrostatique la couche double peut accélerer ou freiner la réaction à l'électrode lorsque la force ionique varie[16,17]. La croissance de la concentration saline accélère la réduction des ions non chargés ou chargés négativement et freine la réduction des ions chargés positivement. Bien que la pré-vague soit produite par un complexe du cobalt avec la séléno-cystéine, cette pré-vague, grâce à son caractère catalytique, n'a pas les propriétés qu'on retrouve normalement dans le cas de la décharge d'un complexe.

La variation de la concentration saline influence spécialement la hauteur de la pré-vague. Parmi les sels utilisés, nous notons principalement l'action du chlorure de

lithium (Fig. 13). La croissance de la concentration en chlorure de lithium jusqu'à 0.2 ou 0.5 M augmente simultanément la hauteur de la pré-vague et celle du maximum qui lui correspond. La croissance ultérieure de la concentration en LiCl diminue le maximum et la hauteur de la pré-vague, mais on remarque également une diminution de la vague totale. L'influence de différents sels sur la hauteur de la pré-vague est montrée sur la Fig. 14. On peut observer que le chlorure de lithium a l'effet le plus

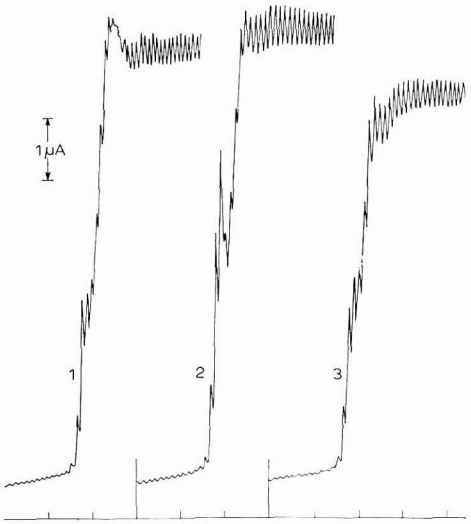

Fig. 13. Influence de la concn. en LiCl sur la hauteur de la pré-vague du cobalt en présence de séléno-cystine. Potentiel de départ, −0.6 V; −200 mV/absc.; anode, E.S.C. Solution: Co^{2+}, 10^{-3} M; NH_4Cl/NH_4OH, 0.1 M; séléno-cystine, $5 \cdot 10^{-6}$ M; gélatine, 0.005%. LiCl: (1), 0; (2), 0.2; (3), 3 M.

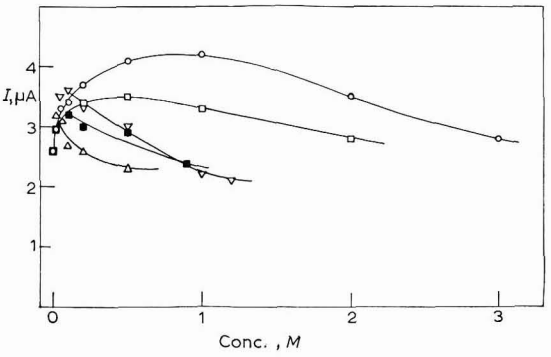

Fig. 14. Influence de la force ionique sur la pré-vague du cobalt en présence de séléno-cystine. Solution: Co^{2+}, 10^{-3} M; NH_4Cl/NH_4OH, 0.1 M; séléno-cystine, $5 \cdot 10^{-6}$ M; gélatine, 0.005%. (○), LiCl; (□), NaCl; (△), $NaClO_4$; (▽), $SrCl_2$; (■), $BaCl_2$.

typique. Dans ce cas, le maximum de la courbe correspond à la concentration de 1 M en LiCl. Pour les autres sels, la valeur du maximum est déplacée vers les petites valeurs de la concentration. De grandes différences peuvent être observées entre le comportement du chlorure de lithium et de sodium d'une part et le comportement du

perchlorate de sodium d'autre part. Le chlorure de strontium a une action analogue au chlorure de barium.

La variation dans un grand intervalle de la concentration saline influence peu les potentiels de démi-vague. Dans tous les cas, on remarque un déplacement des deux vagues vers les potentiels négatifs. L'effet le plus marqué sur les potentiels est manifesté en présence des chlorures de sodium, de strontium et de barium.

DISCUSSION DES RÉSULTATS

La pré-vague du cobalt qui apparaît dans le système cobalt–séléno-cystine est produite par un complexe qui se forme entre le cobalt et la séléno-cystéine; en effet la séléno-cystine est réduite en séléno-cystéine à un potentiel de démi-vague égale à -0.6 V[13,18]. La vague du cobalt en tampon ammoniacal a un potentiel de demi-vague égal à -1.05 V, et la pré-vague catalytique à -0.94 V.

La séléno-cystéine est très active en ce qui concerne la formation de la pré-vague du cobalt puisqu'on observe celle-ci même à une concentration en séléno-cystine de 10^{-6} M. A une concentration de $5 \cdot 10^{-6}$ M en séléno-cystine et une concentration réduite en gélatine, la pré-vague a une hauteur égale à la moitié de la hauteur de la vague totale. Il est à remarquer que par différence à la cystéine, en tampon ammoniacal, où la séparation des vagues peut être observée après un vieillissement relativement long de la solution[3,8] dans le cas de la séléno-cystine la vague apparaît immediatement après la préparation de la solution. Le même effet a été signalé dans le cas du cobalt en tampon au borate et en présence de cystéine[7].

La séléno-cystéine peut avoir plusieurs formes dont la stabilité dépend du pH de la solution. Le groupe carboxylique doit être ionisé au-dessus de pH 7 et les autres groupes ont les formes suivantes:

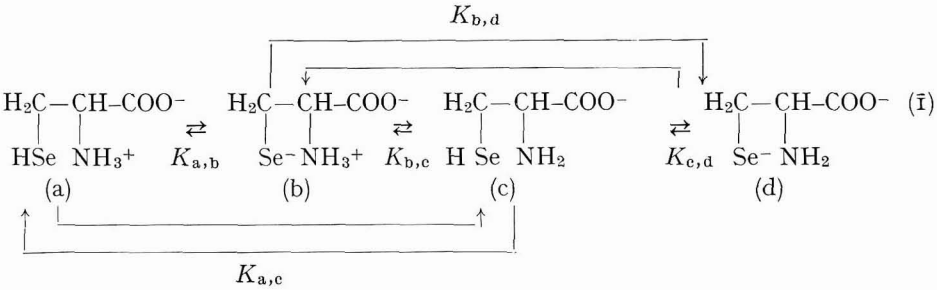

On ne connaît pas les valeurs de ces constantes de dissociation (notées par $K_{i,j}$) et on est obligé de se limiter à une analogie qualitative avec la cystéine[21]. La forme (a) ne peut pas former de complexe avec le cobalt et la forme (d) doit être stable seulement dans les milieux très basiques. Restent les formes (b) et (c) qui peuvent former des complexes avec le cobalt dans les solutions dont le pH n'est pas très éloigné de la valeur 7:

$$\text{Co(II)} + x\text{(b)} + y\ \text{Lig} \rightarrow [\text{Co(II)}\ \text{(b)}_x(\text{Lig})_y] \quad (2)$$

$$\text{Co(II)} + x\text{(c)} + y\ \text{Lig} \rightarrow [\text{Co(II)}\ \text{(c)}_x(\text{Lig})_y] \quad (3)$$

Par Lig nous avons noté une molécule d'eau ou de composant du tampon.

Grâce à la structure des ligands (b) et (c) ces complexes sont du type chélaté.

Il y a deux possibilités de former le cycle chélaté: (1) avec les groupes carboxyliques; (2) avec le sélénium. On a constaté dans le cas de la cystéine[3] que les complexes qui contiennent les groupes carboxyliques ne sont pas actifs dans le processus de décharge catalytique de l'hydrogène. Nous avons également constaté que les vagues du cobalt ne sont pas déplacées dans la région de la pré-vague catalytique en présence de sérine et de l'hydrochlorure de l'ester méthylique de la sérine. En outre la β-benzyl-séléno-alanine, qui est une séléno-cystéine où l'hydrogène du sélénium est substitué par un groupe benzylique, ne donne aucun effet, ni dans la région de la pre-vague, ni dans la région de la décharge catalytique de l'hydrogène. Ces résultats expérimentaux démontrent que les complexes chélatés avec le groupe carboxylique ne présentent pas d'effet catalytique. Il faut donc considérer que les complexes chélatés du cobalt avec le sélénium forment la pré-vague catalytique du cobalt.

Pour l'explication du caractère catalytique de la pré-vague, il est possible d'utiliser un schéma analogue à celui proposé par MARK ET REILLEY[19], puis adopté dans les autres travaux[6-9]:

$$[\mathrm{Co(Se\text{–}cy)}_x(\mathrm{Lig})_y] \xrightarrow{+2e} \mathrm{Co} + x\ \mathrm{Se\text{–}cy} + y\ \mathrm{Lig} \tag{4}$$

$$x\ \mathrm{Se\text{–}cy} + \mathrm{Co(Lig)_6} \xrightarrow[k]{\text{chim.}} [\mathrm{Co(Se\text{–}cy)}_x(\mathrm{Lig})_y] + (6-y)\mathrm{Lig} \tag{5}$$

De ce schéma il résulte que x molécules de séléno-cystéine participent plusieurs fois dans la formation du complexe avec le cobalt qui se décharge dans la région de la pré-vague. On note par N le nombre d'ions de cobalt qui entrent avec x molécules de séléno-cystéine dans les réactions (4) et (5) et par $\bar{i}_k{}^d$ le courant de diffusion du complexe en l'absence d'effet catalytique, donc dans le cas où la réaction (4) peut se produire; z représente la fraction des x molécules qui complexent le cobalt. Dans ce cas, z est égal à 1, puisque les molécules de séléno-cystéine n'interviennent pas dans la réaction à l'électrode. Par analogie avec l'équation déduite[4] pour la décharge catalytique de l'hydrogène, l'équation de la pré-vague catalytique s'écrit de la façon suivante:

$$i_p = zN\bar{i}_k{}^d/[1+\exp\{(\varepsilon-\varepsilon_p{}^{\frac{1}{2}})\alpha nF/RT\}] \tag{6}$$

où ε est le potentiel, $\varepsilon_p{}^{\frac{1}{2}}$ le potentiel de demi-vague de la pré-vague catalytique, i_p le courant, α le coefficient de transfert, F la constante de Faraday, R la constante des gazes, n la valence de la réaction à l'électrode et T la température absolue. Le nombre x des molécules de séléno-cystéine qui entrent dans la composition du complexe ne peut pas être déterminé en utilisant les données polarographiques, par suite de la complexité du processus. Si on fait l'hypothèse qu'une seule molécule de séléno-cystéine entre dans la composition du complexe ($x=1$) et que toute la séléno-cystéine est complexée, il est possible de calculer la valeur minimum de N. Compte tenue des valeurs expérimentales, il en résulte pour N une valeur d'environ 41. Il est intéressant de comparer cette valeur aux valeurs de N calculées dans le cas de la catalyse de l'hydrogène. On a calculé qu'en présence de nitrohydroxylaminate de sodium le complexe du cobalt décharge 14 protons[4] et en présence de cystéine environ 740 protons[20]. Dans le cas de la décharge catalytique du cobalt N est situé vers les petites valeurs.

Les réactions (1) et (2) montrent qu'en présence d'un grand excès de cobalt la pré-vague doit avoir un caractère cinétique. Dans le cas du système nickel–cystéine, on a établi qu'en effet la hauteur de la pré-vague ne depend pas de la hauteur du réservoir de mercure[6]. On a signalé également en réf. 7 le caractère cinétique de la pré-vague du cobalt en milieu tampon au borate et en présence de cystéine, d'ester méthylique de la cystéine, de cystéamine, d'acide β-mercapto-propionique et d'acide thioglycolique. Dans le cas de l'ester éthylique de la cystéine, la constante de vitesse de la réaction de formation du complexe qui produit la décharge catalytique du cobalt est égale à $4.0 \cdot 10^3$ mol^{-1} l sec^{-1} à 25°[7]. Dans le cas de la séléno-cystéine, la pré-vague a également un caractère cinétique (Fig. 4); mais la variation anormale de la hauteur de la pré-vague en fonction de la concentration du cobalt ne permet pas de calculer la constante de vitesse.

La variation de la pré-vague catalytique en fonction des paramètres étudiés met en évidence certaines propriétés caractéristiques des pré-vagues catalytiques.

La variation de la hauteur de la pré-vague en fonction de la concentration du tampon (Fig. 8) et de ses composants (Figs. 9 et 10) peut être interprétée si l'on tient compte de la concurrence entre la formation du complexe avec la séléno-cystéine et la réaction de formation des complexes amminiques du cobalt. Si dans les conditions de travail utilisées, la stabilité de ces complexes croît on peut s'attendre à une diminution de la concentration du complexe contenant la séléno-cystéine et par conséquant à une diminution de la pré-vague catalytique (Figs. 8 et 10).

La concentration en substances adsorbantes, telles que la gélatine, a une influence très importante sur la pré-vague catalytique. Dans le cas de la cystéine ZIELINSKI ET KŮTA[8,9], ainsi que KOLTHOFF *et al.*[7] ont constaté que les courbes électrocapillaires et les courbes tensammétriques ne mettent pas en évidence l'influence de l'adsorption sur la pré-vague catalytique. Les courbes *i–t* ont un aspect qui montre la complexité considérable du processus à l'électrode où les processus d'adsorption peuvent intervenir directement ou indirectement[8]. Le coefficient de température négatif signalé[8,9] caractérise d'habitude les processus influencés par l'adsorption.

La variation de la hauteur de la pré-vague en fonction de la concentration en séléno-cystéine a la forme normale pour ce type de processus. Cette variation tend vers une limite correspondant à la hauteur totale de la vague du cobalt. La variation du pH influence relativement peu la hauteur de la pré-vague, mais la croissance de sa valeur contribue à accentuer la délimitation entre la pré-vague et la vague du cobalt.

La force ionique a une influence bien caractéristique puisque un certain domaine de la concentration saline fait apparaître un maximum de la hauteur de la pré-vague (Fig. 14). Il est à remarquer que dans le cas des métaux monovalents et de l'ion Cl^-, ce maximum est situé à des valeurs plus grandes de la concentration en électrolyte indifférent, tandis que dans le cas des ions divalents le maximum est déplacé vers le domaine des concentrations très petites. La variation de la hauteur de la vague en fonction de la concentration saline peut être expliquée soit par la modification des processus d'adsorption, soit par la variation de la vitesse de la réaction (2) en fonction de la force ionique. Le déplacement vers les potentiels négatifs du potentiel de démi-vague de la vague catalytique lors de la croissance de la force ionique pourrait indiquer la charge positive du complexe qui se décharge dans la région de la pré-vague.

La diminution de la pré-vague catalytique lors de la croissance de la concentration du cobalt est surprenante. On peut s'attendre normalement à ce qu'une croissance de la concentration des ions de cobalt entraîne également une croissance de la concentration du complexe catalytique. Les données expérimentales de la Fig. 7 infirment cette variation.

RÉSUMÉ

En présence de séléno-cystine nous avons constaté la formation d'une pré-vague catalytique du cobalt, dont le potentiel de démi-vague est situé à environ -0.94 V. La pré-vague se forme à partir de la concentration en séléno-cystine de 10^{-6} M; à $2 \cdot 10^{-5}$ M la vague du cobalt (10^{-3} M) est complètement déplacée dans la région de la pré-vague. La concentration des substances adsorbantes montre une influence très importante sur la pré-vague catalytique. En l'absence de gélatine aucun dédoublement de la vague ne se produit en tampon ammoniacal. A une concentration en gélatine de 0.004% les vagues sont complètement séparées, le maximum du cobalt est supprimé, mais le maximum de la pré-vague reste très fort. Lorsque la concentration en gélatine augmente on observe la diminution de la hauteur de la pré-vague qui pratiquement disparaît à une concentration en gélatine de 0.02%. La hauteur de la pré-vague n'est pas influencée par la variation de la hauteur du réservoir de mercure; ce comportement montre le caractère cinétique de la pré-vague. La hauteur du réservoir influence le maximum de la pré-vague, qui est supprimé dans le cas des grandes hauteurs du réservoir. La variation de la concentration du tampon ammoniacal et de ses composants met en évidence l'équilibre qui existe entre les complexes ammoniacaux et le complexe qui produit la pré-vague catalytique. La force ionique influence peu les potentiels de démi-vague, mais la hauteur de la pré-vague acquiert une valeur maximale pour une certaine concentration saline.

Puisque la séléno-cystine est réduite en séléno-cystéine à un potentiel de démi-vague égal à -0.06 V, la pré-vague du cobalt doit être produite par un complexe qui se forme entre le cobalt et la séléno-cystéine.

SUMMARY

In the presence of seleno-cystine we have established the formation of a catalytic pre-wave of cobalt for which the half-wave potential is about -0.94 V. The pre-wave forms from seleno-cystine concentrations of 10^{-6} M; at $2 \cdot 10^{-5}$ M the cobalt wave (10^{-3} M) is completely displaced into the region of the pre-wave. The concentration of adsorbing substances has an important effect on the catalytic pre-wave. In the absence of gelatine there is no splitting of the wave in ammoniacal buffer. At a gelatine concentration of 0.004% the waves are completely separated, the cobalt maximum is suppressed, but the pre-wave maximum remains very strong. When the concentration of gelatine increases, a decrease in the height of the pre-wave is observed; it practically disappears at 0.02% gelatine. The height of the pre-wave is not influenced by variation of the height of the mercury reservoir; this behaviour shows the kinetic character of the pre-wave. The reservoir height influences the pre-wave maximum, which is suppressed at large heights. The variation of the concentration of the ammoniacal buffer and of its components demonstrates the

existence of equilibria between ammoniacal complexes and the complex which produces the catalytic pre-wave. The ionic strength has little influence on the half-wave potentials, but the height of the pre-wave reaches a maximum value at a certain salt concentration.

Since seleno-cystine is reduced to seleno-cysteine at a half-wave potential of −0.06 V, the cobalt pre-wave must be produced by a complex formed between cobalt and seleno-cysteine.

BIBLIOGRAPHIE

1 J. HEYROVSKÝ ET J. KŮTA, *Principles of Polarography*, Publishing House of the Czechoslovak Academy of Sciences, Prague, 1965, pp. 380–393.
2 S. G. MAIRANOVSKII, *J. Electroanal. Chem.*, 6 (1963) 77.
3 A. CĂLUȘARU, *J. Electroanal. Chem.*, 15 (1967) 269.
4 A. CĂLUȘARU, *Compt. Rend.*, 262 C (1966) 4.
5 A. CĂLUȘARU ET J. KŮTA, *Collection Czech. Chem. Commun.*, 31 (1966) 814.
6 J. KŮTA, *Abhandl. Deutsch. Akad. Wiss. Berlin, Elektrochem. Meth. Prinz. Molekular-Biologie. Conf. Iéna, mai, 1965*, Akademie Verlag, Berlin, 1966, p. 423.
I. M. KOLTHOFF, P. MADER ET S. E. KHALAFALLA, *J. Electroanal. Chem.*, 18 (1968) 315.
8 M. ZIELINSKI, Thèse, Technische Hochschule für Chemie, Leuna-Merseburg, 1966.
9 M. ZIELIŃSKI ET J. KŮTA, *Abhandl. Deutsch. Akad. Wiss. Berlin, Elektrochem. Meth. Prinz. Molekular-Biologie, Conf. Iéna, mai, 1965*, Akademie Verlag, Berlin, 1966, p. 432.
10 R. BRDIČKA, *Collection Czech. Chem. Commun.*, 5 (1933) 112.
11 A. CĂLUȘARU ET J. KŮTA, *Nature*, 207 (1965) 750.
12 P. PAINTER, *J. Am. Chem. Soc.*, 69 (1947) 229.
13 B. NYGRAD, *Arkiv. Kemi*, 27 (1967) 341.
14 M. VON STACKELBERG, W. HANS ET W. JENSCH, *Z. Elektrochem.*, 62 (1958) 839.
15 S. G. MAIRANOVSKII, L. D. KLIUKINA ET A. N. FRUMKIN, *Dokl. Akad. Nauk SSSR*, 141 (1960) 147.
16 A. A. VLČEK, *Coordination Compounds*, en *Progress in Inorganic Chemistry*, Vol. 5, edited by ALBERT COTTON, Interscience, New York, 1963, p. 211.
17 P. DELAHAY, *Double Layer and Electrode Kinetics*, Interscience, New York, 1965.
18 A. CĂLUȘARU ET V. VOICU, résultats non publiés.
19 H. B. MARK, JR. ET C. N. REILLEY, *J. Electroanal. Chem.*, 4 (1962) 189.
20 A. CĂLUȘARU, *Compt. Rend.*, 262 C (1966) 676.
21 R. E. BENESCH ET R. BENESCH, *J. Am. Chem. Soc.*, 77 (1955) 5877.

Elsevier Sequoia S.A., Lausanne – Printed in The Netherlands

SHORT COMMUNICATION

Electrocapillary studies on a partially immersed silver electrode

In a previous work it was shown how the method of liquid capillary rise[1] can be applied to obtain an electrocapillary analogue for a partially immersed mercury-plated gold electrode. The variation in capillary rise with potential was predicted on the basis of our knowledge of the electrocapillary phenomena on mercury as described by the equation:

$$\gamma = \gamma_{max} - \tfrac{1}{2}c(E - E_{max})^2 \quad (1)$$

Concerning the effect of applied potential on the interfacial tension and the YOUNG AND HAGEN[2] equations:

$$\text{Cos}\ \theta = (\gamma_{S/g} - \gamma_{S/L})/\gamma_{L/g} \quad (2)$$

$$\text{Sin}\ \theta = 1 - \varrho g h^2/2\gamma_{L/g} \quad (3)$$

which describe the dependence of the contact angle on the interfacial tensions and the relationship between the same angle and the observed liquid capillary rise.

The present study attempts to apply the same method for the determination of an electrocapillary analogue on a partially immersed silver electrode.

Experimental technique

The apparatus and experimental procedure were described in a previous publication[1]. To allow maximum smoothness and minimum contamination, the silver electrodes were prepared in the form of thin films from the vapour phase on clean microscopic glass slides. Some of the samples were annealed in vacuum for 5 h up to a temperature of 500°. This technique was found useful in increasing the resistance of the deposit against peeling off. In acidic media, however, the peeling took place regardless of any heat treatment and, consequently, no experiments were carried out in such media. Because of a strong hysteresis effect, the data were measured in one and the same direction. This consisted in pre-setting the potentiostat at a certain potential and then reading the advancing capillary rise after turning the apparatus upward so as to wet a new fresh position of the vertically-set electrode.

Results

Figures 1 and 2 show the capillary rise *vs.* potential relationships in 0.1 *N* Na_2SO_4 and 0.1 *N* NaOH for both annealed and non-annealed silver deposits. With 0.1 *N* Na_2SO_4, the minimum, which is located at -580 ± 10 mV (*vs.* NHE), was found to be very reproducible and varied only slightly with the heat treatment. With 0.1 *N* NaOH, the minimum was less reproducible and showed a marked shift to more positive potentials with the non-annealed electrodes. Appreciable faradaic currents were observed with the non-annealed electrodes but were very small with the annealed samples. As can be seen in Figs. 1 and 2, the annealed samples show lower capillary rise values compared with the non-annealed deposits. With all the samples tested, the

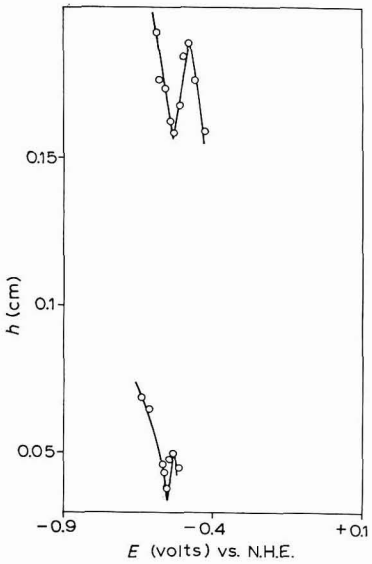

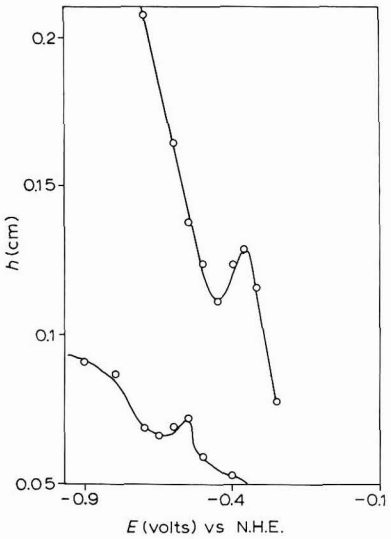

Figs. 1–2. Dependence of capillary liquid rise on potential for a silver electrode in (1) 0.1 N Na_2SO_4, (2) 0.1 N NaOH. Lower curves, annealed electrode; upper curves, non-annealed electrode.

capillary rise minimum is followed at a slightly more anodic potential with a maximum. At lower concentrations of 0.01 N and less, the variation of liquid capillary rise was apparently not much higher than the experimental error in the form of capillary rise fluctuations due to the inhomogenity of the surface crystalline structure. Consequently, no definite pattern of the investigated effect was observed in such concentrations.

Discussion

Ideally, the minimum in Figs. 1 and 2 should, according to eqns. (1)–(3), corresponds to the point of zero charge of silver in the specific solution. The validity of these experimental results will depend on the relevance of such factors as the presence of a chemisorbed layer of oxygen, hysteresis of wetting, adsorption of anions, etc. Before the effect of these can be studied it is important to eliminate any interference from the faradaic currrent due to oxygen reduction. Experiments based on measurements inside an inert gas thermostat are in progress.

Compared with other published data on the p.z.c. of silver, it is interesting to note that in 0.1 N Na_2SO_4 the p.z.c. value reported in this work agrees well with a value of -0.56 V obtained by EYRING *et al.*[4] from the peak potentials of open circuit transients. Compared with the capacity minimum[3], a value of -0.58 V shows at least a 100-mV shift to the anodic side. The capacity value, however, is obtained in very dilute solution and the observed difference might be due, at least partly, to the large differences in electrolyte concentration in both experiments.

The occurrence of a maximum in the capillary rise *vs.* potential plots is interesting for it was not observed in the results obtained on a mercury-plated gold electrode. One explanation that seems possible with the available experimental data is that it is due to the anion chemisorption at the positively charged surface. Such chemisorption could influence the capillary rise not only through increasing the interfacial tension

but also through increasing the friction force between the electrolyte and the solid surface. In this respect, it is noted that the work reported by BOCKRIS AND PARRY-JONES[5], BOWDEN AND YOUNG[6] and STAICOPOLUS[7] has shown that the friction at the interphase varies in a similar manner to the interfacial tension. STAICOPOLUS[7] also showed that higher friction values were observed at potentials positive to that of the maximum friction in the presence of certain anions that were likely to chemisorb at the surface.

The difference in surface energy (or surface tension) between the annealed and non-annealed silver deposits is reflected on the magnitude of liquid rise on both types. This follows directly from the Young equation.

Acknowledgement

The author is much indebted to the "Bundesministerium fuer Wirtschaft" of West Germany for supporting the research.

The author would like to express his thanks to Professor H. FISCHER for his kind interest and encouragement and to Dr. R. PARSONS for his valuable critical comments.

Institute of Physical Chemistry and Electrochemistry,
University of Karlsruhe,
(W. Germany)

IKRAM MORCOS*

1 I. MORCOS AND H. FISCHER, *J. Electroanal. Chem.*, 17 (1968) 7.
2 As described by F. NEUMANN, *Vorlesung ueber die Theorie der Capillaritaet*, Leipzig, 1893.
3 L. RAMALEY AND C. G. ENKE, *J. Electrochem. Soc.*, 112 (1965) 947.
4 D. D. BODÉ, JR., T. N. ANDERSEN AND H. EYRING, *J. Phys. Chem.*, 71 (1967) 792.
5 J. O'M. BOCKRIS AND R. PARRY-JONES, *Nature*, 171 (1953) 930.
6 F. P. BOWDEN AND L. YOUNG, *Research (London)*, 3 (1950) 235.
7 D. N. STAICOPOLUS, *J. Electrochem. Soc.*, 108 (1961) 900.

Received September 21st; in revised form, October 28th, 1968.

* Present address: Metallurgical Engineering Department, McGill University, Montreal, Canada.

Elsevier Sequoia S.A., Lausanne – Printed in The Netherlands

BOOK REVIEWS

La Catalyse au Laboratoire et dans l'Industrie, edited by B. CLAUDEL, Masson et Cie, Paris, 1967, 330 pages, 110 Figures and 7 Tables, 60F.

This book puts into published form a series of lectures given at the National Institute of Applied Sciences, Lyon, in 1966. The contributions, which are essentially of a review nature, take the reader through the subject of catalysis from the mechanisms of simple reactions to the problems met in industrial processes. The standard of the contributions varies appreciably, but those on fundamental mechanisms of heterogeneous catalysis, stereospecific polymerisation and the problems met in an industrial reaction merit special mention. The way in which the experimental techniques of heterogeneous catalysis are described throughout the book is especially welcome.

Because of the wide range of topics covered, the book should appeal to numerous readers already working in the field of catalysis. However, it is doubtful that the book can be recommended for teaching purposes or for those chemists who are new to catalytic research.

R. RUDHAM, University of Nottingham

Coulometry in Analytical Chemistry, by G. W. C. MILNER AND G. PHILLIPS, Pergamon Press, Oxford, 1968, x+207 pages, hard cover 30s, flexicover 21s.

This book is the first in a series intended to present an introduction to selected analytical methods and to create an awareness of the historical development of the subjects by reproducing key papers.

The first four chapters serve as an introduction to coulometry. The choice of material in this section is rather uneven, with a good deal of space devoted to obsolete circuits and instruments, and unnecessary duplication of material appearing in Chapter 7. Some (admittedly less important) coulometric methods are not mentioned and there is little advice to the reader on the subject of commercial instruments. There are numerous minor faults in the presentation. Thus on p. 2 it is implied that the direct reduction of ferric to ferrous iron can be carried out coulometrically at constant current. The impression is corrected on p. 7, but it is easy to imagine that a beginner would be confused by this apparent contradiction. Also, the discussion of end-point detection using polarised electrodes lacks the clarity required in an introductory text. A final example is the repeated reference to "controlled potential coulometric titrators" without comment on the nomenclature. This usage has rightly been criticised because of its inherent ambiguity.

Chapters 5 and 6 consist of very useful tables listing the analytical applications of potentiostatic and constant current coulometry reported up to 1965, with only a few omissions.

The idea of illustrating the development of coulometry by reprinting abridged fundamental papers is an excellent one, and this is done in the final chapter. A surprising omission is of GROWER's paper on the coulometric determination of tin on tinned copper wire, and the inclusion of MCNEVIN AND BAKER's paper on the integration of current–time curves seems hard to justify; otherwise the papers are well chosen and make interesting reading.

The book is well produced and the diagrams are excellent. There are relatively few misprints. On balance, the book succeeds in both of its main objectives, and can be recommended to undergraduates and chemists as an introduction to an intriguing analytical technique.

L. L. LEVESON, Bath University of Technology

J. Electroanal. Chem., 20 (1969) 482–483

ERRATA

V. N. KAMATH AND H. LAL, Kinetics of anodic oxidation of adsorbed films formed on platinized platinum in methanol, formic acid and CO_2 solutions, *J. Electroanal. Chem.*, 19 (1968) 249–258.

eqn. (6), the superscript α should be replaced by $-\alpha$.
p. 250, θ_M should be used in the footnote instead of θ_m.
ref. 3, p. 253 instead of 182; ref. 6, p. 379 instead of p. 397; ref. 17, Vol. 32 instead of 31.

J. Electroanal. Chem., 20 (1969) 483

KABIR-UD-DIN, A. A. KHAN AND M. AIJAZ BEG, Potentiometric estimation of potassium hydroxocyanotungstate(IV) and determination of standard potential, *J. Electroanal. Chem.*, 20 (1969) 239–244.

p. 243, the lines above the Acknowledgement should read: the values at 298°K are 32.4 kcal mole^{-1}, -22.6 kcal mole^{-1} and -18.4 cal deg.$^{-1}$ mole^{-1}, respectively.

J. Electroanal. Chem., 20 (1969) 483

JOURNAL OF ELECTROANALYTICAL CHEMISTRY AND INTERFACIAL ELECTROCHEMISTRY, VOLUME 20, 1969

AUTHOR INDEX

JOURNAL OF ELECTROANALYTICAL CHEMISTRY AND INTERFACIAL ELECTROCHEMISTRY, VOLUME 20, 1969

SUBJECT INDEX

Vol. 20 No. 3 JOURNAL OF ELECTROANALYTICAL CHEMISTRY MARCH 1969
AND INTERFACIAL ELECTROCHEMISTRY

CONTENTS

ADVANCES IN COLLOID AND INTERFACE SCIENCE

An international journal devoted to experimental and theoretical developments in interfacial and colloidal phenomena and their implications in chemistry, physics, technology and biology

Contents of Volume 1

Contents of the first two issues of Volume 2

Subscription price:
Dfl. 75.00, £ 8.14.6 or $ 21.00 per volume of four quarterly issues plus postage Dfl. 3.50, 8s. 3d., or $1.00.

Orders for single issues or full subscriptions may be sent to your regular bookseller or to Elsevier Publishing Company, P.O. Box 211, Amsterdam, The Netherlands.

Elsevier Publishing Company Amsterdam London New York

210 E